

# **Pennsylvania State University**

## **Annual Progress Report: 2008 Formula Grant**

### **Reporting Period**

July 1, 2009 – June 30, 2010

### **Formula Grant Overview**

The Pennsylvania State University received \$7,628,852 in formula funds for the grant award period January 1, 2009 through December 31, 2012. Accomplishments for the reporting period are described below.

### **Research Project 1: Project Title and Purpose**

*Vitamin D and Crohn's Disease: From the Bench to the Bedside* - Decreased outdoor activity and increased pollution and diets that lack adequate vitamin D have combined to create large fluctuations in vitamin D status, especially in populations that experience winter. Since vitamin D regulates the development and function of the immune system, this may account for the increase in autoimmune diseases like inflammatory bowel disease (IBD). Changes in vitamin D status result in more severe forms of experimental IBD, but vitamin D supplementation completely blocks the development of experimental IBD. Our hypothesis is that Crohn's patients have low circulating levels of vitamin D, which may exacerbate IBD. We propose to give Crohn's patients vitamin D and determine whether this dose is well tolerated, induces an increase in circulating vitamin D levels and/or improves health.

### **Anticipated Duration of Project**

7/1/2009 – 6/30/2011

### **Project Overview**

A) Broad objectives/Aims: The incidence of autoimmune diseases like inflammatory bowel disease (IBD) has increased in developed countries over the last 50 years. We propose that decreased outdoor activity and increased pollution and diets that lack adequate vitamin D have combined to create large fluctuations in vitamin D status in developed countries and especially in populations that experience winter. Experimentally we've shown that changes in vitamin D status result in more severe forms of experimental IBD. In addition, active vitamin D (1,25(OH)2D3) completely blocks the development of experimental IBD. The vitamin D hypothesis proposes that vitamin D regulates the development and function of the immune system and that changes in vitamin D status affect the development of the resultant immune response and the development of diseases like IBD. Our hypothesis is that because of low dietary vitamin D intakes and malabsorption of many nutrients, Crohn's patients will have low circulating vitamin D levels that are detrimental for their health. We plan to give

Crohn's patients 1000 IU of vitamin D/d and determine whether this dose is well tolerated, induces an increase in circulating vitamin D levels and has any additional health benefits (improved bone markers, Crohn's disease activity scores, inflammatory markers).

B) Research Design: The plan is to conduct a phase I trial of vitamin D supplementation in 50 adult patients with mild to moderate Crohn's disease. Patients will be recruited from both Hershey and State College. Because the study is a feasibility study no placebo controls will be included. Instead patients will serve as their own controls. Baseline and 6 month data collection will be done on diet, serum vitamin D levels, inflammation, bone mineral density, Crohn's activity scores and quality of life surveys.

### **Principal Investigator**

Margherita Cantorna, PhD  
Associate Professor  
Penn State University  
115 Henning Building  
University Park, PA 16802

### **Other Participating Researchers**

Terryl Hartman, PhD, Jill Smith, MD - employed by Penn State University

### **Expected Research Outcomes and Benefits**

The expected outcomes are 1) to identify what the dietary intakes and circulating levels of vitamin D are in the patient pool, 2) to determine whether vitamin D supplementation will improve vitamin D status, and 3) to determine whether increased vitamin D intakes are associated with health benefits in the Crohn's patients including bone mineral densities, Crohn's activity scores, and quality of life. The information we gather in this study will be used to determine whether a larger clinical study is worthwhile, whether additional selection criteria in the recruitment of Crohn's patients are necessary, whether vitamin D is well tolerated and adequate for improving vitamin D status, and whether clinical and immunologic improvement is seen over the 6-month study period. In addition, the clinical data will be used to help develop new mechanistic experiments aimed at determining what aspects of the immune response and/or health of the Crohn's patients are improved with vitamin D supplementation.

### **Summary of Research Completed**

Our goals have not changed and our project is ongoing. We currently have 7 subjects who have completed the study and 5 who are currently in the study. In addition, we are continuing to recruit and are revising the study protocol in order to increase the recruitment of eligible patients. There are several unexpected impediments to our recruiting efforts. Although our goal continues to be to target only individuals with mild to moderate Crohn's disease, this has limited our ability to enroll several individuals. In addition, the multiple visits required to set the vitamin D dose has limited our ability to recruit individuals who live outside the Hershey and State College

areas. To address this, we plan to alter our IRB application to allow for a phlebotomist to travel to the patient's location to draw blood samples, or to pay for the necessary blood draws and transportation of samples from more remote locations. At this time, we plan to stop enrolling subjects as of January 1, 2011 so that we can have all participants completed in the 6 month intervention by June 30, 2011 and have the data ready for analyses. We have not analyzed any of the data we currently have because we don't want to bias the study.

## **Research Project 2: Project Title and Purpose**

*Epigenetic Regulation of Inactive X Chromosome Expression* - Personalized medicine, or the tailoring of pharmaceuticals and treatments to specific individuals, is an important goal of genomic medicine in the 21<sup>st</sup> century. It is increasingly apparent that even subtle gene differences may impact common traits. We are interested in evaluating gene differences that effect the female sex chromosome (X) where most, but not all, genes on the second X must be silenced. The goal of these experiments are to evaluate the variation in gene expression for genes on the X chromosome and to design an assay that can quickly and effectively assess inactive X expression for specific genes to assess their role in common diseases.

## **Duration of Project**

1/1/2009 – 12/31/2009

## **Project Overview**

Gender differences are well documented in normal traits and in the prevalence or presentation of many diseases. Hormonal and cultural milieus play major roles, but genetic differences contribute as well. The genomic content of the sex chromosomes differ widely although most inequity is erased by X chromosome inactivation that silences genes on one of a female's X chromosomes to functionally balance X gene dosage between XX females and XY males. Nonetheless, not all genes on the inactive X are silenced. The role of these genes that "escape" inactivation in gender-specific medicine has not yet been widely considered.

To identify genes that escape inactivation, we established an X inactivation profile of the human X chromosome. Our data from 642 X-linked transcripts indicate that the majority of genes are subject to inactivation, but 15% escape inactivation and are expressed from both active and inactive Xs. Few genes have Y homologues, suggesting that a significant proportion of X-linked genes may be expressed at higher levels in females than males. Surprisingly, an additional 10% of genes assayed were variable; that is, they escaped inactivation in some female cell lines but not others, raising the intriguing possibility that some could contribute to individual female trait variation.

To better understand these genes that escape X inactivation and the genes that show variable expression, we propose (1) to measure levels of inactive X expression for seven genes that cluster in Xp11.3 in a panel of 40 primary cell lines that have been previously been used to effectively monitor inactive X expression; (2) to correlate inactive X expression with epigenetic modification by measuring DNA methylation at the CpG islands of these genes in multiple

female cell lines; and (3) to establish a methylation assay that could be used to effectively predict expression levels from the inactive X and evaluate the role that inactive X genes contribute to traits that show gender differences.

### **Principal Investigator**

Laura Carrel, PhD  
Assistant Professor  
Penn State College of Medicine  
Department of Biochemistry and Molecular Biology, H171  
Hershey Medical Center, C5757  
Hershey, PA 17033

### **Other Participating Researchers**

Jill Stahl - employed by Penn State College of Medicine

### **Expected Research Outcomes and Benefits**

These studies have both basic biological and clinical relevance. These experiments will be important for understanding the general mechanics of X chromosome inactivation, a critical process that turns off genes on one X chromosome in early female development and also will give important insight into the role that specific DNA sequences play in coordinately controlling clusters of genes not only on the X, but on other chromosomes as well. Of clinical importance is that the inheritance of an abnormal number of X chromosomes or portions of an X is a common birth defect, accounting for 1 in 650 live births. Many problems in these individuals result from inappropriate gene dosage due to the specific subset of X-linked genes that will be studied in this project. It is essential to better understand these genes and how they are regulated in order to explain clinical features and to improve genetic counseling recommendations. Finally, personalized medicine, or the tailoring of pharmaceuticals and treatments to specific individuals, is an important goal of genomic medicine in the 21st century. Gender differences are well recognized in a large number of disorders ranging from heart disease to cancer. Hormonal and cultural differences play major roles, but chromosomal (genetic) differences must be considered in many of these disorders as well. Some genes on the X chromosome are expressed at higher levels in normal females compared to normal males and at variable levels between different females and become candidates to explain gender differences in normal traits and in the prevalence or in the presentation of many diseases. The following studies will give a basic understanding of these genes that will be quite important for understanding the female genome and will guide future studies to explore their roles in gender aspects of genomic medicine.

### **Summary of Research Completed**

The overall goal of this one-year research project was to evaluate and correlate inactive X expression and methylation for seven genes within a region of Xp11.3 in order to assess variation of these genes and to establish a rapid assay that could be used to determine whether these genes contribute to trait variation in different females. We previously established SNP expression

assays for seven genes within Xp11.3 and our previous progress report described surprising results that indicated that only one gene, DDX3X, shows high levels of escape in the lines tested. Therefore, these results indicated that inactive X expression levels vary across an escape domain and show wide variation of inactive X expression levels amongst different individuals.

The milestone for the second six months of this project was to evaluate methylation levels in these cell lines in order to correlate methylation and inactive X expression. We developed methylation assays for two of the genes within the region, USP9X and DDX3X, and again had unexpected results. Methylation was tested by pyrosequencing of bisulfite modified DNA. Male lines (not shown) were completely unmethylated as expected since they only contain an active X chromosome. X inactivated alleles should be fully methylated and therefore we expected to observe 50% methylation in female lines that showed silencing of the inactive X allele since both chromosomes are measured. Conversely, lines that highly escape X inactivation are anticipated to be hypomethylated on both the active and inactive X chromosomes. We previously reported inactive X expression levels for USP9X ranged from 2-18% of active X levels whereas DDX3X ranged from 2-55%. Given such variation, we expected similar methylation variation, yet all samples were completely hypomethylated (Fig. 1). These data suggest that methylation of Xp11.3 genes does not correlate with inactive X expression.

These results prompted us to ascertain an additional locus to evaluate whether aspects of inactive X gene expression in Xp11.4 differ from that of the rest of the chromosome. We developed methylation assays and monitored inactive X expression using a quantitative allele-specific expression assay for two genes mapping to an escape domain in Xq28. HCFC1, like the genes in Xp11.4 is hypomethylated in all lines despite inactive X expression levels in some lines that approach 25% of active X levels (Fig. 2). ARD1 methylation, in contrast, did appear to correlate with inactive X expression; samples that showed the highest levels of inactive X expression have the lowest methylation and higher levels of methylation were seen in the samples with lower inactive X expression levels.

These data allow us to make a number of interesting conclusions. It is clear that methylation is not sufficient to allow inactive X expression and this feature alone cannot predict inactive X expression. It appears that the hypomethylation domain in Xp11.4 is an escape prone domain, but what additional features allow for inactive X expression remain unknown. Given these results, Aim 3 for this project is not feasible. Whether a hypomethylated CpG island is a necessary prerequisite is unknown. It is likely that additional epigenetic features are critical. Such modifications, e.g. histone methylation, particularly H3 trimethylated at lysine 27, could be an important diagnostic of inactive X expression and will need to be further evaluated. A manuscript describing these results is in progress. Further, we remain interested in identifying genetic and epigenetic features that predict inactive X expression as an approach towards evaluating whether these genes are impacting traits and disorders that show gender differences and variation amongst females.

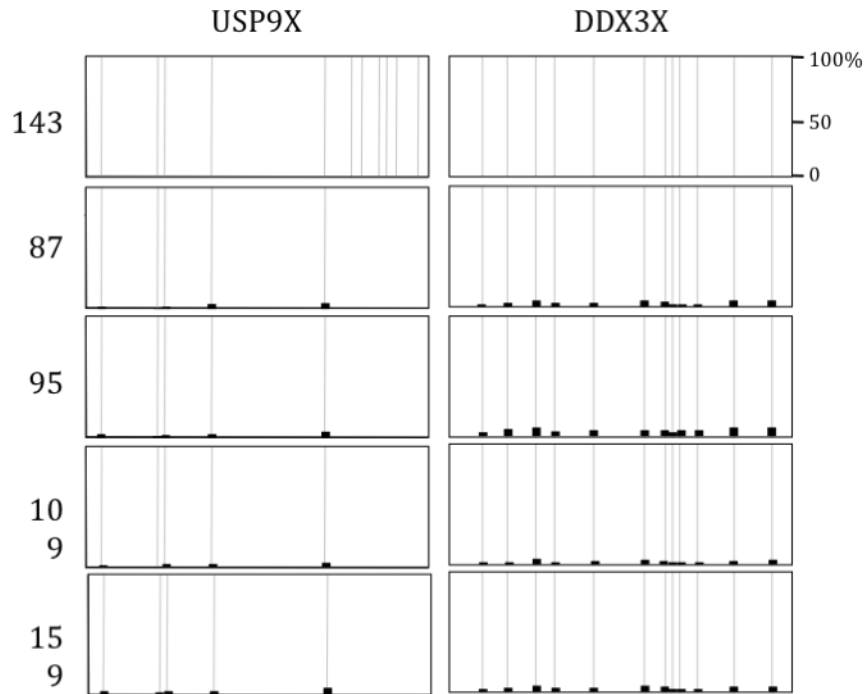


*Fig. 1. Methylation of genes in Xp11.3 does not correlate with inactive X expression. Methylation in five primary fibroblast lines was assayed by pyrosequencing of bisulfite modified DNA. 100 bp regions within CpG islands for the USP9X and DDX3X genes are shown.*

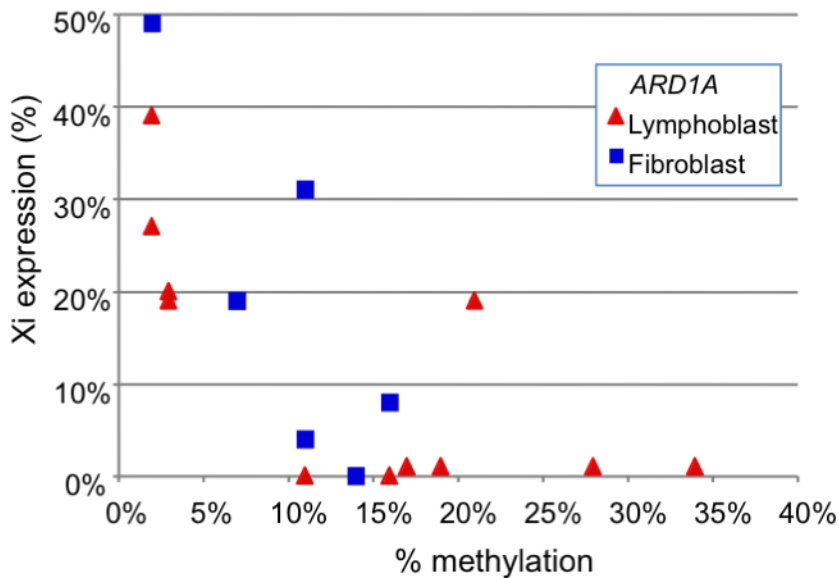
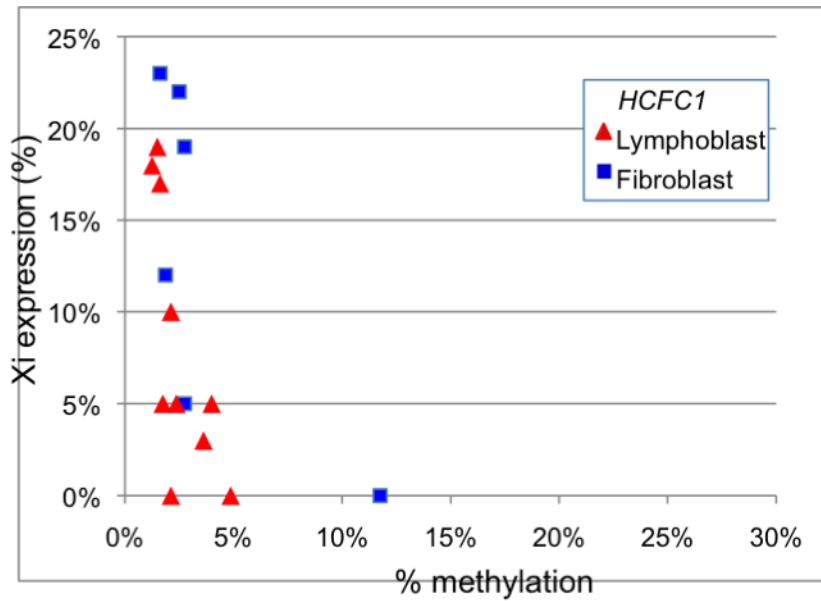


Fig. 2. Methylation and expression of genes in Xq28. Methylation in fibroblast and lymphoblast samples was assayed by pyrosequencing of bisulfite modified DNA. Methylation reflects average methylation of 4-10 sites within the sequenced region.

### **Research Project 3: Project Title and Purpose**

*Role of UGT2B7 Genotype in Patient Response to Tamoxifen* - The glucuronidation phase II metabolic pathway is an important factor in breast cancer recurrence and toxicity associated with tamoxifen (TAM) treatment, and genetic mutations in the enzyme responsible for metabolizing TAM may play a key role in determining overall patient response to TAM. We propose to test this hypothesis by measuring levels of TAM metabolites in patients on TAM and correlating these levels with the presence of genetic mutations. Using detailed clinical questionnaires, we will also examine the potential association between the presence of mutations and patient toxicity and side effects (hot flashes, arthralgias, deep vein thrombosis and uterine cancer). Long-term goals will include studies examining whether these genetic mutations impact breast cancer recurrence and metastasis.

### **Anticipated Duration of Project**

5/1/2009 - 6/30/2011

### **Project Overview**

This project focuses on evaluating individual patient differences in overall response and efficacy of tamoxifen (TAM) treatment based upon individual differences in metabolism and pharmacogenetics. We hypothesize that the glucuronidation phase II metabolic pathway is an important factor in breast cancer recurrence and toxicity associated with TAM treatment. We hypothesize that genetic variations in the UGT enzymes responsible for the glucuronidation of TAM, specifically polymorphisms in UGT 2B7, play an important role in inter-individual differences in TAM metabolism and an important role in inter-individual variability in patient response to TAM. In the preliminary results presented in this project, we show that several UGTs exhibit significant glucuronidating activity against 4-OH-TAM and endoxifen and that a common SNP of one of the most active UGTs, UGT2B7, exhibits significantly lower activity against these metabolites *in vitro*. The goal of the present study is to examine the effects of the UGT2B7 variant on TAM metabolite profiles and toxicity in women taking TAM. We propose to test this hypothesis by measuring levels of TAM metabolites in patients on TAM and correlating levels with UGT2B7 genotype. Using detailed clinical questionnaires, we will also examine the potential association between UGT2B7 genotype and patient toxicity and side effects (hot flashes, arthralgias, deep vein thrombosis and uterine cancer). Long-term goals will include studies examining whether UGT2B7 genotype impacts breast cancer recurrence and metastasis.

### **Principal Investigator**

Leah Cream, MD  
Assistant Professor  
Penn State University  
500 University Drive, HO46  
Hershey, PA 17033

## Other Participating Researchers

Philip Lazarus, PhD, J. Stanley Smith, MD - employed by Penn State University

## Expected Research Outcomes and Benefits

By understanding the role of mutations in enzymes responsible for the metabolism of tamoxifen (TAM), we hope to be able to individualize drug dosing in order to maximize efficacy and minimize toxicity. In addition, these studies should enable us to assess whether patients are better suited for treatment with TAM or an aromatase inhibitor. The results from this study may ultimately lead to identifying optimal protocols for breast cancer treatment and prevention, including tailoring of tamoxifen dosage regimens and the selection of tamoxifen versus other treatment protocols (e.g., aromatase inhibitors). These studies should help minimize breast cancer recurrence and limit toxicity and is consistent with the goals of the National Institutes of Health mandate of individualized medicine and disease prevention. The effect of these studies on human health is enormous since there are over 200,000 new breast cancers a year in the U.S., the majority of which are hormone positive, and millions of women in the U.S. and around the world are currently taking TAM.

## Summary of Research Completed

This clinical trial received institutional review board approval in March 2009 and we began recruiting patients in early April 2009. Current enrollment is 41 patients. We have recently begun submission of an IRB amendment to increase accrual to 100 patients. Accrual was faster than anticipated and we have many more eligible patients than we expected. Patients in the study are followed for one year so over the next year the study will be complete and data analysis will begin. We have begun working with the serum samples and a summary of our laboratory work is included below. We are also collecting hot flash diaries and the hot flash data will be correlated with the pharmacogenomic data.

The serum samples are being used to characterize the effect of pharmacogenetics of functional SNPs in UGT2B7 and CYP2D6 on TAM metabolism profiles in patients treated with tamoxifen (TAM).

The goal of the present study is to study TAM metabolism vs. metabolic profiles (Figure 1). The procedure used for this analysis was developed and performed by Dr. Dongxiao Sun in the laboratory of Dr. Philip Lazarus. TAM, N-desmethyltamoxifen (NDT), *trans*-4-hydroxy (OH)-TAM, *cis*-4-OH-TAM, *trans*-endoxifen, *cis*-endoxifen, and venlafaxine were purchased from Sigma-Aldrich (St Louis, Missouri, USA) and used as standards for methods development. TAM-d5, NDT-d5, *trans*-4-OH-TAM-d5, endoxifen-d5 (1:1 *trans/cis* isomer), and venlafaxine-d6 were purchased from Toronto Research Chemicals (North York, Ontario, Canada) and were used as internal standards. This procedure involved the following experimental milestones:

### *1. Preparation of calibration curve*

Preparation of standards for examination in plasma from healthy, untreated subjects. Calibration samples were prepared freshly by spiking 5 ul standard working solution to 300 ul control human

plasma. Take 100 ul plasma with spiked standards and add 300 ul internal standard working solution in acetonitrile to extract the compounds. The mixture was vortexed and centrifuged at  $16,100 \times g$  for 10 min at 4 °C. The supernatant was dried by vacuum and was then resuspended in 50 ul acetonitrile and 50 ul buffer (5 mmol/L NH<sub>4</sub>Ac, pH 7.5). The 100 ul sample was transferred to UPLC autosampler vial, and 5 ul was loaded onto UPLC/MS/MS.

Linearity and detection limit. Calibration curves were derived using the peak area ratio of standard compound vs. corresponding internal standard. Eight non-zero calibration standards were assessed through the linear least squares regression calculation with a weighting factor of 1/X. The detection limit was defined by the signal/noise > 3~5. A daily linear calibration curve was prepared with each clinical sample batch to be analyzed.

Clinical sample preparation. After thawing on ice, a 100 ul aliquot of plasma sample was transferred to 1.5 ml polypropylene tube and added to 300 ul acetonitrile with internal standards. The preparation procedure was the same as that of standard samples in control plasma. Every sample was prepared and analyzed in triplicate independently.

## Results

We developed a sample pretreatment method to extract TAM metabolites from plasma and eliminate matrix including lipids and proteins. We also developed analytical methods to determine TAM metabolite concentrations in plasma by UPLC/MS/MS.

### 2. Development and optimization of analytical methods for determination of TAM metabolites in plasma by UPLC/MS/MS.

Standards representing the major metabolites of TAM, including *trans*-4-OH-TAM, *cis*-4-OH-TAM, *trans*-endoxifen, *cis*-endoxifen, NDT and TAM, are easily separated and detected when added to plasma and processed in a manner identical to that utilized for plasma samples from TAM-treated patients. In addition, venlafaxine standard (venlafaxine is used as an anti-depressant in virtually all of the TAM-treated patients) was well-separated from TAM metabolites in our UPLC/MS/MS methodology. Data not shown.

### 3. Calibration curve and linearity

The reported concentrations of TAM metabolites in patient plasma are within the TAM metabolite standard linear range analyzed in our developed method. The calibration curves shown for each TAM metabolite in exhibit a correlation coefficient of  $r > 0.999$  in all cases, and are within the reliable criteria for quantification of TAM metabolites in clinical plasma samples.

### 4. Determination of TAM metabolites in plasma from untreated healthy controls by UPLC/MS/MS.

As shown in Fig. 2, the detection limit of *trans*- and *cis*-4-OH-TAM is about 0.5 ng/ml, while the detection limit of *trans*- and *cis*-endoxifen is about 1 ng/ml as determined by signal to noise ratio > 3~5. The reported concentrations of 4-OH-TAM and endoxifen in the plasma of patients treated with TAM are higher than the detection limits for all metabolites. For NDT and TAM, the

lowest concentrations in the calibration curve demonstrated clear peaks, and the signal to noise ratio  $\gg 5$ . Clear peaks with a slightly lower signal:noise ratio were also observed for 4-OH-TAM and endoxifen isomers. Thus, our method is valid for the determination of TAM metabolites in plasma.

5. Determination of TAM metabolites in plasma from subjects treated with TAM by UPLC/MS/MS.

As shown in Fig. 3, clear peaks corresponding to *trans*-4-OH-TAM (1.65 ng/ml), *cis*-endoxifen (2.09 ng/ml), *trans*-endoxifen (10.95 ng/ml), NDT (128.14 ng/ml), and TAM (103.75 ng/ml) could be detected and quantified for each of the major plasma TAM metabolites in plasma from a patient treated with TAM. In addition, two additional peaks likely corresponding to the *cis* and *trans* isomers of TAM-N-oxide (based on molecular weight) are also clearly detected; this will be verified using purchased internal standards. The levels of each metabolite are within range of previously reported plasma levels for patients treated with TAM. *cis*-4-OH-TAM was not detected in this individual's plasma; perhaps the levels of this metabolite were too low for detection in this individual.

This is the first report where the isomers of 4-OH-TAM and endoxifen have been separated and quantified. This is important since it is the *trans* isomers of these metabolites that exhibit the majority of the anti-estrogenic activity of TAM, with their respective *cis* isomers postulated to contribute an estrogen agonist activity.

The plasma venlafaxine concentration (1.94 ng/ml) was lower than the lowest point screened in our calibration curve, but a clear peak with a signal/noise  $\gg 5$  was still detected in this individual. We will re-perform the venlafaxine calibration curve using lower concentrations (3-fold that of the detection limit) to assure that we are within range of detecting this agent in patient plasma and that it is not confounding our TAM metabolite analysis for each individual.

The optimized sample preparation and analytical methods have now been established for the measurement of TAM metabolites in plasma of patients treated with TAM. We are currently analyzing all of the patient samples recruited into this study. Genotyping of known functional SNPs in UGT2B7 and possibly CYP2D6 using lymphocytes from the same blood specimens used for metabolite analysis will also be performed.

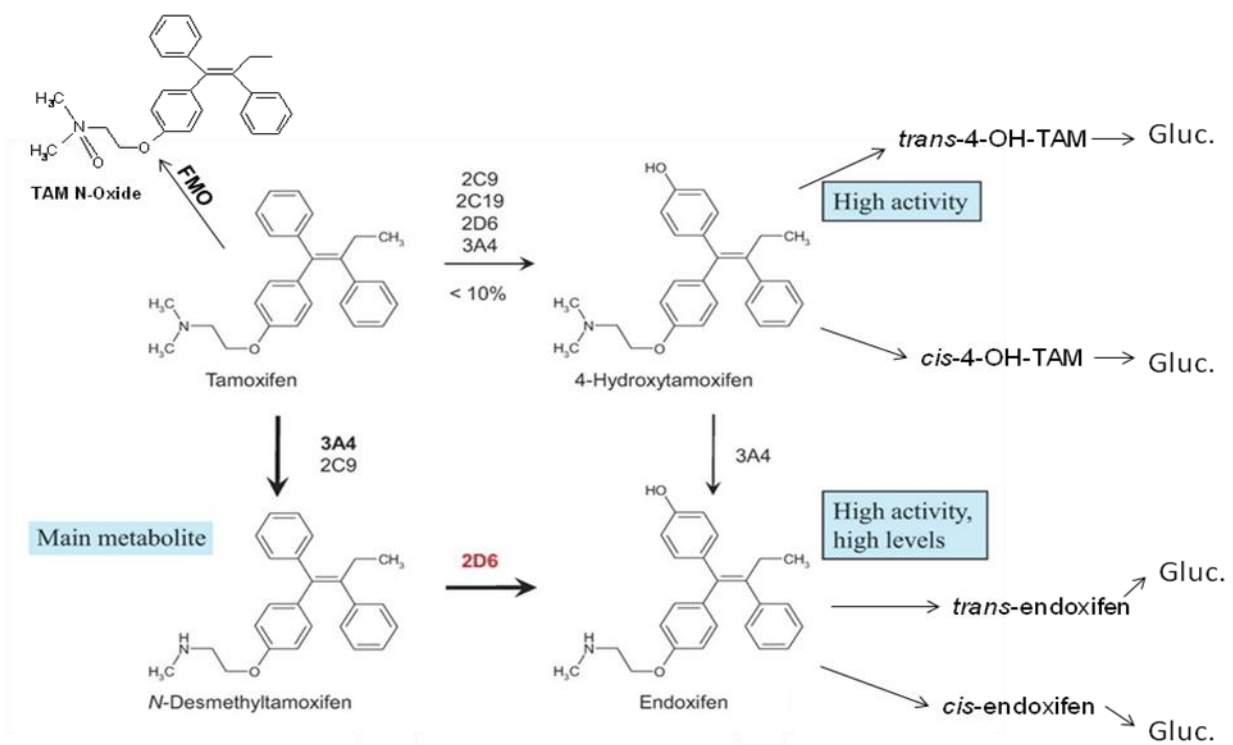


Fig. 1 Schematic of TAM metabolites

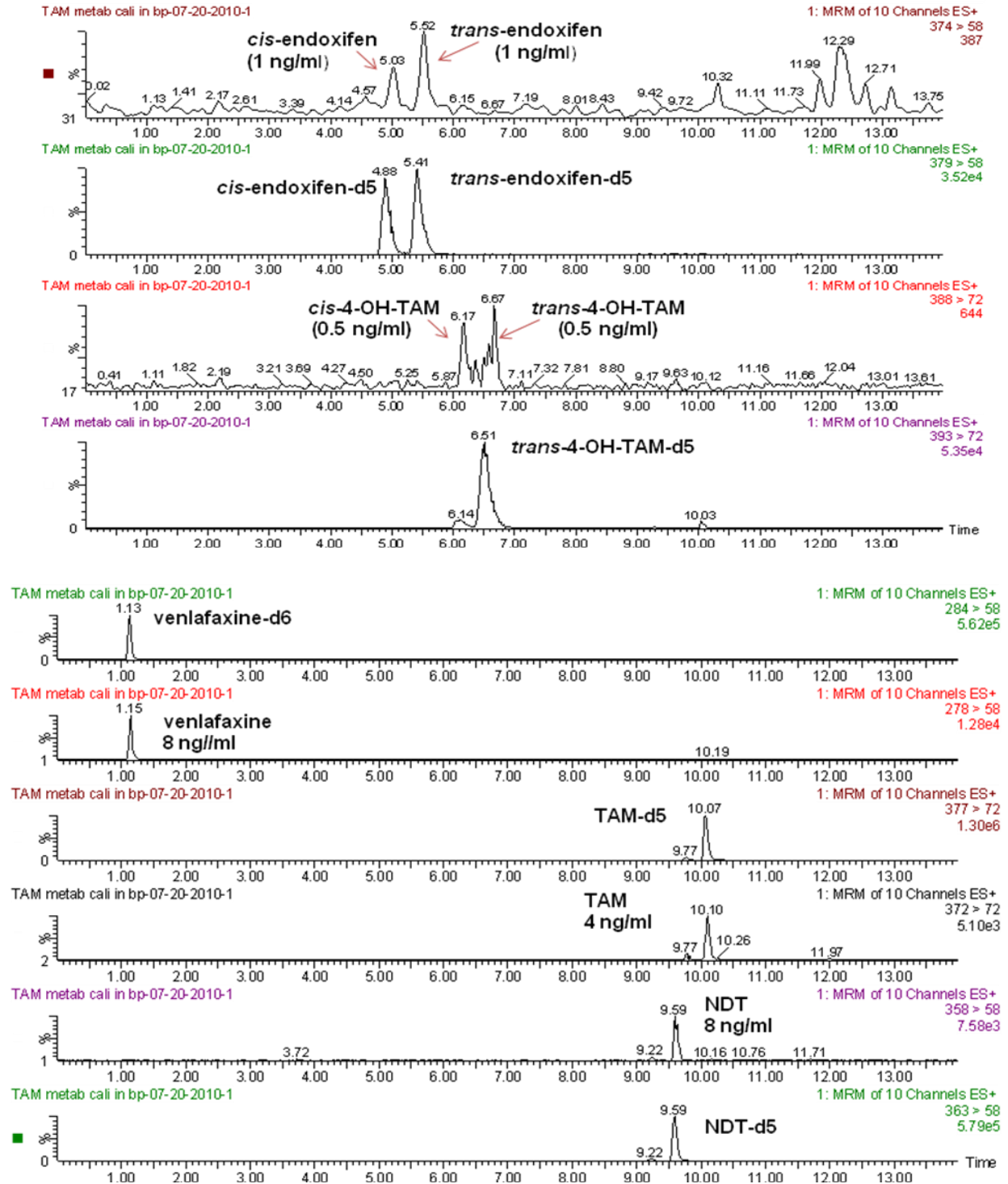


Fig. 2. Representative UPLC/MS/MS MRM chromatograms of TAM metabolites and venlafaxine in plasma from untreated subjects at the lowest concentration of the calibration curve for each compound.

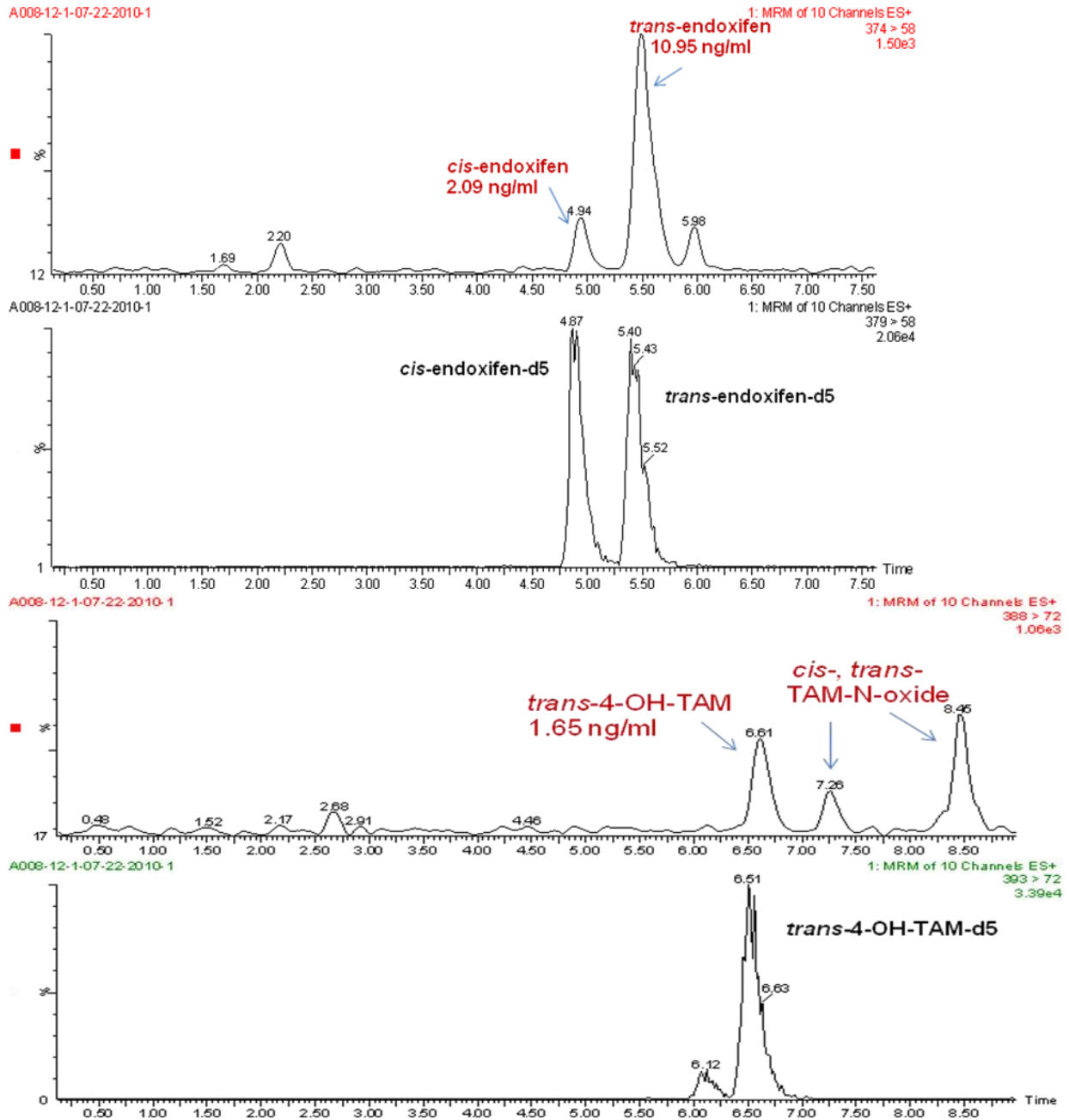


Fig. 3. Representative UPLC/MS/MS MRM chromatograms of TAM metabolites in plasma from a single patient treated with TAM

## **Research Project 4: Project Title and Purpose**

*Functional Brain Imaging of Memory and Language for Epilepsy Surgery* - The purpose of this project is to translate procedures and findings in experimental functional MRI (fMRI) into clinically validated techniques for localizing language and memory systems in the brain of patients undergoing surgery for epilepsy (i.e., temporal lobectomy). The current Wada procedure, which is used to localize systems in the brain, was developed over 50 years ago and is highly invasive, and does not always provide interpretable data. We propose to investigate the feasibility of using fMRI procedures as reliable indicators of language and memory localization to replace the Wada Test.

### **Anticipated Duration of Project**

6/1/2009 - 6/30/2011

### **Project Overview**

The specific aims of this project are:

- (i) Determine the fMRI characteristics most associated with typical left hemisphere language dominance. We hypothesize that areas where there is no fMRI activity detected across three language tasks can be safely resected during anterior temporal lobectomy for intractable epilepsy.
- (ii) Test the hypothesis that an asymmetry index of medial temporal lobe activity during memory retention tasks will be concordant with Wada memory test result asymmetry and of greater predictive value than the Wada for post-surgical memory function.
- (iii) Test the hypothesis that pre-operative fMRI language and memory asymmetries will be predictive of 6-month post-operative re-organization of function.

We plan to study 10 patients who are diagnosed with Temporal Lobe Epilepsy (TLE) and undergo Anterior temporal lobe resection (ATLR) for relief of intractable seizures. The fMRI and cognitive tests will be given to the clinical subjects prior to and 6 month post surgery in addition to the standard clinical tests used for preoperative surgery planning. The memory and language fMRI protocols based on previous studies will be validated with 10 age- and sex-matched healthy volunteers.

Participants will complete three basic language activation tasks including: verbal generation, picture naming, and sentence comprehension. Tasks associated with naming and reading were chosen because these skills are most closely associated with ATLR complications. This will be examined in a 6-month follow up fMRI study by identifying the areas of fMRI activation that nonetheless were necessary to resect and comparing both out-of-magnet neurocognitive testing of language function and activation patterns.

Additionally, 3 different memory activation tasks, designed to stimulate material-specific memory and multi-material memory activations in the medial temporal region, will be used. During the encoding phase, stimuli will be presented in a block design format, with the participant responding to a specific question about what the stimulus is. These include: (1) single

word with high semantic content; (2) nonverbal-visuospatial patterns; and (3) face-name pairs. The 3 types of stimuli will be intermixed in 3 runs of 45 stimuli (15 items for each category) and participants will respond with whether the stimulus is a word, nonverbal design, or face-name pair. After 10 minutes of rest, stimuli will be presented in event-related formats that are either (a) repeated from the initial encoding set or (b) novel stimuli not previously presented, for participant memory about whether they occurred 10 minutes before.

### **Principal Investigator**

Paul J. Eslinger, PhD  
Professor  
Milton S. Hershey Medical Center  
500 University Drive, Mail code: EC037  
Hershey, Pa 17033

### **Other Participating Researchers**

Dan T. Nguyen, MD, Kevin M. Cockroft, MD, Matthew Eccher, MD, Claire Flaherty-Craig, PhD, Paul Kalapos, MD, James McInerney, MD, Qing X. Yang, MD - employed by Milton S. Hershey Medical Center

### **Expected Research Outcomes and Benefits**

fMRI has the potential to provide noninvasive brain mapping of critical cognitive functions such as language and memory with less cost, less health risk, higher reliability, and more information for surgical planning. It is the hope of the research team that this research will produce data that will lead to future clinical trials for the replacement of the Wada test for pre-operative planning. Additionally, successful completion of this project will advance the development of similar techniques for other neurosurgical conditions such as brain tumors and vascular malformations.

### **Summary of Research Completed**

There has been substantial research progress this past year with development of new experimental methods, recruitment of study participants, and initial analysis of data. The summary of research completed follows.

#### **Research Methods**

We have developed or adapted seven (7) cognitive fMRI paradigms to achieve the aims of this study. The experimental tasks, along with high resolution T1 anatomical imaging, requires a total scan time of 55 minutes, which is feasible for patients and controls. The tasks include: Word Encoding (*6 minutes*), Picture Encoding (*6 minutes*), Word Recognition (*8 minutes*), Picture Recognition (*8 minutes*), Verbal Fluency (*6 minutes*), Face-Name Encoding/Recognition (*8 minutes*), and Sentence Completion (*6 minutes*), as follows.

## *Encoding and Memory Recognition Paradigms*

*Word Encoding and Picture Encoding* tasks are set up identically. They are both constructed in a block design format, with a TR of 2000. The blocks alternate between strings of stimuli that participants try to memorize (experimental blocks) and then strings of stimuli that participants passively view (baseline blocks). Each block lasts 40 seconds, separated by an 8 second rest period. During the experimental blocks, participants view 10 stimuli lasting 4 seconds each, totaling in 30 experimental stimuli. They are instructed to try to memorize each stimulus (either a word or a picture) and to press down with both index fingers whenever they notice the stimulus changes. During each baseline block, participants view 10 stimuli (either a pseudo word or scrambled picture) and are instructed to look at each stimulus (but not memorize) and again press down with both index fingers whenever the stimulus changes. Before each block there is an instruction slide, reiterating what the participant should do next and if they need to respond in any way.

*Word Recognition and Picture Recognition* tasks are also designed similarly, differing only by the verbal vs. visuospatial material. They are programmed in a mixed design. The experimental stimuli are presented using an event-related design and the baseline stimuli are presented using block design. The TR is 2000. In both tasks, participants see strings of words (or pictures), but now they must decide (using a keyboard) if they saw words (pictures) from the previous encoding task or if it is a novel word (picture). Each experimental block contains 6 stimuli lasting 4 seconds each, separated by 2 – 10 second blanks. In total, there are 15 “learned” stimuli and 15 “novel” stimuli in each task. During the baseline blocks, participants see strings of 4 stimuli lasting 4 seconds each, separated by a 0.5 second blank (either a pseudo word or scrambled picture). The instructions are presented in the same manner as the Encoding tasks.

*Face/Name Encoding & Recognition* tasks are programmed in a block design, with a TR of 3000. Participants view a string of 4 faces (one at a time); each face has a name below it and they are instructed to memorize each face and the associated name. Next they have a Distractor period lasting for 48 seconds. During this block, they see alternating “+” and “0”, lasting for 3 seconds and 1 second, respectively. Finally, they see the same 4 faces (one at a time), but now all 4 names are listed below each face. Participants are instructed to decide which of the 4 names was associated with each face. During the Recognition block the faces are never presented in the same order as initially presented and the names are in a scrambled order. The task cycles through Encoding → Distractor → Recognition 4 times, twice with male faces and twice with female faces (16 faces total). Stimuli in Encoding and Recognition blocks are presented for 4 seconds each, without any separation.

## *Language Paradigms*

*Verbal Fluency* is set up in a block design, with a TR of 3000. Participants are first presented with three letters (one at a time) and they are instructed to silently think of as many words beginning with the letter on the screen as they can (e.g., for the letter S → “sauce”, “shoe”, “sundae”, etc.). Then they are presented with three categories (one at a time) and instructed to silently think of as many words associated with that category as they can (e.g., for the category

of Fruit → “apple”, “banana”, “watermelon”, etc.). Each letter or category is presented for 30 second, followed by a 20 second rest.

*Sentence Completion* is presented in a block design, with a TR of 3000. Participants first view a string of 8 nonsense sentences (baseline block), and are instructed to simply look at each sentence (e.g., “Rdse sdkln seke \_\_\_\_\_ lewo lskd.”). Then they are presented with a string of 8 simple sentences (experimental block) and instructed to silently fill in the blank in each sentence (e.g., “A young cat is called a \_\_\_\_\_.”). For both blocks, each stimulus is viewed for 3 seconds, separated by a 0.5 second crosshair. Each block lasts for 28 seconds, and there are 6 baseline blocks and 6 experimental blocks.

### Participants

Ten healthy adults have been recruited for standardization studies and all have completed fMRI studies. The Clinical Surgical Epilepsy Program has been reorganizing (with 2 faculty departures and recruitment of new faculty) and recruitment of temporal lobe epilepsy and anterior temporal lobectomy patients has been slower than expected. These factors have been beyond our control but Dr. Eslinger has been working with this program to increase the number of study participants. To date, we have completed presurgical fMRI studies on 2 temporal lobe epilepsy patients (both completed without difficulty) and 6 more have been identified and contacted for studies. This brings our recruitment to 10 controls and 8 patients, with 2 patients yet to be identified. With recent progress in recruitment, we believe we can meet the full recruitment for this study.

### Data Analysis

Data analysis has been steadily progressing. Image data from 8 of the 10 control participants have been processed using SPM5 and quality of studies has been very good. fMRI data from 2 temporal lobe epilepsy patients have been processed as well.

### Initial Results

Representative results are shown because of the large dataset. Among the encoding and memory recognition tasks, *word learning and retention* paradigms have generated clear findings. These are shown in Figure 1. Specifically, medial temporal activation was predominantly on the left and in the region of the hippocampus, which is a main site of anterior temporal lobectomy (see Figure 3 below). In a patient with left temporal lobe epilepsy, who showed a deficit in word recognition memory, there was a specific lack of left medial temporal (hippocampal) activity during this task (see Figure 2 below). Thus, initial results suggest that the word recognition memory task may provide sensitive and specific differences in brain organization subserving verbal short-term memory and may be a good predictor of post-surgical outcome after temporal lobectomy.

The picture recognition memory generated specific medial temporal activations as well. As expected, these clusters were predominantly in the right hemisphere (see Figure 3 below). The activation map of a right temporal lobe epilepsy patient showed lack of typical activity in the right medial temporal lobe region during this task (See Figure 4 below). Thus, initial results

suggest that the picture recognition memory task may provide sensitive and specific differences in brain organization subserving visuospatial short-term memory and may be a good predictor of post-surgical outcome after temporal lobectomy.

The sentence completion task appears provide a very reliable biomarker of language dominance in the brain. The typical activation map of healthy controls is shown in Figure 5 below, with clusters in the region of Broca's and Wernicke's areas. The 2 temporal lobe epilepsy patients studied to date showed divergent results during this task. The patient with left temporal lobe epilepsy showed additional recruitment of right hemisphere resources during this task (Figure 6 below) while the right temporal lobe epilepsy patient did not (data not shown). These differences may be extremely important in guiding neurosurgical treatment of temporal lobe epilepsy and predicting language outcome after surgery.

## Word Recognition: Correct responses - Baseline

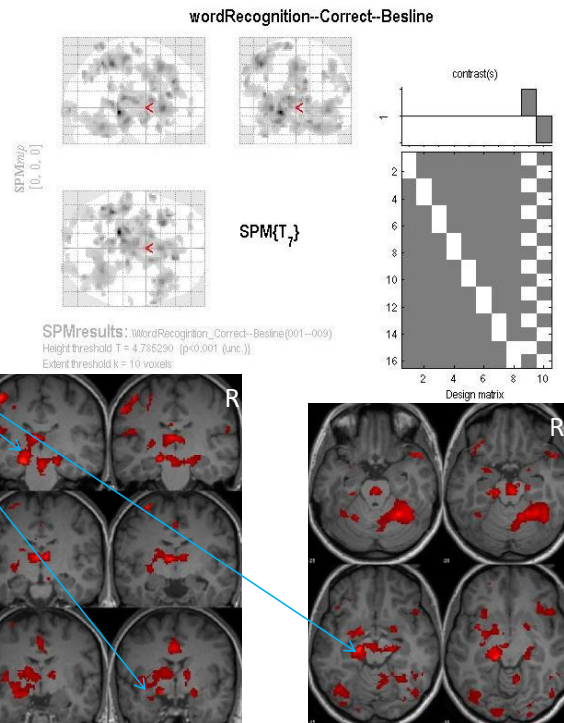
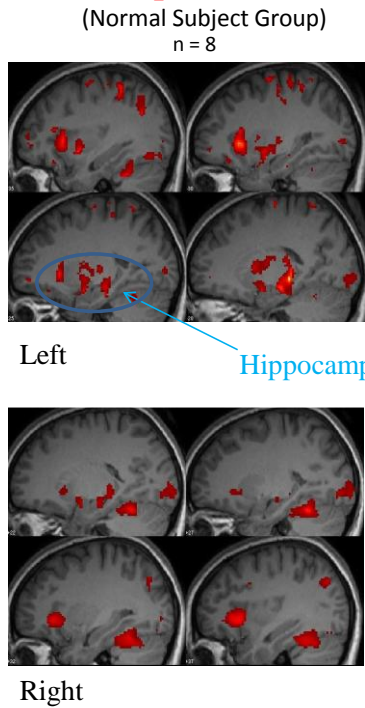
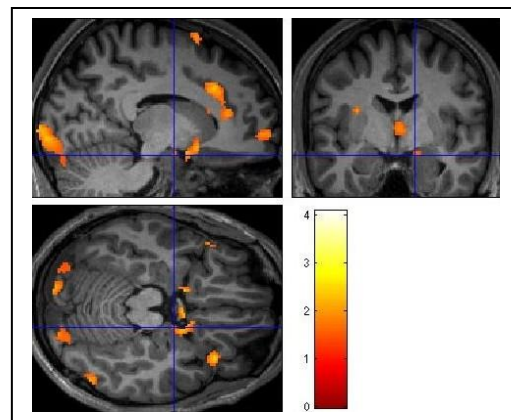


Figure 1. Activation maps of healthy control sample generated by word recognition memory task.

Figure 2. Activation map of a left temporal lobe epilepsy patient showing lack of left medial temporal activation during the word recognition task. Only a small cluster of activity was detected in the right medial temporal region.



## Picture Recognition Memory Correct Responses - Baseline

(Normal Subject Group)

n = 8

### Group analysis

- Paired t-test ( $p = 0.001$ )
- Compared Recognition Correct - Baseline
- Compared Recognition - Encoding
- Activation area: Para-hippocampus

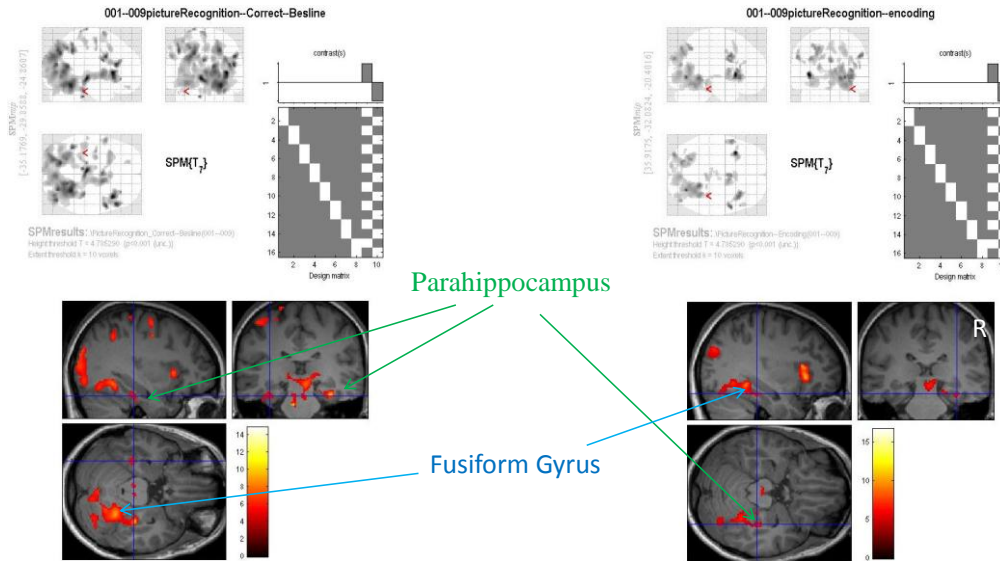
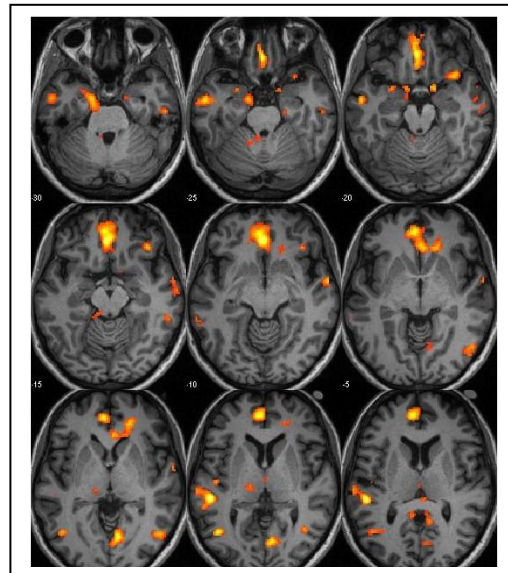


Figure 3. Activation maps of healthy control sample generated by picture recognition memory task, comparing activations under 2 different contrast conditions (i.e., correct recognition responses only and all recognition responses).

Figure 4. Activation map of a right temporal lobe epilepsy patient showing mainly left medial temporal lobe recruitment during the picture recognition memory task. This is the opposite pattern from what healthy controls show.



## Sentence Completion

(Normal Subject Group)  
n = 8

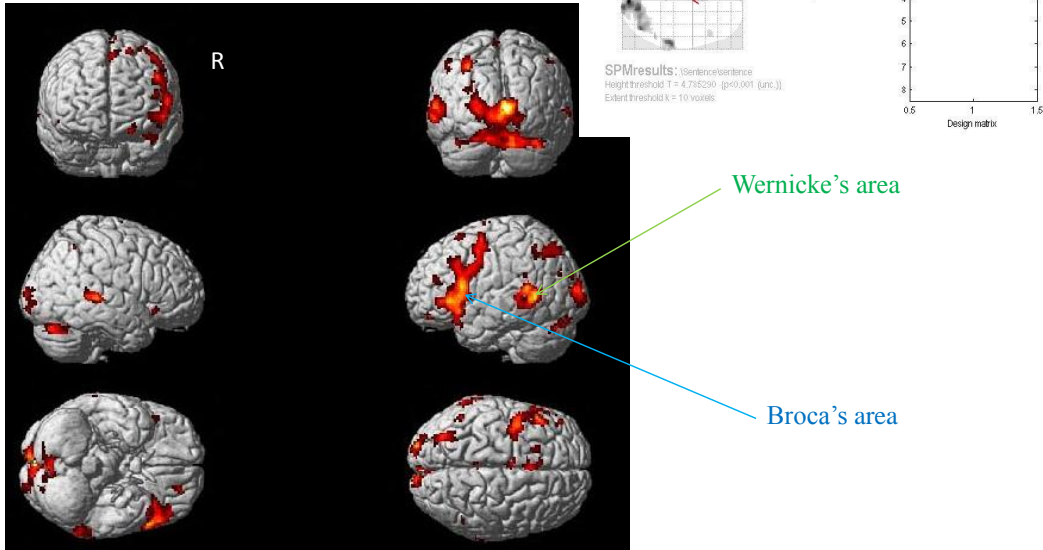
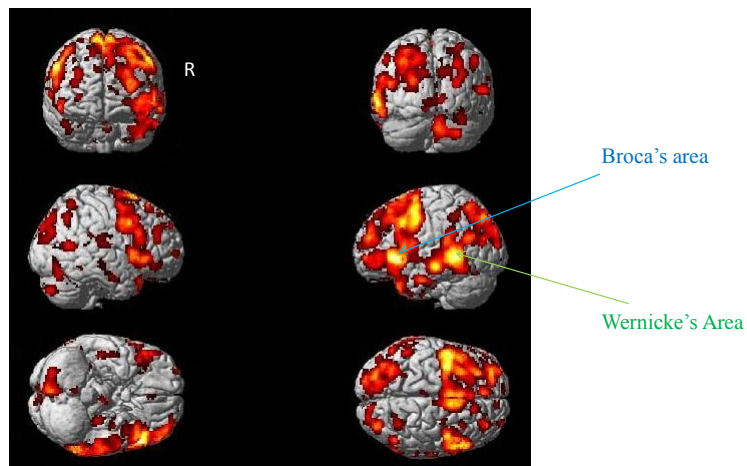


Figure 5. Brain activation map of healthy controls during the sentence completion task. Findings confirm highly asymmetric left hemisphere activity typically associated with dominant hemisphere mediation of language

## Patient 1

Sentence Completion

Figure 6. Activation map of left temporal lobe epilepsy patient during the sentence completion task showing bilateral recruitment of frontal-temporal regions, unlike the highly left asymmetric pattern of healthy controls seen above.



## **Research Project 5: Project Title and Purpose**

*Molecular Targets for Preventing Loss of Skeletal Muscle Mass* - The loss of skeletal muscle mass that occurs in a number of physiological and pathological conditions has adverse effects on functional strength and mobility, and in many conditions is associated with an increase in morbidity and mortality (e.g., aging, sepsis, cancer). In order to design appropriate therapeutic interventions to ameliorate skeletal muscle atrophy, the molecular mechanisms that regulate skeletal muscle size must be thoroughly understood. Significant strides have been made recently with regard to elucidating the pathways involved in the regulation of both protein synthesis and degradation in muscle, but many gaps still remain in our understanding of the complex processes regulating muscle growth in adults. The purpose of this project is to more fully characterize a molecular target identified as key in the regulation of protein synthesis.

### **Anticipated Duration of Project**

1/1/2009 – 12/31/2009

### **Project Overview**

Eukaryotic Initiation factor 2B (eIF2B), a key regulatory and rate-controlling factor in the initiation of mRNA translation, can affect global rates of protein synthesis and has been recently investigated in an experimental rat model of resistance exercise. Previous results from the Principal Investigator's laboratory indicate that the translational efficiency of the mRNA for the catalytic epsilon subunit of eIF2B (eIF2B $\epsilon$ ) is uniquely upregulated following resistance exercise in a rapamycin-sensitive manner. Cell culture experiments have further demonstrated that the mammalian target of the rapamycin complex 1 (mTORC1) signaling pathway is both necessary and sufficient for upregulation of eIF2B $\epsilon$ . The implication of mTORC1 signaling in the post-exercise signaling in muscle and the time course of increased protein synthesis seem to be consistent between rat and human models of exercise; however, changes in the expression of eIF2B subunits in response to resistance exercise in humans has not been previously reported. Furthermore, the contribution of the eIF2B $\epsilon$  expression to increased protein synthesis in muscle and the mechanism of its translational regulation are poorly understood. Considering the potential role of the upregulation of eIF2B $\epsilon$  in the increased rate of global protein synthesis observed in the rat model of resistance exercise, it is important to address these questions. This project seeks to examine the role eIF2B $\epsilon$  in skeletal muscle hypertrophy and its regulation in relation to mTORC1 signaling by employing human, animal, and cell culture models. The goal of the project is to establish that resistance exercise in humans results in increased expression of eIF2B $\epsilon$  in skeletal muscle, to elucidate the mechanism by which the increased expression occurs using molecular and cell biological techniques, and to demonstrate that increased expression of eIF2B $\epsilon$  alone *in vivo* can increase muscle protein synthesis and lead to hypertrophy. The central hypothesis of the project is that activation of the mTORC1 signaling pathway leads to a post-transcriptionally regulated increase in expression of eIF2B $\epsilon$  protein and that an increase in eIF2B $\epsilon$  expression alone is sufficient to increase muscle protein synthesis and skeletal muscle fiber size. The following Specific Aims are designed to characterize the role and regulation of eIF2B $\epsilon$  in skeletal muscle hypertrophy: (1) to validate that an acute resistance exercise bout results in increased eIF2B $\epsilon$  protein expression in human skeletal muscle; (2) to demonstrate that

*in vivo* modulation of eIF2B $\epsilon$  expression directly affects muscle protein synthesis and muscle fiber size; and (3) to validate the role of miR-133 in the translational repression of eIF2B $\epsilon$  mRNA.

### **Principal Investigator**

Leonard S. Jefferson, Jr., PhD  
Evan Pugh Professor and Chair  
Pennsylvania State University College of Medicine  
Department of Cellular & Molecular Physiology  
500 University Drive, MC H166  
P.O. Box 850  
Hershey, PA 17033-0850

### **Other Participating Researchers**

Alexander P. Tuckow, MS - employed by Pennsylvania State University College of Medicine

### **Expected Research Outcomes and Benefits**

The results from this project will advance our understanding of the mechanisms of skeletal muscle hypertrophy and identify a potential target for future physiological or pharmacological interventions aimed at potentiating skeletal muscle hypertrophy and/or ameliorating skeletal muscle wasting in a number of conditions and disease states by favoring net protein synthesis.

### **Summary of Research Completed**

One aim of the project was to examine the effect of overexpression of the catalytic epsilon subunit of eukaryotic initiation factor 2B (eIF2B $\epsilon$ ) on skeletal muscle protein synthesis. In this regard, we have optimized the technique of *in vivo* electro gene transfer delivering plasmid DNA to rat tibialis anterior muscles. We have demonstrated successful transfection of the majority of muscle fibers utilizing a plasmid expressing green fluorescent protein (GFP) and visualizing a transverse section of the muscle via fluorescence microscopy. Utilizing the same electro gene transfer technique, we have been able to achieve a consistent overexpression of eIF2B $\epsilon$  protein in the tibialis anterior muscle (~2-fold mean increase above endogenous expression in the contralateral tibialis anterior) 24 h post-transfection. An assay measuring the guanine nucleotide exchange activity of eIF2B revealed an ~23% increase in eIF2B activity in muscles overexpressing the eIF2B $\epsilon$  subunit compared to contralateral controls 24 h post-transfection, demonstrating functional significance. Rates of protein synthesis showed a trend toward an increase when eIF2B $\epsilon$  was overexpressed. With regard to knockdown of eIF2B $\epsilon$ , we have generated two new shRNA constructs that are being tested in a cell culture model to verify targeting of eIF2B $\epsilon$  prior to *in vivo* animal experiments.

Unexpectedly, longer-term experiments revealed difficulty in maintaining plasmid-based expression of eIF2B $\epsilon$  at 5-7 d post-transfection despite co-transfection with other plasmids (e.g., GFP) that continue to be expressed. Moreover, protein expression driven by other plasmids, such

as the ribosomal protein S6 kinase S6K1, was also maintained at 5-7 d post-transfection. The basis for the downregulation of eIF2B $\epsilon$  expression at later times after transfection is unknown, but it appears to be due to enhanced degradation of the protein (see later paragraph).

Following up on our experiments examining the overexpression of eIF2B $\epsilon$  *in vivo*, we utilized the electroporation technique to express the FLAG-eIF2B $\epsilon$  construct in the skeletal muscle of septic rats. Using a rat model of chronic sepsis in which both protein synthesis and eIF2B activity have been previously shown to be impaired, we expressed the catalytic epsilon subunit in one tibialis anterior muscle of control and septic rats and were able to demonstrate a rescue of eIF2B activity and protein synthesis in the muscle transfected with FLAG-eIF2B $\epsilon$  in spite of the septic condition. The data from the healthy and septic rat studies were published in the manuscript entitled “Ectopic expression of eIF2B $\epsilon$  in rat skeletal muscle rescues the sepsis-induced reduction in guanine nucleotide exchange activity and protein synthesis” (*Am J Physiol Endocrinol Metab* 299: E241–E248, 2010. First published May 18, 2010; doi:10.1152/ajpendo.00151.2010.)

**Abstract:** Eukaryotic initiation factor 2B (eIF2B) is a guanine nucleotide exchange factor (GEF) whose activity is both tightly regulated and rate-controlling with regard to global rates of protein synthesis. Skeletal muscle eIF2B activity and expression of its catalytic  $\epsilon$ -subunit (eIF2B $\epsilon$ ) have been implicated as potential contributors to the altered rates of protein synthesis in a number of physiological conditions and experimental models. The objective of this study was to directly examine the effects of exogenously expressed eIF2B $\epsilon$  *in vivo* on GEF activity and protein synthetic rates in rat skeletal muscle. A plasmid encoding FLAG-eIF2B $\epsilon$  was transfected into the tibialis anterior (TA) of one leg, while the contralateral TA received a control plasmid. Ectopic expression of eIF2B $\epsilon$  resulted in increased GEF activity in TA homogenates of healthy rats, demonstrating that the expressed protein was catalytically active. In an effort to restore a deficit in eIF2B activity, we utilized an established model of chronic sepsis in which skeletal muscle eIF2B activity is known to be impaired. Ectopic expression of eIF2B $\epsilon$  in the TA rescued the sepsis-induced deficit in GEF activity and muscle protein synthesis. The results demonstrate that modulation of eIF2B $\epsilon$  expression may be sufficient to correct deficits in skeletal muscle protein synthesis associated with sepsis and other muscle-wasting conditions.

Based on our observation of the very rapid loss of the exogenously expressed eIF2B $\epsilon$ , we have also pursued potential mechanisms of degradation of the protein. We have experimentally verified that the mRNA for the FLAG-eIF2B $\epsilon$  is still present in transfected muscles despite the absence of expression of the protein, indicating regulation at the level of translation or degradation. Following up on these results, we have obtained evidence that the eIF2B $\epsilon$  protein is ubiquitinated under certain conditions and we are further pursuing the regulation of this mechanism particularly with regard to its potential role in regulating eIF2B $\epsilon$  expression in muscle wasting conditions. We have recently submitted a manuscript examining the effect of the cholesterol lowering drug simvastatin on eIF2B subunit expression in C2C12 myoblasts (under review: *Am J Physiol Endocrinol Metab*). Treatment with simvastatin resulted in a proteasome-dependent decrease in the eIF2B subunits with concomitant reductions in protein synthesis and eIF2B activity.

Finally, we have generated plasmid constructs (cloned from human skeletal muscle) containing the 5'-untranslated region (UTR), the 3'-UTR, or both the 5'- and 3'-UTR of the eIF2B $\epsilon$  mRNA with a firefly luciferase coding region to investigate their potential role in the translational regulation of eIF2B $\epsilon$ . Several cell lines (HEK293, Rat2, C2C12) were transfected with the various eIF2B $\epsilon$ -luciferase fusion constructs to examine the effects of manipulating the mTOR pathway (e.g., serum and leucine deprivation followed by replenishment; treatment with rapamycin) on expression of the constructs. The luciferase activity of the eIF2B $\epsilon$  reporter constructs was not altered in the context of these experiments. Additionally, we investigated the role of several microRNAs predicted to target the 3'-UTR of eIF2B $\epsilon$  by utilizing the luciferase construct with co-transfected pre-miRNAs. Co-transfection of the microRNAs investigated did not dramatically affect luciferase reporter activity of the eIF2B $\epsilon$ -3'-UTR construct, nor did they affect expression of endogenous eIF2B $\epsilon$  protein as determined by Western blotting.

### **Research Infrastructure Project 6: Project Title and Purpose**

*Research Infrastructure - Biological Research Laboratory Construction* - The purpose of this project is to design and build an Animal Biosafety Level three (ABSL-3) research laboratory for the study of immunology and infectious diseases requiring high level Biocontainment. This project is a continuation of the project funded by the 2007-08 formula grant.

### **Anticipated Duration of Project**

1/1/2009 - 12/31/2011

### **Project Overview**

The scope of this project is to design and build an animal biosafety level three (ABSL-3) research laboratory for the study of immunology and infectious diseases requiring high level Biocontainment. Even with the knowledge and biotechnology now available, we still face serious threats to human and animal health and well-being from serious and highly transmissible infectious diseases and / or potential agents of bioterrorism such as avian influenza and anthrax. To respond, we must create a research environment and provide the infrastructure necessary to allow investigators to study these pathogens and discover new ways to detect, prevent or cure these diseases. The proposed Biological Research Laboratory will provide space, support, and biocontainment for basic, applied and diagnostic research; national, state and community outreach; and education on important human and animal pathogens. It will include state-of-the-art laboratories and animal resources, facilities and services that are recognized within and outside the University as being of the very highest quality consistent with our talents and resources. This facility will be composed of a number of ABSL-3 suites for *in vivo* research using small animal models of disease (primarily rodents and poultry). Each suite will have independent air locks to support multiple agent research as well as providing compartmentalization to mitigate cross-contamination concerns. Changing rooms and shower out facilities are included as required. Supporting the ABSL-3 suites will be BSL-3 laboratories for *in vitro* bacteriology, virology, and molecular biology procedures. Outside of the biocontainment area another support laboratory provides preparatory space for the activities within the barrier. The strategically located management office allows for oversight of the main

entry way as well as the loading dock. A conference/classroom/break room allows for on-site training sessions and staff meetings. This \$8,000,000 building project will encompass over 15,000 gross square foot, and will provide laboratories as well as animal holding space that will support the critical need for biocontainment research space at the Pennsylvania State University. This facility will be a unique and much needed resource for infectious disease research. In addition, support space (to house an IVIS imaging camera) and an adjacent biohazard animal holding room in Henning building will be renovated to support preliminary infectious disease studies. This imaging system has the flexibility to image fluorescent and/or bioluminescent reporters both in vivo and in vitro to facilitate non-invasive longitudinal monitoring of disease progression, cell trafficking and gene expression patterns in living animals.

### **Principal Investigator**

Mary J. Kennett, DVM, PhD, Diplomate ACLAM  
Director Animal Resource Program and Professor of Veterinary & Biomedical Sciences  
101 CBL  
The Pennsylvania State University  
University Park, PA 16802

### **Other Participating Researchers**

Biao He, PhD, Craig Cameron, PhD, Vivek Kapur, PhD – employed by Pennsylvania State University

### **Expected Research Outcomes and Benefits**

The proposed Biological Research Laboratory, an Animal Biosafety Level 3 (ABSL-3) facility, presents excellent opportunities for infectious disease research and will greatly enhance the research capabilities on campus. It is not possible to do research with highly infectious agents such as anthrax and avian influenza with out proper protection and biocontainment. This facility will provide special air handling capabilities to filter the exhausted air, liquid and solid waste decontamination, high security, and standard operating procedures within the facility to ensure the safe handling of such agents. The facility is organized into a central spine that connects all of the research spaces to the central decontamination and support areas of the project.

### **Summary of Research Completed**

This project is progressing well, has increased in scope, and is moving into final design. The project was temporarily put on hold while the Penn State design team put together an expanded design and grant proposal for the National Center for Research Resources (NCRR) Recovery Act Construction Program. The goal of the grant proposal was to expand the ABSL-3 facility to include an insectary, and additional laboratory and animal holding space. In addition the expanded facility will have increased redundancies to meet National Institutes of Health (NIH) construction guidelines. The proposal was successful and an award of \$14.8 million was received to expand the facility. In accordance with the guidelines of the award, a phase 1 archeological review was performed and an environmental assessment is in progress. In

addition, we have redesigned the facility to include additional features such as an insectary, a second BSL-3 laboratory and a second shower, as well as improved the redundancy of the building systems. The enhanced building project consists of a 20,000 GSF animal biosafety level three (ABSL-3) facility. The expanded facility will include microbiology and virology laboratories, cell sorting capabilities, animal biocontainment suites, and an insectary. This enhanced facility will support the study of emerging and zoonotic agents, vector borne diseases, the host pathogen interface, and vaccine development. As there is currently no ABSL-3 space on campus, the proposed building represents the fulfillment of a significant need for space to safely study highly infectious agents. Our immunology and infectious disease research program is growing rapidly, and to complement and enhance our current programs several new faculty members whose interests span the broad theme of pathogen evolution have been hired. In particular, we have recruited a new faculty member with ABSL-3 experience who will serve as the scientific director of the new facility. Two centers of excellence, the Center for Infectious Disease Dynamics and the Center for Molecular Immunology and Infectious Disease have formed around the core research groups in this area. Major thematic areas of research include the dynamic modeling of diseases, the evolution of viruses and bacteria in response to drugs and vaccines, the effects of climate change on pathogens, and the transmission dynamics of zoonotic infections.

We met with interested faculty groups to identify equipment needs, and designed the facility with respect to the identified and predicted need for each type of equipment and space with as much flexibility as possible within the constraints of BSL-3 design. The site for the building, near the current Animal Diagnostic Lab, was chosen as it is easily accessible from central campus and yet not near dense student populations. Now that the NIH proposal has been funded, we plan to submit a combined design document and schematic design document package to the NIH for their review prior to July 2, 2010.

The lack of BSL-3 facilities has prevented our faculty, from working with BSL-3 agents. Without a BSL-3 facility, we are also limited in our ability to hire new faculty with an interest in BSL-3 pathogens, or to train the next generation of scientists to work with these agents. Although some of our faculty members presently study BSL-3 level pathogens, much of their work is analyzing sequence data and dynamic modeling based on epidemiology. We need to be able to test the assumptions and hypotheses relating to these pathogens in *in vitro* experiments or in animal models to validate our theoretical models, and we are simply unable to do so without the proposed facility.

The ABSL-3 facility named the Biological Research Laboratory (BRL) will include state-of-the-art laboratories, animal housing and procedure room suites, and a BSL-3 insectary. Specifically, the building will contain two single ABSL-3 animal holding room (AHR)/procedure room suites (an animal holding room with an associated procedure room and ante-room), and two double AHR suites (two AHRs separated by a procedure room and ante-room/air-lock). One of the double AHR suites will have enhanced (ABSL-3E) filtration and air handling capacity and will be designed to hold poultry isolators for avian influenza studies. The other AHR suites will hold up to three biocontainment rodent racks per animal holding room. The building will also contain two BSL-3 laboratories for *in vitro* microbiology and virology studies, as well as two smaller labs for flow cytometry, and PCR. A small insectary will also be housed within the containment

space for work with vector-borne agents. Completing the containment space are a feed and bedding storage space, a gas/decontamination chamber, an autoclave, and shower out facilities. The new containment zones are illustrated in Figure 1. Outside of containment, there will be a preparatory/support laboratory, a conference/ training/ break room, the manager's office, the loading dock with secure waste and cylinder storage, as well as the main entrance and restroom facilities. The research space will be located on the ground floor with the HVAC and mechanical, electrical and plumbing (MEP) systems, including a liquid effluent decontamination system, on the floors above and below. An artist's rendering of the BRL is shown in Figure 2.

The building will be designed to meet construction and redundancy standards as described in the NIH Design Policy and Guidelines for ABSL-3 and ABSL-3 enhanced research space for high pathogenicity infections (such as avian influenza). The building will feature numerous security features including a perimeter fence, card or proximity reader access, biometric security to access the containment zone, as well as motion detectors, lights and security cameras. Several levels of security will be in place, only limited access to the facility will be allowed, and all entries will be documented. Training and security clearances will be required prior to entry according to a biosafety manual specific to the BRL. Standard Operating Procedures (SOPs) will be developed specifically for the BRL to train and certify all personnel working within containment, to ensure safety and security according to Occupational Health and Safety guidelines. Specific policies will be developed for practices such as showering, minimal sharps use, and decontamination. Procedures will be in place to minimize the production of aerosols, and all animal specific regulations and biosafety procedures will be followed. Biohazardous materials use authorization (Recombinant DNA or Human Pathogen registration, Select Agent use, etc.) will be instituted as appropriate.

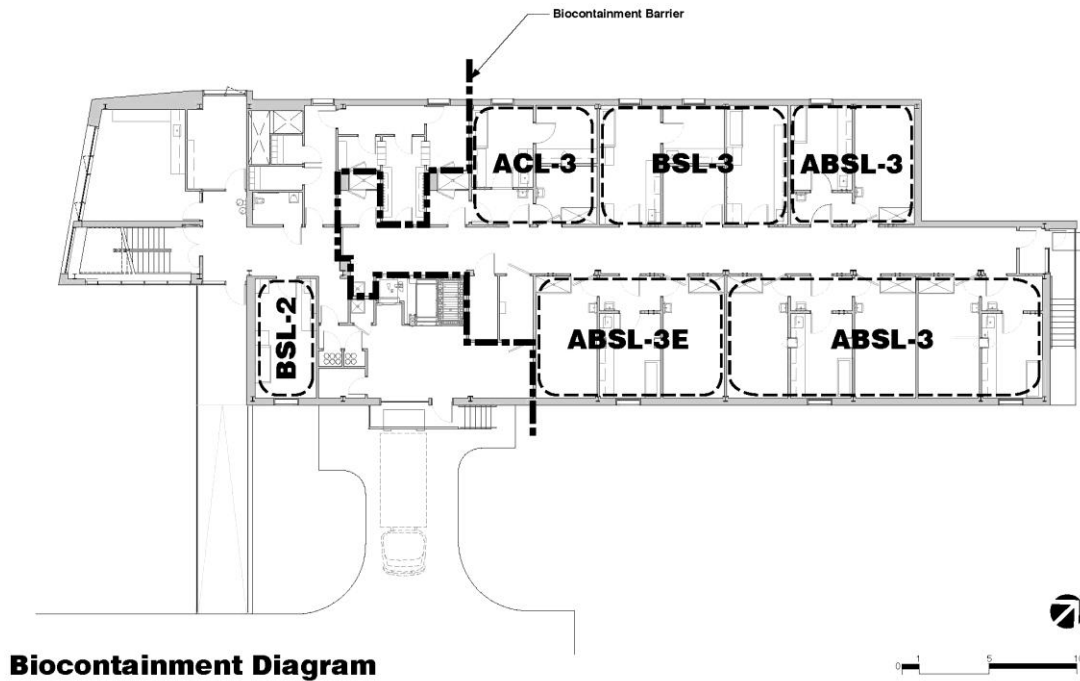


**Figure 1.** Containment zones for the ABSL-3 facility include the insectary (arthropod containment level-3 (ACL-3), Biosafety Level 2 and 3 (BSL-2 and BSL-3) laboratory space, and Animal biosafety level-3 (ABSL-3) and enhanced ABSL-3 (ABSL-3E) space.



**Figure 2.** An artist's rendering of the BRL, showing the main personnel entrance and loading dock.

## **Research Project 7: Project Title and Purpose**

*Regulation of Nutrient Sensing and Muscle Wasting by Alcohol* - Metabolic balance is maintained at the cellular and whole-body level by responding to signals from the environment and from inside the body, namely growth factors, hormones, and stress signals. Chronic consumption and acute ingestion of alcohol reduces the muscle mass of those abusing this drug by changing the body's ability to respond to some of these signals. The purpose of the project is to elucidate how alcohol decreases the ability of the amino acid leucine to increase the synthesis of muscle proteins. If we can determine this mechanism, therapeutic interventions can potentially be developed which prevent the loss of muscle under this condition and as a result of other stress conditions, such as immobilization, trauma, infection, which have similar effects on muscle protein balance.

### **Duration of Project**

1/1/2009 – 6/30/2010

### **Project Overview**

The long-term goal of the project is to determine the mechanism by which alcohol impairs cap-dependent translation and protein synthesis in skeletal muscle under basal conditions and in response to the anabolic agent leucine. This goal will be achieved by three specific experiments. Experiment 1 will determine the role of altered 4E-BP1 and S6K1 interaction with the scaffold protein raptor as a mechanism for the alcohol-induced decrease in mTOR activity in muscle. The endogenous prevailing level of the mTOR-raptor complex will be isolated from whole muscle or cultured myocytes after alcohol treatment  $\pm$  leucine by immunoprecipitation of raptor, and then the IP blotted for mTOR, raptor, G $\beta$ L, and 4E-BP1. The amount of total and phosphorylated 4E-BP1 bound to raptor will be assessed by Western blot analysis. mTOR kinase activity will be determined and correlated with in vivo-determined rates of protein synthesis in the same muscle. The following endpoints will be determined: a) protein synthesis, b) mRNA translation rate, c) mTOR kinase activity, d) phosphorylation of 4E-BP1, S6K1 and mTOR, and e) protein-protein interactions related to TORC1 formation. Experiment 2 will elucidate the mechanism by which alcohol impairs binding activity of the eIF3 scaffolding complex. Muscle from each treatment group will be homogenized and eIF3 immunoprecipitated. Western blotting will be performed on the IP for total and phosphorylated mTOR, S6K1, eIF4B and eIF4G. We will also examine the temporal correlation between mTOR and S6K1 activation and the binding or dissociation of preinitiation complex components with eIF3 and the 5' cap following stimulation with leucine. In Experiment 3 we will determine whether an alcohol-induced alteration in the binding of PDCD4 to eIF4A impairs eIF4A helicase activity and thereby inhibits translation in skeletal muscle. Hence, PDCD4 will be immunoprecipitated and blotted for PDCD4, eIF4A, and eIF4G. Furthermore, PDCD4 is also a phosphoprotein and a downstream substrate of S6K1. Activation of the mTOR pathway enhances S6K1 kinase activity leading to phosphorylation of PDCD4. As a consequence of this phosphorylation event, PDCD4 is rapidly degraded by the E3 ubiquitin (Ub) ligase complex SCF <sup>$\beta$ TRCP</sup> (SKP1-CUL1-F-box) which tags its substrates with Ub molecules for proteasome degradation. Finally, using immunoprecipitated PDCD4, we will also Western blot for SCF <sup>$\beta$ TRCP</sup> which is the endogenous

E3 ligase for PDCD4. Collectively, these studies will help provide information related to the molecular mechanism by which alcohol impairs muscle protein synthesis.

### **Principal Investigator**

Charles H. Lang, PhD  
Distinguished Professor  
Penn State College of Medicine  
Cellular & Molecular Physiology (H166)  
500 University Drive  
Hershey, PA 17033

### **Other Participating Researchers**

None

### **Expected Research Outcomes and Benefits**

The ability of the body to control protein synthesis in muscle is important for the maintenance of muscle mass. Various stress states, such as alcohol, infection, trauma and disuse, decrease muscle mass by inhibiting muscle protein synthesis. In turn, protein synthesis is a complicated metabolic process which is controlled by various proteins and factors. Each of the proposed projects addresses whether alcohol interferes with these specific steps under basal conditions or in response to the nutrient leucine. By examining each of these three specific regulatory steps we should be able to determine how to circumvent the alcohol-induced defect.

### **Summary of Research Completed**

*Effect of PRAS40 knockdown in C2C12 myotubes.* C2C12 stable cell lines deficient in PRAS40 or scramble controls were created using short hairpin RNA (shRNA). shRNA were retrovirally delivered to myoblasts and some of these myoblasts were allowed to differentiate and form myotubes following puromycin selection. shRNA directed towards PRAS40 in myotubes reduced PRAS40 protein levels by greater than 80%, compared to scramble control values. As anticipated, PRAS40 knockdown also reduced the PRAS40 mRNA content by ~65% in infected myotubes. In contrast, PRAS40 knockdown did not alter the mRNA content for 4E-BP1, mTOR, S6K1 or raptor, proteins central to the functioning of the mTOR signaling pathway. Knockdown of PRAS40 in differentiated myotubes did not alter global protein synthesis compared with scramble controls as measured by <sup>35</sup>S-methionine incorporation into protein. To determine whether the responsiveness of the PRAS40 knockdown cells to external stimuli was altered, cells were incubated with either an anabolic (IGF-I) or catabolic (AICAR) agent. Addition of IGF-I to the myotubes increased protein synthesis, whereas, AICAR inhibited protein synthesis. Contrary to expectations, the magnitude of the changes produced by these agents in myotubes was the same in both control and PRAS40 knockdown cells. To confirm protein synthesis data, we performed Western blotting for mTOR and its substrates and binding partners. PRAS40 knockdown cells remained responsive to both types of stimuli and their response was similar and comparable to the scramble controls. For example, IGF-I increased

phosphorylation of S6K1 (T389) and PRAS40 (T246), while AICAR increased raptor phosphorylation (S792).

*PRAS40 knockdown decreases protein synthesis in C2C12 myoblasts.* While the preceding data were obtained from post-mitotic differentiated myotubes (>95%), we also determined whether myoblasts would yield comparable results. In myoblasts, the knockdown of PRAS40 decreased global protein synthesis by ~25% under basal conditions. Despite the decrease in basal protein synthesis in the PRAS40 knockdown cells, the ability of these cells to respond positively or negatively to IGF-I or AICAR, respectively, was unaltered. Contrary to expectations, the decreased protein synthesis observed in PRAS40 knockdown cells under basal conditions was not associated with any difference in the phosphorylation state of the mTOR substrates S6K1 and 4E-BP1, compared to the scramble control values or changes in protein-protein interaction of PRAS40-raptor-eIF3 between the two groups. In myoblasts, the ability of IGF-I to stimulate T389 phosphorylation of S6K1 and AICAR to increase S792 phosphorylation of raptor did not differ between scrambled and PRAS40 knockdown cells.

*PRAS40 knockdown alters myoblast cell size and proliferation.* Vander Haar et al reported that overexpression of wildtype PRAS40 decreased cell size in HEK 293 cells, whereas, knockdown of Lobe (a PRAS40 ortholog in *Drosophila*) increased cell size. Hence, we hypothesized that knocking down PRAS40 would also increase cell size in myocytes. PRAS40 knockdown increased the diameter ( $16.8 \pm 0.1 \mu\text{m}$ ) of low passage proliferating (~60% confluent) myoblasts compared to scramble control cells ( $14.0 \pm 0.1 \mu\text{m}$ ) as measured using either the Coulter counter particle size analyzer or FACS flow cytometry analysis (data not shown). Mean cell volume was also increased in PRAS40 knockdown cells. However, unexpectedly we found that PRAS40 knockdown cells grew slower compared to time-matched scramble controls, although both cell types were seeded at the same initial density. To exclude anchorage-dependence and altered capacity to attach, cells were seeded and counted 4-8 h after seeding to allow for attachment. An equal number of cells were harvested following trypsinization in both the control and PRAS40 knockdown cells, suggesting no significant difference in the ability of PRAS40 knockdown cells to attach to the culture plates (data not shown). To confirm that the proliferation rate of PRAS40 knockdown cells was slower, we used an independent colorimetric assay based on the conversion of the MTT tetrazolium salt to its formazan product. Consistent with the above presented data, the MTT assay revealed that PRAS40 knockdown cells had a 25% lower rate of proliferation.

*PRAS40 and apoptosis.* To determine whether increased apoptosis in PRAS40 knockdown cells was responsible for the slower proliferation rate, we isolated low molecular weight DNA and performed an apoptosis DNA laddering assay. There is no difference between the scramble control and the PRAS40 knockdown cells and that neither group of cells were undergoing active apoptosis within the detectable limits of the assay. These findings were confirmed by Western blotting for caspase-3/ PARP cleavage which failed to detect a significant difference between the groups. Myoblasts incubated with staurosporine were used as a positive control and demonstrated increased caspase-3 and PARP cleavage. Collectively, these data suggest that the decreased protein synthesis and reduced proliferation in PRAS40 knockdown myoblasts cannot be attributed to increased apoptosis.

PRAS40 knockdown inhibits cell cycle progression. To determine the mechanism for the lower proliferation rate in PRAS40 knockdown cells, we stained myoblasts with propidium iodide to study cell cycle events. PRAS40 knockdown myoblasts had a greater proportion of cells in G1/G0 of the cell cycle and fewer cells in active S – phase, compared to control values. Because PRAS40 knockdown cells were arrested in G1/G0 of the cell cycle we assessed whether proteins regulating cell cycle, especially the G1 – S transition, were concomitantly altered. There was a 25-30% reduction in S807/811 phosphorylation of Rb, consistent with reduced progression from G1 to S phase. In myoblasts with PRAS40 knockdown a 20-30% reduced expression of p21 was also detected in these cells. There was no difference in the other proteins analyzed which regulate cell cycle - p53, cdk 4/6, p27 and cyclin D1. PRAS40 alters myogenesis. Our data demonstrate the presence of a concomitant delay in proliferation and altered cell cycle in PRAS40 knockdown myoblasts. Since mTOR also regulates autophagy which in turn plays an important role in cell differentiation, we determined the expression of proteins important in regulating autophagy. While there were no changes in the early markers for autophagy including, Atg 7 and Beclin 1, our data indicate that PRAS40KD decreases the ratio of LC3B-II/LC3B-I.

Next we determined whether such changes might be of physiological relevance to skeletal muscle development. In this regard, we seeded the same number of myoblasts and tracked their progression to form myotubes. We observed that control cells reached confluent status earlier than the PRAS40 knockdown and began fusion to form substantial number of myotubes by day 5, whereas PRAS40 knockdown cells only sparsely formed myotubes by day 5. These data suggest that myotube formation and myogenesis is delayed in PRAS40 knockdown cells. To quantitate these findings, cell lysates were collected at various stages of development of myoblasts and myotubes to measure the expression of myosin heavy chain (MHC) – a protein expressed only in differentiated matured myotubes. While MHC expression was absent in myoblasts (day 3) and there was an initial delay in MHC expression in PRAS40 knockdown cells (days 5 and 7), by day 9 the expression of MHC in both scramble control and PRAS40 knockdown cells were comparable. There were no differences between scramble control and PRAS40KD in their expression of the muscle transcription factor MyoD.

### Summary

PRAS40 is an mTOR binding protein which has complex effects on cell metabolism. Our study tests the hypothesis that PRAS40 knockdown (KD) in C2C12 myocytes will increase protein synthesis via up-regulation of mTOR-S6K1 pathway. PRAS40 KD was achieved using lentiviruses to deliver shRNA targeting PRAS40 or a scrambled control. C2C12 cells were used as either myoblasts or differentiated to myotubes. Knockdown reduced PRAS40 mRNA and protein content by greater than 80% of time-matched control values but did not alter the phosphorylation of mTOR substrates, 4E-BP1 or S6K1, in either myoblasts or myotubes. No change in protein synthesis in *myotubes* was detected as measured by the incorporation of <sup>35</sup>S-methionine. In contrast, protein synthesis was reduced 25% in *myoblasts*. PRAS40 KD in myoblasts also decreased proliferation rate with an increased percent of cells retained in G1 phase. PRAS40 KD myoblasts were larger in diameter and had a decreased rate of myotube formation as assessed by myosin heavy chain content. Immunoblotting revealed a 25-30% decrease in total p21 and S807/811 phosphorylated Rb protein considered critical for G1 – S phase progression. Reduction in protein synthesis was not due to increased apoptosis as cleaved

caspase-3 and DNA laddering did not differ between groups. In contrast, the protein content of LC3B-II was decreased by about 30% in the PRAS40 KD myoblasts, suggesting a decreased rate of autophagy. Our results suggest that a reduction in PRAS40 specifically impairs myoblast protein synthesis, cell cycle, proliferation, and differentiation to myotubes.

### **Research Project 8: Project Title and Purpose**

*Murine Induced Pluripotent Stem Cells: Differentiation and Bone Formation* - The goals of the project are to assess the potential of stem like cells called induced pluripotent stem cells (iPS) to differentiate toward mesenchymal stem cells (MSCs) and to make bone and cartilage *in vivo*, thus to understand the future application of the cells for the repair and regeneration of musculoskeletal tissues.

### **Duration of Project**

1/1/2009 – 6/30/2010

### **Project Overview**

With aging, the yields of adult derived stem cells decrease and some studies have shown that the cells may exhibit reduced proliferation and differentiation potential. Embryonic stem cells (ESC) derived from the inner cell mass of the blastocyst can give rise to any cell type of the body and can be expanded indefinitely without losing their pluripotency, thus these cells are better suited for regenerative medicine. Because of ethical concerns however, little progress has been made in harnessing the power of these cells. Recently, it has been demonstrated that mouse and human fibroblasts can be reprogrammed into an ESC-like state by introducing combinations of four transcription factors Oct-3/4, Sox2, c-Myc and Klf4. The therapeutic potential of such induced pluripotent stem (iPS) cells remains undefined. In the present exploratory project, we propose to generate mouse specific iPS and to assess them for mesenchymal stem cell differentiation (MSCs) and for bone and cartilage formation *in vivo*. The central hypothesis of the project is that iPS cells can be directed to MSC differentiation and will give rise to osteoblasts, chondrocytes and adipocytes and will make bone *in vivo*. To test this hypothesis, we will pursue the following aims; aim 1, we will generate and characterize mouse iPS from tail tip fibroblasts and in aim 2 we will test the hypothesis that iPS cells can be differentiated into MSCs and the cells will form bone and cartilage *in vivo*. To accomplish these aims we will construct retroviruses containing the four defined factors (Oct-3/4, Sox2, c-Myc and Klf4); these factors will be transfected into tail tip fibroblasts harvested from the 4-day old mice. The transduced cells will be cultured following ESC protocols and will then be assessed for ESC like state. In aim 2, the iPS cells will be assessed for MSC differentiation and will then be evaluated for osteoblast and chondrocyte differentiation *in vitro* and for bone and cartilage formation *in vivo* when the cells are incorporated in scaffolds and implanted into the mice from which the reprogrammed fibroblasts were harvested. The results from the project will provide important information regarding the future application of ESC like stem cells generated from reprogrammed fibroblasts for musculoskeletal tissue repair and regeneration.

## **Principal Investigator**

Christopher Niyibizi, PhD  
Associate Professor  
Penn State University  
Department of Orthopaedics and Rehabilitation  
H089  
500 University Drive  
Hershey PA 17033

## **Other Participating Researchers**

Sarah Bronson, PhD, Feng Li, PhD - employed by Pennsylvania State University

## **Expected Research Outcomes and Benefits**

We expect that we will generate mouse stem like cells (iPS) from tail tip fibroblasts as we have demonstrated in the preliminary studies. The cells will make teratomas in vivo containing tissues derived from the three germ layers thus confirming that we are able to generate iPS that exhibit characteristics with the mouse embryonic stem cells (mESC). The rationale for reprogramming fibroblasts harvested from the tail tips of the 4-day old mice is that we plan to maintain the mice in which the fibroblasts come from to later use the mice as cell recipients to assess bone and cartilage formation in vivo. The mice will receive their own cells and thus avoid cell rejection and offer an opportunity to study stem cell function in vivo. Preliminary data also demonstrate that we are able to generate cells from iPS that exhibit mesenchymal stem cell (MSCs) characteristics in terms of surface antigen expression. The cells will be sorted based on a combination of various surface antigens, and we will generate several subpopulations that will be assessed for bone and cartilage formation initially in vitro. Using this approach we should be able to generate iPS directed MSCs that will be evaluated for bone and cartilage formation in vivo. Comparison of iPS directed MSCs and embryoid bodies (EBs) should inform as to whether generation of MSCs is necessary for bone and cartilage formation or EBs will make bone and cartilage efficiently as well as iPS directed MSCs. We however anticipate that iPS directed MSCs would make bone or cartilage exclusively while iPS directed EBs would generate heterogeneous tissues that would include bone and cartilage. We expect to therefore generate MSCs like cells from iPS. The iPS directed MSCs will make bone and cartilage in vitro and perhaps in vivo. The results from the project will provide important information regarding the future application of ESC like stem cells generated from reprogrammed fibroblasts for musculoskeletal tissue repair and regeneration.

## **Summary of Research Completed**

*Aim 1: Generation of induced pluripotent stem cells from murine tail tip fibroblasts:* Fibroblasts were harvested from the tails of 4-day old mice and propagated in culture. The cells were treated with a retrovirus carrying each of the reprogramming factors (Oct4, Sox2, c-Myc and KLF4) using established protocols. Transduced fibroblasts were maintained in culture and the cells reprogrammed into ESC-like state were picked at 16 days and propagated in culture on murine

fibroblasts feeder layers. The clones were propagated in culture using established protocols. Figure 1 below shows a schematic diagram leading to the establishment of the induced pluripotent stem cells.

Results: We succeeded in generating iPSC and the cells were demonstrated to exhibit embryonic like characteristics (ESC) by their ability to give rise to the three germ layers as assessed by teratoma formation (Mesoderm, Ectoderm and endoderm) (Fig. 2). We were therefore successful in accomplishing studies proposed in aim 1.

*Aim 2: Induced pluripotent stem cells (iPSC) can be differentiated into mesenchymal stem cells (MSCs) lineage and form bone in vitro and in vivo.*

The major focus of the project was to demonstrate that iPSC will differentiate into cells that exhibit mesenchymal like characteristics. Established iPSCs were treated with differentiating factors; retinoic acid and transforming growth factor beta 1 (TGF- $\beta$ 1). The results showed that iPSCs treated with this combination of factors gave rise to cells exhibiting mesenchymal stem like cells (MSCs) found in bone marrow and other mesenchymal tissues. The resulting cells were shown to differentiate into osteoblasts in vitro and deposited mineral in vitro, a characteristic of osteoblasts (Fig. 3). The results suggested that cells reprogrammed from adult cells (somatic cells) behave like embryonic like stem cells and can be directed for differentiation toward cells of mesenchymal lineage. *These data were published in a recent manuscript that appeared in the Journal of Cellular Biochemistry (Li F, Bronson Sarah and Niyibizi Christopher, J Cell Biochem, March 2010). The published findings were highlighted in this journal as significant findings.*

We had also proposed to direct iPSC derived MSCs into cartilage cells. We were not successful in directing the cells to cartilage formation.

In summary, we demonstrated that mouse cells can be converted into embryonic like stem cells by reprogramming somatic cells with defined factors ( Oct 4, Sox2, cMy-c and KLF4); these data agree with published reports by other investigators. The novel findings of our studies are however that embryonic like stem cells can be directed for differentiation toward mesenchymal stem cell lineages and that transforming growth factor 1 (TGF- $\beta$ 1) may play a role in this process. The attractive feature of these cells is that patient specific embryonic like stem cells can be generated for transplantation and drug screening. Production of these cells bypasses ethical concerns associated with human embryonic stem cells. The following selected figures illustrate work completed.

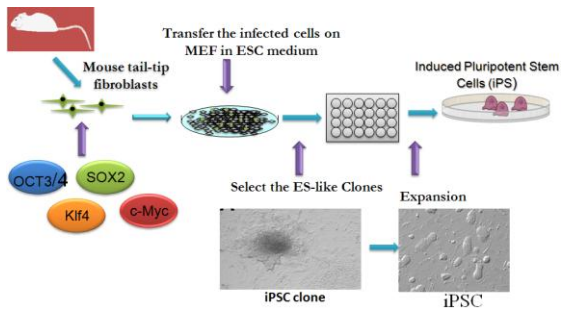
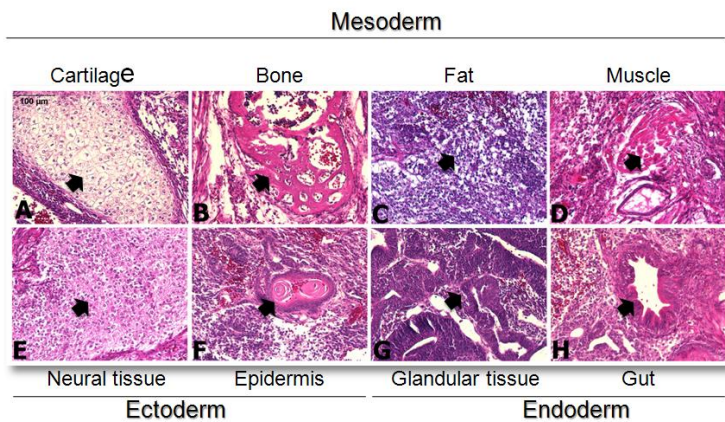


**Fig. 1. Schematic diagram illustrating generation of iPSC from mouse tail tip fibroblasts.** Mouse tail tip fibroblasts were treated with a virus that contained each of the reprogramming factors shown; resulting cells that were converted into ESC like state were peaked and propagated in culture (adopted from Li et al. J. Cell Biochem. 2010).



Bar: 100μm

**Fig. 2. Teratoma formation by the iPSC generated from the murine tail tip fibroblasts.** The xenografts of mouse iPSC generated well-differentiated teratoma-like masses containing all three embryonic germ layers. Immunodeficient mouse recipients were injected with mouse iPSC intramuscularly. Resulting teratomas demonstrated the features characteristic of ectoderm, mesoderm, and endoderm (Adopted from Li et al J. Cell Biochem. 2010).

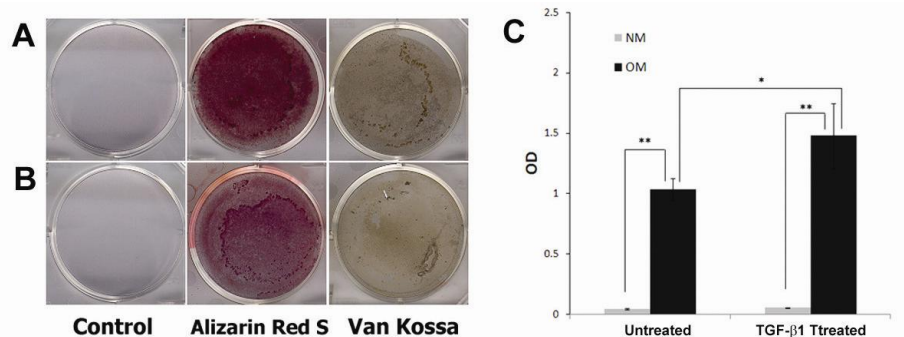


**Fig. 3. Osteoblastic differentiation of MSCs-like cells generated from iPSC with or without TGF-β1 treatment.** A: MSC-like cells derived by treatment of iPSC-directed EBs (embryoid bodies) with TGF-β1, cultured in the presence or absence of osteogenic factors and stained with Alizarin red at 28 days. B: MSC-like cells derived from iPSC-directed EBs without TGF-β1 but exposed to retinoic acid treatment, cultured in the presence or absence of osteogenic factors and stained with Alizarin red at 28 days. C: Relative amount of calcium deposited by cells derived by treatment of iPSC with or without TGF-β1. MSCs-like cells derived by TGF-β1 treatment showed higher mineral deposition than non-TGF-β1- derived MSCs following culture in osteogenic medium (OM). Alizarin red deposits shown in (A) and (B) were extracted and their absorbance was determined. The absorbance levels represent calcium deposits. (Adopted from Li et al. J. Cell Biochem. 2010).

### **Research Project 9: Project Title and Purpose**

*Evaluation of mTOR as a Chemoprevention Target in Skin Cancer* - The object of these studies is to validate the mammalian target of rapamycin (mTOR) as a target for chemoprevention of non-melanoma skin cancer. Since skin cancers are the most common form of malignancies, with increasing numbers world-wide, identification of possible targets for their prevention are particularly relevant to public health.

### **Anticipated Duration of Project**

1/1/2009 – 12/31/2009

### **Project Overview**

The overall goal of these experiments is to validate mTOR as a potential target for chemoprevention of nonmelanoma skin cancer (NMSC). This project is intended to complement experiments described in an R03 application that was funded by the National Cancer Institute (NCI). The specific aims of the funded grant are: 1) to generate and characterize mice with a targeted deletion of mTOR in the skin (K14CreER<sup>T</sup>/mTOR<sup>lox/lox</sup> mice), and 2) to use these mice in DMBA/TPA skin carcinogenesis experiments. The reviewers of the funded R03 recommended that we perform additional experiments using UVB exposure rather than chemical carcinogenesis. Inducing skin tumors by UVB exposure mimics more accurately sun exposure, which is the primary cause of human NMSC. The reviewers also recommended that we use wild-

type mice treated topically with the mTOR inhibitor rapamycin in our experiments. Knocking out mTOR in the skin using the Cre/lox approach would affect the activities of both the mTORC1 and mTORC2 complexes, while rapamycin treatment inhibits primarily mTORC1. Thus, this experiment would help determine which TOR complex is the better target for chemoprevention. The combination of these experiments will provide a stronger set of preliminary results for a future NIH application.

### **Principal Investigator**

Lisa M. Shantz, PhD  
Associate Professor  
Penn State College of Medicine  
500 University Drive  
Hershey, PA 17033

### **Other Participating Researchers**

Shannon L. Nowotarski - employed by Penn State College of Medicine

### **Expected Research Outcomes and Benefits**

The central idea of the project is that the mammalian target of rapamycin (mTOR) is an important target for chemoprevention of non-melanoma skin carcinogenesis. mTOR responds to changes in cellular nutrients by controlling the synthesis of proteins essential for multiple processes, including cell proliferation and organization of the cell cytoskeletal. A large number of cancer-promoting mutations are known to result in mTOR activation. A role for mTOR-controlled pathways in skin carcinogenesis has been suggested in recent clinical trials, which have shown that renal transplant patients administered the specific mTOR inhibitor rapamycin as an immune suppressant suffer from significantly fewer non-melanoma skin cancers compared to patients taking calcineurin inhibitors. Our studies, in combination with these promising clinical trials, will provide a strong rationale for continued development of rapamycin analogues as chemopreventive agents.

### **Summary of Research Completed**

*Rapamycin sensitizes keratinocytes to UVB-induced apoptosis and attenuates UVB-mediated hyperproliferation.* Studies were performed using Rapamycin to determine if inhibition of mTORC1 alters the epidermal response to UVB. Studies have shown that UVB stimulates phosphorylation of mTOR, 4EBP1, S6K1, and AKT(Ser473) in keratinocyte cell lines and primary keratinocytes. We performed these experiments to determine if Rapamycin treatment sensitizes keratinocytes to UVB-induced apoptosis and inhibits UVB-stimulated hyperplasia *in vivo*. FVB/N mice were used at 7-9 weeks of age, during the resting phase of the hair cycle (telogen). The dorsal surface of the mice was shaved and treated with 100 nmol Rapamycin 1 h prior to exposure to 120 mJ/cm<sup>2</sup> UVB using FS20 UVB bulbs (National Biologic). 24 and 48 h after exposure skin sections were fixed, paraffin embedded, and sections stained with hematoxylin-eosin (H-E). The number of apoptotic epidermal keratinocytes was quantified by

counting the number of sunburn cells (SBC) /hpf (high power field) in 5 non-overlapping fields (3 mice for each condition). SBCs are apoptotic cells, characterized by condensed nuclei and eosinophilic cytoplasm. There was a significant increase in SBC in Rapamycin treated UVB-exposed skin sections (Fig 1), indicating that inhibition of mTORC1 sensitizes keratinocytes to UVB-induced apoptosis.

We also examined the effect of Rapamycin on UVB-induced hyperproliferation and hyperplasia. Proliferation was measured directly by injecting mice with BrdU (100 µg/g) 1 h prior to harvesting tissues and performing immunohistochemical (IHC) staining using an antibody specific for BrdU (Fig 2A). The Proliferation Index (percentage of BrdU positive cells per 1000 basal cells) from 4 different skin sections was averaged per mouse (3 mice per condition). In control mice, UVB induces a 5-fold increase in proliferation at 48 h (Fig 2B), and rapamycin significantly attenuated this effect. The epidermal thickness was also measured at 4 different locations and averaged for each mouse (3 mice for each condition). UVB caused a significant increase in epidermal thickness in control mice, but this effect was blocked by Rapamycin (Fig 2C). These studies indicate that mTORC1 is a critical regulator of UVB-induced cell survival and proliferation, suggesting that depletion of mTORC1 activity will be protective in skin carcinogenesis protocols by inhibiting the survival of DNA-damaged cells and reducing the clonal expansion of initiated cells.

*Inducible Deletion of mTOR in the epidermis.* Because homozygous deletion of mTOR is lethal *in utero*, we used an inducible Cre-LoxP mouse model to ablate mTOR in the epidermis. Mice containing a floxed mTOR allele were crossed with the K5CreER<sup>T2</sup> mice that express Cre fused to the estrogen receptor driven by the cytokeratin 5 (K5) promoter. Application of 4-hydroxytamoxifen (4OHT) triggers nuclear translocation of Cre and deletion of genomic fragments flanked by two LoxP sites. The K5 promoter drives expression of genes in the basal layer of the epidermis and the hair follicle outer root sheath, including the keratinocyte stem cells located in the bulge region of the hair follicle. K5CreER<sup>T2</sup> and K14CreER<sup>T</sup> mice have been used successfully to study the impact of gene deletion in the epidermis. The floxed mTOR mice (mTOR<sup>LoxP/LoxP</sup>, generously provided by Dr. CJ Lynch, Penn State College of Medicine) were created with LoxP sites flanking exons 49-50 (Fig 3). Cre-induced removal of this genomic fragment results in a frameshift mutation and a loss of the essential kinase domain (personal communication with Dr. CJ Lynch). To obtain all of the experimental and control mice needed to study the effects of mTOR deletion, K5CreER/mTOR<sup>+/LoxP</sup> mice were bred with mTOR<sup>+/LoxP</sup> mice. Figure 4 shows the results of our genotyping procedure to identify mice for use in these experiments. Tail DNA is assayed for the presence of the K5-Cre transgene, and also for the presence of the wild-type and floxed mTOR alleles. The genotypes produced are as follows: K5CreER/mTOR<sup>LoxP/LoxP</sup>, K5CreER/mTOR<sup>+/+</sup>, mTOR<sup>LoxP/LoxP</sup>, and mTOR<sup>+/+</sup>.

Initial studies were performed on K5CreER/mTOR<sup>LoxP/LoxP</sup> mice to verify ablation of mTOR using topical application of 4OHT to the skin. All mice used were on the FVB/N background and genotyped as described above. When mice were 7-8 weeks old, 1 mg 4OHT was applied daily to the shaved dorsal surface for 5 days. Mice were sacrificed on days 6 and 14. Epidermal protein was collected and used for Western blot analysis detecting either phosphorylated 4EBP1 (an mTORC1 target) or phosphorylated AKT (an mTORC2 target). 4OHT treatment was sufficient to reduce both mTORC1 and mTORC2 signaling, as measured by reduced phosphorylation

levels of both 4EBP1 and AKT(Ser473) (Fig 5). Additionally, a small group of 4OHT-treated mice are currently being monitored for gross skin and hair changes. At the deadline for this report the mice were 16 weeks old and no discernable abnormalities were noted. This model establishes a novel system to study the role of mTOR in the epidermis. Breeding is ongoing to generate mice for carcinogenesis experiments using both chemical carcinogenesis and exposure to UVB.

### Conclusions

These studies establish for the first time that mTOR can be conditionally deleted in the basal layer of the interfollicular epidermis. These mice, used in combination with mice treated with the mTORC1 inhibitor Rapamycin, will not only serve to validate mTOR as a target for chemoprevention, but will also lead to work identifying the genetic and epigenetic changes necessary for tumor promotion that are controlled by mTOR.

These studies were used as Preliminary Results in a current application to the National Institute of Environmental Health Sciences (ES019242)

Figures

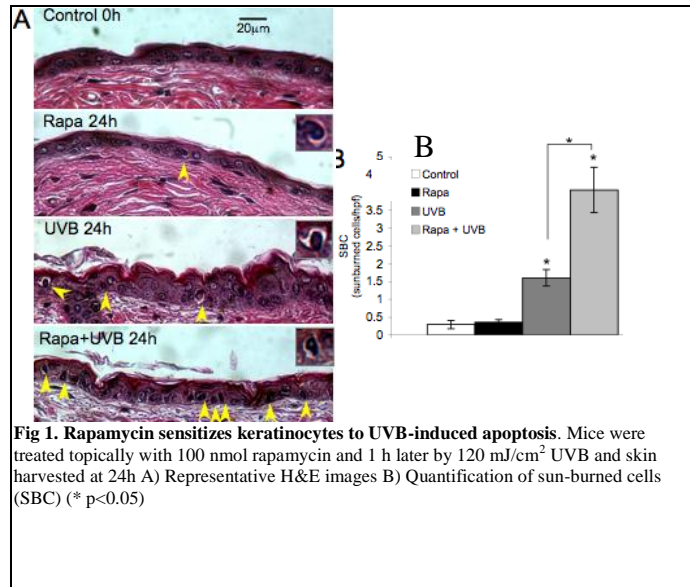


**Fig 1. Rapamycin sensitizes keratinocytes to UVB-induced apoptosis.** Mice were treated topically with 100 nmol rapamycin and 1 h later by 120 mJ/cm<sup>2</sup> UVB and skin harvested at 24h A) Representative H&E images B) Quantification of sun-burned cells (SBC) (\* p<0.05)

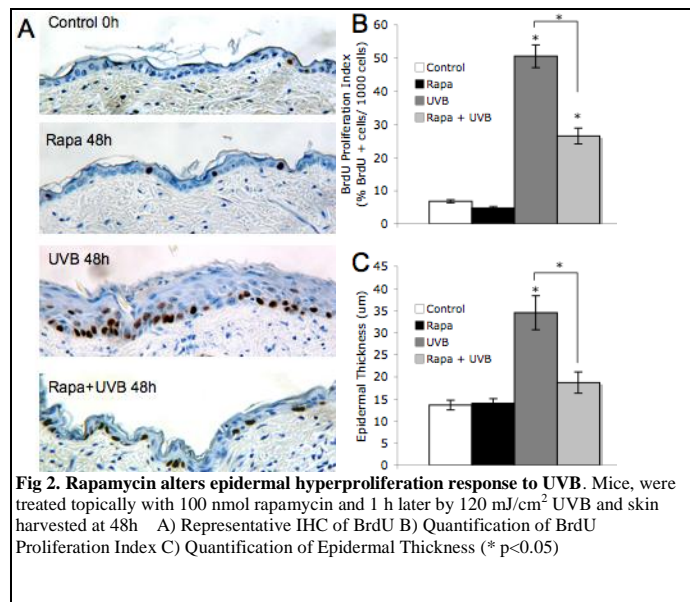


**Fig 2. Rapamycin alters epidermal hyperproliferation response to UVB.** Mice, were treated topically with 100 nmol rapamycin and 1 h later by 120 mJ/cm<sup>2</sup> UVB and skin harvested at 48h A) Representative IHC of BrdU B) Quantification of BrdU Proliferation Index C) Quantification of Epidermal Thickness (\* p<0.05)

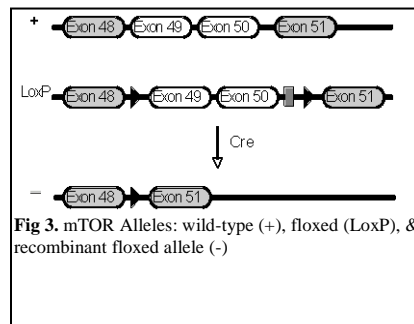


**Fig 3. mTOR Alleles:** wild-type (+), floxed (LoxP), & recombinant floxed allele (-)

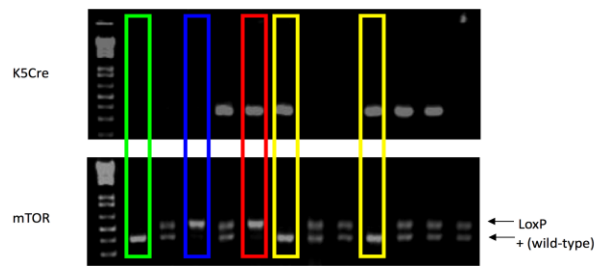
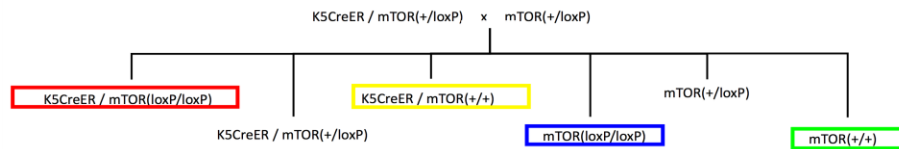


**Fig 4.** Genotypes produced to study the effects of mTOR deletion. The genotypes produced are as follows:  $K5CreER/mTOR^{LoxP/LoxP}$  (red),  $K5CreER/mTOR^{+/+}$  (yellow),  $mTOR^{LoxP/LoxP}$  (blue), and  $mTOR^{+/+}$  (green).

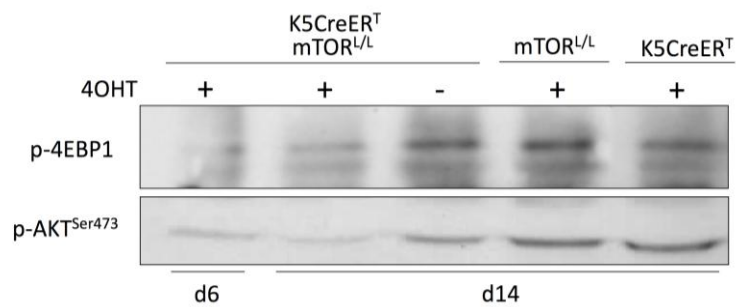


**Fig 5.** Western showing reduced mTORC1 (p-4EBP1) and mTORC2 (p-AKT) signaling with 4OHT application to  $K5CreER;mTOR^{L/L}$  mice

## **Research Project 10: Project Title and Purpose**

*IRES-Mediated Synthesis of Proteins Integral to Adaptation to Hyperoxia* - The purpose of this project is determine if exposure of human lung cells to high concentrations of oxygen alters the processes responsible for synthesis of specific proteins. In particular, our goal is to understand how high ambient oxygen concentrations increase the synthesis of some proteins while decreasing the synthesis of others. We believe, that oxygen “uncovers” alternative synthetic processes inherent in some protein templates, thereby enabling increased synthesis during periods of stress.

### **Anticipated Duration of Project**

1/1/2009 - 12/31/2010

### **Project Overview**

Exposure of the lung to hyperoxia generates reactive oxygen species capable of modulating the translational control of gene expression. Although nearly all eukaryotic mRNAs are translated by a 5'-cap-dependent process under basal conditions, a select group of transcripts containing internal ribosome entry sites (IRES) within 5'-UTR (untranslated region) may be preferentially translated in a cap-independent manner during periods of stress. It is the tenant of our recent R01 resubmission that hyperoxia alters cap-dependent mRNA translation by influencing the activity of mammalian target of rapamycin complex 1 (mTORC1) in the lungs of newborn rodents. We postulate that hyperoxia will acutely depress cap-dependent mRNA translation in the parenchymal epithelium and augment the expression of select proteins integral to O<sub>2</sub>-tolerance translated by cap-independent mechanisms. Specifically, using dual-luciferase, dicistronic constructs containing the 5'-UTR of GADD45 $\alpha$  and p53 mRNAs, we will determine the changes in the relative translational efficiency of cap-dependent and IRES-mediated translation of each transcript in human lung epithelial cell lines. This project seeks to provide additional evidence for the R01 by illustrating that hyperoxia promotes cap-independent mRNA translation in lung epithelial cells.

### **Principal Investigators**

Jeffrey S. Shenberger, MD  
Associate Professor  
Hershey Medical Center  
Department of Pediatrics  
Hershey Medical Center, H085  
500 University Drive  
P.O. Box 850  
Hershey, PA 17033-0850

### **Other Participating Researchers**

Lianqin Zhang, MD – employed by Penn State College of Medicine

## Expected Research Outcomes and Benefits

We anticipate that exposing human lung cells to high concentrations of oxygen will alter the mechanisms used to synthesize proteins. Specifically, we anticipate that high oxygen levels will enhance the production of proteins the cells need to repair oxygen-mediated injury. This information will be used as part of a National Institutes of Health R01 grant proposal investigating how oxygen-mediated changes in protein synthesis modify the expression of factors essential to normal human growth and development. As such, these preliminary, basic science findings have the potential to lead to innovative therapies promoting normal lung development in premature infants requiring oxygen therapy for treatment of surfactant deficiency.

## Summary of Research Completed

After completing our initial experiments using bicistronic plasmid constructs for HIF-1 $\alpha$ , VEGF, and p53, we concluded that accurately determining the effect of hyperoxia on IRES-mediated translation required a modified approach. First, we selected cells with increased transfection efficiencies, HEK293 and HeLa cells. We also decided to study a gene with established hyperoxia-induced differences in protein expression, but not in mRNA expression, indicative of IRES-mediated upregulation. In this case, we chose BiP/GRP78 (immunoglobulin binding protein), an ER-resident chaperone whose protein expression was recently shown to be modified by hyperoxia (Gewandter, et al. *Free Rad Biol Med*, 2010). The expression of BiP is also easily induced by brief incubations with thapsigargin via activation of the unfolded protein response, providing an effective positive control. We also used deletion mutagenesis to isolate the effects of the plasmid, minus the IRES-containing 5'-UTR sequence, on luciferase activity. Finally, we performed a detailed dose-response curve using easily transfected HEK293 and HeLa cells with the intent on establishing the optimal times for hyperoxia exposure.

Methods: Cell growth conditions and transient transfection. HEK293 and HeLa cells were seeded into 6-well plates at densities of 50k/cm<sup>2</sup> and 18k/cm<sup>2</sup>, respectively, and propagated in DMEM containing 10% fetal bovine serum, 2 mM glutamine, penicillin (100 U/ml), and streptomycin (100  $\mu$ g/ml). Twenty four hours later, bicistronic constructs containing the IRES of BiP were transfected into both cell types using Effectene Transfection Reagent (QIAGEN). Briefly, 0.4  $\mu$ g BiP plasmid or negative control construct DNA were diluted in buffer EC to a total volume of 100  $\mu$ l prior to adding 3.2  $\mu$ l enhancer and incubating for 4 min at room temperature. Ten  $\mu$ l of Effectene transfection reagent was added to the DNA-Enhancer mixture and the complete transfection solution added to cells in 600  $\mu$ l of fresh medium. Transfections were carried out for 12-72 hrs in order to construct a time course of gene expression.

Deletion mutagenesis. The pRLuc BiP IRES Fluc bicistronic plasmid was gift from Dr. Celeste Simon at University of Pennsylvania. To generate a negative control plasmid, we deleted the BiP 5'-UTR sequence by deletion mutation. In brief, two oligonucleotides (sense: 5' GATACCGTCGACCTCGAATCGTTGGTAAAGCCACCATGGAA3', antisense: 5' GATTCGAGGTCGACGGTATC3') were synthesized by the core facilities at Penn State University College of Medicine (PSUCOM). To eliminate the BiP-IRES fragment from the

construct, both oligos were used for PCR amplification with the construct pRLuc BiP IRES Fluc as a template according to the instructions in the Site-directed mutagenesis kit (Stratagene, La Jolla, CA). After PCR and digestion with Dpn I, the DNAs were transformed into *E. coli* cells using standard methods, three positive clones selected, and the mutated plasmid DNA confirmed by DNA sequencing.

Luciferase assay. A dual-luciferase assay was performed with the Dual-Luciferase Reporter Assay System (Promega, Madison, WI). In brief, transfected cells were harvested 12-72 hrs after transfection. The wells were washed once with PBS and lysed in 500  $\mu$ l of passive lysis buffer (Promega) with gentle rocking for 15 min at room temperature. Collected cell lysates were cleared by centrifuging and 20  $\mu$ l of lysate combined with 100  $\mu$ l of luciferase reagent I. Tubes were placed into an FB12 luminometer (ZyLux, Maryville, TN) and 100  $\mu$ l of Stop & Glow reagent added to each tube. Firefly (FL) and *Renilla* (RL) luciferase luminosities were recorded and the FL/RL ratio calculated. Three trials for each clone were performed with each trial measured in duplicate.

Results. In order to construct negative control plasmids, we sequenced the portion of the BiP plasmid from the SV40 promoter to the *Renilla* luciferase reporter. By matching the published BiP IRES sequence to the plasmid sequence, we were able to remove the BiP 5'-UTR from the plasmid using mutagenesis. Eighteen ampicillin-resistance *E. coli* colonies were selected and mutated DNA amplified by PCR. Six of the eighteen colonies showing appropriate DNA sizes on agarose gel electrophoresis were sequenced, of which 3 showed exact matches to the devised plasmid deletion. To confirm the absence of luciferase activity, the 3 negative control plasmids were transfected into HEK293 cells along with the native BiP plasmid. As shown in Figure 1, all three negative controls displayed little IRES activity (Firefly luciferase, low FL:RL ratio). The BiP 5'-UTR, on the other hand, possessed nearly 100-fold greater activity for the IRES than the negative control plasmids under basal conditions (48 hrs after transfection).

We next performed time course studies to identify the conditions at which changes in both Firefly (FL) and *Renilla* (RL) could be detected. Figure 2 illustrates that the transfected HEK293 cells lead to time-dependent increases in both FL and RL activities. From 30-48 hrs post-transfection maximal rates of change in both luciferase activities were observed. Importantly, this time frame corresponds to the period when it is possible to detect relative changes in IRES activity (FL:RL ratios) in either a positive or negative direction (Figure 3). These studies indicate that finishing hyperoxic exposure between 28-42 hrs post-transfection in HEK293 cells will provide the best conditions for the identification of either an increase or decrease in IRES activity.

We also performed an identical time course in HeLa cells. Although the experiment produced a similar curve for Firefly luciferase, time-dependent alterations in *Renilla* luciferase activity were markedly less dramatic (Figure 4), resulting in a "flat" FL:RL curve. This result suggested that HeLa cells are less optimal for conducting hyperoxia experiments due to the low basal *Renilla* activity. In addition, transfection efficiency is much greater in HEK293 cells than in HeLa cells.

Preliminary studies indicate that exposure of A549 and HeLa cells to 95% O<sub>2</sub> for 6 hours transiently increases the expression of BiP protein. Similar studies in non-transfected HEK293

cells will be used to identify exposure times correlating altered BiP protein expression. These periods will then be utilized for investigations of transfected HEK293 cells. Treatment of A549 cells with thapsigargin (100  $\mu$ M) has also been shown to dramatically increase BiP protein expression after 3-6 hours (not shown). We plan to perform these same trials in HEK293 cells to provide a suitable positive control for our transfection studies.

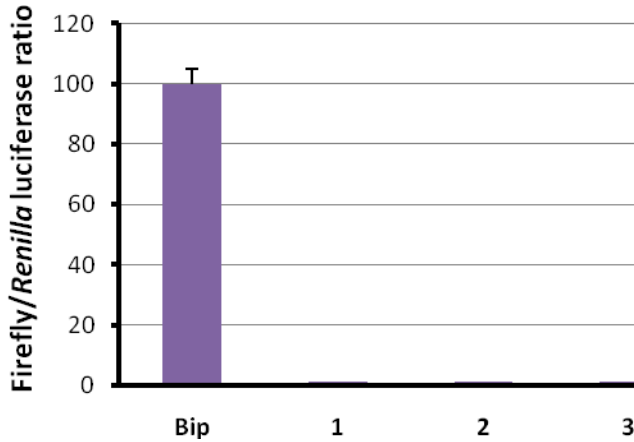


**Figure 1. Relative activity of BiP IRES in HEK293 cells.** Cells were transfected with a dual-luciferase plasmid containing the BiP IRES sequence or with control plasmids (clones 1-3) with the BiP IRES sequence removed. Luciferase activity corresponding to the IRES- (Firefly) or cap-mediated (*Renilla*) mRNA translation was expressed as a ratio (columns = mean of 3 reactions and bars standard error). As illustrated, removal of the IRES sequence dramatically reduced Firefly luciferase activity and the Firefly:*Renilla* ratio, indicating a lack of inherent Firefly luciferase activity in the control plasmid.

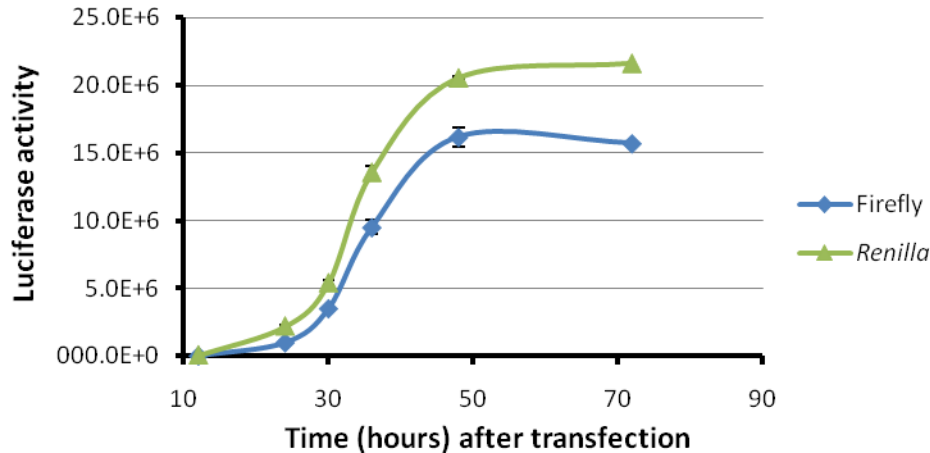


**Figure 2. Time course of IRES- (Firefly) and cap-dependent (*Renilla*) luciferase activity in HEK293 cells.** The graph shows luciferase activity in cells transfected with a dual-luciferase plasmid containing the BiP IRES sequence studied 12-72 hrs after transfection. Results demonstrate that both Firefly (blue diamonds) and *Renilla* (green triangles) activity is time-dependent with the greatest increase in activity occurring between 30 and 48 hrs. Each point represents the mean of 3 wells and bars standard error.

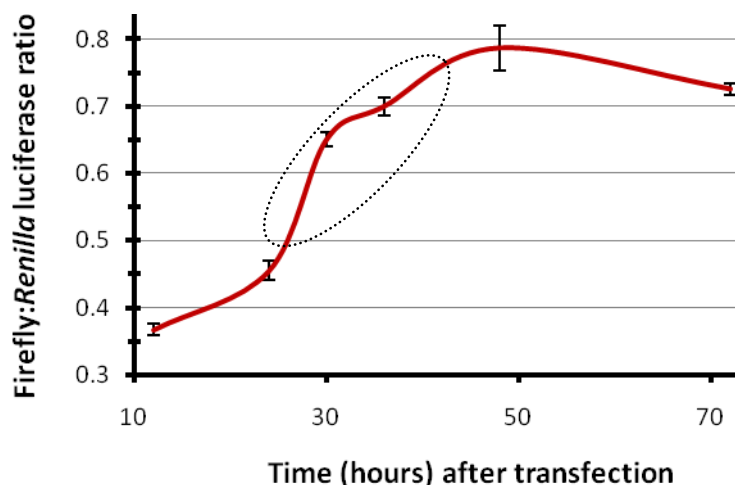


Figure 3. Time course of Firefly:*Renilla* luciferase activities in HEK293 cells. Graph depicts IRES-mediated (Firefly luciferase) translational activity relative to cap-mediated (*Renilla* luciferase) translational activity. Higher ratios indicate a relative increase in IRES activity. Times corresponding to the maximal slope (dashed circle) represent optimal conditions for conducting hyperoxia exposure as neither luciferase reporter is maximally or minimally active. Each point represents the mean of 3 wells and bars standard error.

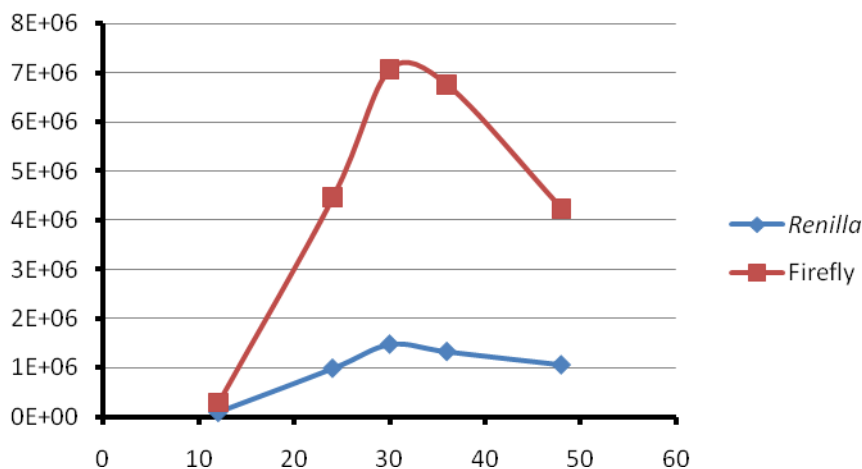


Figure 4. Time course of IRES- (Firefly) and cap-dependent (*Renilla*) luciferase activity in HeLa cells. Graph shows luciferase activity in HeLa cells transfected with a dual-luciferase plasmid containing the BiP IRES sequence. Results demonstrate that Firefly (red squares) luciferase activity is time-dependent, but that *Renilla* (blue diamonds) luciferase activity changes much less. Low endogenous *Renilla* activity makes detection of changes in activity in the presence of hyperoxia more difficult. Each point represents the mean of 4 wells.

## **Research Project 11: Project Title and Purpose**

*Stroke Recovery in Type II Diabetes* - The overall objective of this project is to determine the role anti-diabetic agents have on stroke outcome. Although it is well established that diabetics are at an increased risk of mortality and morbidity following an ischemic stroke there are no known therapies that are specifically targeted at diabetics to improve stroke recovery. This is a significant public health problem considering that the worldwide diabetic population is growing at an alarming rate and thus the incidence of strokes is undergoing the same dramatic increase. This project will test both the chronic and acute effect of several anti-diabetic agents on stroke outcome with the specific objectives of determining which are the most efficacious in promoting recovery in the diabetic animals and the mechanism(s) by which the respective agents elicit their actions.

### **Duration of Project**

1/1/2009 - 3/31/2010

### **Project Overview**

The overall objective of this project is to determine the role of anti-diabetic agents on stroke outcome. Currently, the most commonly prescribed drugs to control blood glucose in patients with Type II diabetes are thiazolidinediones (TZD) (rosiglitazone, pioglitazone, and darglitazone), metformin, and sulphonylureas (glipizide, glyburide, and gliclazide). Both TZDs and metformin act by enhancing insulin sensitivity and regulating glucose and lipid metabolism. TZDs also exhibit anti-inflammatory properties while sulphonylureas work by increasing insulin secretion but are without systemic effects. Diabetics are at an increased risk of morbidity and mortality following a stroke that results from a combination of hyperglycemia, dyslipidemia, and an impaired inflammatory response. Hence, it is anticipated that these anti-diabetic agents will have differential effects on stroke outcome. Our preliminary data using the *ob/ob* mouse as an animal model of Type II diabetes demonstrate that the TZD, darglitazone is highly effective in restoring euglycemia and reducing the infarct volume following stroke induced by a cerebral hypoxic/ ischemic (H/I) insult. Two Specific Aims are proposed to address these questions.

*Specific Aim 1:* To determine the effects that the anti-diabetic drugs darglitazone, metformin and glyburide have on stroke outcome in the diabetic *db/db* mouse and its heterozygous control (*db/+*) following an H/I insult. Male *db/db* and *db/+* mice will receive chronic treatments of darglitazone, metformin or glyburide for 7 days pre-stroke and maintained throughout recovery. The temporal evolution of damage will be monitored by determining: 1) infarct volume by hematoxylin-and-eosin staining (H/E); 2a) pro- and anti-inflammatory cytokine and growth factor mRNA expression by RT-PCR; 2b) cytokine protein levels by BioPlex protein array; 3) microglial, macrophage, neutrophil, and lymphocyte levels and activation by fluorescent flow cytometry; and 4) *In situ* hybridization to localize microglial and astroglial activation and cytokine expression.

*Specific Aim 2:* To determine the effect that the anti-diabetic drugs darglitazone, metformin, and glyburide have on stroke outcome when administered acutely in the diabetic *db/db* mouse and its

heterozygous control (*db/+*) following an H/I insult. Male *db/db* and *db/+* mice will receive acute treatments of darglitazone, metformin, and glyburide by sc. injection 20 min post H/I. The efficacy of the respective reagents on stroke outcome will be assessed using the same array of methodologies as in Aim 1.

### **Principal Investigators**

Ian A. Simpson, PhD  
Professor, Dept. of Neural & Behavioral Sciences  
Penn State University College of Medicine  
Department of Neural & Behavioral Sciences  
Penn State University/Hershey Medical Center  
P.O. Box 850  
Hershey, PA 17033

### **Other Participating Researchers**

Robert H. Bonneau, PhD, Jay K. Krady, PhD, Shyama Patel, BS – employed by Penn State University College of Medicine

### **Expected Research Outcomes and Benefits**

This research project is designed to address the question as to which class of anti-diabetic drugs is most efficacious in reducing damage associated with stroke in diabetic mice. The outcome of these studies may well provide impetus to perform retrospective studies in diabetic patients recovering from stroke to determine whether comparable outcomes are observed and whether such observations might influence subsequent treatment regimens.

It is anticipated that darglitazone, will be more effective than either metformin or glyburide in reducing the severity of the stroke in the diabetic animals. Although, each drug is capable of reducing the glucose levels within the same range, the defining factor may reside in the drug's ability to modulate the rest of the complications associated with diabetes, such as hyperlipidemia and an impaired wound healing response particularly as they are associated with stroke recovery. Therefore, darglitazone should have the greatest effect on the infarct because it can, not only reduce glucose levels, but can significantly improve the lipid profile and the inflammatory response. This improvement in recovery should be seen as a decrease in the peripheral macrophage, neutrophil, and cytokine level which has been associated with improved stroke outcome. Furthermore, there should also be a decrease in cerebral pro-inflammatory cytokines, which could be the result of a decrease in microglial activation, as demonstrated by previous studies.

With acute drug treatment, we will assess the efficacy of the respective agents under circumstances where hyperglycemia or lipid profile will not be improved and thus will provide insight into potential properties that the drugs might hold as an effective post-stroke treatment in addition to restoring euglycemia.

## Summary of Research Completed

As indicated in the previous report, we were unable to complete our original specific aims and therefore elected to examine the role that the peripheral immune system plays in the impaired stroke recovery in the *db/db* mouse compared to non-diabetic littermates. Our underlying hypothesis is that diabetic *db/db* mice exhibit a compromised peripheral inflammatory response resulting in greater leukocyte infiltration, BBB breakdown and poorer stroke recovery. We have tested this hypothesis in the diabetic *db/db* mice and their heterozygous non-diabetic (*db/+*) controls following a hypoxic/ischemic insult ((H/I) - stroke).

During the past year, we have made significant progress toward this objective. Figure 1 illustrates the increased breakdown of the BBB following an H/I insult as indicated by the leakage of fluorescent albumin observed in the ipsilateral hemisphere of the *db/db mouse*. We then investigated what might underlie this increased permeability and measured the levels of the proteases that have been shown to mediate permeation of the BBB.

As illustrated in Figure 2 we observed that the levels of both metalloproteases (MMPs) 2&9 were elevated in the ipsilateral hemispheres of *db/db* mice as compared to their non-diabetic *db/+* littermates. The question then arose as to the source of the MMPs and could they be derived from circulating white cells.

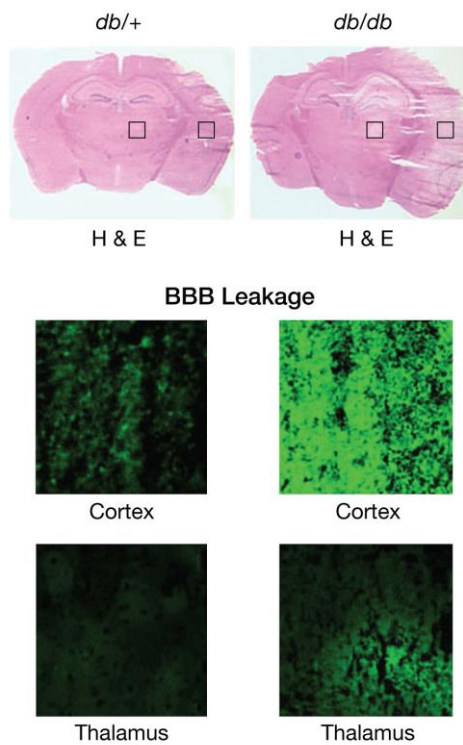
As illustrated in Figures 3-5, we investigated the effects of H/I on the levels of circulating white cells. We observed that both B and T lymphocyte levels declined following H/I and there were similar changes in sham animals that underwent surgery and subsequent hypoxia but without ligation of the right carotid. In the case of T cells, the decline was not observed until 24 h of H/I recovery in the *db/db* animals (Figure 3).

Figure 4 illustrates the effects of surgery and H/I on circulating macrophage levels. In the non-diabetic *db/+* mice, there is a decline in the levels at 4 h in both sham and H/I animals and the levels remained low over 24 h. The baseline macrophage levels in the *db/db* mice are greater than in the *db/+* mice and remain elevated in both sham and H/I mice at 4h of recovery but decline to baseline levels in the *db/+* mice at 24 h of recovery.

In contrast to the other white cells, the neutrophil levels increased at 4 hours of recovery from H/I. In the *db/+* mice, the levels doubled while in the *db/db* a 4-fold increase was observed. In both cases, neutrophil levels returned to approximate baseline levels by 24 h. This initial increase in neutrophils levels does not appear to coincide with the increase in MMP-9 activity (Figure 2) or the expression of the adhesion molecule ICAM (Figure 6), which mediates the binding of neutrophils and macrophages to endothelial cells, as both activities appear to peak at 48 h of recovery.

As illustrated in Figure 6, the levels of ICAM were measured by Western blotting whole brain homogenates derived from ipsilateral and contralateral hemispheres at 24 and 48 h of recovery. While ICAM is expressed in sham treated animals, it is greatly increased in the ischemic hemisphere particularly in the *db/db* animals. We are currently developing the confocal microscopic techniques to quantify the binding of neutrophils and macrophages with the endothelial cells, their subsequent extravasations, and the breakdown of the BBB.

**Fig.1** Blood Brain Barrier Permeability



*Fig.1 compares BBB permeability in db/+ and db/db mice following 48 hr of H/I. H&E staining of the adjacent section represent the infarction both in cortex and thalamus.*

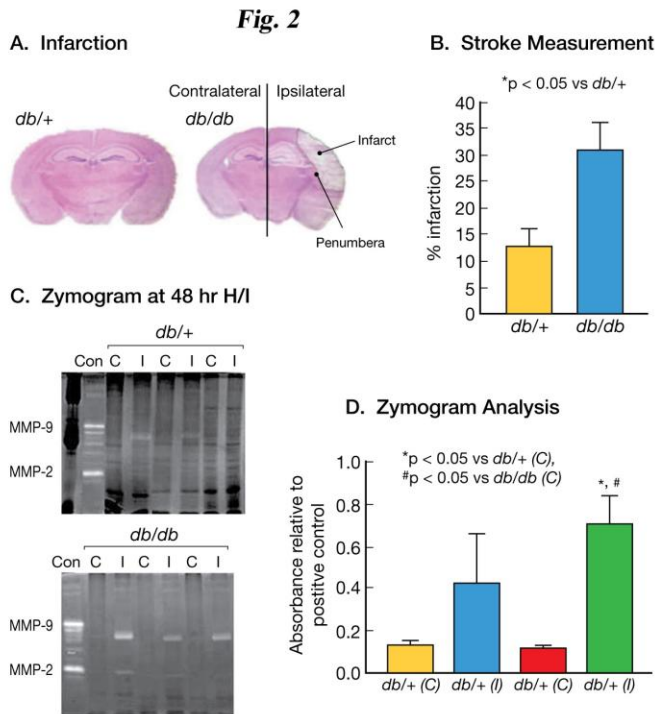
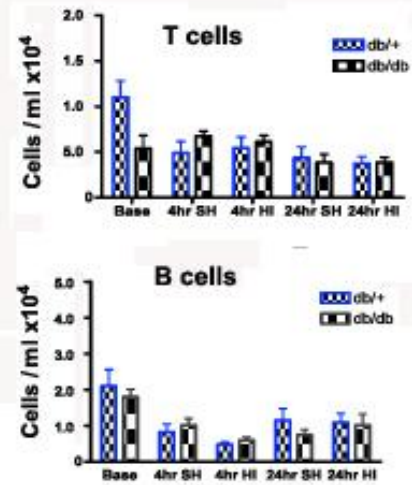
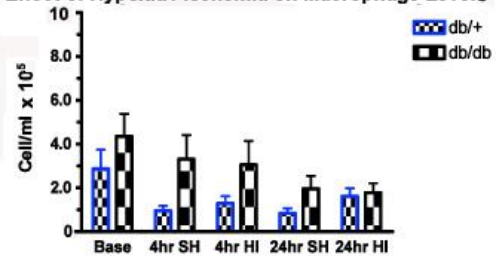


Fig 2A & 2B represents the typical infarcted area in db/+ (n=20) & db/db (n=20) mice following 48 hr of H/I. 2C & 2D shows MMP-9 protease activity in both contralateral (C) and ipsilateral (I) hemispheres in control (n=3) and diabetic (n=3) at 48 hr of stroke.

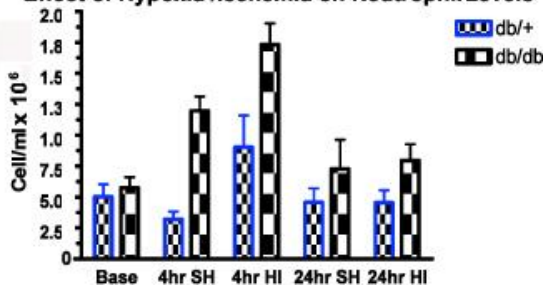
**Fig. 3**  
**Effects of Hypoxia / Ischemia on T & B Cell Levels**



**Fig. 4**  
**Effect of Hypoxia / Ischemia on Macrophage Levels**



**Fig. 5**  
**Effect of Hypoxia / Ischemia on Neutrophil Levels**



Leukocytes were isolated from 100  $\mu$ l of whole blood from 8-16 mice at baseline, and 4 and 24 hr post sham or post hypoxia/ischemia and counted by flow cytometry. B & T Lymphocyte counts are illustrated in Figure 3, Macrophages in Figure 4 and Neutrophils in Figure 5

**Fig.6**

**ICAM-1:**

Western Blot Analysis: 24 & 48 hour of recovery

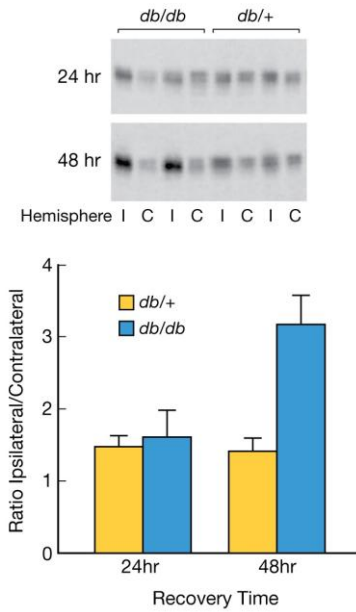


Fig.6 shows ICAM-1 protein expression in *db/+* & *db/db* mice following 24 & 48 hr of H/I Contralateral (C), Ipsilateral (I) (n=3)

## **Research Project 12: Project Title and Purpose**

*Modulation of Basal Ganglia Electrophysiology by Dopaminergic Cell Transplant* - Cell transplants have been shown to provide symptomatic relief for Parkinson's disease patients and in parkinsonian animal models. Separately, researchers have highlighted abnormal brain electrical patterns that occur in Parkinson's disease and are partially reversed with levodopa treatment. This project looks at a crucial related question which has not yet been examined: whether cell transplants change the electrical patterns in the brain. The results of the project will shed crucial light on the utility of cell transplants compared to levodopa treatment and the potential to reduce dyskinesias (a major side effect of prolonged levodopa treatment). The results will also shed light on basic neuroscience questions underlying Parkinson's disease pathology.

### **Anticipated Duration of Project**

6/1/2009 – 12/31/2011

### **Project Overview**

The broad research objective is to better understand the normal electrical properties of the brain, how they are altered in Parkinson's disease and whether "normalizing" the aberrant electrical patterns is critical to restore normal behavioral. Part of this overall objective is to better understand the mechanisms by which cell transplants ameliorate Parkinson's disease symptoms.

The specific research aim is to answer the question: Do dopaminergic cell grafts modulate basal ganglia (BG) electrophysiology in the unanesthetized hemiparkinsonian (HP) rat? Planned subquestions are: Are the changes different in asleep versus awake conditions, do fetal ventral mesencephalic (FVM) cell grafts cause different changes than retinal pigment epithelium (RPE) cell grafts, and is there a difference between striatal-only grafts versus combined striatal-nigral grafts?

The methods involve comparing the recorded electrical patterns from the brains of rats. Rats will be divided into five groups: Normal, Control, and Transplanted (3 different transplant paradigms: FVM-striatal, FVM-striatal/nigral, and (RPE)-striatal). After baseline testing, and induction of hemiparkinsonism via the 6OHDA neurotoxin-injection paradigm, the rats will be transplanted with cells (or vehicle) and implanted with electroencephalogram (EEG) screw electrodes and chronic electrodes for recording local field potentials (LFPs) from the subthalamic nucleus (STN). After recovery, EEG and LFP signals will be recorded weekly for three months under both asleep and awake conditions. Afterward the brains will be histologically examined. The recorded signals will be examined for differences in specific frequency bands between the different groups.

### **Principal Investigators**

Thyagarajan Subramanian, MD  
Professor

Penn State Hershey Medical Center  
500 University Drive, MC H109  
P.O. Box 850  
Hershey, PA 17033-0850

### **Other Participating Researchers**

Timothy Gilmour - employed by Penn State Hershey Medical Center

### **Expected Research Outcomes and Benefits**

The answers to the main research question and subquestions will advance the current understanding and treatment of Parkinson's disease. Knowledge of the extent to which cell transplants normalize the basal ganglia electrophysiology will be crucial to understanding the long-term safety of cell transplantation therapy. Furthermore, if transplants normalize the electrophysiology better than levodopa does, new research avenues would be opened to investigate whether cell transplants are better able to avoid dyskinesias, since dyskinesias are known to be associated with electrophysiological abnormalities.

Each subquestion will also provide essential information. Knowledge of the cell type which produces the best symptomatic amelioration and electrophysiological normalization will directly translate into improving transplant paradigms for human patients. Likewise the answer to the question of whether dopamine replacement into multiple basal ganglia nuclei is necessary for electrophysiological normalization will directly affect transplant paradigms.

In summary, the outcomes of this project will directly affect therapy implementation for human sufferers of Parkinson's disease, and will shed crucial light on electrophysiological questions about the underlying pathology.

### **Summary of Research Completed**

Table 1 shows the projected number of rats for the entire project, and the number of rats whose experimental procedures were completed during the reporting period 7/1/2009 – 6/30/2010. All rats were tested for baseline apomorphine-induced rotations (APIRs). Group 1 was implanted with electroencephalogram (EEG) screw electrodes and chronic electrodes for recording local field potentials (LFPs) from the subthalamic nucleus (STN) (cf. Sharott et al. 2005, "Dopamine depletion increases the power and coherence of beta-oscillations in the cerebral cortex and subthalamic nucleus of the awake rat", *Eur J Neurosci* 21(5): 1413-22).

Group 2 was lesioned with 6OHDA by Charles River Laboratories prior to transfer to our lab. Then in our lab the rats underwent surgery to implant the EEG screws and LFP chronic electrode.

Groups 3-5 were initially lesioned with 6OHDA by Charles River Laboratories. After verification of hemiparkinsonism, Groups 3-5 underwent cell transplant surgery and were implanted with the EEG screws, EMG electrode, and chronic LFP electrode (cf. Subramanian et

al 2002, “Striatal xenotransplantation of human retinal pigment epithelial cells attached to microcarriers in hemiparkinsonian rats ameliorates behavioral deficits without provoking a host immune response”, *Cell Transplant* 11(3): 207-14). Figure 1 shows a sample cresyl violet stain showing accurate electrode targeting into the STN.

After recovery, EEG and LFP signals were recorded at least once per month in each rat during both daytime (for sleep) and nighttime (for awake) sessions. Sleep was verified using EEG and electromyogram (EMG) recordings and video monitoring. The signals recorded were bipolar STN electrode, two EEG channels, one EMG channel, and a cage accelerometer signal to measure activity. Table 2 lists the behavioral recording sessions obtained during 6/1/2009 – 6/30/2010. Figure 2 shows sample EEG and EMG activity with both awake and asleep periods.

Parkinsonism was assessed monthly by APIR tests and by other standard behavioral tests such as the forelimb stepping test, vibrissae stimulation/forelimb placement test, extended body-axis test, and cylinder test. After three months, the rats were perfused and the brains were histologically examined for graft viability and verification of recording locations.

The analysis of the electrophysiological LFPs and cortico-BG coherence is still in process, as well as the analysis of the histology and behavior.

During the project, a need arose to separate the awake and asleep portions of the recordings. After surveying the literature on available segmentation methods, a new method was devised based on the principal component decomposition of the spectral features. This method was tested, submitted for peer review, and published in *Neuroscience Letters* (Gilmour, T. P., J. Fang, Z. Guan and T. Subramanian (2009). "Manual rat sleep classification in principal component space." *Neurosci Lett* 469(1): 97-101).

Table 1 – Listing of numbers of rats completed

Control Groups		Experimental Treatment Groups		
Group 1 Normal	Group 2 HP	Group 3 FVM-single	Group 4 FVM-dual	Group 5 RPE-dual
Projected for entire project				
10 rats	10 rats	20 rats	20 rats	20 rats
<b>Completed between 6/1/2009 – 6/30/2010</b>				
<b>1 rat</b>	<b>3 rats</b>	<b>2 rats</b>	<b>1 rat</b>	<b>0 rats</b>

Table 2 – Listing of Data Recording Sessions

Rat	Number of sessions	Hours of recorded data
Normal 1	10	171
HP 1	6	101
HP 2	13	150
HP 3	15	287
FVM-single-tx 1	14	125
FVM-single-tx 2	13	127
FVM-dual-tx 1	16	125

Figure 1 – Coronal cresyl violet-stained rat brain slice from rat implanted with chronic STN electrode and euthanized after three months, showing the electrolytic lesion from the tip of the electrode localized in the STN.

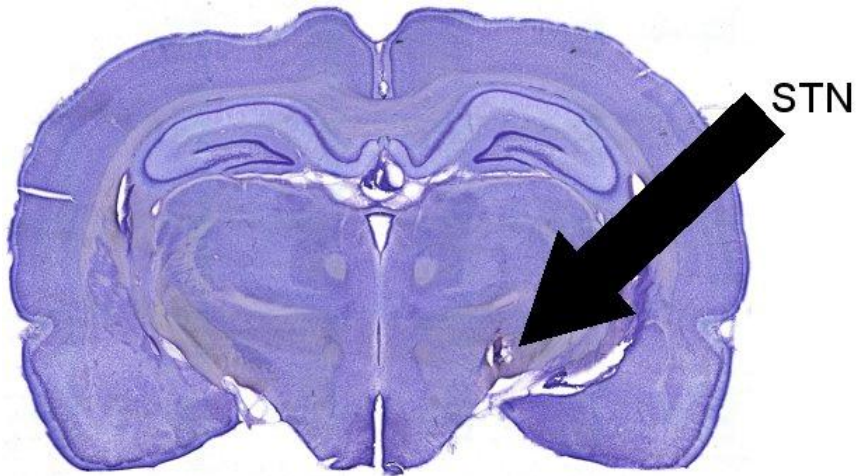
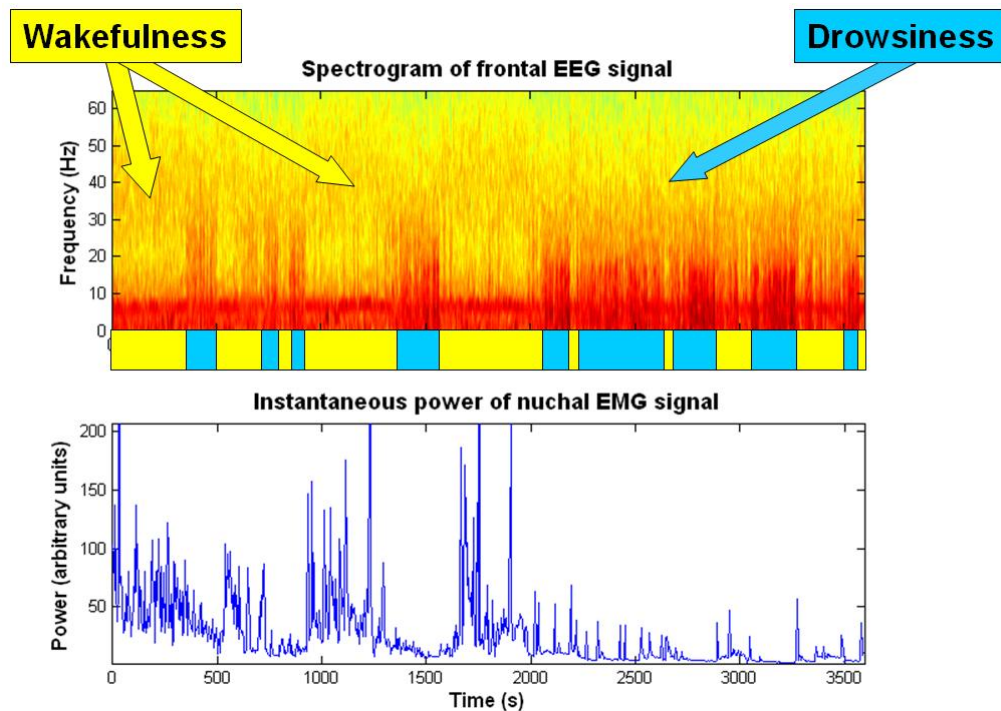


Figure 2 – Spectrogram of EEG signal and concomitant nuchal EMG signal showing periods of wakefulness and drowsiness.



## **Research Project 13: Project Title and Purpose**

### *Identification and Analysis of Arterial Blood Pressure Noise in Baroreceptor Denervated Rats -*

The arterial baroreceptor reflex rapidly and effectively stabilizes blood pressure. A prominent finding, across many species, is that eliminating the baroreceptor input by sinoaortic denervation (SAD) more than doubles arterial pressure variability (APV). Understanding the sources and basic mechanisms of APV is of clinical importance. Using neuromuscular blocked (NMB) rat preparation, we will specifically examine the obligate roles of the baroreflex key way stations, e.g., the rostral ventral lateral medulla (RVLM), in producing the large post-SAD APV. The funds will be used to collect preliminary data for our NIH R03 2<sup>nd</sup> re-submission. Our long-term goal is to develop APV analysis into a non-invasive and economical tool for clinical prognosis and diagnosis of cardiovascular diseases.

### **Anticipated Duration of Project**

1/1/2009 - 6/30/2011

### **Project Overview**

Surprisingly few studies have investigated the neurophysiological sources, and/or regulatory function, if any, of the APV. Understanding APV is of clinical importance. Since the 1980's, despite numerous attempts to catalog APV changes in a range of diseases, the prognostic and diagnostic promise has yet to be realized. A possible reason for this is lack of fundamental understanding of the sources and causes of APV. This current study aims at identifying the potential key central noise sources that are responsible for the large post-SAD APV. Our long-term goal is to further develop APV analysis into a non-invasive and economical tool for the clinical prognosis and diagnosis of cardiovascular diseases.

Previously, using a unique chronically neuromuscular blocked (NMB) rat preparation, we found that SAD more than doubled APV, and that ganglionic block, using chlorisondamine, significantly reduced the large post-SAD APV. These results indicated (1) that the noise sources for APV are endogenous and central, and (2) that normally, APV is attenuated by the baroreflex. Studies have shown that the brain regions rostral to the collicular are not potential noise sources, which suggests that the caudal brain stem is likely to be the source of the noise. Using NMB rats, we will determine the obligate roles of the baroreflex key way stations in the brain stem, e.g., the rostral ventral lateral medulla (RVLM), in the large post-SAD APV. We hypothesize that the RVLM (The Specific Aim) has an important role in the post-SAD APV. The Aim consists of 4 phases: baseline (3 d) -> SAD (3 d) -> bilateral ibotenic lesions of the RVLM (3 d) -> ganglionically block the rat with intravenous chlorisondamine (2 d). A control, of bilateral lesions in a non-cardiovascular area of the brain stem, the cuneate nuclei, will parallel the Aim. The major outcome measurements include the APV, characterized as the standard deviation of the arterial pressure (AP) and the very low frequency (VLF: 0.01-0.2 Hz) power of the AP spectrum. For each variable, separately, a 2 x 3 mixed factorial ANOVA varying experimental conditions (control, lesion) x phases (baseline, SAD, lesion) will be used to determine the RVLM contribution to post-SAD APV.

## **Principal Investigators**

Xiaorui Tang, PhD  
Assistant Professor  
Penn State College of Medicine  
H181 Neural and Behavioral Sciences  
500 University Drive  
Hershey, PA 17033

## **Other Participating Researchers**

Barry Dworkin, PhD, Ralph Norgren, PhD - employed by Pennsylvania State University

## **Expected Research Outcomes and Benefits**

Expected Research Outcome: The arterial baroreceptor reflex is a potent mechanism to stabilize blood pressure. Eliminating the baroreceptor input to the brain stem by sinoaortic denervation (SAD) more than doubles arterial blood pressure variability (APV). We expect that the key central noise source for the largely increased post-SAD APV resides at the rostral ventral lateral medulla (RVLM) in the brain stem.

Benefits: The APV has been related to a variety of cardiovascular diseases, such as hypertension, as well as brain or spinal cord injury. Understanding the primary origins of APV could let us better catalog APV changes in a range of diseases and better understand regulatory functions of the APV. This current project is the first step towards our long-term goal to develop APV analysis into a non-invasive and economical tool for the clinical prognosis and diagnosis of cardiovascular diseases.

## **Summary of Research Completed**

We have made three (3) significant achievements during the period of June 29, 2009- June 11, 2010: (1) we have completed a study investigating the central contribution to the large blood pressure variability after the sinoaortic denervation (the main theme of this supported project), and we published our initial finding at the Experimental Biology meeting this year at the Anaheim, CA, (2) we are currently at the final stage of putting together a manuscript, which we plan to submit to the Journal of American Physiology. Finally (3) with the data collected during the last 12 months, we have re-submitted our R03 application (i.e., the 3<sup>rd</sup> resubmission) to the National Health Institute, and the grant will be reviewed on June 16<sup>th</sup>.

### Summary of our findings:

Interruption of baroreflexes via sinoaortic denervation (SAD) or lesion of the nucleus tractus solitarius (NTS) more than doubles the arterial pressure variability (APV) that sustained chronically. The source of the variability, however, remains controversial. Using a unique chronic neuromuscular blocked (NMB) rat preparation, in which respiration and core temperature are strictly controlled and skeletal activity is absent, we examined the role of the central nervous system (CNS) in producing the exaggerated post-SAD APV. We observed that

(Fig. 1), similar to that in the freely moving rat, SAD almost tripled APV in the NMB rat. Autonomic ganglionic blockade (2.5 mg/kg i.v. Chlorisondamine) significantly reduced both the mean arterial pressure (MAP) and APV to levels below their corresponding baseline; subsequent restorations of the MAP to the basal level, via continuous phenylephrine (Phen: 5 to 73  $\mu\text{g}\cdot\text{kg}^{-1}\cdot\text{min}^{-1}$  at 5 to 33  $\mu\text{l}/\text{min}$ ) and epinephrine (Epi: 2.6 to 36  $\mu\text{g}\cdot\text{kg}^{-1}\cdot\text{min}^{-1}$  at 3 to 13  $\mu\text{l}/\text{min}$ ) infusion (i.v.) only slightly increased APV. These data suggest that there is a substantial endogenous central noise contribution to the large post-SAD APV.

Although carotid sinus denervation had no statistical effect on the APV, aortic denervation significantly elevated variability (i.e., by 143%), suggesting that the aortic baroreflex plays a significant role in buffering the APV (Table 1). APV was analyzed in both the time, as the standard deviation of the systolic arterial pressure (sAP) and the frequency domains, as the Fast Fourier transform. Using electrical stimulation of the baroafferent aortic depressor nerve (ADN), we (Dworkin, Tang, 2000) determined the overall cardiovascular frequency transfer function, and identified a very low frequency (VLF) band of 0.01-0.2 Hz as the principle region, and a low frequency band of 0.2-0.6 Hz as the resonant frequency region of the baroreflex system. Results from this study confirmed our previous finding and further demonstrated that, compared with baroreflex intact control rats, the VLF power was substantially increased, and LF power decreased in the sAP spectra after the SAD. Both VLF and LF power of the sAP spectrum were significantly decreased after the Chlor ganglionic blockade.

## Results

Figure 1 and Table 1 below describes our major finding described above.

Continuous Phen and Epi infusions restored sAP to the baseline level in presence of the Chlor. (B) The APV ( $F(4, 29) = 75.98, p < 0.001$ ). While SAD almost tripled the APV, Chlor decreased APV to the level lower than the baseline. The APV was then increased to the baseline level during the Phen and Epi vasoconstrictor infusions; in other words, compared with the Chlor phase, the APV was significantly increased during the Phen and Epi infusions. (C) The VLF power of the sAP spectrum ( $F(4, 29) = 30.73, p < 0.001$ ). In general, the VLF power changes in a similar pattern as the APV. In brief, SAD significantly increased, and Chlor decreased the VLF power. The VLF power was lower than the baseline during the Chlor stage, and subsequent Phen and Epi infusion returned the VLF power to the baseline level. (D) LF power of the sAP spectrum ( $F(4, 29) = 22.89, p < 0.001$ ). Opposite from the effects of SAD on the APV and the VLF power, the LF power was significantly decreased by the SAD. Chlor further decreased LP power, and subsequent Phen and Epi infusions increased LF power to the SAD level.

\*\* $p < 0.001$ , and \* $p < 0.05$ .

**Fig. 1**

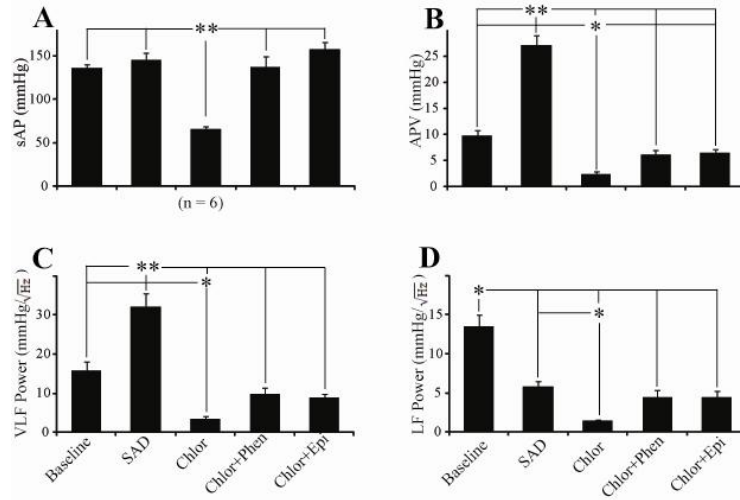


Fig. 1 Summary effects of SAD, Chlor, and Phen and Epi intravenous infusions on the AP, APV, VLF and LF powers of the sAP spectra. APV was defined as standard deviation (SD) of the sAP. VLF and LF powers were calculated as the areas of the frequency bands of (0.01-0.15) Hz and (0.15-0.6)Hz in the sAP spectrum, respectively. Results are presented as the means  $\pm$  SE. (A) The mean systolic arterial pressure (sAP,  $F(4, 29) = 20.44$ ,  $p < 0.001$ ). The mean sAP was similar among all experimental phases, except that Chlor has substantially decreased sAP.

Table 1. Effects of AD, CSD and SAD on AP and HR variabilities

Protocols Variables	AD→SAD (n=4)			CSD→SAD (n=3)		
	Baseline	AD	SAD	Baseline	CSD	SAD
sAP (mmHg)	134±8	140±5	124±8	138±5	142±3	154±4
APV (mmHg)	7±0.3	*17±1.1	†**25±2.7	8±0.8	13±2.8	††**28±1.3
VLF <sub>AP</sub> (mmHg / √Hz)	13±1.4	**26±2.5	†**32±1.2	13±0.6	21±5.3	†*35±2.0
LF <sub>AP</sub> (mmHg / √Hz)	11±1.4	6±0.6	†*5±0.2	12±1.5	9±1.3	*7±0.4
HR (beats/min)	408±28	411±14	390±4	405±12	415±32	412±17
HRV (beats/min)	14±3	9±1	16±2	16±3	12±3	18±3

Table 1 Values are means ± SE. Measurements were made at ≤0.5% isoflurane level. The ‘AD→SAD’ protocol includes procedures of: Baseline → AD → SAD, and the ‘CSD→SAD’ protocol: Baseline→CSD→SAD. APV and HRV were defined as the standard deviation of the sAP and HR, respectively. AD, aortic denervation; CSD, carotid sinus denervation; SAD, (complete) sinoaortic denervation; VLF<sub>AP</sub>, LF<sub>AP</sub>, were the very low and low frequency powers of the sAP spectra. In general, denervation, including AD, CSD and SAD, had no effects on the HR, HRV and the mean sAP, but a significant effect on the APV. Specifically, for the ‘AD→SAD’ protocol (APV: F(2,11)=28.28, p<0.001), VLF<sub>AP</sub>: (F(2,11) = 27.78, p<0.001), and LF<sub>AP</sub>: (F(2, 11)= 13.06, p<0.01), post hoc analysis using Student-Newman-Keuls tests show that, compared with the baseline, AD and SAD increasingly raised the APV and the VLF<sub>AP</sub> power, but decreased LF<sub>AP</sub> power of the sAP spectra. However, for the ‘CSD→SAD’ protocol (APV: F(2,11)=29.16, p<0.001, VLF<sub>AP</sub>: F(2,11) = 11.2, p<0.005, and LF<sub>AP</sub>: F(2, 11)= 4.5, p<0.05), post hoc analysis showed that, compared with the baseline, CSD had no effects on the APV, VLF<sub>AP</sub> and LF<sub>AP</sub> powers of the sAP spectra, but parallel to ‘AD→SAD’ protocol, SAD significantly increased the APV and the VLF<sub>AP</sub> power, but decreased the LF<sub>AP</sub> power of the sAP spectra. Significantly different from the baseline \*\*p<0.001, and \*<0.05; and from the partial denervation ††p<0.001, and †p<0.05.

## **Research Project 14: Project Title and Purpose**

*Myocardial Protein Synthesis after Alcohol Intoxication* - Although the risk of cardiovascular diseases is reduced with moderate alcohol consumption, chronic alcohol abuse leads to heart dysfunction and potentially heart failure. Excessive use of alcohol has a direct toxic effect on the heart demonstrated by a weakening of the heart muscle and the inability to pump blood efficiently. The degree of dysfunction is proportional to the duration and severity of alcohol consumption, with continued heavy drinking leading to an enlarged heart. The purpose of this project is to understand how excessive, chronic alcohol consumption causes structural and functional damage to the heart at the molecular level. Detailed understanding of the defects caused by alcohol will allow for a better understanding of the molecular events surrounding the onset of alcohol-induced heart disease and may allow for the development of targeted therapies.

### **Duration of Project**

1/1/2009 - 6/30/2010

### **Project Overview**

The long-term goal of this project is to understand the mechanisms by which alcohol consumption induces myofibrillar damage characteristic of alcoholic heart muscle disease. Alcohol abuse is associated with an increased premature mortality partly resulting from the development of an alcohol-induced cardiomyopathy, a condition diagnosed in approximately 35% of those individuals who chronically consume excessive amounts of alcohol. Although the mechanisms leading to alcohol-dependent myocardial dysfunction are multi-factorial, altered expression of myocardial proteins stands out as a central mechanism. Alcohol consumption inhibits rates of protein synthesis in heart at the level of mRNA translation. By understanding the alterations in the process of mRNA translation it is hoped that new strategies could be developed to combat the pathologic derangements in cardiac muscle structure and function associated with chronic alcohol abuse. We delineated two regulatory steps in the process of protein synthesis, the formation of an active eIF4E-eIF4G complex and the process of elongation that are responsible, in part, for the inhibition of protein synthesis during chronic alcohol administration, whereas acute alcohol intoxication only affects the formation of an active eIF4E-eIF4G complex. We hypothesize that the normal signaling pathway through mTOR responsible for maintaining the functioning of these two steps in protein synthesis at rates observed in control animals is severely compromised by alcohol intake. The net effect is manifested through alterations in the expression of myocardial proteins, including contractile proteins. We further hypothesize that provision of amino acids either through acute gavage or meal feeding to rats administered alcohol can stimulate mTOR leading to an acceleration of rates of protein synthesis. The experimental design for the project period will test the hypothesis that inhibition of protein synthesis in response to chronic alcohol feeding shifts myocardial protein expression. Overall, the research design will establish the mechanism by which alcohol reduces myocardial protein synthesis.

## **Principal Investigators**

Thomas C. Vary, PhD  
Distinguished Professor  
Penn State College of Medicine  
Cellular & Molecular Physiology (H166)  
500 University Drive  
Hershey, PA 17033

## **Other Participating Researchers**

None

## **Expected Research Outcomes and Benefits**

An alarming 35% of chronic alcohol abusers suffer from a dilated heart, and once the heart muscle becomes enlarged there is no means to return it back to normal. Therefore, it is crucial that these functional changes be identified early. This project will link the progression of structural and functional changes seen via echocardiography to specific alterations in protein expression as a result of chronic alcohol intoxication. By examining this relationship between structural and functional alterations to changes in the content of various proteins, we should be able to define alcoholic heart muscle disease at a molecular level.

## **Summary of Research Completed**

The development of alcoholic heart muscle disease is a complex process involving derangements in numerous pathways. The characteristic feature of alcoholic heart muscle disease is a thinning of the ventricle wall. Remodeling of the ventricular wall requires coordinated changes in multiple cellular compartments. Alcohol-induced cardiomyopathy remains poorly understood despite contributing to about one-half of all cases of heart failure. Heretofore, no systematic analysis of the protein level has been reported, although there are individual reports of changes in some but not all subcellular fractions. An increased understanding of the changes of protein profiles in response to ethanol is important in understanding the pathogenesis of alcoholic cardiomyopathy.

In the studies supported by this funding mechanism, the expression of myocardial proteins was analyzed using a proteomic approach with ICAT technology. The time course of 16 weeks of ethanol consumption was selected because there is evidence of 1) thinning of the ventricular wall at this time based on echocardiography and 2) changes in selective protein content. The ICAT proteomic method labels individual peptides, measures the relative amount of peptide peaks, identifies the peptides with tandem mass spectrometry, and then identifies and quantifies proteins through these identified peptide species. Individual MS/MS spectra were searched against a human sequence database, and a variety of recently developed, publicly available software applications were used to sort, filter, analyze, and compare the results. Although differences in peptide levels could reflect dissimilarity in protein isoforms, multiple peptides covering various locations in the protein sequence contributed to the identification for each of the proteins listed.

The observed ratio between the signal intensities for the unfragmented isotopically-labeled “light” and “heavy” forms of the same peptide yields the relative abundances of that peptide, and hence the protein from which it was derived, in the original samples.

Previously known changes in some proteins were correctly identified by ICAT analysis of peptides, showing that the use of the ICAT gives results consistent with assessment of proteins via Western blot. Both experimental and control groups were given equally nutritionally adequate diets emphasizing that alcohol induces alterations in specific heart muscle proteins and these changes are evident even when the nutrition is the same across groups. We distinguished significant changes in heart proteins in animals fed alcohol compared to pair-fed controls. Chronic ethanol consumption (>15 weeks) depresses actin and myosin content. In the present studies, proteins associated with the contractile elements (myosin alkali light chain 3, myosin alkali light chain 4, heavy chain myosin, actin) were uniformly reduced following feeding a diet containing ethanol.

The decrease in mitochondrial proteins associated with energy metabolism are consistent with observations that mitochondrial respiratory rates and the efficiency of phosphorylation were depressed in rats given 25% alcohol for six months. However, not all proteins identified in this study were decreased upon ethanol exposure. For example, cytochrome b-c1 complex subunit 2, 2,4-dienoyl-CoA reductase, and 28S ribosomal protein S35 were elevated.

Supporting the idea that albumin may be specifically decreased by chronic alcohol ingestion; albumin synthesis by the isolated perfused rat liver was significantly reduced by acute alcohol exposure. Reductions in some of these plasma proteins, including albumin, can be a sign of hepatic dysfunction or protein malnutrition. However, in these studies there is no sign of protein malnutrition, and hence the decrease in albumin most likely represents a failure of the liver to synthesize albumin.

Hemopexin is the plasma protein with the highest binding affinity to heme among known proteins. It is mainly expressed in liver, and belongs to acute phase reactants. Heme is potentially highly toxic because of its ability to intercalate into lipid membranes and to produce hydroxyl radicals. The binding strength between heme and hemopexin, and the presence of a specific heme-hemopexin receptor able to catabolize the complex and induce intracellular antioxidant activities, suggest that hemopexin is the major vehicle for the transportation of heme in the plasma, thus preventing heme-mediated oxidative stress and heme-bound iron loss. As hemopexin is reduced as a result of chronic alcohol intake, this may be a source of reactive oxygen species formation.

Selective protein degradation by the ubiquitin-proteasome pathway has emerged as a powerful regulatory mechanism in a wide variety of cellular processes. Ubiquitin conjugation requires the sequential activity of three enzymes; the ubiquitin-activating enzyme (E1), the ubiquitin-conjugating enzyme (E2), and the ubiquitin-protein ligase (E3). The SCF (Skp1, Cullin, and F-box protein) E3 complex, which is one type of ubiquitin ligase, mediates ubiquitination of proteins targeted for degradation by the proteasome. The function of the F-box protein is to interact with target proteins via protein-protein interaction motifs including leucine rich repeats and tryptophan-aspartate (WD) repeats. The latter domains promote binding of phosphorylated

proteins to the SCF complex. In addition to the ubiquitin-dependent proteolytic pathway, feeding rats a diet containing ethanol affected proteins associated with the lysosomal degradative pathway. In contrast to F-box protein, alcohol ingestion was associated with a 60% increase in P2B/LAMP-1, a lysosomal protein.

One potential mechanism to account for the altered expression of proteins is the generation of reactive oxygen species in hearts from rats fed a diet containing ethanol. In this regard, there are redundant enzymatic systems to control the concentration of reactive species. To this end, chronic alcohol intoxication was associated with reductions in peroxiredoxin 5, antioxidant protein 2, and glutathione transferase 5. Antioxidant protein 2 is the member thiol-specific antioxidant gene family that removes H<sub>2</sub>O<sub>2</sub>, and in doing so protects proteins, DNA, and lipids from oxidative stress. Overexpression of antioxidant protein 2 protects the pancreas from oxidative stress induced by diabetes. Peroxiredoxin, the antioxidant component of the thioredoxin superfamily, have gained recognition as important redox regulating molecules relevant to the mechanisms underlying ischemia-reperfusion injury. In the present study, the expression of antioxidant protein 2 and peroxiredoxin 5 were reduced by 30%. Likewise, the glutathione-S-transferases catalyze the reaction of the major low molecular mass thiol, glutathione, with reactive oxygen species to form thioesters. The production of increased reactive oxidative defenses could result in the accumulation of reactive oxygen species and cause oxidative stress in the myocardium. Elevated reactive oxygen species affect function of myocardial cells through oxidation of other molecules including DNA, lipids, and proteins.

While much of the discussion is directed towards proteins whose ICAT analysis suggests a decrease in protein content, other peptides suggest proteins are elevated. In particular, proteins associated primarily with the cytosolic fraction appear elevated (CD122, 60 kDa SS-A/Ro ribonucleoprotein, lysosome-associated membrane glycoprotein 1, heat shock 70 kDa protein 14, hepatocyte growth factor-regulated tyrosine kinase substrate, hemogen, suppression of tumorigenicity 5, tyrosine-protein kinase receptor UFO, ribonuclease 1, mitogen-activated protein kinase phosphatase 2, and ras association domain-containing protein 10).

In summary, the results of the present investigation provide evidence that myofibrillar, mitochondrial, glycolytic, membrane-associated, cytosolic, and plasma proteins in cardiac muscle are altered following chronic administration of ethanol. The identified proteins presented, for the first time, represent a detailed analysis of some of the proteins affected by long-term alcohol consumption. Specifically, this study used a mass spectrometry-based proteomic approach to identify differentially deregulated proteins in the myocardium following feeding rats a diet containing ethanol. Chronic alcohol appears to have selective effects on particular proteins, and the effects were not directly ascribed to overt malnutrition. This may explain some of the functional and morphological characteristics observed in alcohol-induced heart muscle disease, including reduced contractility. Further investigations on the role of these deregulated proteins may shed new insights into developing novel therapeutic approaches for patients who abuse alcohol.

## **Research Project 15: Project Title and Purpose**

*Development of Nanoliposomal Therapeutics for Leukemia* - Leukemia is a cancer of the blood which is expected to cause 21,710 deaths in 2008 in the United States. Research continues to find mutations that cause leukemia. Inhibitory RNA (RNAi) is a silencing mechanism that turns off a gene. RNAi directed at a cancer-causing mutation can specifically kill cancer cells. However, RNAi must be delivered to cells and protected from degradation in order to work. Small vesicles called nanoliposomes create an efficient and non-toxic delivery vehicle for RNAi as well as other drugs. Another drug that selectively kills cancer cells is ceramide. Ceramide is a lipid produced in the body during many chemotherapy treatments that is partly responsible for the action of these drugs. This project seeks to test anti-leukemia treatment with nanoliposomes containing ceramide, RNAi, or both, initially in mouse and ultimately in future projects in human leukemia.

### **Duration of Project**

5/1/2009 – 6/30/2010

### **Project Overview**

Human acute leukemias represent a growing public health problem. For most patients with these lethal disorders, no truly new therapies have been brought to the clinic in the last 30 years. However, much biological information is now available concerning the varied molecular pathways mutated and involved in the pathogenesis of these diseases. This body of knowledge is best exemplified by observations of bcr-abl, a mutation in chronic myelogenous leukemia also responsible for many cases of adult acute lymphoblastic leukemia. The successful targeting of this molecule with small inhibitors represents a rare bright spot in the development of targeted therapy for human leukemias.

The nanotherapy expertise at Penn State presents a unique opportunity to drive the development of targeted therapies for cancer in general and leukemia in particular. The abundance of molecularly defined therapeutic targets in human leukemias makes these diseases attractive for therapy via nanotechnology. This project seeks funding for a nascent collaboration utilizing hematology-oncology and nanoliposomal expertise.

*Specific Aim 1: Optimize nanoliposomal ceramide for therapy of leukemic mice.* Nanoliposomal ceramide has been shown to be an effective anti-cancer therapeutic agent in multiple solid tumor models and shows *in vitro* activity against murine leukemia. This aim will explore doses and schedules to optimize the therapeutic effect of this preparation in a murine model of myeloid leukemia.

*Specific Aim 2: Develop ceramide-cationic nanoliposomes containing anti-bcr-abl siRNA for therapeutic depletion of bcr-abl in vitro.* The effect of anti-bcr-abl siRNAs will be assayed for ability to knock down the bcr-abl transcription and translation products in bcr-abl expressing cell lines when delivered in a ceramide-cationic liposomal formulation.

*Specific Aim 3: Evaluate the anti-leukemic effect of anti-bcr-abl siRNA with and without ceramide in an in vivo mouse leukemia model.* The material with the highest capacity to knock

down bcr-abl, as identified in *Specific Aim 2*, will be tested for *in vivo* activity against a bcr-abl-dependent leukemogenic murine line. RNAi targeted to bcr-abl will be tested for the ability to decrease tumor burden and extend survival of leukemia-challenged mice.

### **Principal Investigators**

David F. Claxton, MD  
Professor of Medicine  
Penn State Milton S. Hershey Medical Center  
500 University Drive  
Hershey, PA 17033

### **Other Participating Researchers**

Mark Kester, PhD, Nikki R Keasey, PhD, Sriram Shanmugavelandy – employed by Penn State Milton S. Hershey Medical Center

### **Expected Research Outcomes and Benefits**

An important challenge in the field of oncology is to kill cancerous cells while leaving healthy cells unharmed. While treatments exist that can kill cancerous cells, side effect profiles are not ideal due to harmful effects on normal cells in the body. This project aims to develop very small or nano-scale liposomes which successfully kill or control leukemia but leave normal cells unharmed. The intent is to bring these products to the clinic and ultimately contribute to the cure of these otherwise lethal diseases.

Specifically this project will combine ceramide, a natural material which kills cancer cells, with RNAi. RNAi is a silencing mechanism that can turn off genes. This technology can be targeted to cancer-causing genes which may be active in particular leukemias. Because normal cells do not contain the cancer-causing gene, they will be unharmed by the silencing. However, cancer cells cannot tolerate the inactivation of the cancer gene, and will undergo cell death.

A challenge to RNAi-mediated therapies is the delivery of the RNAi molecules to cells, and the protection of these molecules from degradation. The packaging of these molecules into very small complexes called nanoliposomes provides protection from degradation and can also facilitate delivery of liposomal contents to cells. In this way, the nanoliposomal expertise will aid in the development of RNAi-based therapies for the clinic. This technology can be readily tested with mouse leukemia models currently in use in the Claxton lab.

### **Summary of Research Completed**

#### Materials and Methods

##### Colony formation assay

Colony assays were performed in 12-well plates using Methocult complete media for human cells according to manufacturer's instructions (H4434 StemCell Technologies, Vancouver, Canada). Briefly, cryopreserved primary patient samples were thawed, washed, and allowed to

recover for 2-3 hours in RPMI + 10% FBS. A 10x cell stock was made in IMDM + 2% FBS (StemCell Technologies, Vancouver, Canada) and combined with 9 volumes medium containing the appropriate concentration of liposome. Components were vortexed and allowed to settle. A syringe and blunt tip needle were used to deliver 0.5 mL to each of three wells per condition. Colonies of 10 or more leukemic blasts or 50 or more cord blood stem cells were counted following an incubation of 10-12 days in a humidified chamber at 37° and 5% CO<sub>2</sub>.

#### Animal studies

32D cells (congenic with C3H/HeJ mice) transformed with BCR-ABL and transfected to stably express the green fluorescent protein molecule were obtained as a kind gift from Dr. Ling. Animals received leukemia infusions via IV tail vein injection. Injection of 1 x 10<sup>6</sup> cells yielded reliable leukemic death and thus was administered for all subsequent experiments. Male C3H/HeJ mice were obtained from Charles River Laboratories at 7-8 weeks of age. Animals were kept in conventional animal facilities using minimum conventional feed and water and were monitored for illness and survival. Using the models described here, lethargy and inability to feed preceded death by less than 24 hours. Thus, the primary experimental endpoint was death or near moribund status requiring sacrifice. All procedures were reviewed and approved by the Penn State Institutional Animal Care and Use Committee.

#### Analysis of peripheral blood

To analyze circulating tumor burden in some experiments, blood was subjected to flow cytometric analysis for quantification of 32D/BA-GFP cells. Blood (15 µL) was drawn via tail snip and red blood cells were lysed in 200 µL RBC lysis solution (5 Prime, Gaithersburg, MD). White blood cells were pelleted by centrifugation for 2 min in an Eppendorf 5415 C centrifuge at 300 x g, washed in 1 ml phosphate-buffered saline (PBS) and resuspended in 400 µL PBS. Analysis was performed on a FACS Calibur instrument. List Mode multiparameter data files (each file with forward scatter, side scatter, and 4-fluorescent parameters) were analyzed using CellQuest Pro Software. Files were gated to exclude red cell debris. A minimum of 20,000 gated events was acquired.

#### Nanoliposomal ceramide treatment

To prepare the neutral, C6 ceramide-containing, nanoliposome, aliquots of DSPC (1,2-distearoyl-*sn*-glycero-3-phosphocholine), DOPE (1,2-dioleoyl-*sn*-glycero-3-phosphoethanolamine), DSPE-PEG2000 (1,2-distearoyl-*sn*-glycero-3-phosphoethanolamine-N-[methoxy(polyethylene glycol)-2000]), C8-Ceramide-PEG750 (N-octanoyl-D-*erythro*-sphingosine-1-[succinyl(methoxy(polyethylene glycol))-750]), and C6-Ceramide (N-hexanoyl-D-*erythro*-sphingosine), initially prepared in chloroform, were made in a 3.75:1.75:0.75:0.75:3 molar ratio. To prepare the neutral, non-ceramide, ghost nanoliposome, aliquots of DSPC, DOPE, and DSPE-PEG2000, initially prepared in chloroform, were made in a 5.66:2.87:1.47 molar ratio. All aliquots were completely dried under a stream of N<sub>2</sub> gas. The dried mixtures were re-suspended in an isotonic 0.9% NaCl hydration fluid, heated to 60°C, and sonicated until light no longer diffracted through the suspensions. The suspensions were quickly extruded through a 100 nm polycarbonate filter, using an Avanti Mini Extruder, at 60°C, and cooled on ice to room temperature.

Treated animals received PBS, ghost nanoliposome, or C<sub>6</sub> ceramide nanoliposome by IV (intravenous tail vein injection). Treatments began on day 3 post-leukemic challenge and continued until day 24. IV administration volume was 100 µL.

### Statistical Analysis

Animal survival was documented by the method of Kaplan and Meier and statistical significance of survival data was analyzed by the Mantel-Cox log-rank test using GraphPad Software version 5.00 for Windows, San Diego California USA, [www.graphpad.com](http://www.graphpad.com). This software was also used to plot and analyze data using the Student's t-test.

### Results

Ceramide nanoliposomal treatment has been shown to slow expansion of 32D Bcr-Abl cells *in vivo* as measured by flow cytometry (Figure 1). This slowed tumor progression is associated with extended survival of leukemic C3H/HeJ mice (Figure 2).

The survival benefit seen during ceramide treatment is statistically significant, but it is possible that a combinatorial therapy will further extend survival in an additive or synergistic manner. To explore this possibility, we have initiated studies of the microtubule inhibiting chemotherapeutic vincristine in combination with ceramide nanoliposomes. KG-1 is a human AML line that shows minimal cell cycle disturbances in the presence of 0.01 µM vincristine or 24 µM ceramide liposome treatments (Figure 3). However when these drug treatments are combined, a strong induction of sub-G1 debris is present as well as a sharp increase in G2 arrest. These results are consistent with a synergistic interaction between ceramide and vincristine, and this drug combination warrants further study.

Ceramide liposomes, but not ghost liposomes, inhibit the formation of colonies by primary AML cells in semi-solid medium (Figure 4).

Lipofection with siRNA designed against Bcr-Abl was found to decrease viability of Bcr-Abl positive human cell line K562 while scrambled siRNA control had no effect (Figure 5). U937, a Bcr-Abl<sup>-</sup> cell line, was unaffected by lipofection with these molecules (data not shown).

In conclusion, these studies indicate that ceramide nanoliposomes are active against leukemia cell lines, human primary AML cells, and murine leukemia. Ceramide shows promise in combinatorial therapy with the cytotoxic agent vincristine and the suggestion of a synergistic interaction between these compounds shows great promise. Additionally, siRNA molecules have been successfully directed against Bcr-Abl as measured by viability assays. These findings are expected to result in publication as a result of the funding made possible by this feasibility grant.

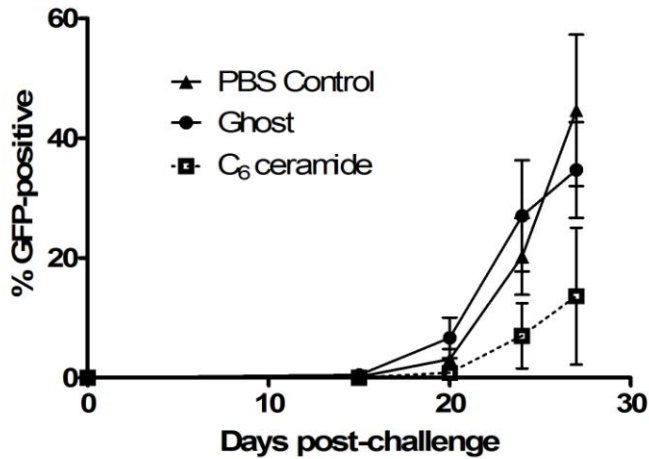


**Figure 1.** C3H/HeJ mice were rendered leukemic by tail vein injection of  $10^6$  32D Bcr/Abl-GFP cells. Mice were treated every 2-3 days with tail vein injections of C<sub>6</sub> ceramide liposomes (36 mg/kg), or ghost liposomes (liposomes containing all lipids except C<sub>6</sub> ceramide). Flow cytometry reveals a slower tumor progression trend in ceramide treated mice relative to PBS or ghost liposome treated mice. (mean and standard error of the mean are shown, n = 5)

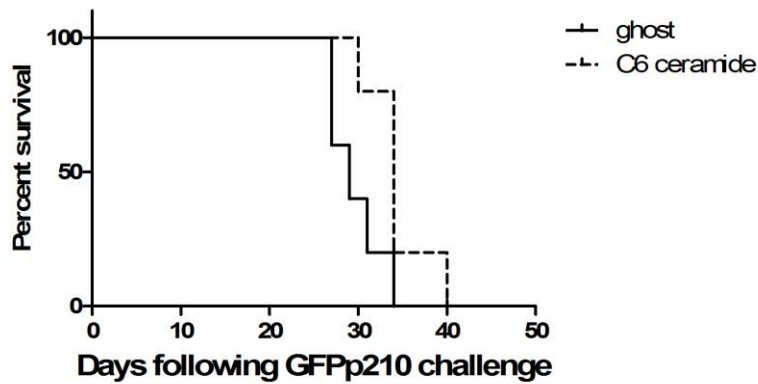


**Figure 2.** Nanoliposomal ceramide improves survival of C3H/HeJ mice with myeloid leukemia. C3H/HeJ mice were rendered leukemic by tail vein injection of  $10^6$  32D Bcr/Abl-GFP cells. Mice were treated every 2-3 days with tail vein injections of C<sub>6</sub> ceramide liposomes (36 mg/kg), or ghost liposomes (liposomes containing all lipids except C<sub>6</sub> ceramide). Survival is extended in ceramide-treated mice (ghost vs. ceramide,  $p < 0.05$ ).

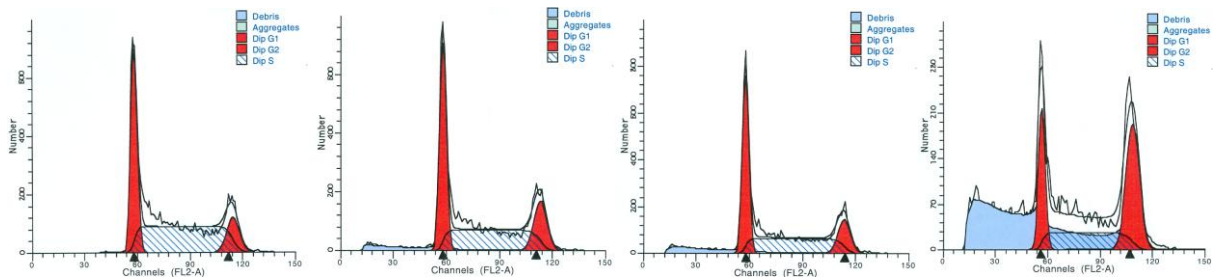


**Figure 3.** KG-1 cells were grown for 48 hours in the absence of drugs (1<sup>st</sup> panel), in the presence of 0.01 μM vincristine (2<sup>nd</sup> panel), 24 μM C<sub>6</sub> ceramide (3<sup>rd</sup> panel), or 0.01 μM vincristine and 24 μM C<sub>6</sub> ceramide.

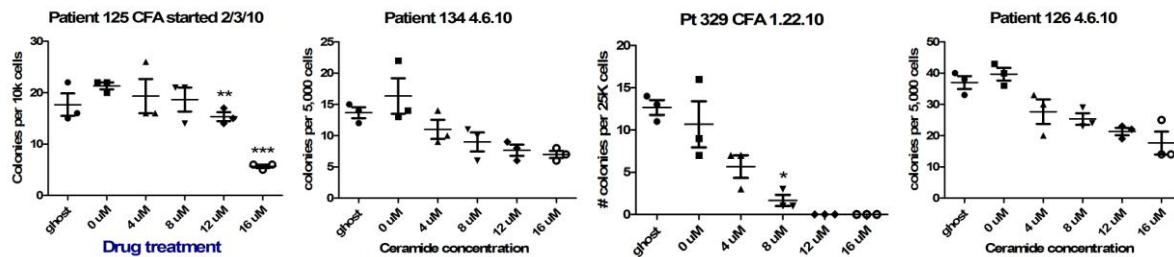


**Figure 4.** Primary human AML cells were grown for 10-12 days in semi-solid medium containing the indicated concentration of ceramide or ghost nanoliposomes. Ceramide inhibits colony formation in a dose-dependent manner. (\* p<0.05, \*\* p<0.01, \*\*\* p<0.001)

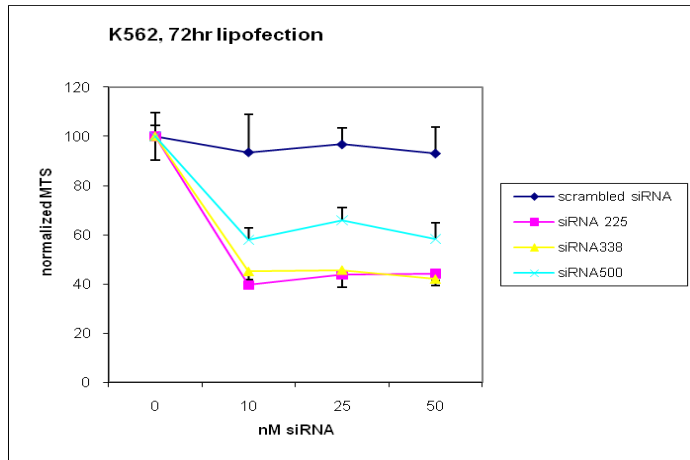


**Figure 5.** K562 cells were lipofected with three siRNA molecules directed against the Bcr-Abl fusion, or a scrambled control. Following a 72-hour incubation, an MTS assay was performed. Each anti-Bcr-Abl siRNA decreased MTS signal at the concentrations tested.

## **Research Project 16: Project Title and Purpose**

### *P16 Alteration and BRAF Mutation and Patient Outcomes in Papillary Thyroid Cancer -*

Thyroid cancer represents the most common endocrine malignancy, with papillary thyroid cancer (PTC) accounting for 90% of malignant thyroid tumors. Although outcome is generally favorable, a group of patients develop local recurrence and/or distant metastases and ultimately die of their disease. For these patients with aggressive disease, better diagnostic and prognostic tools are clearly needed. Molecular markers that accurately predict tumor behavior are lacking. In the past, p16 gene alterations and BRAF mutations have individually been implicated in tumor aggressiveness in PTC. We hypothesize that presence of these mutations simultaneously in patients with PTC is a predictor of worse clinical outcomes and tumor aggressiveness.

### **Anticipated Duration of Project**

5/1/2009 – 6/30/2011

### **Project Overview**

Papillary thyroid carcinomas (PTC) represent about 90% of all thyroid cancers. Although, incidence of PTC has increased in recent years, the mortality has remained low. There is a subgroup of high risk patients with PTC that develop local recurrence and/or distant metastases and ultimately die of their disease. Genetic markers are clearly needed to prognosticate disease-specific mortality, risk of recurrence and death risk in PTC. Several studies have shown that BRAF mutations may confer worse clinical prognosis in PTC. Alterations of the tumor suppressor gene p16 are common in human cancers. Its role in thyroid cancer is not clearly defined. Although BRAF mutation clearly indicates poor outcomes in PTC, p16 as it relates to aggressive thyroid cancer is not well studied and certainly the outcome of thyroid cancer patients whose tumor harbors both the genetic aberrations have never been studied. We propose that in the presence of BRAF mutation, the presence of p16 protein expression is associated with tumor aggressiveness and worse clinical outcomes.

*Specific Aims:* 1) To analyze surgical specimens of PTC for the presence of p16 alterations and BRAF mutations. 2) To correlate the concurrent presence of p16 alterations and BRAF mutations with patient outcomes as manifested by distant metastases, local recurrence and loss of iodine avidity.

*Research Design and Methods:* Retrospective study. We will collect thyroid tissue from 30 patients with PTC that underwent surgery at HMC along with 30 normal thyroid samples (controls). Tissue samples were cryofrozen after surgery and then held in the Penn State Cancer Institute (PSCI) Tissue Bank. Tissue will be allocated to the basic scientist lab, for p16 and BRAF analysis. AS-PCR will be performed to screen for the (V600E) BRAF mutation. P16 protein expression will be detected by Immunohistochemistry. Subsequently we will make the correlations between the presence of these markers and clinical outcomes.

## **Principal Investigators**

David Goldenberg, MD, FACS  
Associate Professor of Surgery  
Director, Head and Neck Surgery  
Department of Surgery  
Penn State University College of Medicine  
500 University Drive-H091  
Hershey, PA, 17033

## **Other Participating Researchers**

Gavin P Robertson, PhD, Saima Durvesh, MD, Andrea Manni, MD, David Mauger, MD, SubbaRao Madhunapantula, PhD – employed by Penn State College of Medicine, Milton S Hershey Medical Center

## **Expected Research Outcomes and Benefits**

We expect that 30% of the samples will test positive for both p16 alteration and BRAF mutation and these will be the patients with the poorest clinical outcomes at presentation. These include short term signs of aggressive disease such as large tumor size, extra-capsular spread and local metastasis. With the findings from this pilot study, we anticipate to propose a larger scale, randomized clinical study to further look at the correlation between these mutations, the long term follow up including development of iodine resistance and the effect on long term survival.

Correlation between p16 and BRAF, if confirmed, will serve as a diagnostic and prognostic tool to help us identify the high-risk subgroup of patients with PTC that have the potential to develop aggressive cancers. These are the patients that stop responding to conventional treatment and ultimately die of their disease. These patients may benefit from earlier more aggressive treatment, with potential improvement in overall clinical prognosis. Thus, *our project has the potential to impact human health by providing better tools to diagnose and treat a more deadly form of thyroid cancer.*

## **Summary of Research Completed**

This is a study with correlative type objectives, which have been performed during the execution of the project. The Specific Aims are 1) to analyze surgical specimens of PTC for the presence of p16 alterations and BRAF mutations. 2) To correlate the concurrent presence of p16 alterations and BRAF mutations with patient outcomes as manifested by distant metastases, local recurrence and loss of iodine avidity.

The following has been accomplished. Thyroid tissue from 30 patients with PTC that underwent surgery at HMC along with 30 normal thyroid samples (controls) have been collected according to an IRB approved protocol, which is a part of this study. Tissue samples were cryofrozen after surgery and then held in the Penn State Cancer Institute (PSCI) Tissue Bank. These samples were processed to obtain protein or DNA using standard techniques. Samples have been

analyzed by Western blotting to measure levels of pAkt or pErk. BRAF mutational analysis has also been undertaken using AS-PCR to screen for the (V600E) BRAF mutation. Finally, P16 protein expression is being measured by Immunohistochemistry.

Methods. The methods used for this project are routine. Western blotting is a standard technique, as too is, ASPCR for the (V600E) BRAF mutation. The p16 immunohistochemistry is also an established technology

Results of data generated and analyzed. The project is still in the data collection stage. Results of Western blotting suggest unique patterns of pAkt and pErk expression; however, data analysis is still pending. ASPCR and p16 data collection are underway. Finally, correlation between the presence of these markers and clinical outcomes remains to be completed.

### **Research Project 17: Project Title and Purpose**

*The Interaction of Environmental Agents and LDL-Cholesterol in Parkinson's Disease* - This project seeks to characterize the apparently paradoxical observation that low cholesterol (LDL-C) is a risk factor for Parkinson's disease (PD), and to examine some of the possible underlying mechanisms. One aim is to collect pilot data and support the planning of testing the association between low LDL-C and PD further via a prospective study in the "Atherosclerosis Risk in the Communities" (ARIC) cohort. The second aim is to test the idea that lower LDL-C is etiologically-linked to PD because it affects the distribution or toxicity of trace environmental toxicants. The data provided by this pilot study will set the stage for more detailed examination of the health consequences of these findings and their underlying mechanisms with the collaboration of a PD clinician, epidemiologist, and basic neuroscientist.

### **Anticipated Duration of Project**

5/1/2009 – 6/30/2011

### **Project Overview**

Parkinson's disease (PD) is the second most common, age-related neurodegenerative disorder about which there are many unexplained "paradoxes". PD patients are generally more cardiovascularly-healthy than controls. Smoking, a major cardiovascular risk factor, is protective in PD. Whereas the apolipoprotein E (APOE)  $\epsilon$ 4 allele is associated with increased risk of Alzheimer's disease (AD), it is the  $\epsilon$ 2 allele that we have linked to increased PD prevalence. Interestingly, the  $\epsilon$ 2 allele is associated with lower plasma low-density lipoprotein-cholesterol (LDL-C), longevity in general, and lower risk of AD. Such paradoxes led to the central hypothesis that lower LDL-C is associated with increased risk of PD. Four studies have provided early support for this hypothesis. If confirmed, this hypothesis may have critical clinical and public health impact, especially if lower LDL-C is etiologically linked to PD. The first aim is to test the central hypothesis with a prospective study using the "Atherosclerosis Risk in the Communities" (ARIC) cohort. The ARIC cohort of ~16,000 participants, with baseline fasting lipid profiles since 1986, could provide a rigorous test of our central hypothesis already supported by four prior studies. We shall perform preliminary data analysis on these PD cases,

establish feasible PD case validation procedures, and plan for a successful independent grant application to further the research in this cohort. The second aim is to test the hypothesis that peripheral cholesterol-APOE status affects the metabolism and or central entry of toxicants that can cause Parkinson's like damage. This work will focus on the hypothesis that low cholesterol either increases central nervous system (CNS) availability of environmental toxicants, or affects repair associated with injury. We shall modify cholesterol levels using dietary manipulations and test the effects of rotenone and MPTP, two human-relevant model toxicants. We shall inject these compounds at various doses, and follow the toxicokinetics of the parent compounds and some selected metabolites using high-performance liquid chromatography (HPLC)/mass spectroscopy. In addition, we shall assess the effects of these compounds on brain dopamine neuronal function and integrity initially using neurochemical approaches. Together, these experiments will provide important data that might link genetic and environmental factors in the causation of "idiopathic" PD.

### **Principal Investigators**

Richard B. Mailman, PhD  
Professor and College of Medicine Distinguished Senior Scholar  
Penn State University College of Medicine  
Department of Pharmacology, R130  
500 University Dr.  
Hershey PA 17033-0850

### **Other Participating Researchers**

Xuemei Huang, MD, PhD – employed by Penn State Hershey Medical Center

### **Expected Research Outcomes and Benefits**

The clinical arm of this study will be an important addition to the existing literature suggesting the surprising idea that lowering cholesterol levels without a specific medical rationale may have unforeseen negative consequences. If this idea is supported by Aim 1 of this study, then low cholesterol may be important in other neurodegenerative diseases as well. If true, it may suggest caution in the practice of giving medication to lower cholesterol when a patient is not at cardiovascular risk.

The second aim is the first attempt to elucidate possible mechanisms that may be involved in the clinical findings. There are three general types of mechanisms by which low cholesterol may predispose to Parkinson's disease, and the proposed studies test one of these hypotheses rigorously.

In total, we expect that the studies will provide further support for the central hypothesis that lower LDL-C is associated with an increased risk of PD, and also provide pilot data that lower LDL-C cholesterol might be etiologically linked to PD via changing the CNS availability of environmental toxicants. These data will have critical clinical and public health impact, and

warrants larger scale projects that we shall pursue using National Institutes of Health (NIH) or foundation extramural grants.

## **Summary of Research Completed**

We summarize the progress on each of our two specific aims.

### *Aim 1: Test the central hypothesis further in the “Atherosclerosis Risk in the Communities” (ARIC) prospective cohort.*

The ARIC cohort of ~16,000 participants, with baseline fasting lipid profiles since 1986, is an excellent testbed of our central hypothesis. We have gained approval from ARIC Committee to gather preliminary data in this cohort by identifying potential PD cases through self-reporting, medication history, and death records. Initial analysis of the relationship between potential PD subjects and cholesterol levels did not show a significant association between the occurrence of PD and fasting cholesterol profiles (both at baseline and follow-ups). A major problem, however, is that potential PD subjects identified by self-report, or by medication, or death records can be confounded by high rates of false positive diagnoses. For example, self reported Parkinson's disease may include many subjects with Parkinson's look-alike diseases such as Progressive Supranuclear Palsy (PSP), multisystem atrophy (MSA), normal pressure hydrocephalus, essential tremor, or stroke-related parkinsonism, etc. Moreover, potential cases identified by medication also can be confounded by a restless leg syndrome (RLS) that recently became a popular diagnosis and uses similar medication to Parkinson's disease, but with very different pathoetiology.

To tease out the false diagnosis of Parkinson's disease from idiopathic Parkinson's disease, Dr. Huang has been working closely with Dr. Honglei Chen (from NIEHS), Dr. Tom Mosley (ARIC PI at Jackson, MI center), and Dr. Alvaro Alonso (ARIC PI at the University of Minnesota) to develop a case-confirmation strategy. This strategy will include interviewing all potential PD subjects identified from the self report or medication list. With each subject's permission, we are going to contact the treating physician and Dr. Huang will review the records of each of these potential subjects. This endeavor had gained approval from ARIC committee, and is partially funded by NIEHS. All the forms have been developed and in the process for IRB approval of each of the ARIC coordinating centers..

In addition, we became aware of a second cohort that would allow prospective testing of the hypothesis that lower plasma cholesterol may be associated with faster progression (in addition to prevalence) of PD. These cohorts were from the Parkinson's Study Group DATATOP and PRECEPT studies. Because there were no funds for this extension of Aim 1, we wrote an application to the PSG requesting access to this important dataset, as well as funds to perform needed analyses. This competitive application was funded (see above), and the work has been completed, and is an integral part of this Aim.

The DATATOP and PRECEPT data are important because they were two large neuroprotection studies that took place in two distinct epochs in relationship to the availability of statins. The DATATOP study started in late 1980's (pre-statin era), whereas PRECEPT began in the mid-

2000's after FDA statins approvals in mid-late 1990's. This unique feature can help to explore potentially intriguing relationships among cholesterol and statins in relation to PD. Our initial case control studies found a negative association between statin usage and PD occurrences, a finding supported independently by two groups but contradicted by two others. The possible negative association between statin usage and PD occurrence, coupled with possible neuroprotective properties independent of its cholesterol lowering properties has prompted a data-mining effort by the epigenetic work group of the PSG.

*Aim 2 Progress: Testing the hypothesis that peripheral cholesterol-APOE status affects the metabolism and or central entry of toxicants that can cause Parkinson's like damage.*

We are testing the working hypothesis that cholesterol status influences the metabolism and/or distribution of trace toxicants to which PD-susceptible people are exposed, or alternately, that cholesterol status influences the distribution of such toxicants, permitting greater entry into the brain. The model toxicants we plan to use are rotenone (modestly dopaminergically selective) and MPTP (highly selective). Aim 2 has progressed more slowly. The study depended on having high and cholesterol groups, and the first step was to determine how long dietary intervention was needed before a stable concentration of blood cholesterol was reached. We therefore established two groups of mice: one fed a high-cholesterol diet and one fed a low-cholesterol diet. The mice have now been on their respective diets for 29 weeks. Because we needed to confirm cholesterol status without sacrificing the mice, we required an assay kit that could measure cholesterol from very small serum samples that were collected via a submandibular bleed. We purchased a commercial enzymatic test kit for this purpose from Biovision that required only 2 µL of serum per assay. Unfortunately, this experiment-limiting test has been highly problematic. Initially, we found average levels of 337 mg/dL for the high-cholesterol group and 241 mg/dL for the control group. Although the reproducibility of the assays was good, we hypothesized that the values were inaccurate since they were far higher than expected from the literature when similar manipulations were done.

Therefore, we collected pooled serum samples from each group, and had them assayed by the Penn State Hershey Medical Center clinical laboratory. The results that we have recently gotten showed that the high-cholesterol group has a value of 296 mg/dL whereas the control mice had a value of 124 mg/dL. These values are in the range that we had predicted, and indicate that the dietary manipulation is working, but that the microassay we had used was problematic. It should be noted that blood can only be collected from the mice safely every three weeks, so it has necessary to run follow-up assays around this schedule. We are now in the process of testing a newer version of the assay provided by Biovision (at no cost), in which Biovision's representatives believed there may be a problem with the original stock standard. The new assay will be compared to the clinical lab results to verify if it works. Once this is accomplished we can initiate the planned studies on effects of the neurotoxicants. In addition, while the cholesterol issues are being resolved, we have made operational the needed HPLC assay for dopamine and metabolites.

## **Research Project 18: Project Title and Purpose**

*Moving Experimental Cancer Therapeutics from the Research Bench to the Clinic* - The Penn State Melanoma Therapeutics Program has a Therapeutic Drug Portfolio of ~20 experimental therapeutic compounds at various stages of development. Unfortunately, agents proceed through preclinical development at which point progress halts. The purpose of this project is to establish the necessary expertise and infrastructure to more rapidly move these compounds to the clinic. This involves developing interactions with companies to make clinical grade compound for testing in patients; undertaking necessary toxicological and pharmacological evaluation for an Investigational New Drug (IND) application; and interacting with the Food and Drug Administration (FDA) to enable experimental agents to obtain IND status so that they can be evaluated in the Pennsylvania State University (PSU) Cancer Institute Clinics in phase I trials. Accomplishing these objectives for one of the compounds from the current melanoma drug portfolio is the objective of this project.

### **Anticipated Duration of Project**

5/1/2009 – 6/30/2012

### **Project Overview**

Clinicians treating cancer believe that agents targeting key pathways deregulated in cancer cells are necessary for more effectively treating these diseases. Unfortunately, relatively few agents are available in the clinic to treat cancer in this manner. Malignant melanoma is a prime example of a devastating disease needing more effective agents for treatment of metastatic disease. The hope is that targeted agents inhibiting the activity of aberrantly behaving proteins would be more effective than those untargeted drugs currently available to patients. To develop better cancer therapies to treat melanoma, The Penn State Melanoma Therapeutics Program is identifying genes causing the disease, developing drugs to target these genes and drug delivery systems to get the agents more effectively to the cancer cells, and finally testing the agents in clinical trials in patients. However, the biggest hurdle is the final step, which involves testing the agents in the clinic. Therefore, the objective of this project is to develop the organizational structure necessary to move agents developed within the Melanoma Therapeutics Program from the preclinical to clinical arena. Development of an agent known as ISC-4, which inhibits the Akt3 kinase deregulated in ~70% of melanomas will be emphasized. Therefore, the *objective of this project* is to undertake the necessary characterization to move ISC-4 from the preclinical arena to the clinic. First, a large batch of GMP grade ISC-4 is required, which will be compared to currently used smaller laboratory generated batches. By-products and physical characteristic will be determined. Next efficacy for inhibiting tumor development using the larger synthesis scale will be compared to smaller scale synthesis together with toxicological evaluation. Second, toxicology as well as pharmacokinetic and pharmacodynamic properties of ISC-4 in a second animal model will be evaluated. Collectively, these studies will form the foundation for an IND from the FDA for ISC-4. Once these data are obtained, The Penn State Cancer Institute plans to test the compound's toxicity in humans as well as determine any efficacy in a phase I melanoma clinical trial. Note: A phase I trial testing of the agent in melanoma is not the objective of this project, rather it is to successfully obtain IND status for the compound. Thus, the *central*

*hypothesis* for these studies is that targeting Akt3 signaling using ISC-4 would be an effective targeted approach for inhibiting melanoma development. This discovery would be highly significant, evaluating the therapeutic implications of targeting a major signaling pathway promoting melanoma development.

### **Principal Investigators**

Gavin P. Robertson, PhD  
Associate Professor of Pharmacology, Pathology, and Dermatology  
Associate Director for Translational Research  
The Pennsylvania State University  
College of Medicine  
The Milton S. Hershey Medical Center  
Department of Pharmacology, R130  
500 University Drive, P.O. Box 850  
Hershey, PA 17033-0850

### **Other Participating Researchers**

SubbaRao Madhunapantula, PhD, Raghavendra Gowda, PhD – employed by Pennsylvania State University, College of Medicine

### **Expected Research Outcomes and Benefits**

One person in the United States dies from melanoma every hour. Currently, no effective treatment exists for patients suffering from the metastatic stages of this disease. In spite of the widely appreciated magnitude of the problem, there is still a critical gap in knowledge regarding key deregulated signaling pathways causing melanoma and therapies specifically targeted to correct these defects to inhibit tumorigenesis and metastasis. *Availability of ISC-4 as a melanoma therapeutic targeting Akt3 signaling in melanoma has the potential of leading to a more effective rationally targeted therapeutic agent for melanoma patients.* Therefore, as a direct outcome of the project, it is expected that a scaled-up clinical batch of ISC-4 will be generated; the compounds physiochemical and biological characteristics will be evaluated in preclinical models and compared to small-scale lab generated batches. Second, toxicity as well as pharmacokinetics and pharmacodynamics will be determined in a second animal model, which is critical data necessary to apply for an IND for ISC-4 from the FDA so that the compound can be tested in phase I clinical trials. Clinical availability of ISC-4 is predicted to have a significant positive impact on the currently poor prognosis faced by advanced-stage melanoma patients by contributing to availability of more effective therapies, which would increase the length and quality of life for melanoma patients. Therefore, the positive impact for cancer patients suffering from melanoma will be significant.

### **Summary of Research Completed**

A significant amount of work has been completed during the first year of this project.

First, a 1 kg of ISC-4 has been synthesized and compared to smaller laboratory generated batches. HPLC, NMR and Mass Spec have been used to verify the identity and purity of the ISC-4. Measuring of the efficacy of the ISC-4 drug to kill cultured cancer cells following synthesis at a larger scale, has been compared to this agent synthesized in smaller batches and shown to be equally effective, resulting in similar IC<sub>50</sub> values. Second, efficacy for inhibiting cutaneous tumor development using the larger synthesis scale together with toxicological evaluation has been evaluated. The chemopreventive efficacy of topical ISC-4 was evaluated in a laboratory-generated human skin melanoma model containing early melanocytic lesions or advanced-stage melanoma cell lines and in animals containing invasive xenografted human melanoma. Cumulative topical application of ISC-4, reduced melanocytic or melanoma developed in the skin model by 80-90% and decreased tumor development in animals by ~80%. Histological examination of ISC-4 treated skin showed no obvious damage to skin cells or skin morphology and treated animals did not exhibit markers indicative of major organ related toxicity. Mechanistically, ISC-4 prevented melanoma by decreasing Akt3 signaling leading to a 3-fold increase in apoptosis rates. Thus, topical ISC-4 can prevent melanoma in preclinical models and has potential to profoundly impact melanoma incidence and mortality rates in humans if similar chemopreventive results are observed. With this proof of principal demonstration, the goal is now to develop a topical formulation, which would be evaluated in clinical trials in humans to prevent melanoma.

#### Detailed description

The results of this experimentation are detailed in the sections that follow under headings detailing the discoveries.

ISC-4 kills melanocytic lesion cells more effectively than normal skin cells. ISC-4 has been derived from naturally occurring isothiocyanates by increasing the carbon chain length to 4 and replacing sulfur with selenium. ISC-4 can kill aggressive invasive advanced stage melanoma cells following systemic administration, but its effect on early melanocytic lesion and normal cells present in skin is unknown. Human skin is composed of multiple cell types including fibroblasts, keratinocytes and melanocytes, with the latter developing into melanocytic lesions, which later progress into melanoma. Therefore, effective topical chemopreventive agents would need to kill early melanocytic lesion or aggressive melanoma cells with negligible effect on normal skin cells. To determine the appropriate concentration range and IC<sub>50</sub> of ISC-4 for topical use applications, cell proliferation using the MTS assay was examined after exposure of melanocytic lesion, melanoma or normal skin fibroblast cells to ISC-4. An ISC-4 concentration of 26  $\mu$ M was required to kill 50% of normal human fibroblast compared to 3.4  $\mu$ M for early stage WM35 cells line derived from an early stage melanocytic lesion in the radial growth phase or 10  $\mu$ M for invasive UACC 903 melanoma cells derived from an invasive cutaneous melanoma. Thus, ISC-4 is 2.6-7-fold more effective at killing melanocytic lesion or melanoma compared to normal cells, indicating potential utility for topically applications at concentrations  $\leq$ 25  $\mu$ M.

ISC-4 decreases Akt3 activity and triggers apoptosis in early stage melanocytic lesion cells derived from the radial growth phase. To measure ISC-4 inhibition of Akt3 activity in early stage melanomas, WM35 cells were exposed to 2.5 to 12.5  $\mu$ M of ISC-4 or control PBITC and cell lysates analyzed by Western blotting. ISC-4 decreased pAkt3 levels at lower concentrations

than control PBITC with negligible effect on total Akt protein levels. Furthermore, ISC-4 decreased levels of downstream pPRAS40 more effectively than control PBITC, which had little effect on this downstream signaling target. As a consequence of decreased Akt3 activity, cleaved PARP and caspase-3 indicating increased apoptosis rose more dramatically in ISC-4 compared to PBITC treated cells. Thus, ISC-4 functions to decrease Akt3 activity resulting in increased apoptosis in radial growth phase melanocytic lesion cells.

Mechanism leading to death of cultured melanocytic lesion cells following ISC-4 treatment is by decreasing proliferation and triggering apoptosis. The mechanism by which ISC-4 kills cultured early stage melanocytic lesion WM35 cells was examined by determining whether inhibition of melanoma cell growth using ISC-4 resulted from inhibition of proliferation or induction of apoptosis. Caspase3/7 activity, a marker of apoptosis, and the percentage of cell population in the sub-G0-G1 phase indicating apoptotic debris were examined after 24 h of treating melanocytic lesion cells with increasing concentrations of ISC-4, PBITC or vehicle control using a BrdU ELISA kit. Both ISC-4 and PBITC decreased proliferation and increased apoptosis. However, ISC-4 was more effective at inhibiting proliferation and triggering apoptosis than PBITC. Thus, ISC-4 is effective at killing cultured early stage melanocytic radial growth phase lesion cells.

Topical ISC-4 treatment inhibits melanocytic and melanoma lesion development in laboratory-generated skin.

Human skin containing melanocytic lesions resembling benign or aggressive tumors can be generated in the laboratory and the effects of anticancer agents can be evaluated on tumor development in this model. These cell lines form tumors in the skin, which resemble early and late stage lesions occurring in skin for WM35 and UACC 903, respectively. Furthermore, both WM35 and UACC 903 cell lines express green fluorescent proteins (GFP) making melanocytic nodule development detectable and quantifiable using fluorescence microscopy.

A decrease in cutaneous melanocytic lesion development was observed in laboratory generated skin following ISC-4 treatment compared to controls. H&E stained and fluorescent images of cross sections of skin at day 11 show dramatically fewer melanocytic lesions or melanoma cells in the skin compared to controls. In contrast to ISC-4 treated skin having little melanocytic lesion development, control skin contained nests of cells for the WM35-GFP cells line and many invading disseminating cells for the UACC 903-GFP cell line. At the end of ISC-4 treatment, most melanocytic lesion cells for both cell lines were barely detectable. ISC-4 also caused no detectable damage to the keratinocytes, fibroblasts or skin morphology present in this model, again suggesting that a topical formulation would cause negligible effect on normal skin cells.

To assess the effect of ISC-4 treatment on melanocytic lesion development overtime, serial measurement was made on the same skin. Doses of ISC-4 ranging from 7.5-25  $\mu$ M were evaluated for inhibition of melanocytic lesion development in the 3-dimensional human skin model. Regression in area occupied by WM35-GFP and UACC 903-GFP tumors was observed when treated with ISC-4 compared to controls. A similar trend was observed for PBITC but ISC-4 was more effective leading to an 80-90% reduction in average area occupied by the end of treatment compared to a 50-60% decrease for PBITC. Thus, ISC-4 is effective at inhibiting melanocytic lesion development in the laboratory generated skin model containing melanocytic

lesions at concentrations ranging from 7.5-25  $\mu$ M, supporting topical use of ISC-4 for preventing melanocytic lesion development.

Topical application of ISC-4 prevents melanocytic lesion development in the skin of nude mice with negligible changes in animal body weight. To demonstrate that topical ISC-4 inhibits melanocytic lesion development in animals, UACC 903 melanoma cells, which are tumorigenic and have high Akt3 signaling activity, were injected subcutaneously and 24 h later in animals treated topically everyday with ISC-4 or acetone vehicle. WM35 cells could not be evaluated in mice since these cells are not tumorigenic. Topical ISC-4 treatment led to a 77% decrease in UACC 903 tumor size compared to vehicle control. Body weights of mice treated with ISC-4 compared to control showed no significant differences between groups, suggesting negligible toxicity. Thus, use of topical ISC-4 inhibited cutaneous melanocytic lesion development without weight loss was suggestive of systemic toxicity.

Mechanistically, ISC-4 inhibits melanocytic lesion development in animals by triggering tumor cell apoptosis. To determine the mechanism causing tumor inhibition, size and time matched tumors from mice treated with ISC-4 or vehicle were compared. Western blot analysis of matched tumors lysates harvested at day 13 from animals treated with ISC-4 showed decreased active pAkt ( $p < 0.05$ ; t-test) and downstream target pPRAS40 ( $p < 0.001$ ; t-test) compared to vehicle control treated tumors.

To show that decreased Akt3 activity led to an increase in tumor cell apoptosis, rates of apoptosis (TUNEL staining) and proliferation (Ki-67 immunohistochemistry) were compared in size and time matched melanoma tumors excised from ISC-4 treated animals and compared to vehicle control. Tumors harvested at day 11 and 13 from mice treated with ISC-4, showed an ~3-fold ( $p < 0.01$ ; t-test) more TUNEL positive cells compared to control animals treated with vehicle control. In contrast, no statistically significant difference was seen in rates of proliferation between different treatment groups. Thus, treatment of animals with ISC-4 decreased Akt3 signaling leading to increased rates of tumor cells apoptosis.

ISC-4 causes negligible major organ related toxicity. To determine whether ISC-4 would cause systemic toxicity, blood parameters (serum glutamic oxaloacetic transaminase, serum glutamate pyruvate transaminase, alkaline phosphatase, blood urea, glucose, and creatinine) indicative of organ toxicity were measured following systemic administration. None of these indicators were significantly different from controls. Furthermore, histologic examination of H&E-stained vital organ sections revealed that ISC-4 treatment did not significantly alter cell morphology or structure of liver, kidney, adrenal, lung, spleen, heart, pancreatic, or intestinal tissue. Thus, ISC-4 caused negligible systemic toxicity and would be effective for preventing melanocytic lesion development.

## **Research Project 19: Project Title and Purpose**

*Changes in Oxygen-induced Proliferative Retinopathy in 4E-BP1/2 Knockout Mice* - The purpose of this project is to determine if dysregulation of protein synthetic pathways contributes to the aberrant development of retinal blood vessels in oxygen-exposed newborn rodents. Using newborn mice deficient in proteins (4E-BP1/2) regulating the initiation phase of protein synthesis, we seek to determine the impact of high concentrations of oxygen to retinal blood vessel growth and vascular endothelial growth factor expression. We believe that the findings from this project will provide a useful framework from which to develop clinical and therapeutic interventions to protect premature newborns from the detrimental effects of oxygen exposure.

### **Anticipated Duration of Project**

5/1/2009 – 12/31/2010

### **Project Overview**

Premature infants exposed to high concentrations of oxygen to treat pulmonary disease often develop retinopathy of prematurity (ROP), a condition associated with long-term visual impairment and blindness. The objective of this project is to determine the contribution of protein synthetic regulatory pathways in the development of oxygen-induced retinopathy in newborn mice. Specifically, we will investigate the role of cap-dependent mRNA translation on the expression of vascular endothelial growth factor (VEGF) protein expression and the subsequent development of neovascularization. We hypothesize that loss of cap-dependent mRNA regulatory proteins, 4E-BP1/2, will reduce retinal neovascularization and retinal VEGF protein expression during the proliferative stage of retinopathy. The project will utilize 7-day-old mice exposed to 75% O<sub>2</sub> for 5 days followed by 5 days of room air recovery; a well-established model of proliferative retinopathy. In the first aim, we will assess the effect of 4E-BP1/2 on the magnitude of oxygen-induced retinal neovascularization using immunohistochemistry. Aim 2 will delineate changes in VEGF protein expression secondary to the altered regulation of cap-dependent mRNA translation induced by the loss of 4E-BP1/2. Specifically, we will determine changes in VEGF and hypoxia-inducible factor-1 (HIF-1) expression by immunoblotting and real-time PCR, respectively. Overall, this project will provide evidence for a role of translational regulation of protein synthesis in the pathogenesis of retinopathy of prematurity.

### **Principal Investigators**

Jeffrey S. Shenberger, MD  
Associate Professor  
Department of Pediatrics  
Hershey Medical Center  
500 University Drive, H085  
Hershey, PA 17033-0850

## Other Participating Researchers

Leonard S. Jefferson, PhD, Tabitha L. Schrufer, MS, Lianqin Zhang, MD – employed by Pennsylvania State University, College of Medicine

## Expected Research Outcomes and Benefits

Each year, approximately 15,000 premature infants in the U.S. develop some degree of retinopathy of prematurity (ROP), a form of oxygen-induced eye injury associated with life-long visual impairment. We anticipate that loss of the protein synthetic regulatory proteins, 4E-BP1/2, will diminish abnormal blood vessel growth in the newborn retina induced by exposure to high concentrations of oxygen. Specifically, we anticipate that animals without 4E-BP1/2 proteins will demonstrate a reduction in aberrant blood vessel budding and in the level of blood vessel growth factors within the eye. This information will be used as part of a National Institutes of Health grant proposal investigating how oxygen-mediated changes in protein synthesis modify the expression of factors essential to normal and pathologic retinal growth and development in the newborn. Because effective strategies to prevent or treat abnormal retinal blood vessel development do not currently exist, this project's findings may ultimately lead to the identification of novel therapeutic targets aimed at ameliorating or averting harmful new vessel formation. Given the potential for blindness, a better understanding of ROP may dramatically improve the lives of hundreds of preterm infants and their families.

## Summary of Research Completed

Thus far, we have studied the vascular development of wild type (WT) and 4E-BP1/2 double knockout (DKO) BALB/c mice at varying time points. Our progression has been somewhat hindered by small litter sizes and the need to re-derivatize the DKO animals. As such, we have limited data available for quantitation of the avascular and neovascular area in oxygen-induced retinopathy (OIR). Similarly, we have yet to measure our primary vascular growth factor, VEGF, by ELISA. Within the next several months, we anticipate an increase in the number of litters from both WT and DKO animals.

Methods: *Experimental Design.* BALB/c mice in dam/pup pairings were placed into plexiglass exposure chambers overnight, in room air, for habituation. Dams were supplied with standard mouse chow and water *ad libitum*. Routine day/light cycles of 12 hrs were used and temperature and humidity maintained at 26°C and 75–80%, respectively. Animals were studied using two treatment protocols. In the OIR protocol, mice were exposed to 75% O<sub>2</sub> for 5 days (P12) after which they were returned to room air for an additional 5 days (P17). Delivery of O<sub>2</sub> at these time points and concentrations recapitulates human ROP. Administration of O<sub>2</sub> was continually adjusted and monitored using a computerized system (BioSpherix Oxyclyer, Reming Bioinstruments, Redfield, NY). In the control protocol, animals were exposed to ambient air in identical chambers through P17. In both chambers, CO<sub>2</sub> concentrations were adjusted by the degree of chamber “leak” and kept <0.5%. Retinal vascularity and VEGF expression were studied in pups at P7, 12, 15 and 17.

*Avascular and neovascular area.* BALB/c mice exposed to either room air or 75% O<sub>2</sub> were euthanized and eyes enucleated. The eyes were fixed in 4% paraformaldehyde for 60 min at room temperature. After 60 min, eyes were washed 3 times in PBS and stored at 4°C. Retinas were separated from the sclera, retinal pigmented epithelium, lens, and cornea and marked for orientation. Retinal vessel staining was performed using 500 µl of Alexa Fluor 594 conjugated to isolectin (B4-594, Molecular Probes/Invitrogen, Carlsbad, CA) incubated overnight at 4°C in the dark. Following rinsing, retinas were flat-mounted ganglion side up on glass slides and cover-slipped in aqueous mounting medium containing anti-fade reagent. Digital images were acquired using a laser confocal microscope (TCS SP2 AOBS, Leica Microsystems).

*Immunoblotting.* Flash-frozen retinas were homogenized in RIPA buffer, cleared by centrifugation, and protein concentration determined using the BCA assay. Twenty µg of sample was separated by SDS-PAGE, transferred to PVDF, and blocked with 5% milk in TBST. Membranes were incubated overnight with antibodies directed against VEGF, FGF2, ribosomal S6 kinase 1 (S6K1) phosphorylated on threonine 389, ribosomal protein S6 (S6rp) phosphorylated on serine 235/236, and 4E-BP1. Blots were developed using chemiluminescence and quantified using the GeneGnome imaging system (SynGene, Frederick, MD).

*Results.* Initial studies examining the retinal vascularization in WT BALB/c and DKO mouse pups show identical arborization and vessel distribution patterns from post-natal day 7 (P7) through P17. As expected, exposure of pups to the OIR protocol produced large areas devoid of retinal vessels at P12 and a marked increase in neovascularization at P17 (Fig. 1). The observed findings at P17 do not appear to be as robust as those reported in the C57BL/6 mice. It has been noted elsewhere that BALB/c display an accelerated “recovery” from neovascularization when compared with C57BL/6 mice. We are in the process of studying mice P14 and P16 to identify the time of maximal neovascularization. Exposure of DKO mice to the OIR protocol demonstrated that loss of 4E-BP1/2 accelerates recovery from vascular regression and induces less pronounced neovascularization (Fig. 2 and Fig 3).

Examination of the retinal growth factors VEGF and FGF2 in whole retinal lysates demonstrates that at P17, OIR decreases VEGF<sub>164</sub> and VEGF<sub>120</sub> relative to room air exposed controls in WT mice. In DKO mice, however, OIR increased VEGF<sub>164</sub> and VEGF<sub>120</sub> relative to room air controls. With regard to FGF2, OIR increased protein expression in both WT and DKO mice but the increase in DKO was substantially greater (Fig. 4). Finally, we examined retinas for changes in mTOR signaling cascade of which 4E-BP1/2 is part. We found that neither OIR nor loss of 4E-BP1/2 alter the phosphorylation of the mTOR target, S6K1 (Fig. 5). The phosphorylation of S6K1 target, S6rp, however, was increased by OIR in WT, but decreased in DKO mice. As anticipated, we could not detect 4E-BP1 in DKO mice, but noted that OIR increased 4E-BP1 phosphorylation (increased density of band shift) in WT mice.

In summary, we have found that loss of 4E-BP1/2 ameliorates OIR-induced neovascularization coincident with an increase in VEGF and FGF2. We are working to determine if these changes retinal growth factors represent a direct effect of 4E-BP1/2 deficiency or are reflective of an accelerated restoration of appropriate vascular development. Studying additional mice at earlier time points than P15 will help resolve these issues.

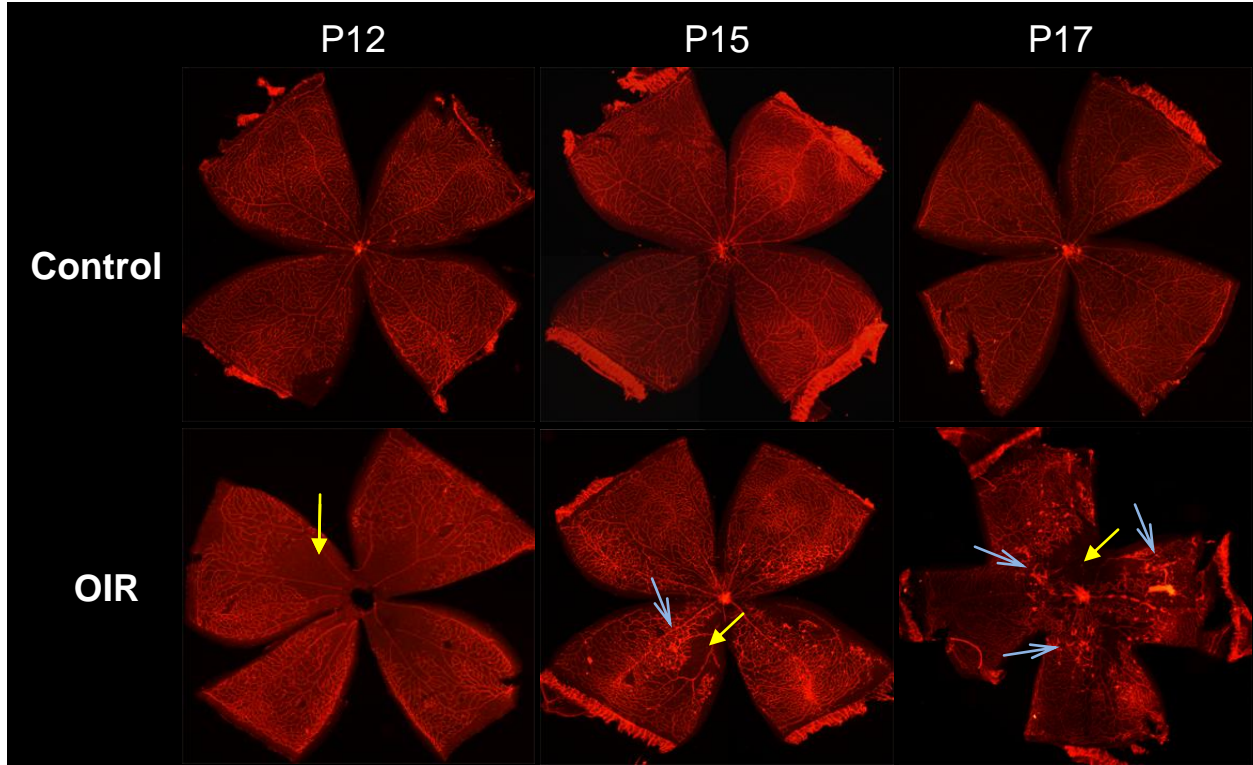


**Figure 1.** Effect of OIR on retinal vascularization in WT BALB/c mice. Mouse pups were exposed to 75% O<sub>2</sub> from P7-P12 and then returned to room air. Retinal images shown were stained with isolectin B4. At P12, O<sub>2</sub> lead to centripetal vascular regression (yellow arrows). By P15, vascular regression was improved, but early neovascularization (blue arrows) began to appear, which became more apparent at P17. Images representative of retinas from 3 animals in each group.

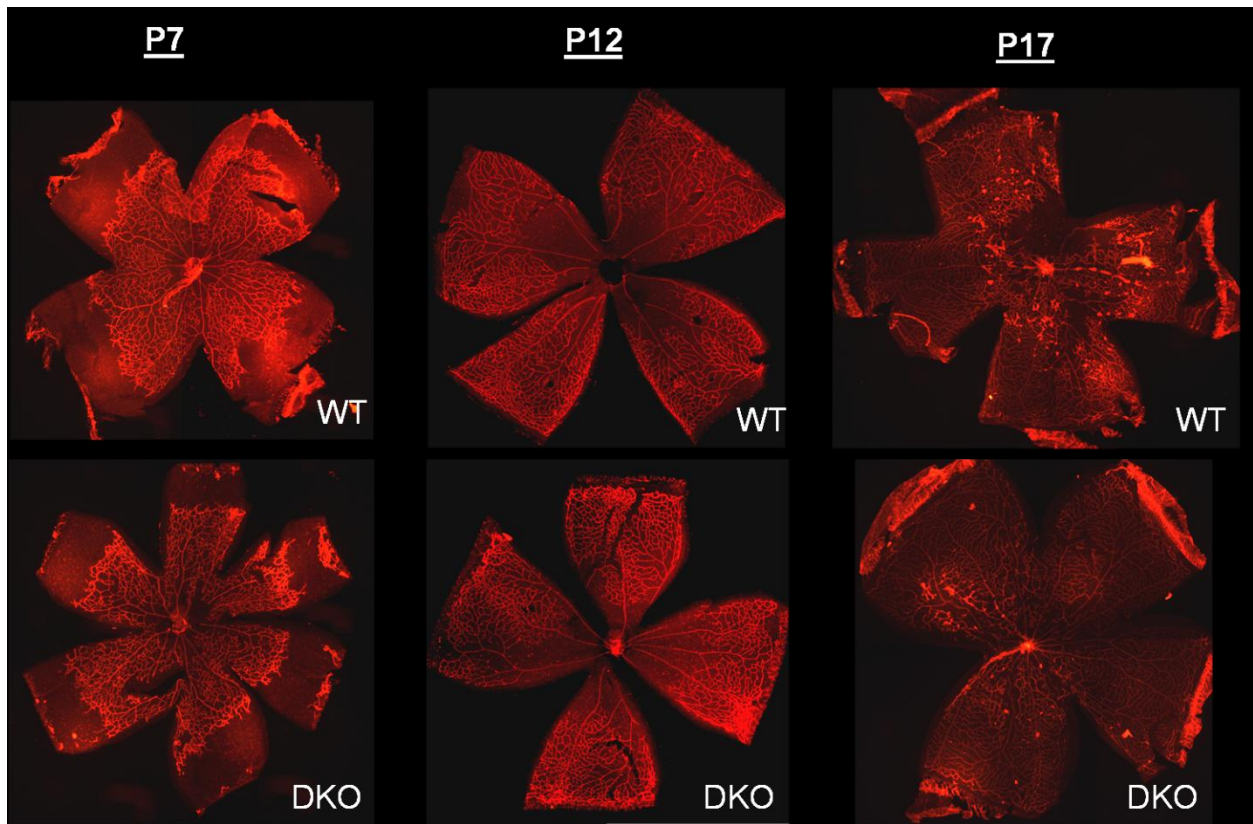


**Figure 2.** Effect of OIR on retinal vascularization in WT and DKO mice. Mouse pups were exposed to 75% O<sub>2</sub> from P7-P12 and then returned to room air. Retinal images shown were stained with isolectin B4. At P12, O<sub>2</sub> lead to centripetal vascular regression in both mouse strains. By P17, vascular regression was improved to a greater degree in DKO mice. Likewise, there was less neovascularization in DKO mice compared to WT at P17.

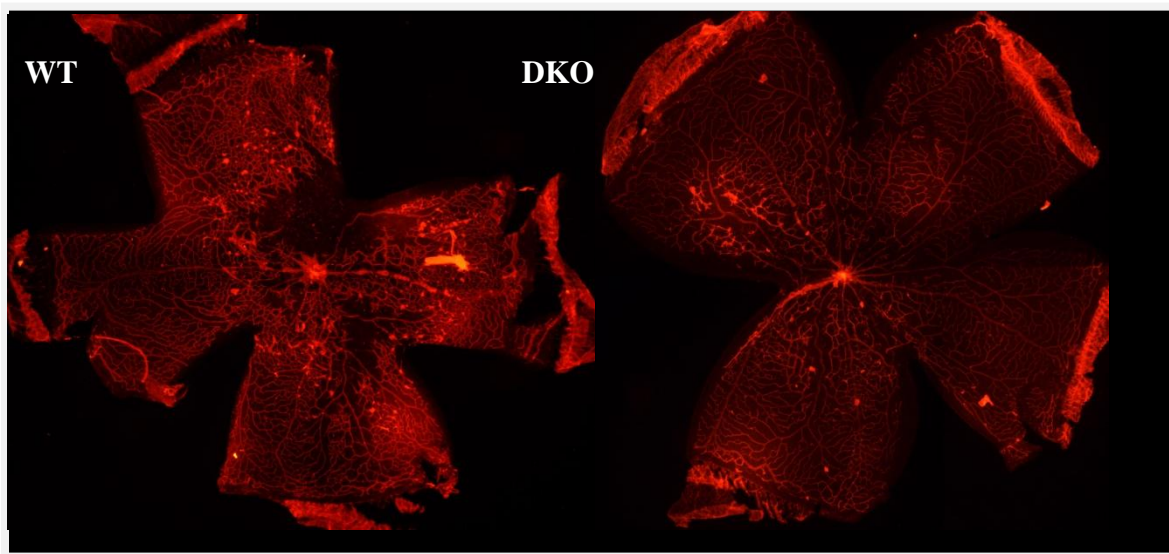


**Figure 3.** Effect of OIR on retinal vascularization in WT and DKO mice at P17. Expanded images show WT and DKO mouse retinas at P17 in the OIR model.

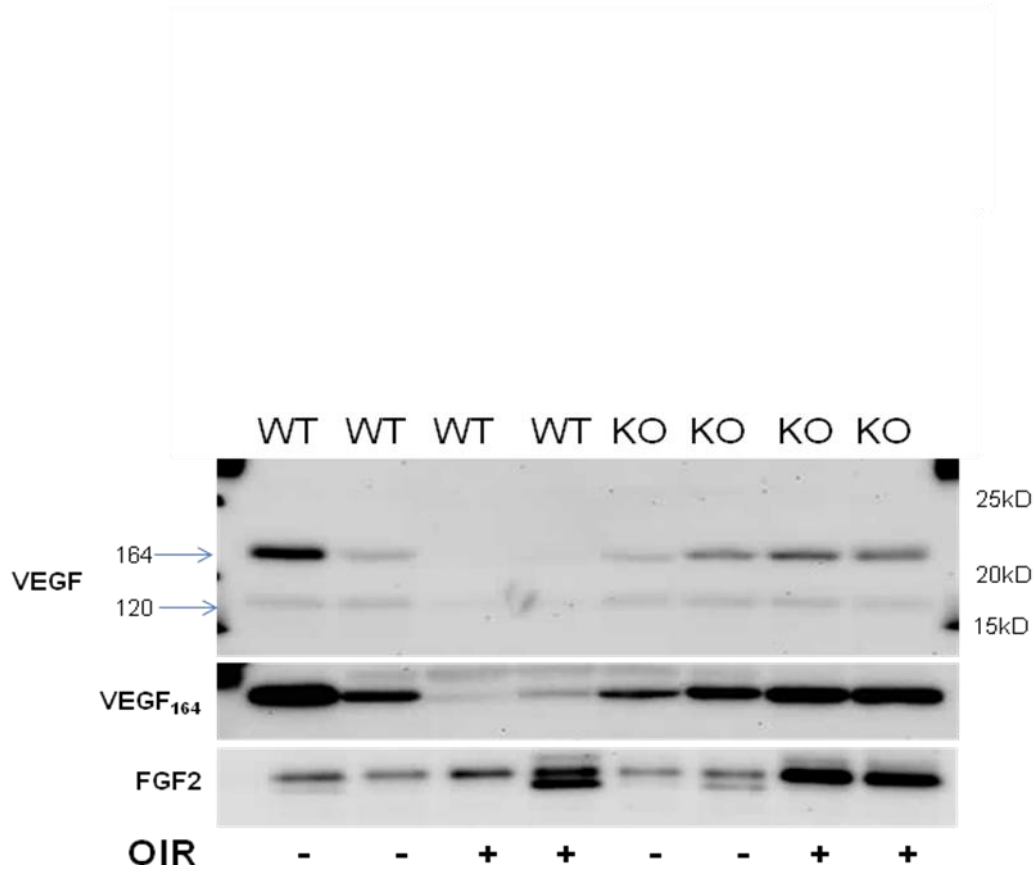


**Figure 4. Effect of OIR on VEGF and FGF2 expression.** Mouse pups were exposed to 75% O<sub>2</sub> from P7-P12 and then returned to room air until P17. We found that OIR decrease VEGF<sub>164</sub> and VEGF<sub>120</sub> in WT mice at P17, but had the opposite effect in KO (4E-BP1/2 knockout) mice. OIR increased FGF protein expression in both WT and DKO mice though the effect was greater in KO mice. The two immunoblots for VEGF represent the same samples blotted with antibodies to different VEGF epitopes.

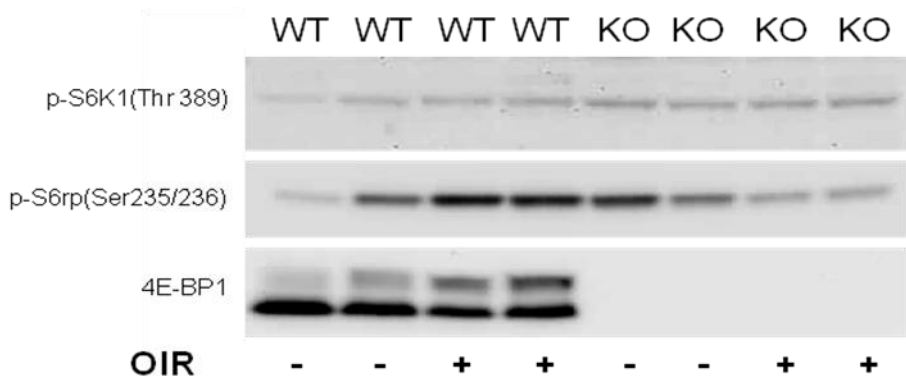


**Figure 5. Effect of OIR on mTOR signaling at P17.** OIR had little effect on S6K1 phosphorylation, but increased S6rp phosphorylation in WT but decreased S6rp phosphorylation in KO mice. 4E-BP1 was not detected in KO mice as expected.

## **Research Project 20: Project Title and Purpose**

*Molecular Mechanisms of Uninfected Red Cell Phagocytosis in Severe Malarial Anemia (SMA)* - The purpose of this study is to determine how uninfected red cells are destroyed by macrophages of malaria-infected mice.

### **Duration of Project**

5/1/2009 – 6/30/2010

### **Project Overview**

The broad research objective is to develop interventions to prevent the destruction of uninfected red cells by the host innate immune system during malaria infection.

#### Specific Aims:

1. Identify the red cell ligands and macrophage receptors involved in phagocytosis of red cells in a rodent SMA model developed in our laboratory.
2. Determine the roles of malaria pigment (hemozoin) and glycosylphosphatidylinositol (GPI) in stimulating in vitro erythrophagocytosis and identify reagents to block this effect.

To achieve the above aims we will study the role of red cell ligands and macrophage receptors on the in vitro phagocytosis of red cells from mice infected with rodent malaria using a new model of SMA developed in our laboratory. Specific ligands and receptors will be blocked using lectins, receptors, and antibodies that have been shown to be effective in blocking the phagocytosis of aged or C3b-coated red cells. In addition, we will study the role of GPI and hemozoin in the stimulation of macrophage-dependent phagocytosis as well as the effect of toll-like receptor (TLR) inhibitors and inhibitors of the transcription factor NF- $\kappa$ B on the erythrophagocytosis of GPI and hemozoin-stimulated macrophages. These studies will identify compounds that potentially could be used for the treatment of SMA and that could be tested in mice in vivo in subsequent studies.

### **Principal Investigators**

José A. Stoute, MD  
Associate Professor  
Penn State Hershey Medical Center  
500 University Drive  
Room C6833, MC H036

### **Other Participating Researchers**

Channe Gowda, PhD, Tiffany Bohr – employed by Penn State College of Medicine

## Expected Research Outcomes and Benefits

*Plasmodium falciparum* is responsible for 1-2 million deaths each year, most of which occur in children as a result of complications such as severe malarial anemia (SMA). Blood transfusions can save the lives of these children but many die because few hospitals in the endemic regions have the resources to maintain an adequate blood supply. Therefore, alternative therapies are needed that can be implemented instead of blood transfusion to stop red cell destruction and increase the number of circulating uninfected red cells during malaria infection. There is substantial evidence to suggest that SMA results from the destruction of uninfected red cells due to the host immune response against the parasite. Red cells can continue to be destroyed despite malaria therapy and after parasites have disappeared from the circulation and this loss can contribute to exacerbation of severe anemia. We hope to develop an intervention that can be given to children with SMA when they present to the hospital and that will result in preservation of the uninfected red cell population and perhaps even increase the number of uninfected red cells by releasing red cells sequestered in the spleen and/or liver.

## Summary of Research Completed

The focus of our investigation on erythrophagocytosis in our rodent SMA model involved the use of labeled red cells whose fluorescence signal increased as a result of internalization by macrophages. The outline of our approach was as follows:

- a) Testing of three fluorescent dyes (cypHer5E, pHrodo and CFSE) for red cell staining
- b) Phagocytosis experiments using the *P.chabaudi*, *P.berghei* and SMA (*P.chabaudi* and *P.berghei*) models
- c) Assessing the effect of potential phagocytosis modulators such as pigment (hemozoin) and glycosylphosphatidylinositol (GPI)

## Methods

### RBC staining for monitoring phagocytosis

We optimized the staining of red cell cells using two pH-sensitive (cypHer5E and pHrodo) and one pH-independent dye (carboxyfluorescein diacetate succinimidyl ester, CFSE). Both cypHer5E and pHrodo fluoresce minimally in neutral environments but exhibit increased red fluorescence in an acidic environment such as in the endosomes formed after particle internalization.

CFSE on the other hand passively diffuses into cells and remains colorless and non-fluorescent until its acetate groups are cleared by intracellular esterases. The green fluorescent conjugates that bind strongly to intracellular amines are retained by the cells following cell divisions and are ideal for tracking cells for weeks.

The procedure for labeling red cells for monitoring phagocytosis began with harvesting blood from a mouse by cardiac puncture using citrate-phosphate-dextrose (CPD) as the anti-coagulant. The blood was centrifuged, plasma removed and a 5% (v/v) hematocrit suspension prepared using phosphate buffered saline (PBS), pH 7.4. Dye was added to the 5% blood suspension to a final dilution of 1:250 (cypHer5E and pHrodo) or 1:600 (CFSE). This was mixed, protected from light by covering the tube(s) with aluminum foil and incubated for 30 min on a rocking

platform. For CFSE stained red cells the reaction was stopped using an equal volume of fetal bovine serum (FBS). The stained red cells were then centrifuged and washed three times with PBS and then analyzed by flow cytometry (Figure 1). After testing the three dyes we proceeded to use pHrodo in our erythrophagocytosis assays.

#### *In vitro red cell phagocytosis assay*

The protocol for determining *in vitro* erythrophagocytosis was as follows. First, macrophages were obtained by cell culture (J774) or isolated from C57BL/6 mice (splenic, peritoneal, PBMCs and bone marrow) using standard procedures. Murine macrophages were harvested from both uninfected and *P. chabaudi*, *P. berghei* or *P. chabaudi*-*P. berghei*-infected (Anemia model) mice. Red cells were also collected from these mice as needed. Three populations of red blood cells were used in our studies: uninfected RBCs from uninfected mice (uiRBC/uiM), uninfected RBCs from infected mice (uiRBC/iM) and infected RBCs from infected mice (iRBC/iM). Separation of infected and uninfected red cells from infected animals was achieved using Percoll/sorbitol density gradients with Percoll densities of 80%, 70%, 60%, 40% and 20% (Figure 2).

The positive control for red cell phagocytosis were uninfected red cells from an uninfected mouse (uiRBC/uiM) coated with a monoclonal against mouse red cell glycoprotein (anti-TER 119) while anti-TER 119-coated RBCs co-incubated with cytochalasin D (a potent inhibitor of phagocytosis) were used as the negative control. A typical assay was set up as follows: on the day before the phagocytosis assay, macrophages cultured in DMEM/10%HI-FBS were plated at a concentration of  $1 \times 10^6$  per well on each of six wells on a 24-well plate to be analyzed by flow cytometry. For comparison between  $4 \times 10^4$  and  $1 \times 10^5$  of the same macrophages were added to each of six wells on an 8-well Labtek chamber slide to be analyzed by light microscopy. The next day the old medium was replaced with fresh medium and in selected wells medium containing 50  $\mu$ M cytochalasin D was added 30 minutes prior to addition of pHrodo-labeled red cells. Red blood cells were then added to the macrophage at a ratio of 10:1 to both the 24-well plate and the 8-well chamber slide. These were then placed on a rotating shaker and incubated at 37°C, 5% CO<sub>2</sub> for 2 hours. Nonadherent red cells were then washed off by replacing the media with RPMI. After removal of the RPMI the macrophages on the 24-well plates were detached using cold PBS/10mM EDTA/1%BSA. To prepare them for analysis by flow cytometry an equal volume of 2% paraformaldehyde was added and the suspension transferred to 5 ml polystyrene round bottom test tubes. The detachable chambers on the 8-well slides were removed and the macrophages fixed with methanol before staining with Giemsa for viewing by light microscopy.

#### Results

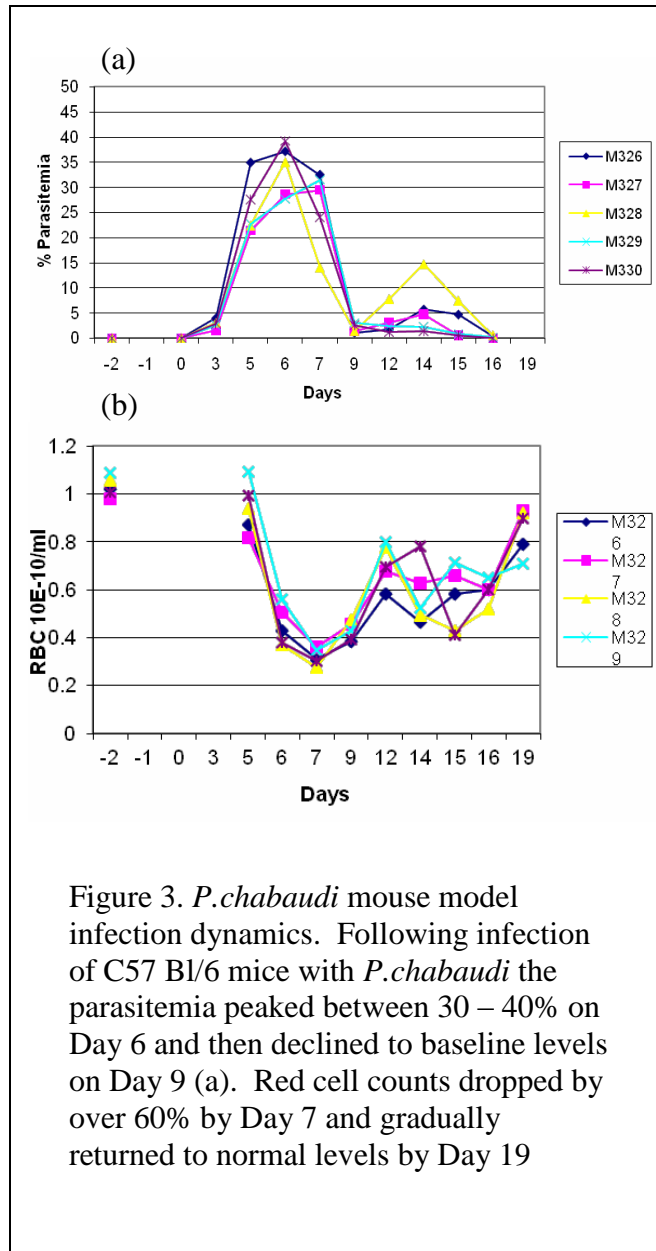
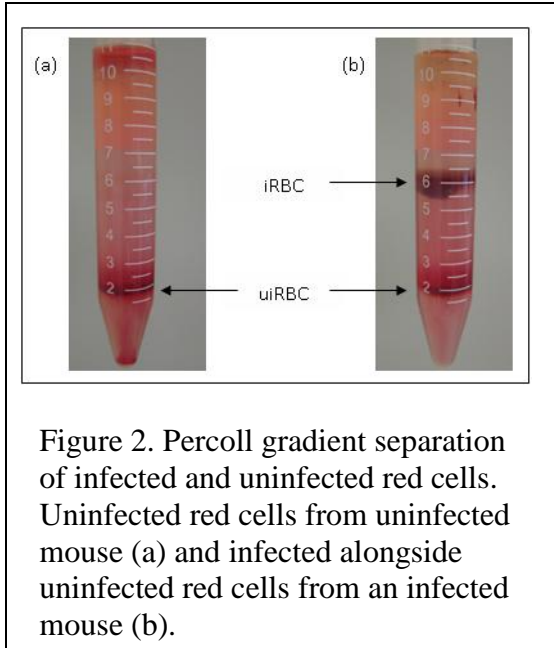
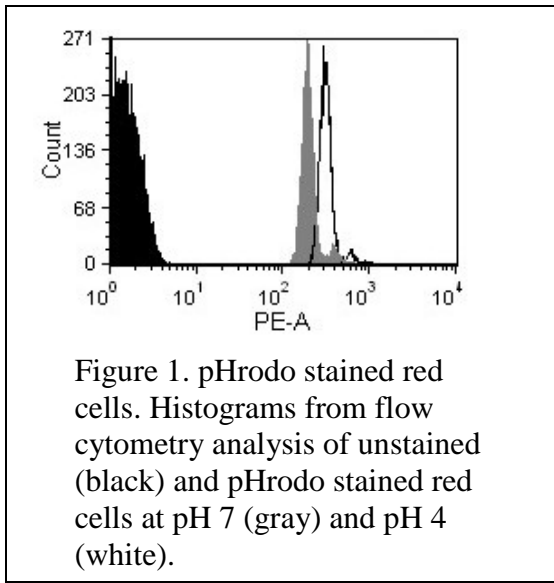
We investigated whether there was an increased susceptibility to phagocytosis of uninfected red cells obtained from infected mice as compared to those from uninfected mice. This was tested in three mouse models: *P. chabaudi*, *P. berghei* and the *P. chabaudi*-*P. berghei* SMA model. The dynamics of these infections differ with the peak parasitemias of 40% noted in both the *P. chabaudi*, and SMA models (Fig.3a and 7a) compared to 15% in the *P. berghei* model (Fig 5a). Anemia was most pronounced in the *P. chabaudi* (60% reduction in RBC count, Fig.3b), and SMA models (50% reduction in RBC count, Fig 7b) while it was less (20% reduction in RBC count, Fig.5b) in the *P. berghei* model. Most of the experiments were done using J774 macrophages as the target macrophages while a number of experiments were performed with

macrophages (splenic, peritoneal and PBMCs) harvested from our anemia model while one investigation was conducted on macrophages from the *P.berghei* model. Similarly, the majority of the red cells used for the assays were obtained from our SMA model given that of the three models we interrogated it is most representative of malaria anemia in humans.

In the *P.chabaudi* model the higher level of phagocytosis of uiRBC/iM compared to uiRBC/uiM was consistent across the three time points tested with the greatest difference observed pre-peak parasitemias (Day 5) with phagocytosis of uiRBC/iM at 38% and that of uiRBC/uiM at 12% (Figure 4). No such difference in susceptibility to phagocytosis was observed in either the *P.berghei* or SMA (*P.chabaudi* and *P.berghei*) models. Overall the extent of erythrophagocytosis was much lower in macrophages isolated from the infected mice in comparison to the J774 cell line.

Our results suggest that erythrophagocytosis of uninfected red cells may have a role in pathophysiology of the non-lethal *P. chabaudi* murine infection. Furthermore our findings do not provide any evidence for red cell destruction due to increased erythrophagocytosis in both the *P.berghei* and SMA (*P.chabaudi* and *P.berghei*) models. Other mechanisms besides phagocytosis may have a greater role in red cell destruction in these models and they remain to be elucidated.

We also tested potential modulators of phagocytosis. The assumption was that such modulators may be essential in onset and sustenance of phagocytosis *in vivo*. These included malaria pigment (hemozoin), human TNF and spleen cytokines from a Day 5 post-infection anemia model mouse. None of these however decisively inhibited or increased the extent of phagocytosis in our positive control (J774 macrophages ingesting anti-TER 119-coated RBCs) and neither did they enhance phagocytosis on our SMA model. Given that we did not detect any significant phagocytosis in our SMA model we could not achieve one of our aims namely, to identify red cell ligands and macrophage receptors involved in this process. It would be important to validate and explore further *P. chabaudi* erythrophagocytosis.



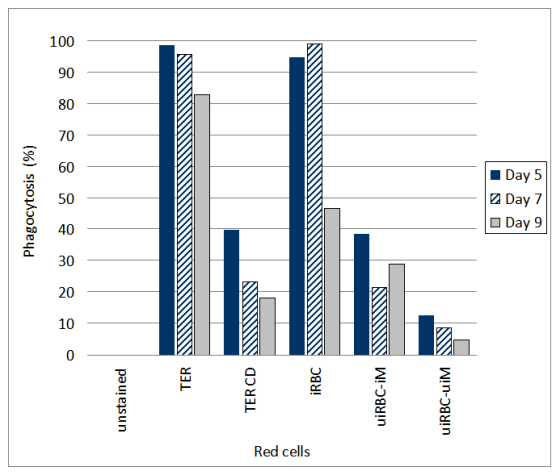
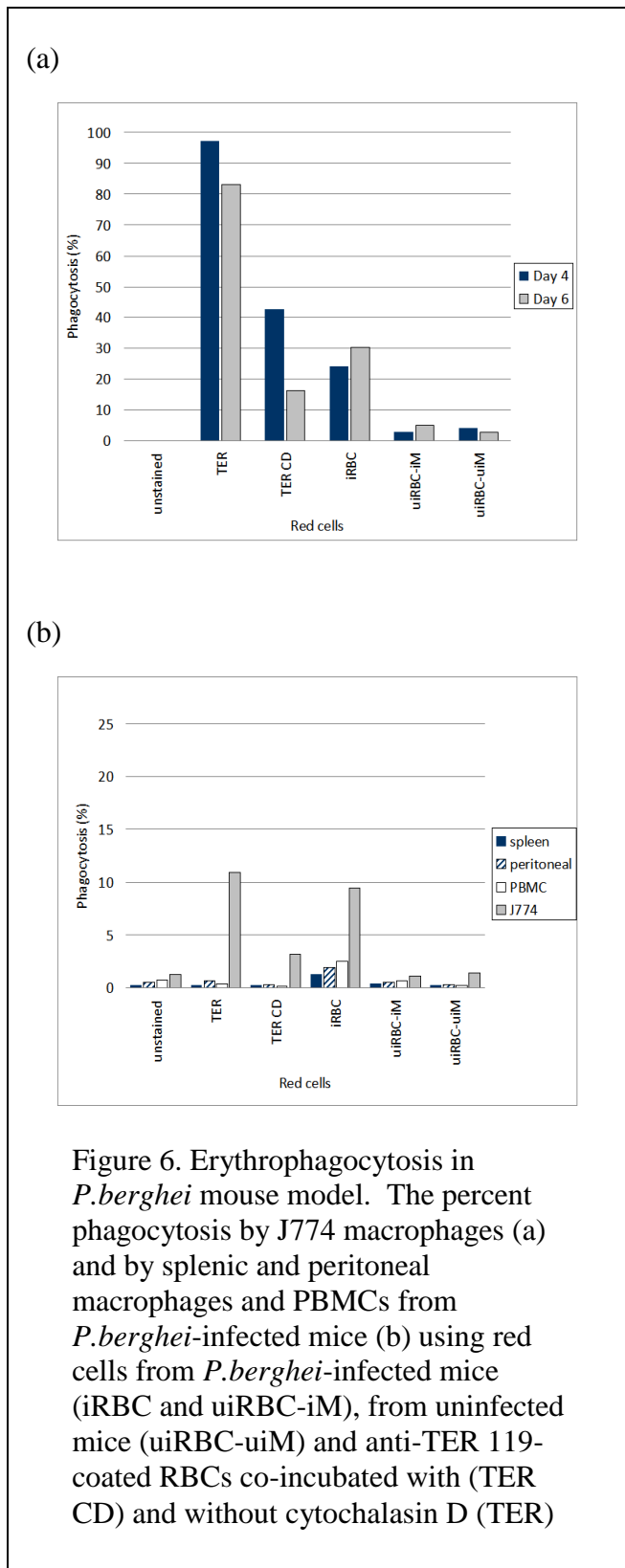
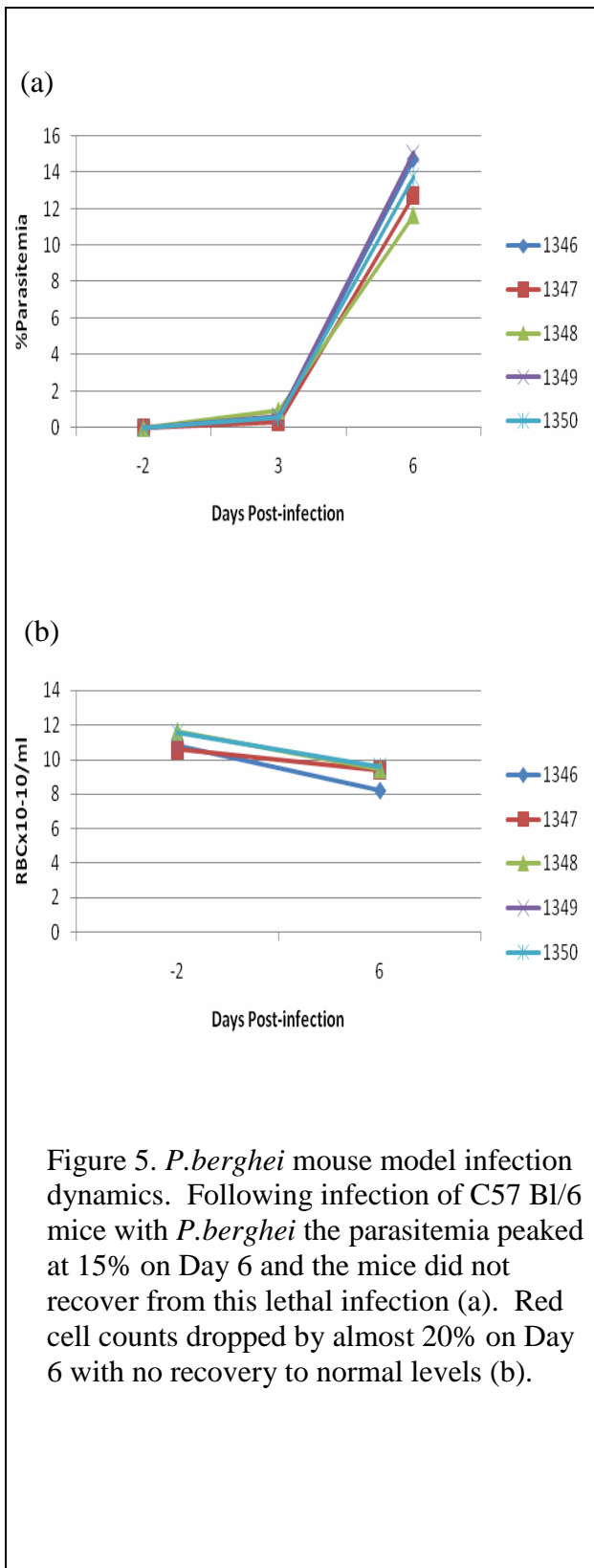
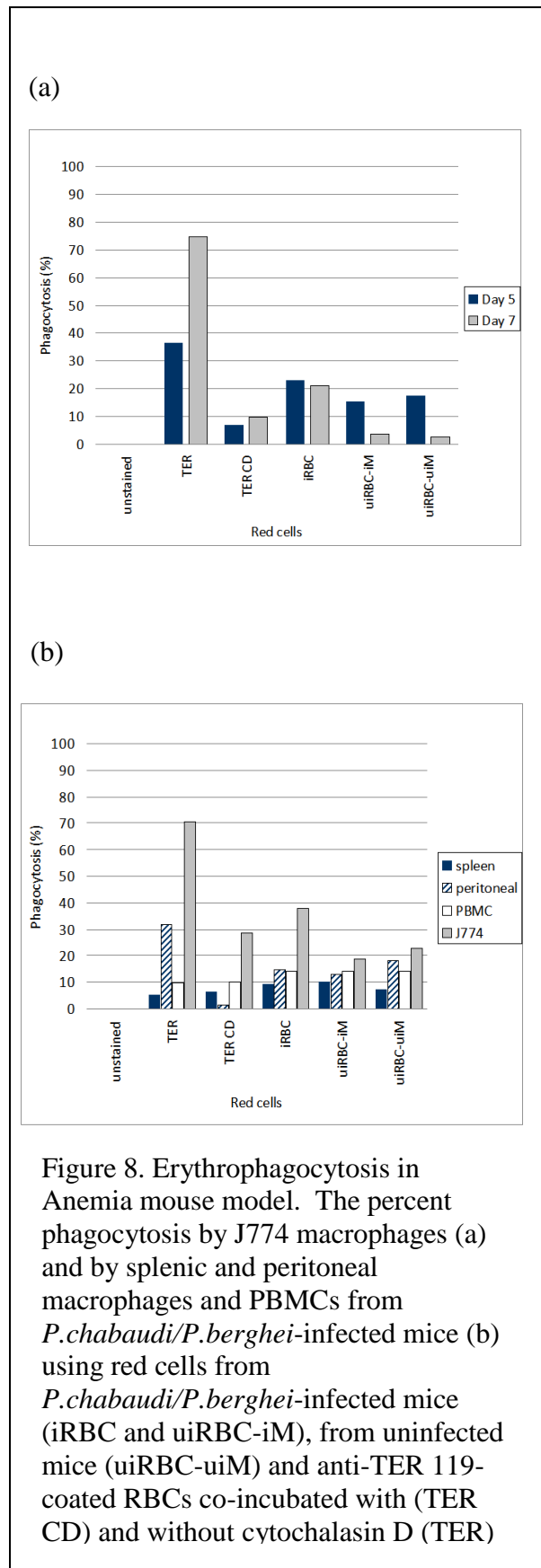
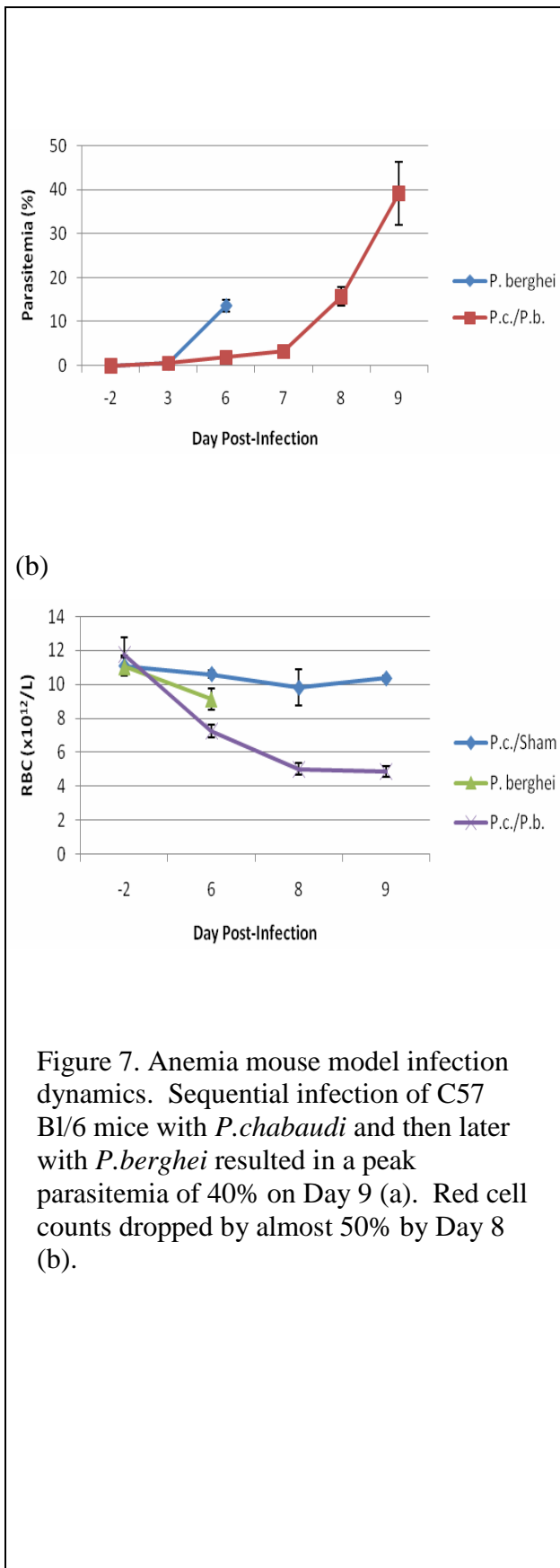


Figure 4. Erythrocytosis in *P.chabaudi* mouse model. The percent phagocytosis by J774 macrophages using red cells from *P.chabaudi*-infected mice (iRBC and uiRBC-iM), from uninfected mice (uiRBC-uiM) and anti-TER 119-coated RBCs co-incubated with (TER CD) and without cytochalasin D (TER)





## **Research Project 21: Project Title and Purpose**

*In Vivo Anti Tumoral Properties of Ceramide Nano-Liposome in Murine Hepatocellular Cancer-*  
Through the use of nanotechnology, ceramide has been encapsulated in tiny bundles called liposomes. Ceramide is a sphingolipid, and is not soluble in blood. However encapsulation of ceramide into nanoliposome allows ceramide to travel in the bloodstream without any toxicity and thus allows it to target the tumor. Previous studies in murine breast cancer models showed that ceramide preferentially induced apoptosis of breast cancer cells, sparing the surrounding healthy tissue and found that very high doses of ceramide was non-toxic to the animals. In this study we will apply ceramide liposome treatments for cancer therapy using a SV40 T- antigen murine model system aimed at the inhibition of the solid tumor of hepatocellular cancer (HCC). These studies are critical in understanding the importance of the liposomal drug therapy, and may be unique for the experimental model.

### **Anticipated Duration of Project**

5/1/2009 – 6/30/2011

### **Project Overview**

Hepatocellular cancer (HCC) is the fifth most common cancer in the world with 5-year survival rates of less than 5%. The incidence of HCC is at least one million new patients per year. HCC primarily occurs in individuals with cirrhosis related to either hepatitis C virus (HCV) or hepatitis B virus (HBV) infections. This tumor is refractory to most chemotherapy, and radiation is rarely possible due to liver toxicity. Treatment relies mainly on surgical management: via resection, transplantation, or ablative techniques. Current treatment modalities, including surgery and liver transplantation, offer limited survival benefits, with the number of deaths from the disease in the US (16,780) nearly equal to the number of newly diagnosed cases (19,160). New therapies are desperately needed.

Ceramide liposome (Lip-C6) has been found to be a potential therapeutic agent demonstrating anti-mitogenic and pro-apoptotic effects on various human cancerous cell lines in vitro. The cytotoxic effect of ceramide liposome acts exclusively on cancer cells even at low concentrations (5 $\mu$ M) and has not been noted on the normal epithelial cells even at very high concentrations. This has resulted in the unprecedented interest in ceramide liposome and has prompted the search for new and innovative preclinical studies. Moreover, reports from literature demonstrate that liposomes play a critical role in reduction of the tumor size in transplantable models. The effects of ceramide liposome on potential chemotherapeutic responses have not been defined in HCC. We have developed a murine model for HCC that spontaneously develops liver tumors under the influence of the large T antigen (T ag) of the SV40 virus. This model represents a unique approximation to human hepatocellular carcinoma, as the mice spontaneously develop malignant tumors through the expression of a viral oncogene. In this model, liver tumors constitutively express the T ag as a tumor-associated antigen and closely resemble the macroscopic and histological characteristic disarrangement seen in liver cancer patients. Therefore, this would be an excellent model to evaluate the liposome treatment effects on liver

cancer kinetics. The overall goal of this project is to gain a new understanding of the effects of treatment with ceramide liposomes on tumor growth in a murine model of spontaneous HCC.

### **Principal Investigators**

Hephzibah Rani S. Tagaram, PhD  
Research Assistant  
Penn State University, College of Medicine  
500 University Drive  
Hershey, PA-17033

### **Other Participating Researchers**

Kevin Staveley-O'Carroll, MD, PhD, Mark Kester, PhD, Harriet Isom, PhD – employed by Penn State University, College of Medicine

### **Expected Research Outcomes and Benefits**

Neo-angiogenesis is the process of formation of new blood vessels in the tumors. It is well accepted that neo-angiogenesis is a critical step required to maintain tumor growth. Multiple therapeutic strategies targeting tumor vessels have demonstrated benefit in delaying solid tumor progression. We hypothesize that treatment with ceramide liposome (lip-C6) delays the progression of liver tumors in a murine model for HCC.

Ceramide liposome (Lip-C6) has been found to be a potential therapeutic agent demonstrating anti-mitogenic and pro-apoptotic effects on various human cancerous cell lines in vitro. However, those anti-mitogenic and pro-apoptotic effects have not been evaluated specifically for tumor blood vessel cells after exposure to ceramide-liposome. Utilizing immunohistochemical techniques we will simultaneously evaluate the expression of cellular proliferation markers like PCNA and Ki67 and apoptotic markers (TUNEL) on cells expressing CD31 and CD105 markers which are specific for endothelial cells. Treatment with Lip-C6 will result in decreased expression of proliferation markers PCNA and Ki67, and increased expression of TUNEL as an indication of the inhibition in tumor growth. This inhibition may be prominent in mice treated with lip-C6 compared to mice treated with ghost liposome or mice without treatment. We anticipate controlled levels of CD31 and CD105 as an indication of anti-angiogenic ability of lip-C6 compared to ghost liposome. The mechanism and pathways underlying the anti-angiogenic properties of Lip-C6 will be the basis for targeted therapy for the future human studies. These studies could lead to new avenues intended to evaluate the immunologic effects of liposome treatment on a hepatic tumor antigen-specific fashion. This in turn will lead to a better understanding of the precise mechanisms by which these novel therapeutic approaches mediate apoptosis in HCC.

### **Summary of Research Completed**

There is a continuing need for innovative and alternative therapies for HCC. Hence we have used the nanoliposomal C6-Ceramide to evaluate the effects on anti-mitogenic and pro-apoptotic

effects on the human Hepatocellular cancer.

1. We have successfully determined the efficiency of ceramide liposome to inhibit proliferation and promote apoptosis in the human Hepatocellular carcinoma cell lines.

We initially evaluated the *in vitro* efficacy of nanoliposomal C6-ceramide for the treatment of human SK-HEP-1 cells, a model of metastatic HCC. SK-HEP-1 human HCC cells were maintained at 37°C, and 5% CO<sub>2</sub>, in MEM supplemented with 10% FBS, 1% sodium pyruvate, 1% non-essential amino acids, 1% sodium bicarbonate, 1% L-glutamine, and 1% penicillin/streptomycin. For subculture, cells were subject to trypsin/EDTA detachment, centrifuged, resuspended in growth media, and replated at appropriate cell density. Proliferation assay was performed by MTT assay (Fig 1A). Nanoliposomal C6-ceramide, pegylated to improve retention and limit toxicity, has been shown to effectively treat cellular and animal models of breast cancer and melanoma. 10 µM nanoliposomal C6-ceramide induced a significant 30% decrease in SK-HEP-1 cellular viability *in vitro*, compared to the PBS control and ghost nanoliposome, as indicated by MTS viability assay (Fig. 1A).

We further determined the apoptotic effect of Lip-C6 on SK-HEP-1 cell by caspase assay, annexin-V staining and TUNEL staining. SK-HEP-1 cells were plated at 5x10<sup>3</sup> cells per well in 96-well tissue culture plates, and grown in 10% serum fortified media for 48 hours prior to treatment. Cells were exposed to PBS, ghost nanoliposomes, or nanoliposomal C6-ceramide for 24 hours in media containing 1% FBS. Caspase 3/7 enzymatic activity was measured following treatment using an Apo-ONE Homogeneous Caspase 3/7 Assay according to the manufacturer's instructions (Promega, Madison, WI). Caspase 3/7 activity was determined by measuring fluorescence of the cleaved substrate using a microplate reader (excitation: 498 nm; emission 521 nm). The results on caspase with 10 µM nanoliposomal C6-ceramide, but not ghost nanoliposomes or PBS controls, stimulated a robust 5-fold increase in caspase 3/7 activity, indicative of an apoptotic death pathway (Fig. 1B).

To further substantiate the apoptotic potential of ceramide in SK-HEP-1 cells, we assessed annexin-V expression and TUNEL staining. SK-HEP-1 cells were treated, harvested and stained (1x10<sup>6</sup> cells/ml of annexin-binding buffer) with annexin-V FITC labeled antibody (Molecular Probes) for 15 min at RT. Stained cells were analyzed by flow cytometry. Annexin V staining of SK-HEP-1 cells showed a 2 fold increase with 10 µM nanoliposomal C6-ceramide (Fig 1C). Terminal Deoxynucleotide Transferase dUTP Nick End Labeling (TUNEL) Assay determines the fragmented DNA as an indication of apoptosis. SK-HEP-1 cells were plated at 1000 – 10,000 cells per well in 8-well chamber slides, and grown in 10% serum fortified media for 48 hours prior to treatment. Cells were exposed to PBS, ghost nanoliposomes, or C6-ceramide-containing nanoliposomes for 24 hours in media containing 1% FBS. Fragmented DNA of apoptotic cells was stained using an ApopTag Red *In Situ* Apoptosis Detection Kit according to the manufacturer's instructions (Chemicon, Temecula, CA), and visualized by fluorescence microscopy using appropriate filters. TUNEL staining of SK-HEP-1 cells further showed that 10 µM nanoliposomal C6-ceramide, but not ghost nanoliposomes, induced apoptosis of SK-HEP-1 cells *in vitro* (Fig. 1D).

## 2. Blockade of G<sub>2</sub>-M phase of cell cycle of SK-HEP-1 cells with Lip-C6 treatment:

SK-HEP-1 cells were grown at  $5 \times 10^3$  in 10% serum fortified media for 48 hours prior to treatment. Cells were exposed to PBS, ghost nanoliposomes, or C6-ceramide-containing nanoliposomes for 24 hours in media containing 1% FBS. Cells were dissociated from culture plates, resuspended in PBS, and DNA stained with propidium iodide. Flow cytometry was used to determine cell cycle distribution based on total DNA content per cell. Cell cycle arrest is often a preliminary event that leads to apoptosis. As ceramide has previously been documented to interfere with cell cycle progression in HCC, we evaluated the effect of nanoliposomal C6-ceramide on the cell cycle. We utilized flow cytometry following DNA staining with propidium iodide, and quantified the proportion of SK-HEP-1 cells in the G<sub>1</sub>, S, and G<sub>2</sub> phases of the cell cycle (Fig. 2). We demonstrate a significant percentage of SK-HEP-1 cells treated with 10  $\mu$ M nanoliposomal C6-ceramide in the G<sub>2</sub> phase ( $37.98\% \pm 0.36$ ), compared to cells treated with ghost nanoliposomes ( $18.34\% \pm 1.65$ ) or control PBS ( $20.22\% \pm 0.43$ ), indicative of blockade at the G<sub>2</sub>-M checkpoint (Fig 2). Similar G<sub>2</sub>-M blockade as well as decreases in cellular viability and increases in caspase3/7 activity and TUNEL staining were shown with C3A human HCC cells lines when treated with liposomal C6 ceramide (data not shown).

## 3. Nanoliposomal C6 decreases the phosphorylation of AKT

AKT phosphorylation is often associated with resistance to apoptosis in cancer cells. The effect of C6 nanoliposomal ceramide on prosurvival AKT signaling was studied by western blot analysis. Cell lysates were prepared by treating tissues with lysis buffer (0.1% NP40, 50mM HEPES, 137mM NaCl, 10mM Na<sub>4</sub>P<sub>2</sub>O<sub>7</sub>, 50mM NaF, 5mM b-glycerophosphate, 1mM EGTA, 2mM EDTA, 1% glycerol, 2mM) containing protease inhibitor (Calbiochem) for 20 min on ice followed by centrifugation at 4 ° C for 15 minutes to sediment particulate materials. The protein concentrations were measured using Bio-Rad protein assay kit. (Bio-Rad Laboratories, Hercules, CA). Protein (30ug) from whole cell extracts were separated on SDS- polyacrylamide gels and transferred onto nitrocellulose membrane. Membranes were blocked with 1% BSA in TBS containing 0.05% Tween and incubated with pAKT and  $\beta$ -actin primary antibodies (Cell Signaling, Beverly, MA) before visualization with enhanced chemiluminescence detection (Thermo Scientific, Rockport, IL). Following 24h of treatment with C6 nanoliposomal ceramide, phosphorylation of AKT was reduced in a dose dependent manner (Fig 3). Equal loading of lanes was confirmed by  $\beta$ -actin staining. The results are consistent with previous studies showing that nanoliposomal C6 ceramide can target cancer cells by diminishing activated AKT signaling.

## 4. Growth of SK-HEP-1 tumors *in vivo* is prevented by systemic administration of nanoliposomal C6-ceramide

Bilateral human HCC tumor xenografts were established in female athymic nude mice (Jackson Laboratories, Bar Harbor, ME) by subcutaneous injection of SK-HEP-1 cells over the rib cage. For each tumor,  $5 \times 10^6$  cells were resuspended in 200  $\mu$ l of cell culture media. Tumors were allowed to establish for one week prior to commencement of treatment regime. Treatments occurred on alternate days via tail vein injection of sterile saline, ghost nanoliposomes, or C6-ceramide-containing nanoliposomes at 36mg/kg body wt of the mice. Each treatment group consisted of 5 animals, each with bilateral tumors. Tumor volumes were quantified by measuring with calipers, and multiplying tumor length, width, and height. At the conclusion of the trial, animals were sacrificed, and tumors were excised and processed for histological analysis by formalin fixation, paraffin embedding, and microtome sectioning. All animal procedures were

approved by, and carried out according to the standards and guidelines of the Pennsylvania State University College of Medicine Institutional Animal Care and Use Committee. Tumor volume was monitored by measuring the length, width, and height of tumors with calipers. We observed that systemic administration of nanoliposomal C6-ceramide completely prevented the growth of human HCC xenografts in athymic nude mice, whereas saline or ghost nanoliposomes did not (Figure 4). Specifically, by the end of the trial (>7 weeks post tumor initiation), mice receiving saline or ghost nanoliposomes had tumor volumes over 3.5 times greater than those in mice that were treated with nanoliposomal C6-ceramide (Fig 4).

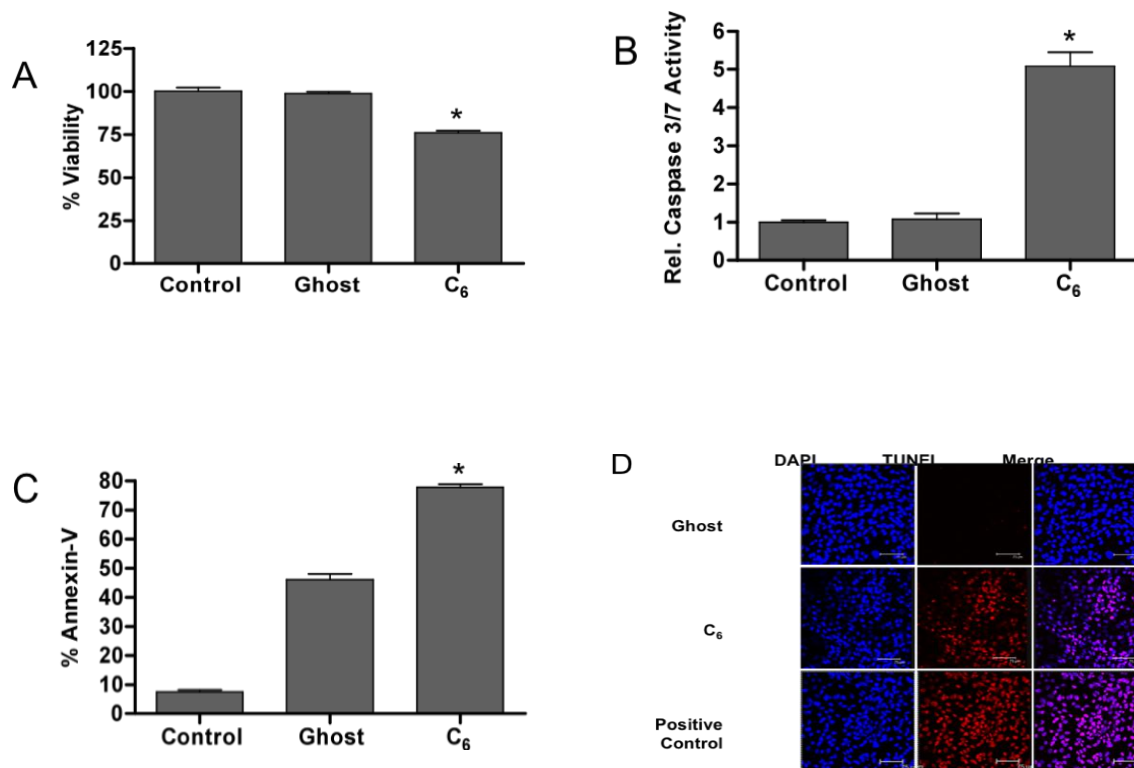


**Figure 1. Nanoliposomal C6-ceramide decreases the viability of SK-HEP-1 cells *in vitro* by inducing apoptosis.** Human SK-HEP-1 hepatocellular carcinoma cells were treated with 10  $\mu$ M nanoliposomal C6-ceramide (C6), nanoliposomes without C6-ceramide (Ghost) or PBS (Control), in growth media supplemented with 1% FBS. (A) Cellular viability was determined by MTS viability assay after 24 h treatment. (B) Caspase 3/7 activity was determined by fluorometric assay after 24 h treatment. (C) Annexin-V staining detects the externalized phosphatidylserine from within the cells to the surface, as an indication of apoptosis. (D) DNA fragmentation was analyzed by TUNEL staining after 24 h treatment. The TUNEL positive control is treated with DNAase. All data represent the averages of at least three independent experiments  $\bar{x} \pm$  SEM, \* $p < 0.05$ , 1-way ANOVA. Images are representative of at least three independent experiments.

Figure 2

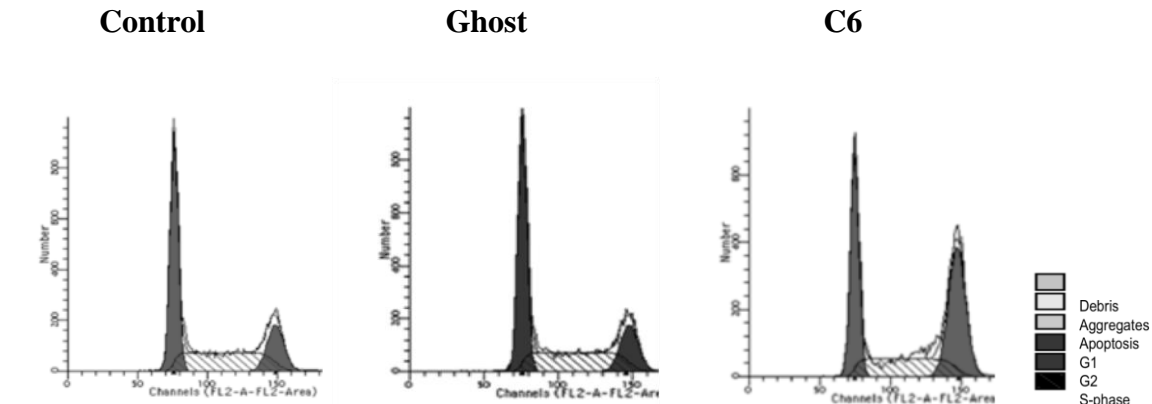


Figure 2. SK-HEP-1 cells treated with nanoliposomal C6-ceramide accumulate in the G<sub>2</sub> phase of the cell cycle. SK-HEP-1 cells were treated with 10 μM ghost nanoliposomes or 10 μM C6 nanoliposomal ceramide in growth media supplemented with 1% FBS for 24 h. Cells were collected, stained with propidium iodide, and analyzed by flow cytometry. DNA histograms are representative of at least three independent experiments.

Figure 3

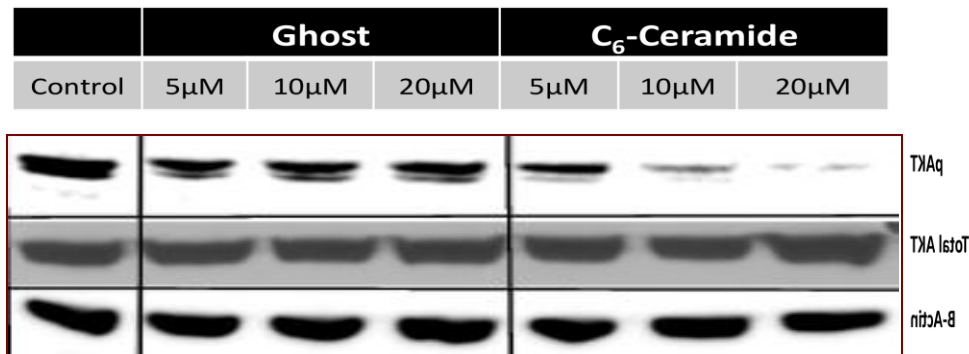


Figure 3. SK-HEP-1 cells treated with nanoliposomal C6-ceramide have diminished phosphorylation of AKT. SK-HEP-1 cells treated with 5, 10, and 20 μM nanoliposomal ceramide, but not ghost nanoliposome and control treatment, have significantly decreased pAKT levels. β-actin and total AKT served as controls for protein loading. A representative blot of n = 2 experiments

Figure 4

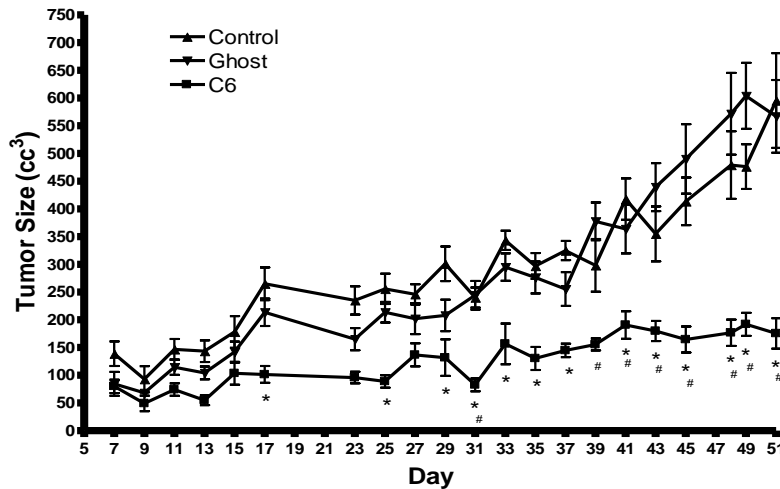


Figure 4. Nanoliposomal C6-ceramide prevents *in vivo* growth of SK-HEP-1 xenografted tumors in nude mice. Bilateral human SK-HEP-1 hepatocellular carcinoma xenografts were established in female athymic nude mice (5 mice per treatment group). Systemic tail vein injections of sterile isotonic NaCl, 36mg/kg of ghost nanoliposomes (Ghost), or 36 mg/kg of nanoliposomal C6-ceramide (C6) were given on alternate days, and tumor volume was determined by caliper measurement. The average tumor volume of the nanoliposomal C6-ceramide group was significantly different from the other treatment groups, as determined by 2-way ANOVA: \* $p < 0.05$  vs. Control, # $p < 0.05$  vs. Ghost.

## **Research Project 22: Project Title and Purpose**

*The Use of Biomarkers to Predict the Onset of Vasospasm in Aneurysmal Subarachnoid Hemorrhage* - The purpose is to create a panel of key molecular markers that can be used as a diagnostic test to predict the occurrence of cerebral vasospasm in the setting of aneurysmal subarachnoid hemorrhage (SAH).

### **Anticipated Duration of Project**

7/8/2009 - 6/30/2011

### **Project Overview**

Of those patients that survive an initial aneurysm rupture and/or re-rupture, the primary cause of death and further disability is cerebral vasospasm. There are no clinical warnings that allow the clinician to predict which patients will experience vasospasm. The pathogenesis of vasospasm is not known. There are over twenty cellular and molecular factors that have been implicated. No one has been able to satisfactorily predict which patients will undergo cerebral vasospasm based on the presence of hemorrhage in the subarachnoid space. Our study will allow us to examine a wide selection of interleukins and growth factors during a patient's hospital stay and correlate these with clinical cerebral vasospasm. This approach to vasospasm diagnosis using a panel of pertinent molecular markers has not been previously studied. With these data we will be able to

create a diagnostic test that will allow for the early prediction of vasospasm.

### **Principal Investigator**

Kevin M. Cockroft, MD, MSc  
Associate Professor  
Penn State Hershey Medical Center  
30 Hope Drive, EC110  
Hershey, PA 10033

### **Other Participating Researchers**

James R. Connor, PhD, Ryan Mitchell, PhD - employed by Penn State College of Medicine  
Akshal S. Patel, MD –employed by Penn State Hershey Medical Center

### **Expected Research Outcomes and Benefits**

Stroke is the third leading cause of death and the primary cause of disability in the United States. Aneurysmal subarachnoid hemorrhage (SAH), a form of hemorrhagic stroke, is a particularly devastating disease. The thirty-day mortality rate after aneurysmal SAH is approximately 50% with the majority of survivors left disabled and unable to return to work. Of those patients that survive the initial aneurysm rupture and/or re-rupture, the primary cause of death and further disability is cerebral vasospasm. Despite its unequivocal clinical significance, the complete pathogenesis of post-hemorrhagic cerebral vasospasm remains poorly understood and there is no accurate, early diagnostic test to predict its occurrence.

We plan to determine a molecular profile that can be used to predict which patients will experience clinically significant cerebral vasospasm. We will use a multiplex immunoassay to evaluate a panel of inflammatory and trophic proteins present in cerebrospinal fluid (CSF) and serum during the course of aneurysmal SAH. Using regression analysis we will develop a panel of biomarkers that can be used to predict cerebral vasospasm.

### **Summary of Research Completed**

#### Clinical components

An institutional review board (IRB) proposal was completed and approved prior to the onset of investigation. (Hershey Medical Center and Penn State College of Medicine IRB 30616). Between July 1<sup>st</sup> 2009 and April 30<sup>th</sup> 2010, 34 patients were enrolled into this study. Patient selection and suitability was based on the presence of subarachnoid hemorrhage due to aneurysmal rupture only. Subarachnoid hemorrhage in this setting was confirmed via radiographic data in all cases. All patients were consented within 48 hours of the onset of their clinical symptoms. All patients were admitted to the Neurosurgical Service at the Penn State Hershey Medical Center. Demographic and radiographic data were collected on point of admission. This included age, sex, location and size of aneurysm, Hunt-Hess grade, Fisher grade, World Federation of Neurologic Surgeons grade, cigarette smoking status and placement of external ventricular drain (Table 1).

Venous blood was obtained on a daily basis for each patient during the admission period. If a patient required an external ventricular drain (EVD), cerebrospinal fluid (CSF) was also obtained daily while access was available. Samples were obtained between 7am and 2pm, to limit variations of circadian rhythm. Once samples were obtained they were immediately hand couriered to the lab on ice (see below).

All patients were subject to daily Transcranial Doppler (TCD) imaging. Two patients had temporal bones too thick for ultrasonographic interpretation. TCD provided the velocity of blood flow in the anterior cerebral artery, the middle cerebral artery, the internal carotid artery and the posterior cerebral artery of both hemispheres. As vessel diameter narrows, velocity increases in order to maintain constant flow, hence vasospasm is correlated with TCD velocity. The highest mean velocity, in any arterial territory was used to categorize the patient's degree of TCD vasospasm. If the mean velocity was less than 80 cm/sec it was considered that the vessel was not spastic or narrowed. Similarly, velocities between 80-120 cm/sec denoted mild spasm, 120-200 cm/sec, moderate spasm and greater than 200 cm/sec, severe vasospasm. In addition, patients were monitored closely for signs of delayed ischemic neurologic deficit (a.k.a. clinical vasospasm). Further imaging was performed with either MRI or CT if clinically warranted. Two patients required intracranial endovascular angioplasty for treatment of clinically symptomatic vasospasm that was refractory to noninvasive ICU management.

#### Laboratory components

Once the samples were received in the lab, they are spun down in a centrifuge at 1000G for 5 minutes. The supernatant was extracted as to leave all particulate matter behind. Protease inhibitor cocktail (Sigma-Aldrich; St. Louis, MO) was then added 1:100. The samples were then stored at minus 80 degrees Fahrenheit in 200uL aliquots. When it was possible to analyze the samples, they were appropriately thawed.

#### Multiplex cytokine bead assay

We performed multiplex analysis on undiluted blood and CSF supernatants using the Bio-Plex Human 27-plex panel of cytokines and growth factors (Bio-Rad; Hercules, CA) (Table 2). The analytes tested are listed in Table 1. One percent bovine serum albumin (BSA, Sigma-Aldrich; St. Louis, MO) was added to 200uL of each of the supernatants. The standards were reconstituted in PBS with 1% BSA. Fifty uL of each sample or standard was added in duplicate to a 96 well plate and mixed with 50uL of antibody-conjugated beads for 1 hour at room temperature. Wells were then washed and 25uL of detection antibody was added to each well. After a 30-minute incubation, wells were washed and 50uL of streptavidin-PE was added to each well for a second 10-minute incubation. A final wash cycle was then completed and 125uL of assay buffer was added to each well. The plate was then analyzed using a Bio-Plex 200 workstation (Bio-Rad). Analyte concentration was calculated based on the standard on the respective standard curve for each cytokine. Analyte concentration was measured in picograms per milliliter. For direct comparison and to measure trends between analytes, the concentration values were normalized. This calculation was based on the analyte concentration on day 1 of patient admission. All data collected from day 1 onwards reflects a change from an arbitrary baseline across all analytes.

Results to date

To date, serum samples from 20 of the 34 patients enrolled have been processed. CSF was collected in 12 patients, at present these samples have not been analyzed. Until all samples are processed no statistical analysis will be performed. Representative figures showing the serum levels of the various analytes in patients within typical vasospasm categories are presented (Figures 1 – 4).

Table 1: Demographic data.

	<b>Total</b>	<b>No TCD Vasospasm</b>	<b>Mild TCD Vasospasm</b>	<b>Moderate TCD Vasospasm</b>	<b>Severe TCD Vasospasm</b>
<b>Total Number of Patients</b>	34	5	6	12	9
<b>Male Gender</b>	26	1	2	3	2
<b>Median Fisher Score</b>	4	3	3	4	3
<b>Median Hunt-Hess Grade</b>	2	2	2	2	2
<b>Median World Fed. Neurol. Surgeon. Score (WFNS)</b>	2	1	1	2	2
<b>Endovascular embolization</b>	28	4	6	9	7
<b>Microsurgical surgical Clipping</b>	6	1	0	3	2
<b>Tobacco Use</b>	18	1	5	6	6

Table 2: List of analytes tested using multiplex bead assay.

IL-1 beta	IL-7	IL-15	Eotaxin
IL-1ra	IL-8	IL-17	Granulocyte-monocyte colony stimulating factor
IL-2	IL-9	VEGF	IFN-gamma
IL-4	IL-10	Fibroblast growth factor basic	Monocyte chemoattract protein-1
IL-5	IL-12	TNF-alpha	Macrophage inflammatory-1-alpha
IL-6	IL-13	PDGF bb	Macrophage inflammatory-1-beta

Figure 1

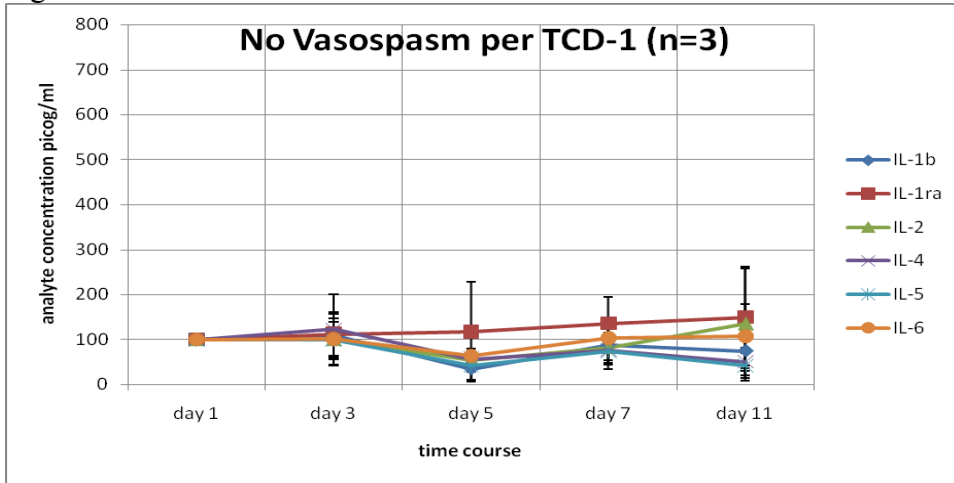


Figure 2

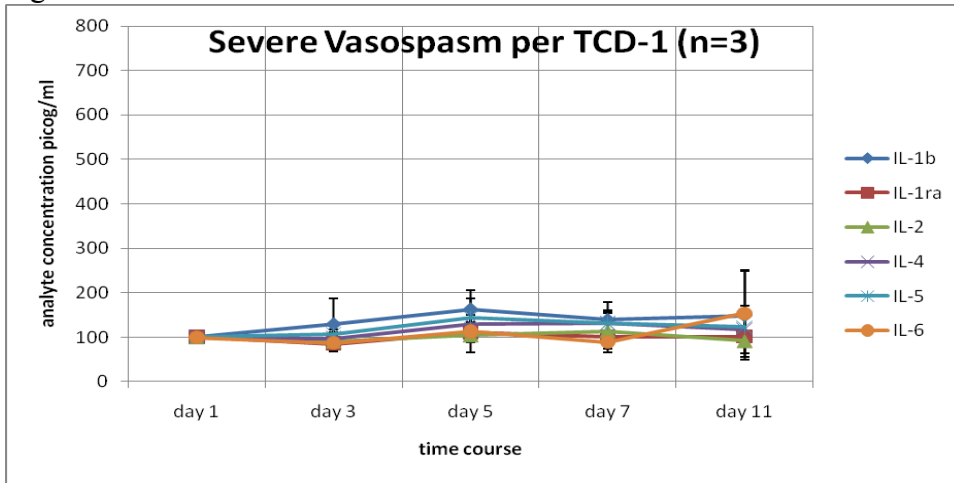


Figure 3

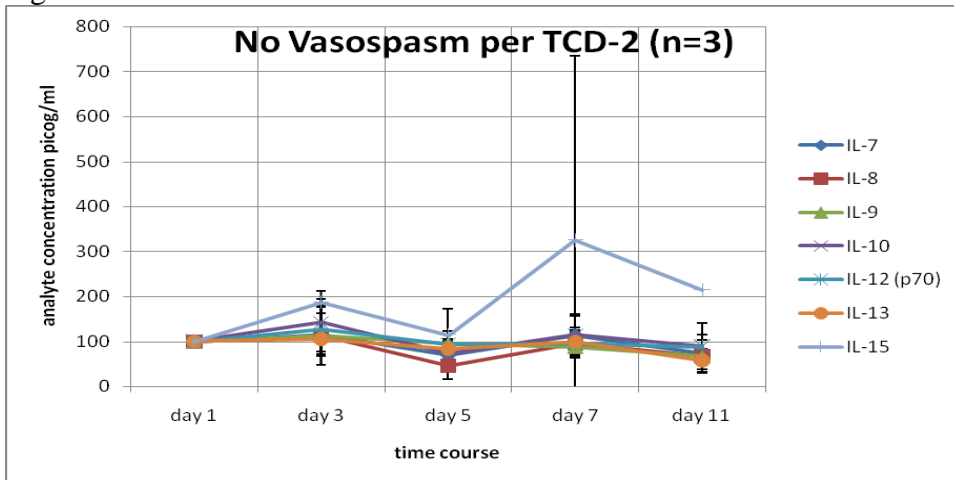


Figure 4

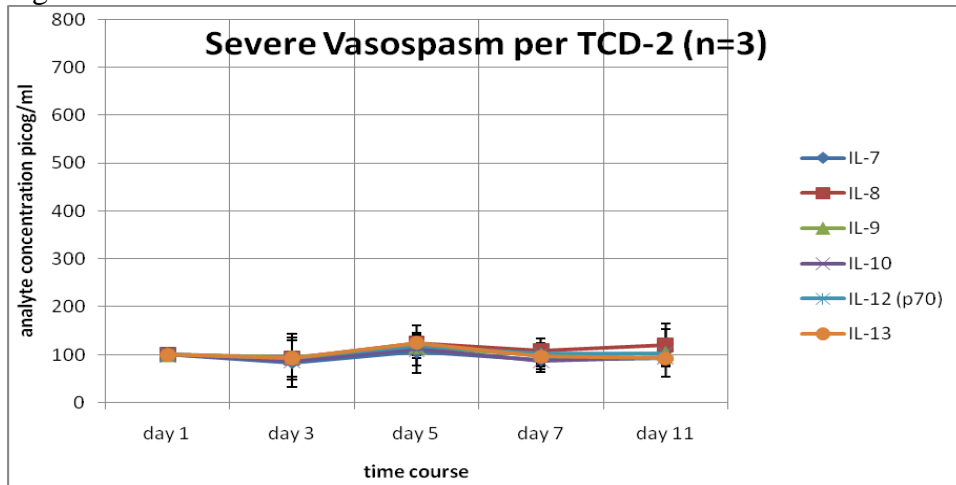


Figure 5

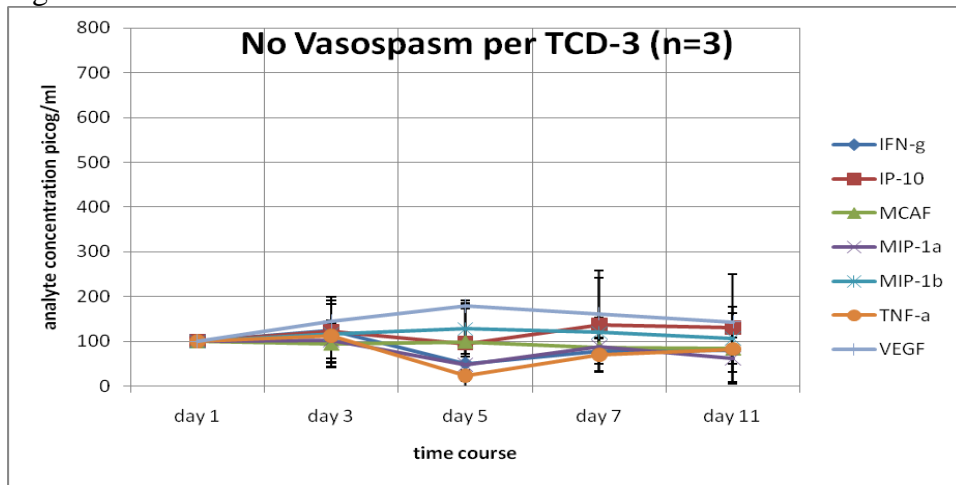
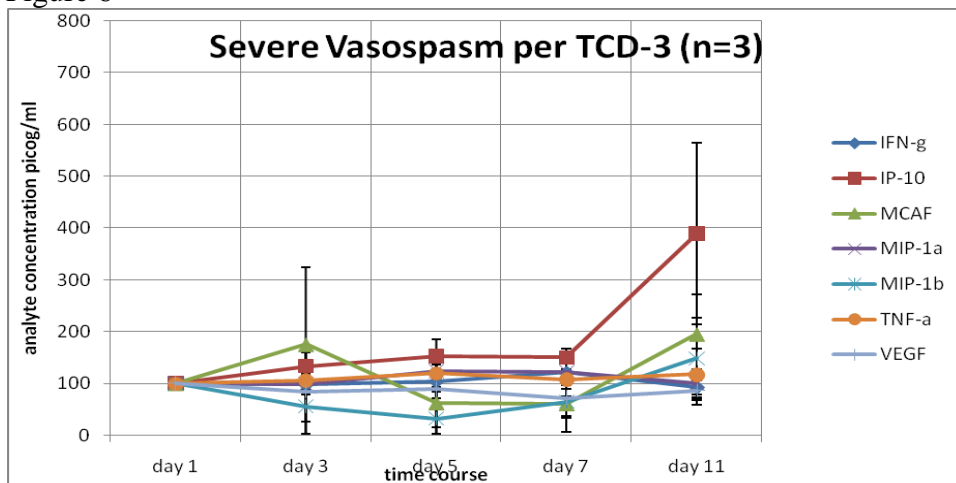


Figure 6



## **Research Project 23: Project Title and Purpose**

*Tim-2 Expression on Oligodendrocytes: A New Immune System Target* – Recently, we have made a novel and exciting discovery that Tim-2 receptor is selectively expressed on oligodendrocytes. One of the ligands for Tim-2 is Sema4A, which is highly expressed in the immune system, and is critical in regulating immune attacks on the myelin in animal models of multiple sclerosis (MS). We have shown that when oligodendrocytes are exposed to Sema4A in a cell culture model they die. This is an exciting and new finding suggesting that the Sema4A/Tim-2 interaction may be the deleterious relationship between oligodendrocytes and immune cells that scientists have been seeking. Therefore, in this project, we want to investigate mechanism of Sema4A-induced oligodendrocyte death.

### **Anticipated Duration of Project**

7/8/2009 - 6/30/2011

### **Project Overview**

Despite the recent advances in our understanding of disease pathogenesis and treatment of multiple sclerosis, this disease still represents a significant source of neurologic disability. Although immunomodulatory drugs are very effective at treating active disease, they are completely ineffective at treating the chronic neurodegenerative phase of MS. To address this, one approach is finding ways of encouraging remyelination by endogenous oligodendrocyte progenitor cells, allowing them to repair myelin and therefore preventing secondary axonal loss and neurodegeneration. We have recently discovered that Tim-2 protein is selectively expressed on cells of oligodendrocyte lineage. Tim-2 is present on mature oligodendrocytes and oligodendrocyte progenitors and functions as receptor for extracellular H-ferritin and Sema4A proteins. Considering that both Sema4A and Tim-2 have an important function in immune regulation and are critical in development of experimental autoimmune encephalomyelitis (EAE), we propose that existence of Tim-2 receptors on oligodendrocytes may predispose these cells to immune attack. There are two specific aims that we intend to accomplish.

**Aim 1:** Test the hypothesis that Sema4A can be detected in demyelinating plaques, but not in normal white matter from human tissue collected at autopsy. A second hypothesis will be tested concomitantly, that Sema4A staining in the plaques will be colocalized with markers of infiltrating lymphocytes (T cells and B cells) and local central nervous system (CNS ) inflammatory cells (astrocytes and microglia).

**Aim 2:** Test the hypothesis that there will be higher concentrations of Sema4A protein in the Cerebrospinal fluid (CSF) of MS patients compared to controls which will be predictive of clinical diagnosis of MS.

### **Principal Investigator**

James Connor, PhD  
Distinguished Professor and Vice Chair, Research

Penn State College of Medicine  
Neurosurgery, H110  
500 University Drive, PO Box 850  
Hershey, PA 17033-0850

### **Other Participating Researchers**

Padma Ponnuru, PhD – employed by Pennsylvania State University

### **Expected Research Outcomes and Benefits**

Our findings will have the potential of identifying a novel mechanism by which oligodendrocytes fail to remyelinate in MS, as well as identifying a novel diagnostic marker and drug target for treatment of MS. Although it will take some time (several years) to develop drugs to inhibit Sema4A-Tim-2 interaction on oligodendrocytes, discovery of Sema4A as diagnostic marker would benefit MS patients immediately, as screening for Sema4A protein could become part of MS diagnostic procedure soon after we publish our findings.

### **Summary of Research Completed**

#### Studies Directed Towards These Aims and Their Results:

The following studies were performed in fulfillment of Aim 2 of the proposal. Aim 2 is now completed. The results are in a manuscript under review in *GLIA*. The manuscript has been accepted pending revisions in *GLIA*.

To begin investigating role of iron delivery systems in oligodendrocyte survival, we subjected primary oligodendrocyte progenitors to transferrin deprivation experiment. Purified rat primary oligodendrocyte progenitors were incubated in complete N2S media and then changed to either complete N2S medium or N2S to which apoTf had not been added. Tf deprived cultures exhibited a four-fold increase in cell death as quantified by both MTT and LDH release assays. To demonstrate that loss of cell viability observed in response to transferrin deprivation is due to iron deprivation, we performed an identical Tf deprivation experiment while adding either increasing concentrations of lipophilic compound TMH-ferrocene or ionic ferric ammonium citrate to the cultures at the time of transferrin withdrawal. Because of its lipophilic nature, TMH ferrocene is able to deliver iron into cytosol, while ionic FAC is unable to do so without a transport system such as Tf/TfnR. In the absence of transferrin (and ferritin) in culture media, membrane-permeant TMH-ferrocene, but not membrane impermeable ferric ammonium citrate was able to prevent loss of cell viability. On the other hand, equimolar concentrations of FAC under identical experimental conditions had minimal effect on cell viability.

To investigate whether H-ferritin was sufficient to replace the transferrin requirement for iron delivery to oligodendrocyte progenitors, we performed the Tf deprivation experiments in the presence of recombinant human H-ferritin. Transferrin deprived cultures of primary OPCs showed loss of cell viability which was prevented in a dose-dependent fashion with the addition of recombinant H-ferritin to the media. To investigate whether this mechanism of H-ferritin rescue is via iron delivery, we assessed intracellular iron content using calcein AM method.

OPCs in Tf deprived N2S media showed approximately 50% increase in fluorescence, which is consistent with iron deprivation of these cells. Conversely, concurrent treatment of Tf deprived OPCs with H-ferritin under identical conditions resulted in reversal of the increased fluorescence signal consistent with an increase in intracellular iron. Overall, transferrin deprivation in oligodendrocyte progenitors leads to loss of intracellular iron, which results in cell death. Adding H-ferritin prevents loss of intracellular iron, which promotes survival and development of oligodendrocyte progenitors.

To evaluate the pro-myelinating potential of extracellular H-ferritin-mediated iron delivery, we treated purified cultures of oligodendrocyte progenitors in N2S complete media with increasing concentrations of recombinant H-ferritin and allowed them to differentiate over a 6 day period. At 6 days post-treatment, cells were evaluated for expression of myelin basic protein (MBP) and olig2 by immunohistochemistry and Western blot. The results demonstrate increased MBP immunoreactivity in rH-ferritin treated cultures compared to untreated controls, while apparent cell number (as demonstrated by DAPI staining, was comparable between the groups). The increase in MBP expression in response to recombinant H-ferritin treatment was dose-dependent, and was confirmed by immunoblot analysis. In addition, we observed an increase in total cellular levels of olig2 in response to recombinant H-ferritin treatment, consistent with increased differentiation of these cells.

The proposed studies for Aim 1 are in progress. The first and second experiments were designed to determine the pattern of expression of Tim2 in the developing rat and if the pattern was disrupted by dietary iron deficiency. The animals have been collected for this study, and the brains have been sectioned and immunostaining is underway. The sections are coded so we are blinded to condition and thus have no in progress data to report at this time. We anticipate this study will be completed in the next 3-4 months.

The third experiment proposed in Aim 1 was to perform binding analyses for H-ferritin in Tim2 knockout mice. The brains for this study have been collected and sectioned and binding is in progress.

#### Significance of the Findings:

We have discovered a novel receptor and its ligand for oligodendrocytes. Given the prevalence of this receptor on oligodendrocytes and the amount of iron delivered, it is likely that this receptor is the predominant iron source for oligodendrocytes. Furthermore, the only known ligand for Tim-2 prior to our discovery is Sema4A. Thus, we have the exciting possibility that we have discovered the mechanism by which the immune system can directly impact oligodendrocytes. If true, this would be the first demonstration of a direct ligand and receptor interaction between the immune system and oligodendrocytes. A grant has been submitted to the NIH and Department of Defense to follow up on this observation.

#### Publications:

- Todorich B, Zhang X and Connor JR. (2010) "H-ferritin and transferrin are complementary iron delivery systems in oligodendrocytes." Accepted with revisions, *GLIA*.
- Todorich B, Olopade JO, Surgaldze N, Zhang X, Neely E and Connor JR (2010) "The Mechanism of Vanadium-Mediated Developmental Hypomyelination Is Related to

Destruction of Oligodendrocyte Progenitors Through a Relationship with Ferritin and Iron.”  
*Neurotox Res* Mar 17. [Epub ahead of print], PMID: 20237879

## **Research Project 24: Project Title and Purpose**

*Mechanisms of Microsatellite Mutagenesis in Human Cells* – Short, repetitive DNA sequences, called microsatellites, are a characteristic feature of the human genome. Mutations within microsatellite sequences are causally linked to the development of several human diseases, including cancer and cardiovascular illness. We have created a new, interdisciplinary program among computational and experimental investigators at Penn State University to elucidate the mechanisms whereby microsatellites arise, mutate, and disappear within individual human genomes. The purpose of this project is to provide direct experimental evidence in support of our new collaborative model in order to improve the competitiveness of our NIH-R01 application.

### **Anticipated Duration of Project**

7/8/2009 - 9/1/2010

### **Project Overview**

**Broad objective:** To elucidate the mechanisms of microsatellite emergence, mutation, and degeneration in individual human genomes.

**Specific Aim 1:** To test the effect of cellular DNA polymerase  $\kappa$  (pol  $\kappa$ ) levels on the degeneration of microsatellite alleles by the interruption pathway.

*Rationale:* Our existing biochemical (in vitro) data clearly implicate pol  $\kappa$  in maintaining the stability of microsatellites. Pol  $\kappa$  specifically produces interruption errors by a single base insertion pathway. We hypothesize that the frequency of this type of microsatellite interruption error occurring in human cells should be directly proportional to the levels of pol  $\kappa$  protein.

*Experimental approach:* To test this hypothesis, we will over-express pol  $\kappa$  in human cells, using a lentiviral expression vector. Mismatch repair-deficient human cells will be transduced, and several clones expressing a range of pol  $\kappa$  protein levels will be selected for mutational studies. Microsatellite-containing shuttle vectors [T/A]<sub>11</sub> and [TC/AG]<sub>11</sub> will be used in the mutation study, as both have been studied extensively in vitro. The HSV-tk mutation rate within the microsatellite region will be determined for each vector and human cell clone combination, using published approaches that are well established in our laboratory.

**Specific Aim 2:** To test the relationship of microsatellite allele length to mutational behavior in human cells.

*Rationale:* In vitro, we have observed that the frequency of mutations within a microsatellite allele increases exponentially with increasing allele length, after a threshold length has been achieved. This result is similar to what our collaborator has observed in computational studies of variation among human genomes. Using our human cell assay, we have previously quantitated the mutation rate for the [TC/AG]<sub>11</sub> microsatellite allele.

*Experimental approach:* We will measure [TC/AG]<sub>n</sub> mutagenesis within alleles of varying length, using a mismatch repair-deficient human cell line. Using techniques that directly follow

our published studies and standard laboratory methods, the mutation frequency and microsatellite specificity will be determined. We will measure the relationship between allele length and mutagenesis in human cells and relate this curve to the existing in vitro and computational studies. This will demonstrate the validity of our interdisciplinary approach for studying human disease risk.

### **Principal Investigator**

Kristin A. Eckert, PhD  
Professor  
Penn State College of Medicine  
Gittlen Cancer Research Foundation  
500 University Drive, H059  
Hershey, PA 17033

### **Other Participating Researchers**

Kateryna Makova, PhD – employed by Pennsylvania State University

### **Expected Research Outcomes and Benefits**

Understanding how microsatellites arise, mutate, and eventually cease to exist within individual human genomes is of importance for several reasons. First, microsatellites are highly abundant elements in the human genome, but have not been widely studied. Microsatellites are believed to function as modifiers of gene expression. Second, microsatellite lengths are highly variable among individuals, leading to their widespread use as markers in forensics and population genetic studies. Third, mutations within microsatellites are directly implicated in common diseases.

This research project will examine mechanisms related to the microsatellite life cycle. A known characteristic of microsatellites is the dynamic nature of their mutations, in which microsatellite sequences both expand and contract at rates greater than other parts of the genome. Our anticipated results will be the first direct experimental analysis of two important aspects of microsatellite behavior in human cells. First, we expect to demonstrate the threshold length that a repetitive sequence must reach to begin behaving as a microsatellite sequence. Second, we expect to directly demonstrate that microsatellites can degenerate due to interruption mutations produced by a specific DNA polymerase. Therefore, we anticipate a high scientific impact value of publications resulting from this project. Moreover, this project will enhance our pending interdisciplinary NIH/R01 application by demonstrating the degree to which biochemical results predict the mutational behavior of microsatellites in human cells.

In the long-term, data resulting from this project will be useful in predicting individuals who may be at risk for common diseases because of the precise DNA sequence composition of their genome.

## Summary of Research Completed

A. Specific Aim 1: To test the effect of cellular DNA polymerase  $\kappa$  (pol  $\kappa$ ) levels on the degeneration of microsatellite alleles by the interruption pathway.

A.1. *Effects of pol  $\kappa$  overexpression on microsatellite mutagenesis* (original approach)

We originally proposed to use a lentiviral vector delivery technique to increase expression of pol  $\kappa$  in the non-tumorigenic, MMR-deficient (PMS2 homozygote) cell line, LCL-1261. However, during the funding period, we discovered (through other ongoing studies in our laboratory) that lentiviral infection of LCL cells alone alters mutagenesis, both mutation frequency and specificity. We therefore began a systematic investigation of other techniques that would result in efficient introduction and integration of foreign DNA into LCL1261 cells. We determined that traditional transfection methods, such as electroporation and lipofection, do not result in high efficiency transfection in this cell line.

Recently, our departmental group purchased an Amaxa nucleofection device; therefore, we sought to determine whether nucleofection would lead to efficient LCL1261 cell transfection. Initial experiments were performed, as directed by the manufacturer, to determine the optimal nucleofection reagent and conditions for these cells. Following optimization, we compared two vectors for short-term transfection efficiency and long term retention following nucleofection: pNC1, an oriP-derived, episomal plasmid; and pMaxGFP, an origin-less, integrative vector. We also compared the efficiencies using supercoiled versus linearized forms of the two plasmids. As shown in Table 1, nucleofection was an efficient method of transfection, as we observed green fluorescence in 70-80% of the cells. Importantly, we continued to observe fluorescence in 5-10% of the cells for 2 weeks following nucleofection, suggesting that the plasmids are stably maintained in the cells. We are very excited by these results, and will continue to use the Amaxa device for the genetic manipulation of LCL1261 cells.

In our original proposal, we intended to use a pIRES/pol $\kappa$  expression vector that we had previously obtained from a colleague. Unfortunately, when we transfected the plasmid into human cells, we failed to observe increased pol $\kappa$  protein levels, using Western analyses. As we were uncertain as to the cause of this failure, we decided to purchase the pol $\kappa$  cDNA (pCMV-Sport6; Invitrogen), and use this cDNA in subcloning. However, when we characterized the Sport6 plasmid, we discovered that it did not encode a full length pol  $\kappa$  protein. We have just recently obtained pcDNA3.1 encoding a full length, flag-tagged pol $\kappa$  cDNA from the laboratory of Dr. Jean Sebastien Hoffman. Both of the technical roadblocks described in this section have resulted in a delay in our ability to complete Aim 1.

A.2. *Effects of UV-irradiation on microsatellite mutagenesis* (alternative approach)

While experiencing the roadblocks described in section A.1., we designed an alternative strategy to test whether pol  $\kappa$  activity can be linked to the production of interruptions within microsatellite sequences. Several publications have indicated that the expression of pol  $\kappa$  and pol $\eta$  may be inducible by DNA damage, and that UV-irradiation of human cells results in the nuclear relocalization of pol  $\kappa$  and pol  $\eta$  into replication foci. Moreover, pol  $\kappa$  has been shown to be required for ~50% of DNA synthesis associated with the repair of UV damage. Our rationale was that UV damage produced within the HSV-tk gene sequence would recruit pol  $\kappa$  to the vicinity of the microsatellite sequence. Our strategy was to UV-irradiate MMR-proficient

(LCL721) or MMR-deficient (LCL1261) cells that stably carry a microsatellite shuttle vector, and examine the types of mutations at the microsatellites before and after UV damage. Initial experiments were performed to determine the UV fluence range that would be mildly lethal to each cell line (Figure 1A). The irradiated cells were cultured for 10 population doublings (2-4 weeks), after which time the shuttle vector DNA was harvested for mutational analyses. We did not observe an increase in the overall HSV-tk mutant frequency with UV dose for either cell line (Figure 1B), suggesting that the majority of UV-induced DNA lesions were efficiently repaired. Nevertheless, DNA sequence analyses of independent mutants from the control and UV-irradiated cultures showed a significant change in the distribution of mutants between the HSV-tk gene and microsatellite target sequence (Figure 1C). In the absence of UV, the majority of mutations were located within the [GT/CA] microsatellite sequence in both cell lines. After UV-irradiation, we observed an increase in the proportion of mutants within the HSV-tk coding region. We conclude that the doses of UV used for this study were mutagenic, and that we did induce a low level of UV damage within the plasmid DNA. Although our numbers are small, we did not observe any interruption mutations among the mutational events at the microsatellite sequence. Unfortunately, this experimental design does not allow us to determine directly whether we were successful at increasing polk activity during plasmid microsatellite DNA synthesis, precluding our ability to interpret the negative data obtained.

B. Specific Aim 2: To test the relationship of microsatellite allele length to mutational behavior in human cells.

An intriguing observation from the computational studies of our collaborator, Dr. Makova, is that the slope of the mutability function is dependent on microsatellite allele length, arguing for unique mutation mechanisms at long microsatellites. We hypothesize that differences in the biochemistry of genomic DNA synthesis may contribute to microsatellite mutational variation across the genome. This is an important topic, as the relative risk for polymorphic microsatellite changes affecting disease may depend on the characteristics of the mutation rate function for that particular microsatellite and genomic region. In this aim, we undertook experimental approaches to ascertain the extent of mutability variation that can be attributed to microsatellite length in human cells. The experimental data shown below will be combined with computational data from Dr. Makova's laboratory in a manuscript describing the mutability of mature human microsatellites.

### B.1. *Experimental Design*

We examined the relationship between [TC/AG]<sub>n</sub> and [GT/CA]<sub>n</sub> microsatellite allele length, MMR, and mutagenesis. We focused on dinucleotide allele lengths between 10 and 30 units, as these lengths represent the second phase of the observed genomic dinucleotide mutability function curve, and dinucleotide microsatellites of lengths above 30 units are virtually absent from the human genome. Mutational analyses of independent human cell clones were performed using our published *ex vivo* shuttle vector assay in MMR<sup>+</sup> (LCL-721 cells) and MMR<sup>-</sup> (LCL-1261 cells). Briefly, OriP-tk shuttle vectors carrying artificial microsatellite alleles of varying length were introduced into each human cell population. Plasmid-bearing cells were selected by growth in hygromycin, after which time independent clones were isolated by limited dilution technique. After 20-30 cell generations, the shuttle vector DNA was harvested and used to electroporate *E. coli* for determination of mutation frequency. Independent mutants were isolated from each clone, and the types of mutational events were determined by DNA sequence

analyses. The experiments using [GT/CA] vectors are still in progress, and final mutational data is not yet available. Below, we summarize our results for the [TC/AG] alleles.

### B.2. Long microsatellite alleles are biased toward expansion mutations in human cells

As expected, in the MMR-proficient cells, we observed an exponential increase in the rate of [TC/AG] mutations as the length increased from 11 to 20 units (Figure 2A). Unexpectedly, the majority of this increase can be explained by the increased production of expansion mutations with length, as the rate of deletions increased only ~2-fold as length increased from 11 to 20 units (Figure 2B). We examined whether the expansion bias could be due to biased MMR by analyzing mutagenesis of the same shuttle vector alleles in LCL-1261 cells. The results at this time are preliminary, as we have completed analysis of only a few clones (Table 2). However, we do observe the same relationship between expansion/deletion microsatellite mutation rates and length in these MMR-deficient cells (Figure 2B). Therefore, the exponential relationship between mutation rate and STR allele length, and the bias towards expansion mutation at longer allele lengths cannot be explained by differential MMR. We hypothesize that the unique expansion bias within [TC/AG] microsatellites may be due to the formation of H-DNA structures in the plasmid, as we have observed S1 nuclease sensitivity over this microsatellite allele.

Various computational models have been developed to describe mutagenesis of mature microsatellites. In the stepwise mutation model (SMM), each mutation either adds or removes one repeat unit at a constant rate. Other models have been derived from the SMM to allow higher mutation rates at long microsatellites, to allow different rates of expansions and deletions depending on length, or to incorporate mutations involving a large number of repeated units. Our experimental data clearly support these latter models.

### C. Outcomes

The purpose of this project was to provide support for a new interdisciplinary research program among experimental and computational investigators at Penn State, and to improve the competitiveness of an R01 application that we had submitted to the National Institutes of Health (NIH). In this light, the project has been highly successful, in that we have new data that will be sufficient for an interdisciplinary publication when completed. In addition, our R01 application to NIH was funded in 2009: NIH/R01 GM087472: “Computational and Biochemical Analysis of Microsatellite Life Cycle”, K. A. Eckert (MPI) and K. Makova, (MPI); \$973,466 Direct costs (total).

### D. Tables and Figures

**Table 1. Nucleofection is an efficient method to transfect LCL-1261 cells**

DNA/ Form	% GFP-positive cells/intensity		
	Day 1	Day 7	Day 14
pNC1			
supercoiled	70-80% / high	70-80% / high	50-60% / high
linear	30-40% /medium	20-30% /medium	5-10% /medium
pMAXGFP			
supercoiled	70-80% / medium	70-80% / medium	50-60% / medium
linear	30-40% /medium	20-30% /medium	5-10% /medium

**Table 2. Mutagenesis of [TC/AG] shuttle vectors in MMR-deficient (LCL1261) cells**

Clone	HSV-tk Mutation Rate x 10 <sup>6</sup> (Number of STR mutants)			
	[TC/AG] <sub>11</sub>	[TC/AG] <sub>14</sub>	[TC/AG] <sub>17</sub>	[TC/AG] <sub>20</sub>
1	1400 (20)	Clones in culture	9100 (19)	13000 (30)
2	340 (4)		680 (44)	n.d.
3	140 (8)		n.d.	n.d.
mean	630		4900	

n.d., not yet determined

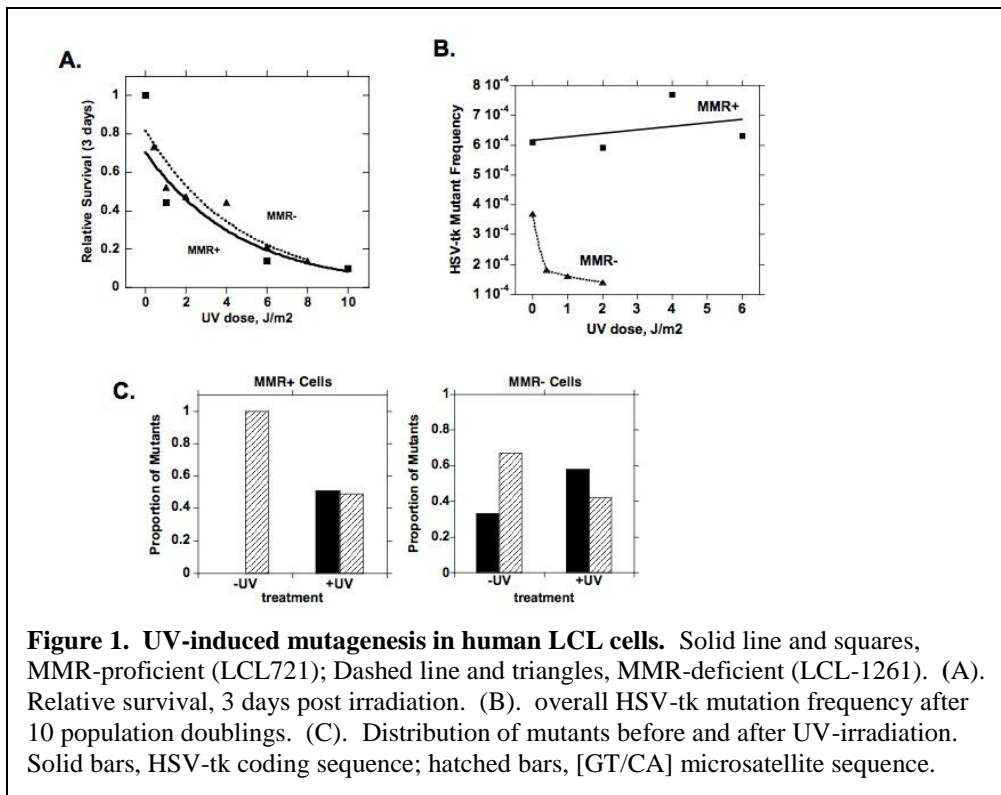
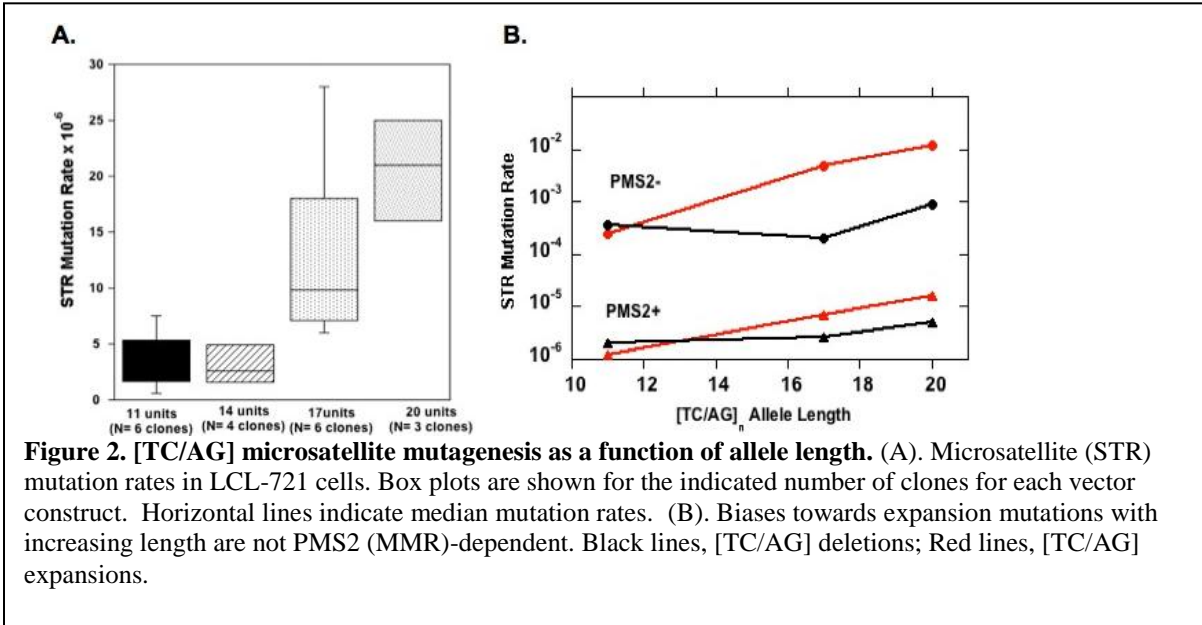


**Figure 1. UV-induced mutagenesis in human LCL cells.** Solid line and squares, MMR-proficient (LCL721); Dashed line and triangles, MMR-deficient (LCL-1261). (A). Relative survival, 3 days post irradiation. (B). overall HSV-tk mutation frequency after 10 population doublings. (C). Distribution of mutants before and after UV-irradiation. Solid bars, HSV-tk coding sequence; hatched bars, [GT/CA] microsatellite sequence.



## **Research Project 25: Project Title and Purpose**

*Epigenetic Therapy of Human B Cell Malignancies* – Cancers of B cells including leukemia and lymphoma are common and mostly incurable. We have used a unique combination of chemotherapy and immunotherapy to achieve durable complete response in B cell malignancies like mantle cell lymphoma. Clinical trials have been initiated to test these hypotheses. Clinical samples will be available from these trials for correlative science studies. The purpose of this project is to use these samples to determine the silenced target genes activated by our treatment regimen and to further study these genes in vitro.

### **Anticipated Duration of Project**

9/1/2009 - 6/30/2011

### **Project Overview**

Epigenetic gene silencing is a common theme in many malignancies. Epigenetic therapeutic agents such as DNA hypomethylating agents and histone deacetylase inhibitors are being tested in a variety of malignancies with some success. B cell malignancies are a group of diseases where improved therapies are needed. We have found that combination therapy with epigenetic agents and the monoclonal antibody rituximab is extremely effective against B cell malignancies such as mantle cell lymphoma, chronic lymphocytic leukemia and other indolent B cell lymphomas. This combination appears more effective and less toxic than other current cytotoxic therapies. We have initiated clinical trials testing these therapies. The objective of this project is to use cell lines and patient samples to demonstrate that the therapy is working via an epigenetic mechanism by identifying genes and microRNAs (miRNA) that are transcriptionally activated with these therapies. We will identify these target genes and further study their roles in the pathogenesis of B cell malignancies.

Thus, the *central hypothesis* for these studies is that epigenetic therapy for B cell malignancies using this combination will be safe and effective and result in the activation of certain silenced target gene(s) that allow rituximab to effect apoptosis much more efficiently. This discovery would be highly significant, highlighting the therapeutic implications of epigenetic therapy for B cell malignancies and other malignancies as well.

### **Principal Investigator**

Elliot M. Epner, MD, PhD  
Professor of Medicine  
Pennsylvania State University  
Penn State Cancer Institute  
500 University Drive, P.O. Box 850  
Hershey, PA 17033-0850

## **Other Participating Researchers**

None

## **Expected Research Outcomes and Benefits**

This project will not support the clinical trials, which will be funded through other sources. However, this project will use the clinical samples generated from these clinical trials to do important correlative science to identify the target of the hypothesized epigenetic mechanism of action. Once putative targets are characterized, they will be studied in vitro in tissue culture systems. We predict this combined epigenetic/immuno therapeutic approach to be potentially curable in B cell malignancies. If successful, we also predict that this approach can be tested in a variety of other malignancies. Identification of the target genes involved will add important scientific validity and encourage adaptation of this approach by the oncologic community. Thus, success of these clinical trials and their scientific correlates is predicted to have a significant positive impact on the currently poor prognosis faced by mantle cell and other B cell lymphoma patients by contributing to availability of more effective therapies, which would increase the length and quality of life for these patients.

## **Summary of Research Completed**

Recently, epigenetic mechanisms have been reported to be critical to the pathogenesis of chronic lymphocytic leukemia (CLL) and mantle cell lymphoma (MCL). We have initiated a clinical trial utilizing combined epigenetic and immunotherapy in B cell malignancies using a purine analogue, cladribine that has novel epigenetic activities. Cladribine inhibits both DNA and histone methylation through inhibition of the methyl donor S adenosyl methionine (SAM) pathway. Cladribine has been demonstrated to inhibit DNA methylation in vitro in a MCL cell line and in vivo in CLL and MCL patients (Fig. 1-2). Our hypothesis is that epigenetic therapy including cladribine and the histone deacetylase inhibitor (HDACi) SAHA (vorinostat) is activating silenced genes in B cell malignancies, including genes required for rituximab induced apoptosis. We have obtained further evidence supporting this hypothesis and are performing correlative science studies in patient samples to identify the gene (s) activated by epigenetic therapy.

Preliminary results with SCR treatment both off and on trial indicate dramatic activity in relapsed and high grade MCL patients, where the cladribine + rituximab regimen is not very active. This regimen also has substantial activity in CLL and other low grade B cell malignancies.

In addition to the inhibition of DNA methylation, inhibition of transfer of methyl groups to either protein such as histones and/or RNA is possible. Histone methylation has recently been shown to have an important role in gene silencing in cancer cells independent of DNA methylation. Treatment of cancer cells with DZnep (Deazaneplanocin A), a nucleotide inhibitor of SAH hydrolase like cladribine, has been shown to affect apoptosis and activate genes in cancer cells. Our experiments have demonstrated that cladribine also inhibits histone methylation in vitro in MCL cells and in vivo in MCL patients (Fig 3-4). Further experiments

to extend this observation in additional MCL cell lines and patient samples are underway.

During the last year, our laboratory has made significant progress in our specific aims. Using mantle cell lymphoma cell lines, we have studied the mechanism of action of cladribine (2-chlorodeoxyadenosine), a purine analogue that is FDA approved for the treatment of hairy cell leukemia. Cladribine is also active in the treatment of other B cell malignancies such as chronic lymphocytic leukemia (CLL) and follicular, mantle cell and other B cell lymphomas. The mechanism of action of this drug and its potent activity in diseases such as hairy cell leukemia are not well defined. Published literature has suggested a potential epigenetic mechanism of action for this drug through the inhibition of the S-adenosyl methionine (SAM) pathway. By inhibiting the donation of methyl groups, cladribine could inhibit both DNA and histone methylation, similar to another published agent DZNep. We have shown that cladribine inhibits global histone methylation in vitro in Granta MCL cells (Fig 3). In addition, in collaboration with Dr. Samir Parekh at Albert Einstein College of Medicine (AECOM), we have demonstrated that cladribine inhibits DNA methylation in MCL and CLL patients using an epigenomic (HELP) assay (Figs 1-2). The HELP (Hpa II Enriched Ligation PCR) assay utilizes the methylation sensitive enzyme Hpa II and the methylation insensitive enzyme Msp. Using this assay, we have identified potential target genes that are silenced in mantle cell lymphoma. Our hypothesis is that silenced genes that are involved in apoptotic signaling and activating these genes facilitate rituximab and cladribine induced apoptosis.

One of these candidate genes (DUSP2; PAC1) is a phosphatase that is involved in p53 mediated apoptotic signaling. We have demonstrated by quantitative RT-PCR that this gene is transcriptionally activated in a MCL cell line treated with cladribine and in some but not all MCL and CLL patients treated with cladribine, SAHA, and rituximab (SCR) on a clinical trial (Fig 5). We have also demonstrated inhibition of histone methylation in vivo in patients treated with cladribine (Fig. 4). We have observed encouraging preliminary results in patients with MCL and CLL treated with this combination. To date 14 patients have been enrolled on trial with several more to be enrolled shortly. Further experiments to use epigenomic assays in patients treated with cladribine +/- HDACi and fludarabine (control) are underway. Using chromatin immunoprecipitation (ChIP) sequencing assays, changes in histone acetylation and methylation at specific promoters will be correlated with patient response and transcriptional changes.

## Genome-wide Hypomethylation by Cladribine in Primary CLL

**Fig. 1. Genomic Hypomethylation in CLL patient samples before and 3 days after treatment with single-agent Cladribine.** A multiplot of fold change (X axis) vs. significance (Y axis) of methylation ratios (log HpaII/MspI) as measured by the HELP assay demonstrates striking hypomethylation after Cladribine treatment in the majority of loci. Two CLL patients were studied.

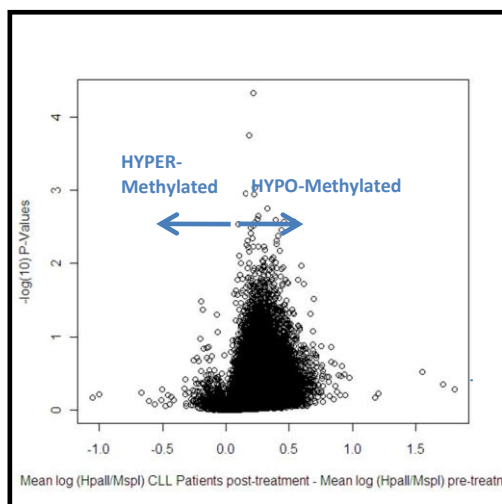
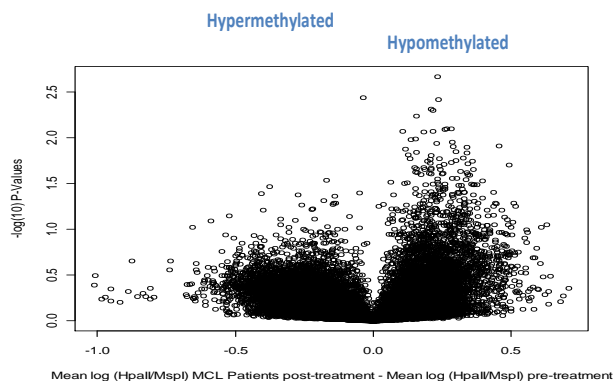


**Fig 2. Genomic Hypomethylation in 2 MCL patient samples before and 3 days after treatment with single-agent Cladribine.** A multiplot of fold change (X axis) vs. significance (Y axis) of methylation ratios (log HpaII/MspI) as measured by the HELP assay demonstrates striking hypomethylation after Cladribine treatment,

**Aberrant promoter DNA methylation in the MCL patient samples before and after Cladribine treatment**



of methylation difference between MCL Patients after and before Cladribine treatment (x-axis) versus statistical significance (y-axis). HYPomethylated HELP probes after treatment are on the right side of the plot.

**Fig 3. Inhibition of global histone methylation in a MCL cell line and patient samples before and 3 days after treatment with single-agent Cladribine.**

Histone Methylation in Granta Cells Following Cladribine Treatment

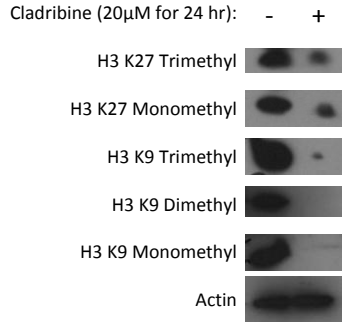


**Fig 4. Inhibition of histone methylation in a MCL cell line and patient samples before and 3 days after treatment with single-agent Cladribine.**

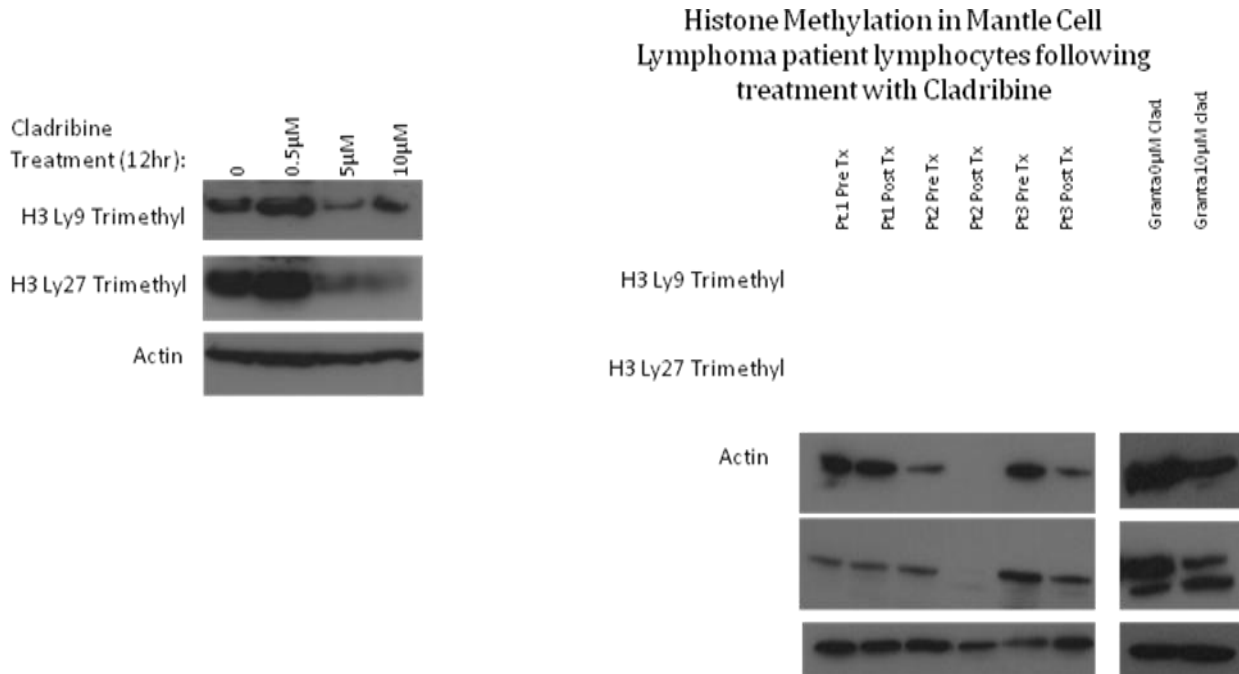
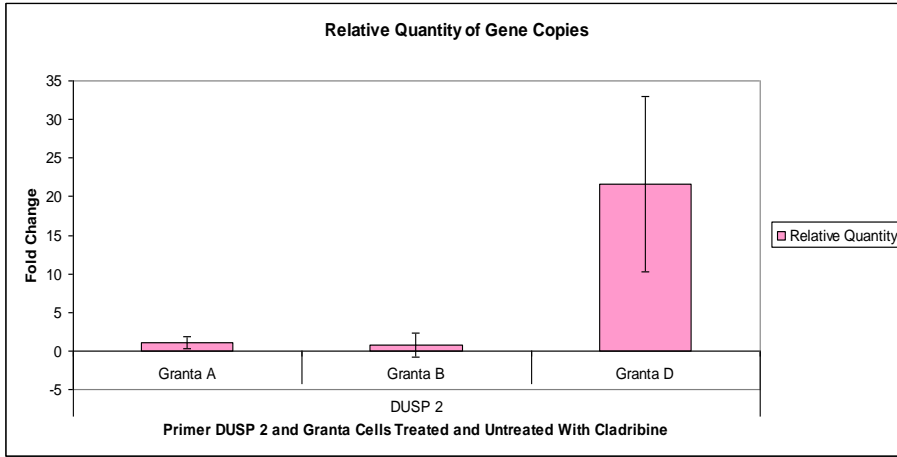
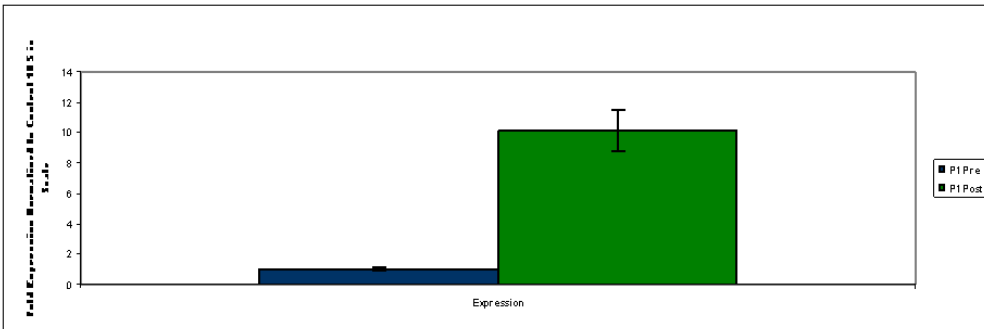


Fig 5. Transcriptional Upregulation of DUSP2 phosphatase in a MCL cell line (Granta) and in a patient samples 5 days after treatment Cladribine. RT-QCR assay was preformed.



Granta A – Treated with 0 uM of Cladribine  
 Granta B – Treated with 1 uM of Cladribine for 24 hours  
 Granta D – Treated with 20 uM of Cladribine for 24 hours  
 Error bars denote standard error of the mean

DUSP 2 increases ~ 20 fold with high treatment of cladribine



Error bars denote standard error of the mean

Post treatment sample shows a 8-9 fold increase of DUSP 2 expression

## **Research Project 26: Project Title and Purpose**

*Novel Multielectrode Recording Techniques for Assessment of Taste Functions in the Brain* – Obesity contributes to a number of life threatening health problems such as non-insulin dependent diabetes, hypertension, and coronary heart disease. The causes of obesity are complex but overconsumption motivated by palatable foods may be an important factor in the etiology of obesity. Since meal size is controlled by sensation originating in the oral cavity, the contribution of oral sensation will potentially provide significant data on ways to control obesity. The present application seeks support to develop novel multielectrode recording techniques necessary to obtain critical pilot data for a future NIH R01 grant application. Specifically, the project will record activity of gustatory-sensory neurons of the hindbrain in high caloric high fat diet-induced obese (DIO) and lean male rats to compare taste responses to palatable sucrose solutions in hungry and sated states.

### **Anticipated Duration of Project**

7/8/2009 - 3/31/2011

### **Project Overview**

Obesity is a global pandemic, and poses extreme concerns for individuals and the society in the United States. According to recent health statistics, in the U.S., two-thirds of the adult population is overweight, and more than 25% is clinically obese. Although the etiology of obesity is complex and includes various environmental and also genetic factors, most obesity is caused by chronic overeating. The project will make use of a currently available animal model of dietary obesity to study the role taste palatability plays in guiding excessive food intake resulting in obesity. The project will employ behavioral and neurophysiological techniques to test whether taste function is altered in obesity and affects the central neural code that is responsible for the hedonic or palatability attribute of sensory information derived from peripheral chemoreceptors. This experiment will test the hypotheses that 1) high energy high fat diet-induced obese rats express reduced neural responses to lower concentrations of sucrose whereas taste neurons respond more vigorously to high concentrations compared with lean rats, and 2) satiation has blunted effect to alter neural code for sweet in obese rats. To test these hypotheses, the across-neuron code for sucrose concentrations and the effects of refeeding (satiation) following an overnight food restriction will be studied using novel multielectrode recording techniques. It is expected that the neural responses will parallel behavioral observations that not only appetite is increased in obese individuals but the effect of satiation to reduce the feeling of pleasantness of sweet is also blunted. This information will help us understand maladaptive changes in the brain that influence the taste and stimulatory effects of certain foods, making them less easily controlled in obese individuals. A future NIH grant application, supported by the findings of this project and the successful demonstration of feasibility of chronic multielectrode recording, will aim at identifying potential pharmacological targets to curb appetite and combat food cravings.

## **Principal Investigator**

Andras Hajnal, MD, PhD  
Associate Professor  
Penn State College of Medicine  
Department of Neural and Behavioral Sciences  
500 University Drive, H181  
Hershey, PA 17033

## **Other Participating Researchers**

Peter Kovacs, PhD – employed by Penn State College of Medicine

## **Expected Research Outcomes and Benefits**

This research is aimed at a highly significant problem in human health — obesity due to overeating. Specifically, it investigates how does taste change with obesity and in turn contribute to sustained overeating of palatable high-caloric meals. The PI will quantify taste changes with behavioral assays and with electrophysiological recordings from taste-responsive neurons in the brain. To achieve this goal in a way that yields data relevant to normal physiology, the project will develop and test novel multielectrode techniques suited for chronic recording in behaving rats. The advantages of chronic recordings are to spare animals, reduce recording time and effort, and make it possible to follow changes within subjects. In addition, the chronic setup provides actual markers from each rat's meal recorded simultaneously with neuronal gustatory activity. Thus, it will be useful for analyzing concomitants of this phenomenon because licking microstructure analysis permits assessment of treatment effects on taste evaluation and inhibitory feedback from the gut. To manipulate such feedback, rats will be overnight food deprived or free-fed. It is hypothesized that not only appetite is increased in obese individuals but the effect of satiation to reduce the feeling of pleasantness of sweet is also blunted. The preliminary data obtained in the PI's lab support such outcome and an in-depth analysis of neural activity is also expected to provide important new data. The outcome of testing novel multielectrode techniques, recorded from a conscious animal, will be critical to submitting an NIH grant application with an improved chance of fundability. This study is critical to developing a non-invasive pharmacological treatment to curb appetite. Such treatment alone or in combination with other therapies could provide the benefits of long-term weight management and eliminate the dieting patients' most disturbing experience, the continuous hunger and craving for sweet or fatty meals.

## **Summary of Research Completed**

During the report period, we have made substantial progress with addressing both hypotheses and also with development and testing chronic electrophysiological techniques to record from the pontine parabrachial taste relays (PBN). Actually, the progress has exceeded our initial plans and expectations in many aspects. Specifically, we have run two behavioral studies and several iterations of semi-chronic and chronic recording tests in naïve rats and also select subjects of the behavioral tests. In this latter experiment we have employed various designs of multielectrode and single electrode microdrives in order to determine which would work the best for our

purpose in terms of durability, longevity in a chronic setting as well as signal quality required for across neuron pattern analysis. Experiment 1 was designed to test effects of various obesogenic (high energy, high palatability) diets for their efficiency to develop a) obesity and b) to alter taste perception of sweet. This study has been completed and all data are analyzed, thus ready for publication. Experiment 2 aimed at investigating effects of satiation on neural coding for sweets in a genetic obese strain, the Otsuka Long Evans Fatty (OLETF) rat. The rationale for starting neural recording in this obese strains and not immediately in dietary obese (DIO) rats was twofold. First, we have previously characterized pontine taste coding in the OLETF rats (Kovacs and Hajnal, Journal of Neurophysiology, 2008). Thus we identified the variables that intestinal satiation may affect, whereas in DIO rats a similar study has not been done. Second, the behavioral experiments with different diets (Experiments 1 and 2, above) revealed larger individual variations in terms of the obesogenic and taste effects in the outbred Sprague Dawley male rats we used for developing DIO compared with the OLETF rats. Nevertheless, we have just started a similar electrophysiology study in DIO rats based on the initial data from the OLETF rats. Both these studies require additional time to be fully completed, and whereas some data have already been analyzed an overall statistics will be required once the tests are fully completed. The following narrative will give a brief summary of the currently available results from the two studies including chronic recording data and the view of one of our microdrive design which has been tested in these studies successfully.

Experiment 1. Obesigenic effects of high energy high fat and high energy high carbohydrate diets. Coupled with reduced physical activity, the most common cause of overweight and obesity is a chronic overeating of highly palatable high energy foods rich in carbohydrates and fats. In a widely used rat model of dietary induced obesity (DIO), it has been found that only about one-half of Sprague Dawley rats (DIO-prone rats) become obese if rats are fed with a moderately high fat (~ 30 kcal%), and high carbohydrate (~ 50 kcal%), high energy (HE) diet. In contrast, other studies showed that all rats significantly gain weight – irrespectively to their genetic background - if they are fed with diets that content similar calories but more fat (~ 60 kcal%) and less carbohydrates (~ 20 kcal%). Furthermore, it has been proposed that switching from an isocaloric low fat diet to one with higher fat content, that body fat mass will increase. These observations together with data on additional effects of chronic fat intake on the brain mechanisms suggest that high-fat diets may alter energy homeostasis and motivational control of food intake – at least partially – independent of its caloric effects. To test this hypothesis and to establish a rat model that is relevant to human obesity we compared the short term (8 weeks) effects of two high caloric obesogenic diets shown in Table 1 on food intake, the body weight, body composition and glucose tolerance in 24 adult male Sprague Dawley rats. In addition, we investigated the effects of the very high-fat diet (DIO-VHF) on the body weight in conditions when the rats were pair-fed, i.e., received it in a restricted amount isocaloric to the daily intake of their controls receiving a balanced normocaloric chow diet.

Our results showed that rats fed with the DIO-VHF- but not with the DIO-HE diet had significantly increased body weight and body fat content during the 8 weeks of the study period (Figure 1A, B). This difference was not related to energy intake, but it was rather a consequence of the different composition and fat content of the two DIO diets (Figure 1C). Supporting this notion is our analysis revealing that the same energy content in the DIO-VHF diet was more effective in increasing the body weight than the equivalent energy content in the CHOW or in the

DIO-HE diet (Figure 1D). In concert with this, we observed that the DIO-VHF diet potently increased weight gain even when intake amount was calorically restricted to normal levels (Figure 2). These findings collectively suggest that increased consumption of dietary fat may result in increased weight gain and body fat content even within a short period of time by mechanisms that appear to be partially independent of total energy intake.

Experiment 2. Effects of satiety from increased blood glucose levels on neural taste coding for sweet in obese compared to lean rats. We recently investigated sucrose coding in the second central taste relay, the pontine parabrachial nuclei (PBN) of obese Otsuka Long Evans Tokushima Fatty (OLETF) rats. These rats express deficits in satiation and prefer sweet tastants. Compared with lean controls (LETO), obese OLETF rats have reduced neural responses to lower concentrations of sucrose and exaggerated responses to higher concentrations. To investigate potential underlying mechanisms by which taste stimulation from sweets may override satiety signals to halt overeating of sweet meals; we compared the effects of acute changes in blood glucose levels on concurrent gustatory activity in the PBN of prediabetic, obese OLETF and lean LETO rats. We used semi-chronic and chronic extracellular single neuron recording while stimulating the tongue with various taste solutions. The analysis included taste responses from 47 neurons, before and after peripheral administration of dextrose (1.25g/5ml, i.p.), following an overnight fasting. For chronic recording – so far producing 17 neurons many of them for a period over 10 days – we used a PCB board microdrive filled with a single electrode or one tetrode electrode assembly (Figure 3).

The results showed that whereas dextrose overall increased taste responses as a function of concurrent blood glucose levels, the magnitude of the effects and the across neuron pattern was significantly different in obese and lean rats (Figures 4 and 5). The overall effect from these changes in taste code was that acute surges of blood glucose reduced neural responses for sucrose relative to NaCl in lean but not in obese rats. These findings demonstrate that satiety from increased blood glucose affects taste processing in the PBN, suggesting a role for across neuron code for sweet taste in the altered sensitivity to this satiety signal in obese rats. In order to determine whether such effect (altered taste coding to blood glucose in obese rats) was due to the obesity or could also be influenced by dietary history we conducted a study to record taste activity by chronically implanted electrodes in normal (non-genetic) obese Sprague Dawley rats receiving different high energy diets identical to those tested and discussed in Experiment 1.

In addition to the result supporting our hypotheses, the technical progress on developing the chronic recording helped substantially in renewal of an R01 grant (DC000240, PI: Hajnal).

**Table 1. Composition and energy content of the applied diets.**

	CHOW	DIO-HE	DIO-VHF
	Teklad Global	Research Diets	Research Diets
	2018	D12266B	D12492
Carbohydrate (kcal %)	60	51	20
Fat (kcal %)	17	32	60
Protein (kcal %)	23	17	20
Energy (kcal/g)	3.4	4.41	5.24

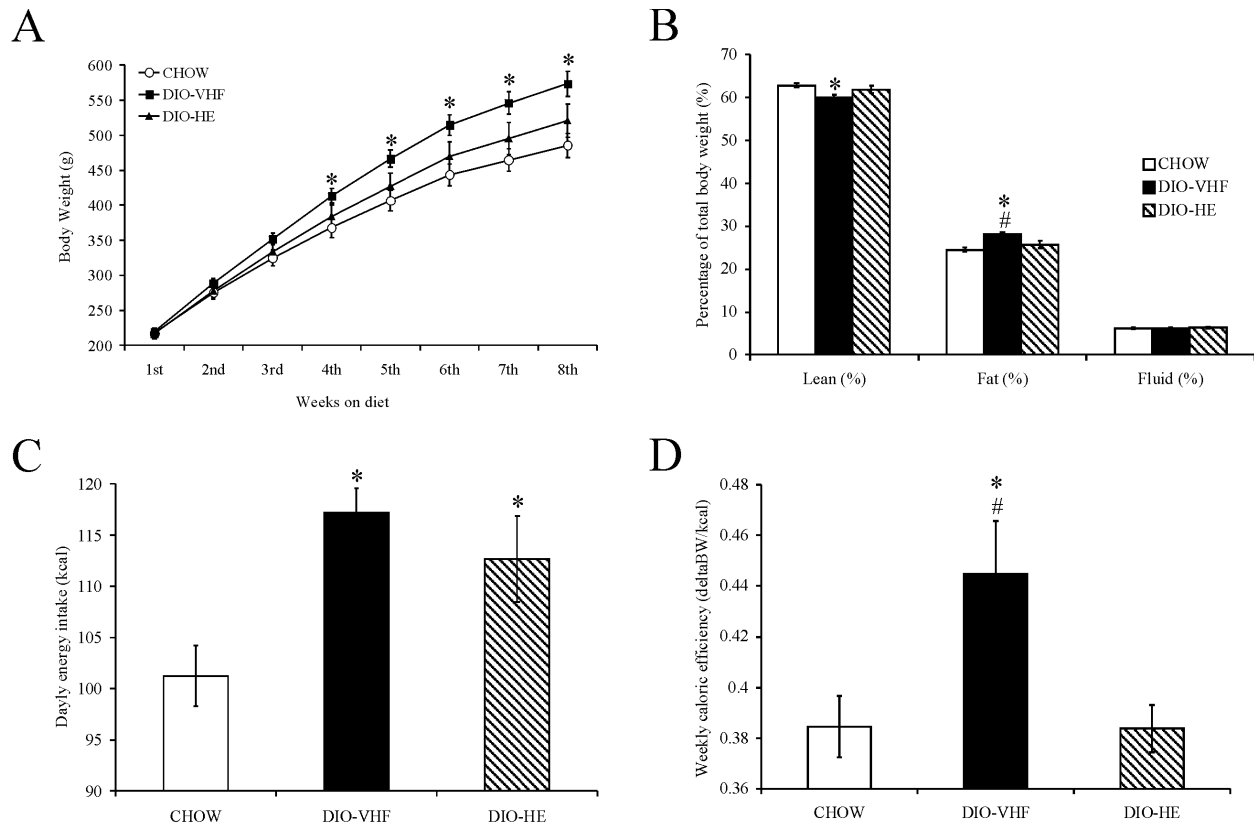


**Fig. 1.** The effects of two different obesogenic (DIO) diets on (A) body weight, (B) body composition, (C) daily energy intake, and (D) caloric efficiency in adult Sprague Dawley male rats. DIO-VHF: very high fat diet ; DIO-HE: high energy diet; CHOW: standard lab chow. Posthoc LSD tests: \* =  $p < 0.05$  compared to CHOW; # =  $p < 0.05$  compared to DIO-HE.

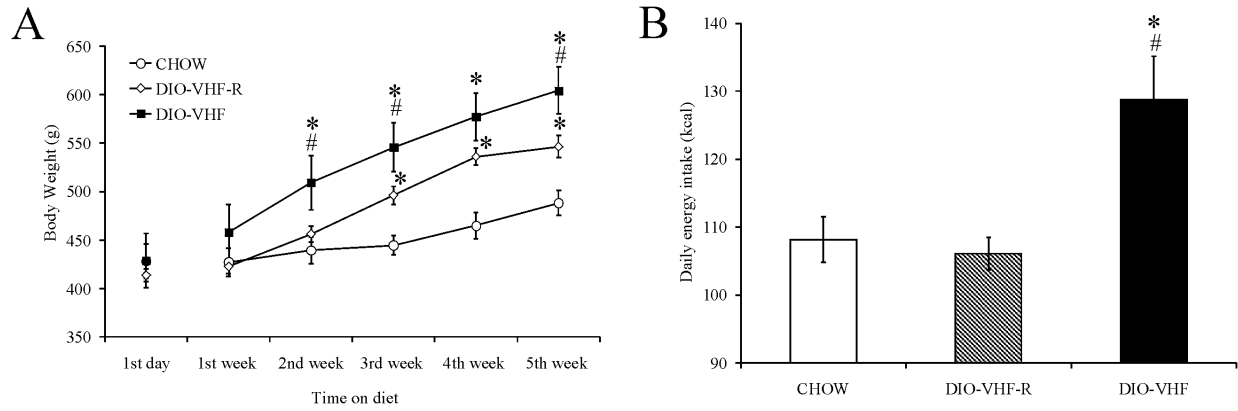


Fig. 2. Effects of restricted and ad libitum access to DIO-VHF diet on the (A) body weight, (B) daily energy intake of Sprague Dawley rats. DIO-VHF-R: very high fat diet restricted access – isocalorically pair-fed with the CHOW group; DIO-VHF: very high fat diet unrestricted access; CHOW: standard lab chow. Posthoc LSD tests: \* =  $p < 0.05$  compared to CHOW; # =  $p < 0.05$  compared to DIO-VHF-R.

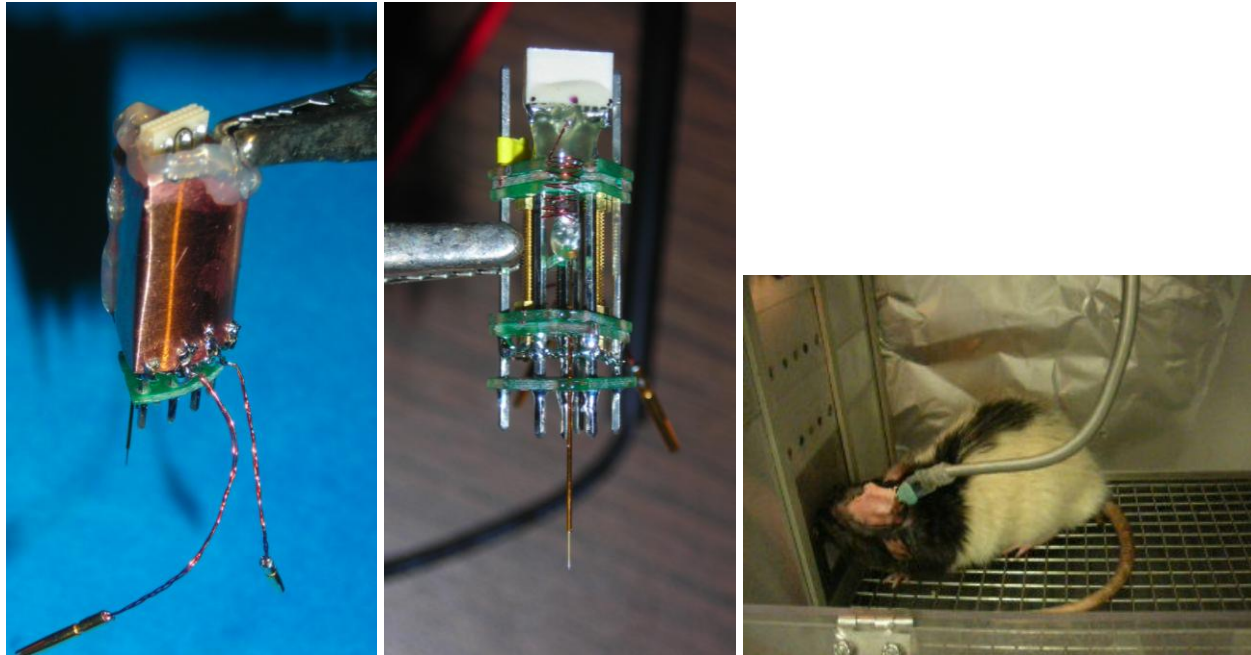


Fig. 3. Our smallest PCB microdrive can move one single tungsten electrode or one tetrode (Left, Center). It is uniquely designed for recordings from PBN taste neurons in freely moving rats during sucrose licking (Right).

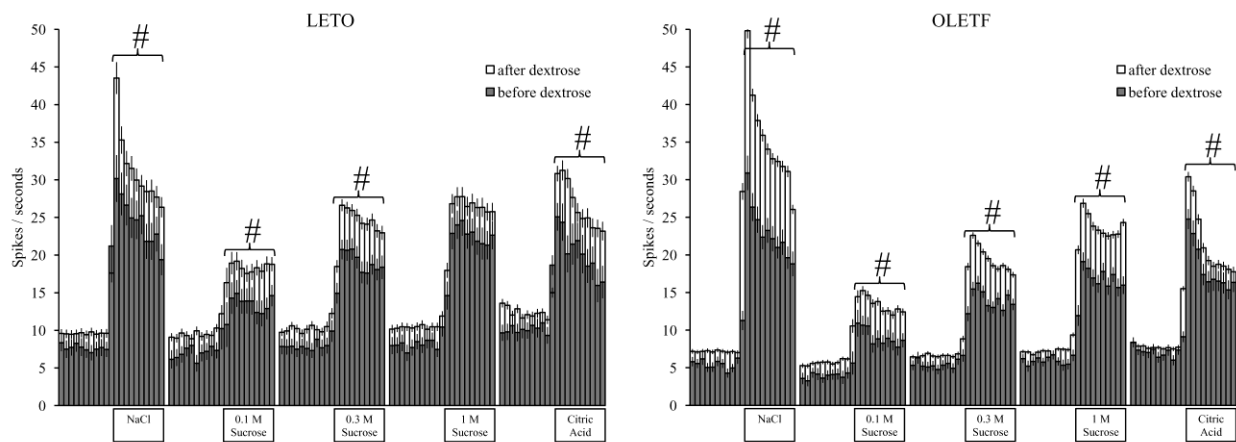


Fig. 4. Systemic dextrose augmented neuronal taste responses in the PBN to oral NaCl, sucrose and citric acid in both LETO and OLETF rats; however the magnitude of the effect for sucrose was reduced in obese rats. Mean ( $\pm$  SEM) neuronal responses to oral taste stimulation in the PBN of 10 LETO and 10 OLETF (20 and 27 neurons, respectively). #  $p < 0.05$  compared to before dextrose (poststimulus 0-10 s mean taste response magnitudes).

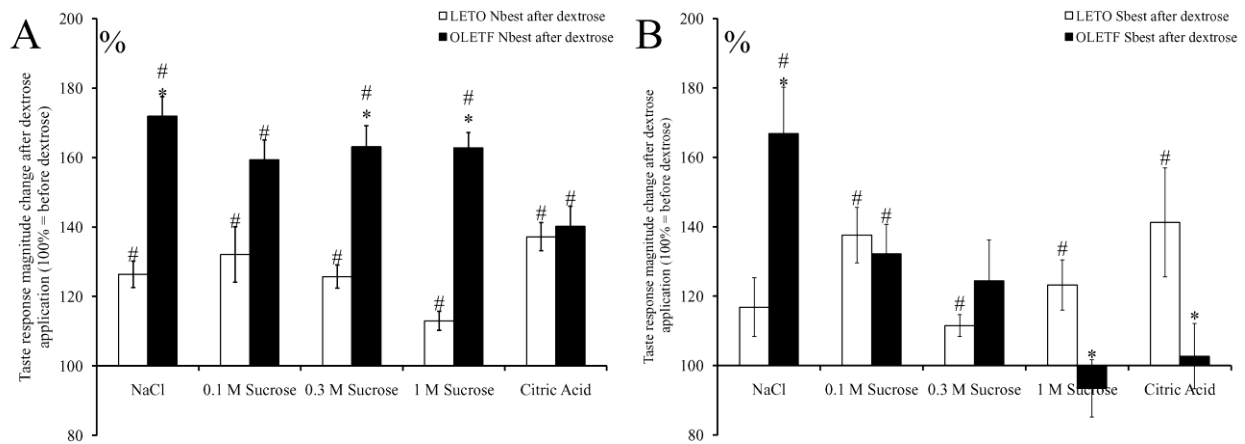


Fig. 5. The across neuron pattern of taste evoked activity following dextrose infusions was significantly different in obese and lean rats. A) Taste response magnitude changes in the N-best population; B) Taste response magnitude changes in the S-best neuronal class. \*  $p < 0.05$  compared to LETO, or #  $p < 0.05$  compared to baseline. The NaCl-best neurons displayed significantly larger responses to NaCl and to 0.3- and 1 M concentrations of sucrose but not to citric acid in obese compared with lean rats (Fig. 6/A; +72% vs. +25%; +60% vs. +35%; +39% vs. +38%, respectively). In contrast, sucrose-best units in obese rats responded more vigorously only to NaCl (+68% vs. +18%), but showed no increase to 1.0M sucrose (-6% vs. +23%).

## **Research Project 27: Project Title and Purpose**

*Glycosphingolipids and Diabetic Retinopathy* – Diabetic retinopathy is the leading cause of blindness among working age adults. We have found that a class of lipids, glycosphingolipids, is elevated in the diabetic retina. The purpose of this study is to understand the consequences of elevated glycosphingolipids within the retina and determine if systemic inhibition of glycosphingolipid accumulation is therapeutic for diabetic complications.

## **Anticipated Duration of Project**

7/8/2009 - 12/31/2010

## **Project Overview**

The overall objective of this project is to understand the molecular basis for vision impairment in diabetic retinopathy. The specific objective is to investigate the role of ceramide metabolism and glycosphingolipid-enriched lipid microdomains (rafts) in insulin signaling and cell survival in retinal neurons. The rationale for the project is based upon several novel observations, including: 1) diabetic retinas demonstrate decreased total ceramide levels; 2) with a concomitant increase in glucosylceramides concomitant with; 3) decreased insulin receptor signaling. We hypothesize that diabetes increases glycosphingolipid production in the retina, which decreases activation of pro-survival signaling cascades contributing to cell death. The significance of this work is that identifying glycosphingolipids as a therapeutic target in diabetic retinopathy has the potential to lead to pharmacological and molecular interventions to prevent the progression of vision loss in patients with diabetes.

*Specific Aim One: Determine the consequence of glycosphingolipids on insulin signaling and cell death in ex vivo retinas.* We will assess the effects of altered glycosphingolipid metabolism upon insulin signaling and resultant cell death in retinal explant models. Here, retinal explants from C56BL/6 mice will be treated with inhibitors to glycosphingolipid metabolism and the effect on the phosphorylation of enzymes within the insulin signaling cascade assessed in addition to caspase 3 activity to assess cell death.

*Specific Aim Two: Determine the consequence of glucosylceramide synthase inhibition on the metabolic milieu.* Our published studies identify glucosylceramide accumulation within lipid rafts as a therapeutic target for diabetic retinopathy. These *in vitro* data support the hypothesis that inhibitors of glucosylceramide synthase may be effective *in vivo* therapeutic modalities. We will administer drugs via a systemic approach and directly assess clinical endpoints in a mouse model of diabetes. Taken together, these studies will provide novel insights into dysfunctional lipid metabolism in diabetes and may identify glucosylceramide accumulation as a therapeutic target for diabetic retinopathy.

*Specific Aim Three: To determine the metabolic profiles of the vitreous samples from patients with/without diabetes.* We will expand on the animal models by next assessing human samples. In this aim, we will undertake a comprehensive assessment of vitreous metabolites by liquid chromatography-mass spectrometry (LC-MS/MS)-based metabolomics approaches. These experiments will identify and monitor soluble non-lipid metabolites that are altered in the vitreous from patients (1) without diabetes, (2) with diabetes, but without proliferative diabetic retinopathy, (3) with proliferative diabetic retinopathy, and (4) with macular edema. Through the analysis of this diverse subset of patients, our objective is to discover factors that change with diabetes and between different severities of diabetic retinopathy.

*Specific Aim Four: To determine the lipid profiles of the vitreous samples from patients with/without diabetes.* In this aim, we will undertake a comprehensive assessment of vitreous lipids by liquid chromatography-mass spectrometry (LC-MS/MS)-based and infusion-based mass spectroscopy lipidomic methodologies. Using the same vitreous samples as above, the end results of these two aims will be the delineation of the vitreous “metabolome” that will lead to new hypothesis driven projects toward new therapies for diabetic retinopathy.

### **Principal Investigator**

Mark Kester, PhD  
Professor of Pharmacology  
Pennsylvania State University  
500 University Drive  
Hershey, PA 17033

### **Other Participating Researchers**

Todd E. Fox, PhD, Megan M. Young, BS – employed by Pennsylvania State University

## Expected Research Outcomes and Benefits

Diabetes is a debilitating chronic disease that has no cure and can only be managed by pharmaceutical or nutritional interventions. Worldwide, the incidence of diabetes and diabetic complications is dramatically increasing. This may reflect the incomplete knowledge base underlying the role of inflammatory or nutritional stresses to exacerbate diabetic complications. Despite the knowledge that hyperlipidemia is a cardinal feature of both type 1 and 2 diabetes, the actual lipid species that contribute to complications such as diabetic retinopathy, have not been well defined, or have not elucidated new treatment strategies. Sphingolipids comprise only a fraction of total lipids but a body of evidence has now identified dysfunctional sphingolipid metabolism and/or generation of specific sphingolipid metabolites as contributors to diabetic complications, including retinopathy. Preliminary data suggest that pharmacological therapies that target dysfunctional sphingolipid metabolism and/or signaling may prove beneficial in decreasing the chronic pathology of retinal disease in diabetes. The project will further investigate these treatment options that may prove beneficial in ameliorating or delaying retinal dysfunction in diabetic patients.

## Summary of Research Completed

Testing the therapeutic efficacy of glucosylceramide synthase inhibition on diabetic retinopathy. Since we have shown glucosylceramide is upregulated in two distinct models of type 1 diabetes, the streptozocotin-induced diabetic rat model and the Ins2<sup>Akita</sup>, we sought to determine if inhibition of glucosylceramide synthase (GCS) would be efficacious for diabetic retinopathy. Initial studies using control animals revealed that the GCS inhibitor did not have any overt toxicology to the retina upon a dosing regimen of subconjunctival injection for 3 straight days. This lack of toxicology was determined by a DNA fragmentation ELISA-based assay (Roche Cell Death Detection kit) to assess drug-induced cell death. We next assessed the efficacy of this drug in a model of diabetes. Using 3 month STZ-induced diabetic rats, we again followed the same dosing regimen to inhibit GCS. Here, we observed a significant increase in DNA fragmentation in diabetic animals compared to controls. We however did not observe any alterations in DNA fragmentation with the GCS inhibitor. These studies are still under further analysis. We are still in the process of determining if the inhibitor successfully decreased glucosylceramide levels in the diabetic retina and/or successfully reached the retina by utilizing mass spectrometry. We are also in the process of assessing several known biomarkers to determine if the inhibitor has any effect on their expression. As GCS inhibition has shown to be effective in type 2 models of diabetes, we are moving forward with a systemic study to determine the effect in type 1 models and peripheral complications. Importantly, we have recently obtained the tools and knowledge needed to further retina research by utilizing electroretinograms (ERGs) and have recently purchased a UTAS Visual Diagnostic System. The ERG will allow us to noninvasively assess retinal function and thus allow us to get a better understanding of the effects of therapeutics on the retina.

Understanding sphingolipid biosynthesis in the retina. Increased *de novo* sphingolipid synthesis has been implicated in many inflammatory responses and to contribute to disease pathogenesis. We have begun studies to examine this biosynthetic pathway and a potential contribution to elevated glycosphingolipid flux. Our mass spectrometry-based studies have revealed that

ceramides are predominantly enriched with C16 and C18 fatty acids. In analysis of the ceramide synthases that regulate this pathway by qRT-PCR demonstrated that CerS4 is the predominant isoform of the retina. CerS1, CerS2, CerS5, CerS6 are also expressed, but at much lower levels. CerS3 was undetectable. Glycosphingolipids are also enriched with C16 and C18 fatty acids, but at a lesser percentage with an increase in longer chain and unsaturated fatty acids. Further studies will examine if the retina preferentially metabolizes longer chain and unsaturated sphingolipids to glycosphingolipids and determine the role of CerS4 in retinal sphingolipid metabolism. These studies will allow us to further understand the pathways that regulate alterations in glycosphingolipids in diabetic retinopathy.

Defining the diabetic milieu for diabetic retinopathy. To further our knowledge of altered sphingolipids in diabetes, we sought to determine what changes are present in the plasma of diabetic animals. We initially assessed the sphingolipid profile from lipids extracted from the plasma of the STZ-diabetic rat and the Ins2<sup>Akita</sup> mouse. By utilizing LC-MS/MS we quantified the long chain bases; sphingosine-1-phosphate (So1P), sphinganine-1-phosphate (Sa1P), sphingosine (So) and sphinganine (Sa). We also determined the quantity of the fatty esterified sphingolipid classes of ceramides, cerebroside and sphingomyelin. Both models of diabetes demonstrated significantly elevated sphingosine-1-phosphate (So1P). Interestingly, the dihydro form, Sa1P, was unaltered as were the metabolic precursors So and Sa.

Ceramides were elevated only in the STZ-induced diabetic rat, but not the Ins2<sup>Akita</sup> mouse. Despite this difference, further examination of the fatty acid profiles of both models reveals a significant decrease in the omega-9, 24:1 fatty acid (nervonic acid). This specific fatty acid decrease was also observed in the sphingomyelin and cerebroside classes of sphingolipids. The difference of the ceramide alteration between the STZ-diabetic rats and Ins2<sup>Akita</sup> diabetic mice may be due to a higher basal level of insulin in the mice compared to the rats. It should also be noted that the Ins2<sup>Akita</sup> mice do not become hyperlipidemic like the STZ-diabetic rats.

As a high-fat/poor diet can lead to obesity and insulin resistance, we determined if such a diet had an effect on nervonic acid containing sphingolipids in controls. We also assessed the effect of the high fat diet in the Ins2<sup>Akita</sup> diabetic mice to determine how these animals respond to the high fat diet-induced stress. After 10 weeks on the high fat diet, both controls and diabetic mice showed significantly elevated sphingomyelins, cerebroside and ceramides of almost all fatty acid species with one exception. The exception was again, a decrease in nervonic acid. The decrease in diabetes for the 24:1 containing sphingomyelin and cerebroside classes was exacerbated with the high fat diet.

As sphingolipids can be found packaged onto lipoprotein complexes in the plasma, this would potentially implicate the liver as a contributory factor in altered sphingolipids in circulation. From the Ins2<sup>Akita</sup> diabetic liver, we observed a similar decrease in 24:1. Similarly, as with the diet-induced changes in the plasma, a high fat diet also induced significant reductions in 24:1 in the liver. Again, while we observe this diminished nervonic acid containing sphingolipids, as observed in the plasma, the high fat diet led to large increases in several types of sphingolipids. Note that we did not observe changes in liver So1P. This may reflect a source of elevated So1P other than the liver.

To further understand this diminished fatty acid content of the plasma, we examined the fatty acid profile of the total lipids present in the plasma of the STZ-induced diabetic rat. By GC-FID analysis of total fatty acids, we observed diminished 24:1. Interestingly, while the percentage of 24:1 in free or esterified form is relatively low compared to other fatty acids in the total lipid pool, the percentage of 24:1 present on sphingolipid classes is considerably higher. This suggests that nervonic acid is selectively esterified to sphingolipids rather than glycerol-containing lipids.

Taken together, these studies demonstrate that the sphingolipid profile of the plasma in diabetic animals differs from that of diabetic-induced changes of the retina. The retinal glycosphingolipids as opposed to the ceramides demonstrate a closer profile to that of the plasma with regards to fatty acids of 20 or longer carbon chain lengths. It is not clear yet if this influences retinal fatty acid composition.

### **Research Project 28: Project Title and Purpose**

*Epithelial/Dendritic Cell Crosstalk in Acute Kidney Injury* – The purpose of these studies is to evaluate the interactions between cells of the immune system and kidney cells in causing drug-induced damage in the kidney.

### **Duration of Project**

7/8/2009 - 6/30/2010

### **Project Overview**

The broad objective of this project is to elucidate how a bidirectional communication between renal epithelial cells and resident renal dendritic cells modulate kidney injury in response to acute renal insults such as ischemia-reperfusion and drug-induced nephrotoxicity. Three specific aims are proposed:

1. Confirm the presence of defective TLR4 signaling in proximal tubule epithelial cells. Renal epithelial cells of mouse and human origin will be cultured in vitro and exposed to TLR4 agonists.
2. Demonstrate specific TNF-alpha gene recombination in the proximal tubules of GGT-cre/TNF flox/flox mice. Proximal tubules will be microdissected from GGT-cre/TNF flox/flox mice and DNA recombination and mRNA expression of TNF-alpha will be determined.
3. Generate a dendritic cell-specific TNF-alpha knockout mouse. TNF flox/flox mice will be bred with a dendritic cell specific cre-transgenic mouse to create a dendritic cell-specific TNF knockout.

### **Principal Investigator**

William B. Reeves, MD  
Professor of Medicine  
Penn State Hershey Medical Center  
Division of Nephrology, C5830

Penn State College of Medicine  
500 University Dr  
Hershey, PA 17033

### **Other Participating Researchers**

WeiWei Wang, BS – employed by Penn State College of Medicine

### **Expected Research Outcomes and Benefits**

The project studies will elucidate the key role of Toll-like receptor 4 and kidney dendritic cells in the induction of the inflammatory phenotype of the kidney during acute injury. These results will be relevant because they are expected to lead to clinical trials to test the efficacy of TLR4 antagonists currently under development and other immunomodulatory strategies for the prevention or treatment of acute renal injury.

### **Summary of Research Completed**

During the award period we made substantial progress towards several aspects of the project. Previously, we identified a profound, and perhaps surprising, protective role for dendritic cells in cisplatin nephrotoxicity and submitted our findings for publication. During July- August additional experiments were completed and a revised manuscript was submitted. (J Am Soc Nephrol 21:53, 2010).

We also determined that endogenous production of IL-10 is an important defense against cisplatin toxicity. While earlier work had established that exogenous IL-10 can ameliorate cisplatin nephrotoxicity, ours is the first demonstration of a role for endogenous IL-10. Using a novel conditional cell ablation approach, we determined that IL-10 production by dendritic cells accounts for a significant portion of the protective effects of endogenous IL-10 and for a portion of the protection afforded by dendritic cells themselves (J. Immunol, in revision). We also progressed in our attempts to produce dendritic cell-specific deletion of TNF-alpha and TLR4 to be used to determine the role of these innate mediators in AKI. Details of our progress are provided below.

#### Determine the impact of renal injury on the activation state of kidney dendritic cells.

Experiments were performed using 6- to 14- week old C57BL6 (CD45.2+) or congenic C57BL6 mice B6.SJL-PtprcaPep3b/BoyJ (CD45.1<sup>+</sup>), and CD11c-DTR mice (B6.FVB-Tg Itgax-DTR/GFP 57Lan/J) harboring a transgene encoding a simian DTR-GFP fusion protein under the transcriptional control of mouse CD11c promoter. Single cell suspensions of spleen and kidney were prepared by enzymatic digestions. Cells were stained with fluorochrome labeled antibodies to leukocyte cell markers and analyzed by flow cytometry.

Properties of renal dendritic cells. Flow cytometric analysis of tissue digests revealed a distinct population of cells expressing high levels of CD11c and MHC class II in both kidney and spleen. Based on this definition, dendritic cells were the most abundant population of leukocytes in the kidney. In contrast to splenic dendritic cells, renal dendritic cells were negative for CD4, CD8 or

Ly6C/G (Gr-1). Renal dendritic cells also differed from the bulk of splenic conventional dendritic cells by their prominent expression of F4/80, a surface marker of monocytes and macrophages. We used transgenic mice (CD11c-DTR) which express GFP and the simian diphtheria toxin receptor (DTR) driven by the CD11c promoter to localize DCs in the kidney. Confocal imaging revealed GFP-positive cells throughout the tubulointerstitium but not in glomeruli. GFP-positive cells had a stellate shape typical of dendritic cells.

*Changes in DC properties during AKI.* We examined changes in kidney dendritic cell expression of MHC class I, MHC class II, CD40, CD80 and CD86 in response to cisplatin treatment. Kidney dendritic cells from WT mice treated with saline or cisplatin showed similar expression of MHC class I, CD40, CD80 and CD86. However, a significant decrease in MHC class II expression was noticed in kidney dendritic cells obtained from cisplatin treated mice, indicating that dendritic cells maintain an immature status in spite of renal injury in cisplatin treated mice, at least when examined 24 hrs after cisplatin treatment.

*Inducible ablation of renal DCs in vivo.* To selectively deplete dendritic cells in vivo, we employed CD11c-DTRtg mice in which expression of the DTR/GFP fusion protein in DCs renders the normally resistant murine cells sensitive to DT- induced cell death. We first examined the efficiency of depletion of renal and splenic DCs in response to DT treatment. DT administration to CD11c-DTRtg mice caused a marked transient depletion of CD11c<sup>+</sup> MHCII<sup>+</sup> cells in both kidney and spleen (Fig. 1). Ablation was maximal at 24 hrs in spleen and at 48 hrs in kidney (Fig. 1C and D). DC depletion in the kidney was more prolonged than in spleen. DT did not deplete CD11c<sup>-</sup> F4/80<sup>+</sup> macrophages in the kidney.

*DC depletion exacerbates cisplatin nephrotoxicity.* DT was injected 24 hrs before cisplatin injection to ablate DCs. Treatment of either CD11c-DTRtg mice or their Wild Type (WT) littermates with DT alone did not result in renal dysfunction as assessed by levels of BUN and serum creatinine (Fig. 2A and B). In comparison to WT mice, CD11c-DTRtg mice injected with DT followed by cisplatin showed both earlier and more dramatic increases in serum creatinine and BUN. The survival at 72 hrs was only 20% in the CD11c-DTRtg mice and 100% in WT mice treated with DT and cisplatin (n=5).

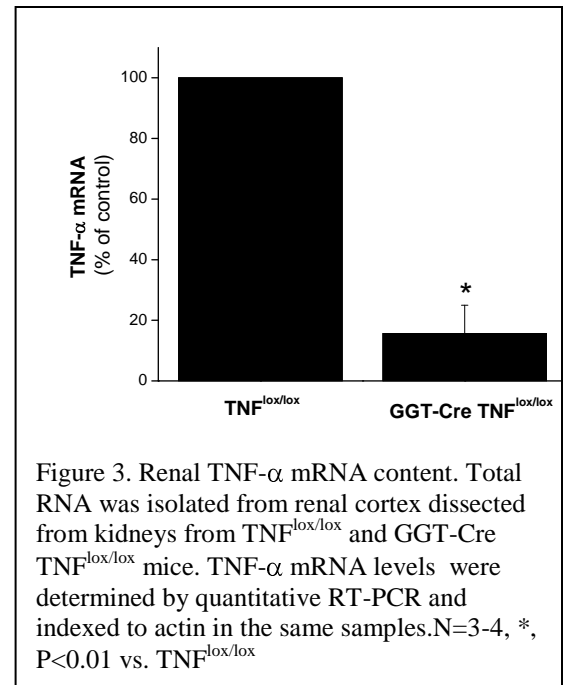
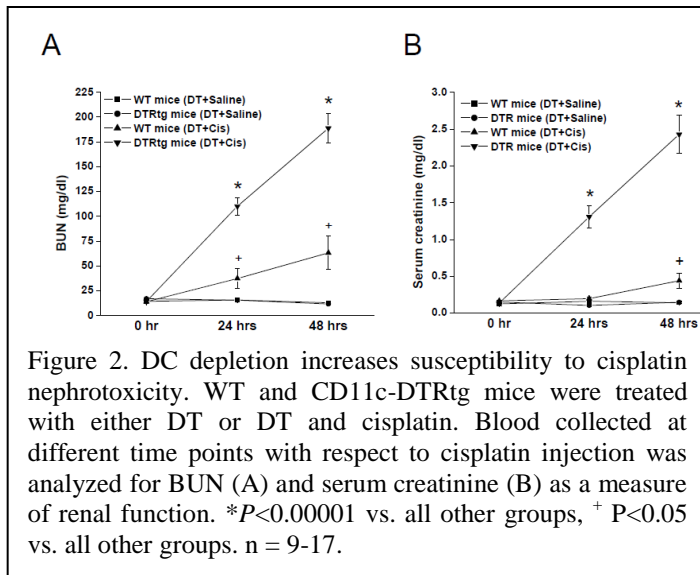
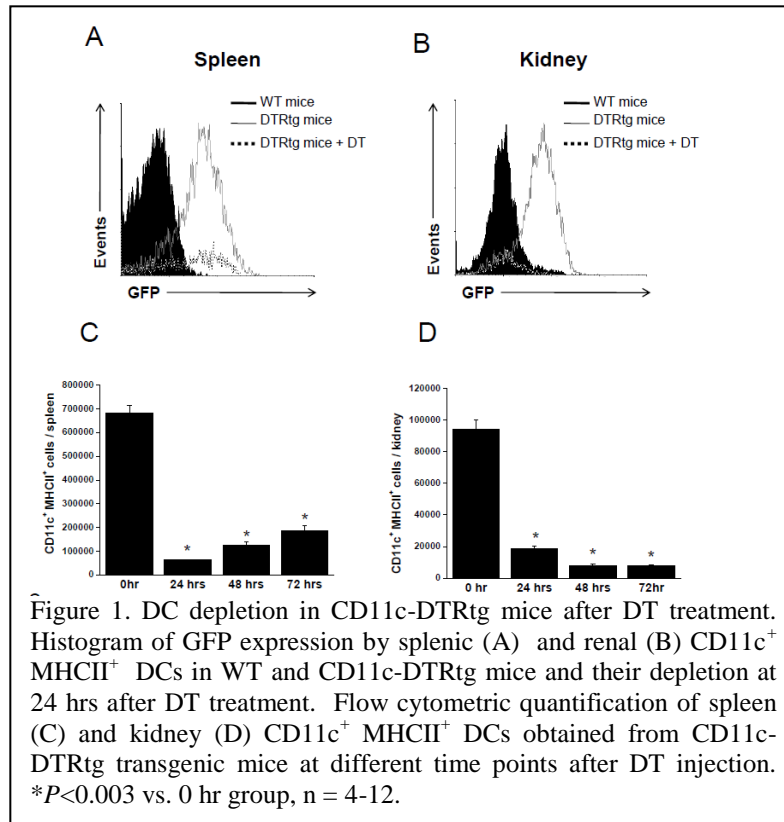
The worsening renal dysfunction in response to cisplatin treatment in DC depleted mice was associated with an increase in tubular necrosis. Kidneys from DT treated WT mice and CD11c-DTRtg mice did not exhibit any visible tubular damage. WT mice treated with DT followed by cisplatin displayed moderate tubular injury characterized by dilation of tubules, loss of brush border and sloughing of epithelial cells. CD11c-DTRtg mice treated with DT followed by cisplatin showed more extensive renal tubular damage compared with mice not depleted of DCs.

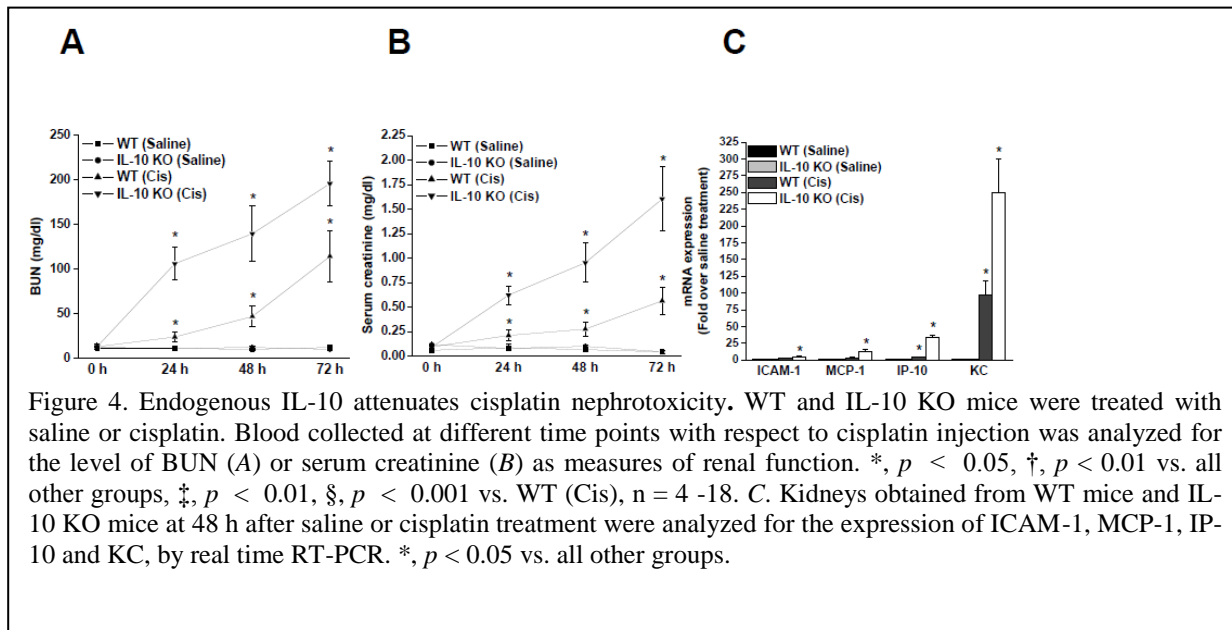
*Demonstrate specific TNF-alpha gene recombination in the proximal tubules of GGT-cre/TNF flox/flox mice.* By breeding a proximal tubule-specific cre mouse (GGT-cre) with a floxed TNF $\alpha$  mouse, we produced the desired GGT-cre/TNF<sup>lox/lox</sup> mice. In initial studies, they demonstrated significantly reduced (~80%) renal cortical TNF $\alpha$  production as determined by RT-PCR of renal cortex (Fig. 3) and by ELISA measurements of TNF- $\alpha$  production by suspensions of tubules prepared from kidney cortex.

However, subsequent generations have displayed variable reductions in TNF expression. We explored this further by genotyping DNA isolated from various tissues to determine the degree and specificity of recombination. We found incomplete recombination of the TNF gene in kidney cortex, but also observed recombinant product in other tissues, including heart, liver and spleen. This suggested low level expression of cre and more generalized expression of cre than we anticipated. However, quantitation and localization of cre expression in the kidney has been difficult to confirm by Western analysis or immunohistochemistry. Other investigators have not reported similar problems using the same GGT-cre mouse (personal communications). We suspected that our breeding colony might have been contaminated by endemic viruses which are present in our facility. Therefore, we re-derived the GGT-cre mouse in SPF conditions. We obtained only 2 mice from that rederivation, unfortunately both female. A second rederivation has produced more pups, still to be genotyped. Further breeding will be needed to determine if the rederived mice provide more specific gene recombination.

Generate a dendritic cell-specific TNF-alpha knockout mouse. These experiments involve the creation of dendritic cell-specific deletion of TNF- $\alpha$  using cre/lox technology. We bred a TNF flox/flox mouse with a CD11c-cre deleter mouse obtained from Jackson labs. The F1 generation has been genotyped. We then bred one of the resulting CD11c-cre TNF<sup>flox/WT</sup> with a TNF<sup>flox/flox</sup>. The F2 generation was just born and the genotyping is still pending. We expect the litter to include several of the desired CD11c-cre/TNF<sup>flox/flox</sup> mice.

Determine the mechanisms whereby kidney dendritic cells suppress AKI. Dendritic cells control immunity through the production of effector molecules, such as cytokines, and by interacting with other effector cells, such as T cells. We explored the role of IL-10 production by DCs in mediating their protective actions in AKI. First, we established that endogenous production of IL-10 did, indeed, suppress AKI. It was known that exogenous IL-10 can reduce AKI, but the role of endogenous IL-10 was not clear. We subjected wild-type and IL-10 KO mice to cisplatin treatment. Cisplatin treatment caused increases in renal IL-10R1 expression and STAT3 phosphorylation. In addition, IL-10KO mice showed more rapid and greater increases in BUN and serum creatinine compared with WT mice, indicating that endogenous IL-10 ameliorates kidney injury in cisplatin nephrotoxicity (Figure 4). Renal infiltration of IFN $\gamma$ -producing neutrophils was markedly increased in IL-10KO mice compared with WT mice. Renal dendritic cells showed high expression of IL-10 in response to cisplatin treatment. We further investigated the effect of dendritic cell-derived IL-10 in cisplatin nephrotoxicity using a conditional cell ablation approach. Mixed bone marrow chimeric mice lacking IL-10 in dendritic cells showed moderately greater renal dysfunction than chimeric mice positive for IL-10 in dendritic cells, suggesting that dendritic cell-derived IL-10 accounts for some, but not all, of DC-mediated protection from cisplatin nephrotoxicity. These data demonstrate that endogenous IL-10 reduces cisplatin nephrotoxicity and associated inflammation. Moreover, a portion of the protective effect of dendritic cells in cisplatin nephrotoxicity is mediated by IL-10 produced by dendritic cells themselves.





## **Research Project 29: Project Title and Purpose**

*Synergistically Acting Targeted Therapeutics for Melanoma* – Malignant melanoma remains the most deadly skin cancer with no effective drugs available for the long-term treatment of patients. The melanoma community believes that targeting Akt3, <sup>V600E</sup>B-Raf and other key kinases deregulated in melanoma is needed to effectively treat this disease. However, the identity of kinases to target using siRNA for synergistically acting tumor inhibition remains unknown and delivery of siRNA in animals remains a challenge. Therefore, the purpose of this project is to develop therapeutic agents inhibiting proteins deregulated in melanoma to shrink tumors in a synergistically acting manner. To accomplish this nanoliposomes containing siRNA designed to target <sup>V600E</sup>B-Raf, Akt3 and other key kinases in melanoma will be developed and efficacy for synergistically inhibiting melanoma development in skin and animals evaluated. Accomplishing these objectives not only identifies key kinases to synergistically inhibit melanoma development but also validates the utility of siRNA-loaded liposomes for treating melanoma patients.

### **Duration of Project**

7/8/2009 - 6/30/2010

### **Project Overview**

Malignant melanoma remains the most deadly skin cancer with no effective drugs available for the long-term treatment of patients. The melanoma community believes that therapies targeting key proteins or pathways promoting melanoma development are needed that act in a synergistic manner to effectively treat this disease. While it's thought that the MAP and PI3 kinase pathways need to be inhibited along with other key pathways, the identity of particular genes to target and therapeutics to accomplish this objective do not currently exist for melanoma. Targeting key

kinases deregulated in melanoma using siRNA-based agents is one approach, but the identity of kinases to target siRNA for synergistically acting tumor inhibition remains unknown and delivery of siRNA in animals remains a challenge. Our *long-term goal* is to develop therapeutic agents inhibiting proteins deregulated in melanoma to shrink tumors in a synergistically acting manner. To accomplish this objective, the *central hypothesis* proposes that siRNA-targeting Akt3, <sup>V600E</sup>B-Raf and other key kinases deregulated in melanoma can be loaded into nanoliposomes and used to synergistically inhibit melanoma development. The central hypothesis will be evaluated by: (1) Identifying which key kinases when targeted along with <sup>V600E</sup>B-Raf and Akt3 lead to synergistically acting tumor inhibition. A siRNA-based screen will be used to identify kinases deregulated in melanoma cell lines, validate involvement in tumor development and determine whether inhibition along with <sup>V600E</sup>B-Raf and Akt3 leads to synergistic tumor inhibition. (2) Evaluating whether nanoliposomes containing siRNA-targeting <sup>V600E</sup>B-Raf, Akt3 and other key kinases deregulated in melanoma can inhibit melanoma in a synergistically acting manner. Nanoliposomes containing siRNA designed to target <sup>V600E</sup>B-Raf, Akt3 and other key kinases in melanoma will be developed and efficacy for synergistically inhibiting melanoma development in skin and animals evaluated. Development of synergistically acting therapeutic agents targeting key kinases promoting melanoma development would be a significant, novel and innovative scientific advancement. These agents would lay the foundation for a new category of therapeutic drugs to more effectively treat patients suffering from melanoma. Long-term it would increase the currently available small arsenal of effective therapeutics for treating melanoma, thereby directly decreasing mortality rates.

### **Principal Investigator**

Gavin P. Robertson, PhD  
Associate Professor of Pharmacology, Pathology, and Dermatology  
Associate Director for Translational Research Penn State College of Medicine  
Pennsylvania State College of Medicine  
The Milton S. Hershey Medical Center  
Department of Pharmacology, R130  
500 University Drive, P.O. Box 850  
Hershey, PA 17033-0850

### **Other Participating Researchers**

SubbaRao Madhunapantula, PhD, Raghavendra Gowda, PhD – employed by Pennsylvania State College of Medicine

### **Expected Research Outcomes and Benefits**

One person in the United States dies from melanoma every hour. Currently, no effective treatment exists for patients suffering from the metastatic stages of this disease. In spite of the widely appreciated magnitude of the problem, there is still a critical gap in knowledge regarding key deregulated signaling pathways causing melanoma and therapies specifically targeted to correct these defects to inhibit tumorigenesis and metastasis. *Identification of synergistically acting kinases regulating melanoma development and design of a novel liposomal formulation*

for delivering these specific agents provide a better therapy for patients suffering from metastatic melanoma. As a direct outcome of the project, it is expected that synergistically acting kinases would be identified; Second, validity of identified kinases will be tested; Third, liposomal formulations will be developed for effective loading of siRNA molecules. Therefore, the positive impact for cancer patients suffering from melanoma will be significant.

## Summary of Research Completed

The *hypothesis* to be tested in aim 1 is that siRNA targeting kinases deregulated in melanoma can be identified, which when combined with inhibition of Akt3 and <sup>V600E</sup>B-Raf, lead to synergistically acting tumor inhibition. Discoveries made in this project show: (1) an siRNA screen can be used to identify kinases deregulated in melanoma; (2) validation of several of these kinases in melanoma development, including Akt3, <sup>V600E</sup>B-Raf and Wee1; (3) use of a siRNA-based approach in cultured cells to identify kinases, which when simultaneously targeted cooperatively inhibit melanoma development; and (4) that siRNA-mediated targeting of <sup>V600E</sup>B-Raf and Akt3 or Akt3 and Wee1 leads to synergistically acting inhibition of cultured cells. The *hypothesis* to be tested in aim 2 is that nanoliposomes containing siRNA-targeting <sup>V600E</sup>B-Raf, Akt3 and other key kinases deregulated in melanoma will synergistically destroy melanoma tumors. Discoveries made in this project show: (1) development of stable, non-toxic nanoliposomes that can be loaded with siRNA, which protect it from degradation; (2) that siRNA contained in nanoliposomes can be taken into melanoma cells and reduce expression of proteins against which the siRNA is targeted; (3) that nanoliposomes containing siRNA targeting two deregulated kinases, <sup>V600E</sup>B-Raf and Akt3 inhibits tumor development in animals in a cooperative, synergistically acting manner; and (4) that intravenously injected nanoliposomes loaded with fluorescent siRNA are taken into tumors in mice thereby inhibiting tumor development with negligible associated toxicity.

The *goals of aim 1* are to identify key kinases deregulated in melanoma and determine which kinases when targeted together with Akt3 and <sup>V600E</sup>B-Raf lead to synergistically acting tumor inhibition. The following was accomplished to achieve this objective.

- siRNA screening to identify kinases regulating melanoma development. A primary and secondary siRNA screen was developed to identify potential kinases deregulated in melanoma.
- Validating targets from the siRNA screen. Since earlier studies have demonstrated the oncogenic role of Wee1, involvement in melanoma was examined to validate the siRNA screen results using a xenografted melanoma model. Wee1, a dual specificity protein kinase, phosphorylates tyrosine, Ser/Thr residues of protein substrates. Wee1 was identified from the siRNA screen. To validate its therapeutic potential in animals, two independent, non-overlapping stealth siRNAs were introduced into metastatic melanoma cell lines UACC 903 and 1205 Lu and their effect on tumor development measured. 36 hours after introduction of siRNA,  $1 \times 10^6$  melanoma cells were injected into right and left flanks of 4 to 6 day old nude mice (Harlan Sprague) and sizes of developing tumors measured using calipers on alternate days up to day 21.5. Note that compared to control cells nucleofected with buffer, or a scrambled siRNA, siRNA targeting Wee1 led to significant decreases in the tumorigenic potential of both cell lines. Thus, the screen can identify potentially important therapeutic kinase targets, which is the goal of aim 1.
- Identifying genes to target with siRNA that lead to synergistic inhibition of cultured melanoma cells. To identify kinases that synergistically inhibit melanoma development, an *in vitro* tissue culture approach examining changes in anchorage dependent or independent cellular growth. To determine

whether the inhibition of anchorage independent growth was additive or synergistic following siRNA-mediated inhibition of Akt3 and <sup>V600E</sup>B-Raf or Akt3 and Wee1, the Chou-Talalay method for determining the combination index (CI) using CalcuSyn software was used (68). Using this approach, CI values less than 0.9 are synergistic, greater than 1.1 are antagonistic, and values between 0.9 and 1.1 are additive. The resulting CI for each combination was calculated to be 0.909, 1.023, and 1.107, for the respective doses of 3, 6, and 12 pmoles of B-Raf siRNA combined with 200 pmoles of Akt3 siRNA. The CI for Akt3 and Wee1 combinations was calculated to be 0.512, 0.095, 0.127, 0.189 and 0.307 for the respective doses of 6.25, 12.5, 25, 50 and 100 pmoles of Wee1 siRNA combined with 100 pmoles of Akt3 siRNA. According to Chou and Talalay doses between 0.9 and 1.1 are considered additive for the Akt3 & B-Raf combination and less than 0.9 are synergistic for the Akt3 & Wee1 combination. *Thus, simultaneous targeting <sup>V600E</sup>B-Raf and Akt3 using siRNA inhibits growth in a cooperatively additive manner and targeting Akt3 and Wee1 is strongly synergistic.*

• *Simultaneously targeting Akt3 and <sup>V600E</sup>B-Raf signaling using siRNA leads to cooperative, synergistically acting tumor inhibition, which validates the utility of the cell culture based screening assay.* To validate the therapeutic potential of simultaneously introducing multiple siRNA into melanoma tumors to synergistically inhibit melanoma development, siRNA inhibiting mutant <sup>V600E</sup>B-Raf and Akt3 was introduced via nucleofection into UACC 903 melanoma cells and the effect on tumor development examined. The size of developing tumors was measured using calipers every other day until day 17. Note, this is a published assay developed by the Robertson groups (Cancer Research May 1, 2008; 68(9): 3429-39. In comparison to controls (buffer, scrambled siRNA and C-Raf siRNA), siRNA against Akt3 or <sup>V600E</sup>B-Raf significantly decreased the tumorigenic potential of the UACC 903 cells. However, an even more dramatic reduction in tumorigenesis was observed following simultaneous inhibition of both Akt3 and B-Raf. Under these conditions, cooperatively acting synergistic tumor inhibition was observed. Tumors removed from mice 8 days after cell injection were found to have reduced Akt3 or <sup>V600E</sup>B-Raf protein expression demonstrating effective knockdown of these proteins in tumors. *These data are important because they show that siRNA targeting of two deregulated kinases, Akt3 and <sup>V600E</sup>B-Raf, can more effectively inhibit melanoma development than either agent alone.*

The *goal of aim 2* is to evaluate the efficacy of novel nanoliposomes containing siRNA-targeting kinases deregulated in melanoma to synergistically inhibit metastatic tumor development. The following was accomplished to achieve this objective.

• *Development of stable cationic nanoliposomes that load siRNA.* Since liposomes have been reported as potential siRNA delivery vehicles, a number of possible formulations to discover that a novel DOTAP, DOPE and DSPE-PEG(2000) ratio of 4.75:4.75:0.5 could efficiently load siRNA. Loading was measured by adding Alexa Fluor 546 tagged siRNA to these nanoliposomes at ratios of 1:5, 1:10, or 1:15 (siRNA: liposome by weight) and complexing for 0.5, 3, or 6 hours. Measuring free fluorescently tagged siRNA present in agarose gels or as a siRNA-liposome complex retained in the gel well was used to directly assess siRNA loading. A 1:5 ratio following 0.5 hours incubation showed presence of both loaded and unloaded siRNA, which was in contrast to the 1:10 and 1:15 ratios where siRNA remained in gel wells indicating complete complexing with nanoliposomes. Since maximal loading occurred following 30 minutes incubation at a 1:10 ratio, this formulation has been selected. Diameter of siRNA-liposome complexes either one day after preparation or 3 weeks later was measured using dynamic light scattering and shows an average diameter of ~50 nm with a range of 34-67 nm, demonstrating that the colloidal structure is maintained over time. Note, ghost nanoliposomes had a similar diameter averaging

~48 nm with a range of 32–64 nm and liposome size had not changed over the 3-week period. *These data are important, because they demonstrate creation of stable cationic nanoliposomes of ~50 nm capable of loading and transporting siRNA.*

- *siRNA in nanoliposomes is protected from serum degradation.* To evaluate the protective effects conferred by nanoliposomes on siRNA, fluorescently tagged free siRNA or siRNA-liposome complexes were exposed to 50% FBS, which is rich in RNA degrading factors, for 10, 30, 60, 180, or 360 minutes. To demonstrate siRNA protection, half of the original sample was treated with 0.5% SDS for 10 minutes, which disrupted the complex to release the siRNA. Similar levels of free siRNA were observed at all time points indicating protection by the complex. *These observations validate the protective effects nanoliposomes confer on the siRNA from degradation by external factors.*

- *Nanoliposomal-siRNA complex can load one or multiple siRNA, is non-toxic, and taken-up into the cytoplasm of normal as well as cancer cells.* A major advantage of these nanoliposomes is that they are uniformly sized due to filtration to exclude large nanoliposomes as shown by the dynamic light scattering system demonstrating an average size of ~50 nm. Thus, each liposome loads and delivers similar amounts of siRNA giving it significant potential as an agent for delivering siRNA based therapeutic agents. Furthermore, pegylation (69) and homogeneous nature of the ~50 nm sized nanoliposomes offers the potential of reduced clinical immunogenicity and inflammation, by minimizing activation of the reticular-endothelial system.

To determine uptake and toxicity of nanoliposomal-siRNA complex, fibroblasts, keratinocytes, and melanocytes were treated with ghost nanoliposomes or nanoliposomes containing Alexa Fluor 546-tagged siRNA (50, 100, or 200 nM). Fluorescence microscopy showed red Alexa fluorescence in ~100% of all cells indicating uptake of nanoliposomal siRNA. To verify siRNA was taken into the cytoplasm of cells, 1205 Lu melanoma cells were treated with 100 nM fluorescein-tagged siRNA-nanoliposomal complex or ghost nanoliposomes. Cells were then trypsinized to remove cell surface bound nanoliposomes and replated overnight followed by fixation. Fluorescence microscopy showed the presence of green fluorescein-tagged siRNA in the cytoplasm of cells surrounding a nuclear shadow indicating nanoliposomal siRNA was internalized. In contrast, no green fluorescence was observed in cells treated with ghost nanoliposomes. *These data validate uptake of the nanoliposomal-siRNA complex into the cytoplasm of normal and cancer cells with negligible toxicity.*

- *SiRNA targeting <sup>V600E</sup>B-Raf decreases mutant but not wild-type protein expression in cells demonstrating the potential for specifically targeting deregulated kinases in melanoma cells.* siRNA can be designed overlapping the T1799A mutation site of <sup>V600E</sup>B-Raf, which has potential to selectively decrease expression of mutant but not wild-type protein. To verify specificity of siRNA targeting <sup>V600E</sup>B-Raf, 100 pmoles (1 μM) was nucleofected into melanoma cells containing mutant (UACC 903) or wild-type protein (C8161.C19). Western blot and densitometric analysis of cellular protein lysates showed that siRNA designed specifically against <sup>V600E</sup>B-Raf reduced protein levels ~70% in mutant UACC 903 but not in wild-type B-Raf expressing C8161.C19 cells. In contrast, siRNA designed to sequences present in both mutant and wild type B-Raf decreased protein expression by ~70% in both cell lines. *These preliminary data are significant because they demonstrate the specificity of the siRNA for decreasing mutant but not wild type B-Raf and Akt3 but not Akt1 or Akt2 in melanoma cells.*

• SiRNA targeting <sup>V600E</sup>B-Raf can be loaded into nanoliposomes, delivered into cells and decrease expression of mutant protein. Having validated the specificity of siRNA for targeting V600E but not wild type B-Raf, 1 $\mu$ M siRNA was loaded into nanoliposomes and protein knockdown measured in 1205 Lu cells containing mutant <sup>V600E</sup>B-Raf in three independent experiments by densitometric analysis and using Western blotting. Examples of protein knockdown at 18 and 32 hours following a single treatment showed a 50-60% decrease of <sup>V600E</sup>B-Raf protein compared to cells treated with scrambled siRNA-nanoliposomal complex. While this result is significant it also suggests that a multiple dosing regime will be needed, as with most drugs for maximal effect, which is proposed in the *Research Design and Methods* section. Duration of knockdown following a single siRNA treatment was measured by introducing siRNA into cells and using Western blotting to measure protein knockdown 2, 4, 6, and 8 days later. Western blots were densitometrically scanned and knockdown of B-Raf protein compared to control cells nucleofected with siRNA targeting C-Raf. A consistent ~60% decrease in protein expression was observed through day 8. *These are significant results demonstrating that siRNA specific to mutant <sup>V600E</sup>B-Raf can be loaded into these cationic nanoliposomes, deliver siRNA into melanoma cells and decrease protein expression by ~60% following a single treatment.*

• Nanoliposomal-siRNA complex targeting <sup>V600E</sup>B-Raf and Akt3 cooperatively decreased melanocytic lesion development in animal skin. 1X10<sup>6</sup> UACC 903-GFP cells were subcutaneously injected into the right flank of nude mice and, under anesthesia, treated on alternate days at the tumor site with ultrasound for 15 minutes followed by topical application of siRNA-nanoliposomal complex. Along with measurement of tumor size, mice were weighed on alternate days. A statistically significant ~30% reduction in tumor size was observed from day 15 in mice treated with complex containing siRNA targeting <sup>V600E</sup>B-Raf compared to animals exposed to complex containing scrambled siRNA ( $p < 0.05$ ; Two-Way ANOVA). In contrast, no statistically significant difference was observed on cutaneous melanoma development following treatment with liposomes containing siRNA targeting Akt3 even though treated tumors were 10-15% smaller than controls treated with liposomes containing scrambled siRNA ( $p > 0.05$ ; Two-Way ANOVA). However, combination treatment showed significant synergistically acting tumor inhibition from day 11 when compared to siScrambled-liposomal complex ( $p < 0.05$ ; Two-Way ANOVA). Weights were monitored on alternate days to ascertain weight-related toxicity and no difference detected (Two-Way ANOVA,  $p > 0.05$ ). *These are very significant results demonstrating that nanoliposomal-siRNA complex targeting <sup>V600E</sup>B-Raf and Akt3 led to cooperative synergistically acting tumor inhibition in animals.*

• Intravenously injected siRNA-liposomal complex is taken up by tumor cells in mice. To demonstrate that liposomes deliver siRNA to tumors in mice, Alexa Fluor 546 tagged siRNA was loaded into liposomes and intravenously injected into mice. Tumors were removed from the mice 2 hours later. Ghost liposome-injected control mice showed the presence of no fluorescence. Fluorescent siRNA-liposomal complex was injected directly into tumors to serve as a positive control, which showed the presence of fluorescent siRNA within the tumors. Intravenously injected fluorescently-tagged siRNA liposomal complex led to the presence of fluorescently-tagged siRNA similar to the positive control. Accumulation was likely due to passive accumulation in tumors due to the presence of a leaky vasculature. Note, minimal uptake was seen in the lungs and no visible uptake was observed in the liver for mice treated intravenously or intra-lesionally with siRNA-liposomal complex. *Therefore, the liposomes can deliver siRNA to tumors following intravenous injection.*

• Intravenously injected siMutB-Raf-liposomal complex inhibits tumor growth in mice with negligible toxicity. To determine whether uptake of siMutB-Raf-liposomal complex into tumors would inhibit tumor growth in mice,  $2.5 \times 10^6$  1205 Lu or  $5 \times 10^6$  UACC 903 cells were injected into the flanks of nude mice. Beginning on day six when a fully vascularized tumor had developed, mice were injected daily via the tail vein with siMutB-Raf-liposomal complex (50 mg; UACC 903 and 100 mg; 1205 Lu) and compared to siScrambled-liposomal complex, ghost liposome, or free siMutB-Raf. Statistically significant decreases in UACC 903 and 1205 Lu tumor development of ~30% were observed for mice treated with siMutB-Raf-liposomal complex compared to control mice, which was predicted based on direct topical treatment with this agent. Additionally, weights of 1205 Lu tumor bearing nude or Swiss Webster mice treated with the siRNA-nanoliposomal complex were measured on alternate days, showing no differences compared to controls indicating negligible toxicity. This observation was confirmed by examining blood parameters indicative of major organ related toxicity or histological analysis, which also showed no differences compared to controls. Levels of SGOT, SGPT, alkaline phosphatase and blood glucose of mice injected with control siScrambled-liposomal complex or siMutB-Raf-liposomal complex were similar to that of normal uninjected control mice..

### **Research Project 30: Project Title and Purpose**

*Diabetic Changes in Contractile Proteins and Contractility in Arterial versus Venous Grafts –* Coronary artery disease is the leading cause of death and disability in patients with diabetes mellitus. Because of this, more than 300,000 patients with diabetes undergo coronary revascularization procedures annually in the U.S. to clear coronary blockages. Unfortunately, the benefit of percutaneous coronary intervention in diabetic patients is limited by their tendency to develop coronary restenosis by nearly 2- to 4-fold compared with nondiabetic patients. To date, the extent of alterations in contractile protein levels and the contractile responses in arterial vs. venous grafts remain unclear. Hence, the current project will compare diabetic vs. nondiabetic alterations in contractile proteins that regulate smooth muscle contractility in arterial and venous grafts, which will be obtained from patients undergoing coronary artery bypass grafting surgery.

### **Anticipated Duration of Project**

9/1/2009 - 6/30/2011

### **Project Overview**

Broad Research Objectives and Specific Research Aims: The overall goal of this project is to gain new understanding into the contractile properties of arterial vs. venous grafts. The specific objective is to investigate the relationship between contractile protein levels and the contractile responses in arterial vs. venous grafts in diabetic patients. Saphenous vein grafts have been shown to have worse coronary outcomes compared with left internal mammary artery (LIMA) grafts. We hypothesize that contractile proteins and/or contractile responses in vein grafts are compromised to a greater extent compared with arterial grafts. The Specific Aim of this project will determine diabetic and nondiabetic changes in contractile protein levels and contractile responses using saphenous vein and LIMA tissues from patients undergoing coronary artery bypass grafting surgery (CABG).

Research Design and Methods: Saphenous vein tissues (leftover segments) will be obtained from diabetic (n = 6) and age-matched nondiabetic (n = 6) patients undergoing CABG surgery. In addition, LIMA tissues (leftover segments) will be obtained from diabetic (n = 6) and age-matched nondiabetic (n = 6) patients undergoing CABG surgery. Saphenous vein and LIMA specimens from diabetic and nondiabetic subjects will be cleansed free of blood, adherent fat, and connective tissues. A portion of the tissue will be flash frozen in liquid nitrogen and stored at -80° C until analyses (for protein analysis and contractile protein quantification by immunoblotting). Immunoblot analysis will be performed with the total tissue lysates using primary antibodies specific for SM  $\alpha$ -actin, smooth muscle myosin heavy chain, calponin, and caldesmon. For *ex vivo* contractility studies, ring preparations of tissues will be immersed in Krebs-Henseleit solution (pH 7.4) that is gassed with 95% O<sub>2</sub> and 5% CO<sub>2</sub>. Contractility studies (isometric tension measurements) with saphenous vein and LIMA will be performed using the myograph chamber. We will determine the contractile responses to cumulative concentrations of serotonin (1 nM to 10  $\mu$ M) in the respective ring preparations.

### **Principal Investigator**

Lakshman Sandirasegarane, PhD  
Assistant Professor  
Penn State College of Medicine  
500 University Drive  
Hershey, PA 17033

### **Other Participating Researchers**

Mark Kozak, MD, Ann Ouyang, MD – employed by Penn State College of Medicine

### **Expected Research Outcomes and Benefits**

Expected outcomes: From the studies described in the current research project, it is expected that diabetes would decrease the expression of one or more contractile proteins in the blood vessel wall. In this regard, the decreases in contractile proteins would be much greater in saphenous vein grafts compared with left internal mammary artery (LIMA) grafts. Functionally, diabetic decreases in contractile protein expression will be reflected by corresponding alterations in the contractile responses in the blood vessels.

Benefits: The current project will determine the biochemical and functional abnormalities (contractile protein levels and contractile responses) in arterial and venous blood vessel specimens from both diabetic and nondiabetic patients. This will provide a better understanding of blood vessel wall contractile disorder and restenosis in diabetic *vs.* nondiabetic patients.

### **Summary of Research Completed**

The contractile properties of blood vessels such as saphenous vein (SV) grafts and left internal mammary artery (LIMA) grafts are attributed to smooth muscle cells (SMCs), which are present

in the medial layer of the vessel wall. Several contractile proteins are expressed in SMCs and they include smooth muscle  $\alpha$ -actin (SM  $\alpha$ -actin), SM22 $\alpha$ , calponin, caldesmon, smooth muscle myosin heavy chain (SM MHC), desmin, and smoothelin. To demonstrate the expression of these contractile proteins, a number of studies have previously employed the use of SMCs and blood vessels from rodents and several other animal species. Nevertheless, the expression profile of contractile proteins in human vascular SMCs or blood vessels is not fully understood.

*Rationale for the use of normal human vascular SMCs as controls for SV and LIMA grafts to determine contractile protein expression:* To determine the expression profile of contractile proteins in the SMCs of human origin, we used the commercially available SMCs that are derived from normal human aorta (Lonza Inc.). The determination of contractile proteins in normal human vascular SMCs has the following advantages: i) it provides the initial first step to characterize contractile proteins in normal human vascular SMCs, and subsequently use them as controls to compare with the contractile proteins that are expressed in SMCs of the diseased blood vessels such as SV and LIMA grafts, which will be obtained from diabetic and nondiabetic patients undergoing CABG surgery; ii) it allows us to examine whether the chosen primary antibodies are specific toward the detection and quantification of respective contractile proteins in human vascular SMCs; and iii) it also allows us to confirm the expression profile of contractile proteins at the level of contractile gene promoter activity and mRNA.

*Immunoblot analysis to determine contractile protein expression in human vascular SMCs:* When SMCs are maintained in culture in the presence of medium and growth supplements, they exhibit the properties of proliferative/synthetic phenotype characteristic of SMCs in the neointima in patients with restenosis after angioplasty. The proliferative phenotype of SMCs is associated with diminished expression levels of contractile proteins. Of importance, serum deprivation upregulates the expression of contractile proteins (e.g., SM  $\alpha$ -actin) in SMCs characteristic of differentiation/contractile phenotype in the vessel wall seen under physiological conditions *in vivo*. To determine the expression of contractile genes at the protein level in serum-deprived human aortic SMCs, we performed immunoblot analysis using primary antibodies specific for SM  $\alpha$ -actin, SM22 $\alpha$ , calponin, SM MHC, desmin, and smoothelin. In brief, the whole cell lysates (10  $\mu$ g protein each) from human aortic SMCs were subjected to electrophoresis using pre-cast 4-12% NuPage mini-gels (Invitrogen). The resolved proteins were transferred to nitrocellulose membranes (Hybond C, GE Healthcare). The membranes were then blocked and probed with the indicated primary antibodies. After extensive washes, the immunoreactivity was detected using specific HRP-conjugated secondary antibodies followed by enhanced chemiluminescence (Amersham Biosciences). The protein bands were quantified using Biorad GS-800 calibrated densitometer.

Figure 1 shows the progressive increase in the expression levels of SM  $\alpha$ -actin in human aortic SMCs after serum deprivation as a function of time. Figure 2 compares the contractile protein expression in human aortic SMCs using the respective primary antibodies. To verify the specificity of the chosen primary antibody, we used control SMCs (mock-transfected conditions) and the SMCs that were transfected (Amaxa device) with serum response factor (SRF) siRNA. SRF siRNA is expected to downregulate SRF transcription factor expression. In addition, SRF downregulation is associated with downregulation of contractile protein expression, as evidenced in rodent vascular SMCs. As shown in Figure 2, we were able to detect the expression of

contractile proteins such as SM  $\alpha$ -actin, SM22 $\alpha$ , and calponin in human aortic SMCs using specific primary antibodies. The expression of these three contractile proteins was further confirmed by: i) its downregulation by SRF siRNA; and ii) its downregulation by platelet-derived growth factor-BB (PDGF-BB) compared with the respective controls. However, we were unable to detect SM MHC and desmin using the respective primary antibodies ([Figure 2](#)). In addition, the specificity of the primary antibody in detecting smoothelin was not clear; and also there was no apparent downregulation of smoothelin by SRF siRNA ([Figure 2](#)). To address the problems associated with contractile protein detection using the primary antibodies for SM MHC, desmin, and smoothelin, we therefore performed RT-PCR analysis to determine contractile protein expression at the mRNA level.

*RT-PCR analysis to determine contractile protein mRNA expression in human vascular SMCs:* Total RNA was extracted from human aortic SMCs using QIAshredder and RNeasy mini kit (Qiagen). Using RT-PCR kit (Qiagen), 1  $\mu$ g total RNA was primed with random primers to synthesize the cDNA. The primer sequences for contractile genes (Integrated DNA Technologies) used in PCR amplification are listed in [Table 1](#). The PCR amplification conditions were: 95°C and 45 sec for initial denaturation; 57°C and 45 sec for annealing; 72°C and 1 min for chain elongation; 27 cycles for amplification. This was followed by a final extension at 72°C for 10 min. GAPDH was used as the house-keeping gene. The PCR reaction products were separated on 2% agarose gels using ethidium bromide and 100 bp DNA ladder. [Figure 3](#) shows the mRNA expression levels of contractile genes in comparison with c-Fos and GAPDH. We obtained distinct PCR products representative of SM22 $\alpha$  and GAPDH. Further studies are required to optimize the conditions for mRNA expression of other genes.

*EMSA analysis to determine the promoter activity of contractile protein gene in human vascular SMCs:* In human arterial/venous grafts and vascular SMCs, the molecular basis underlying contractile protein expression remains unclear. Previous studies using rodent arterial SMCs suggest that the contractile protein expression is primarily controlled at the level of transcription. In this regard, CARG-A and CARG-B containing DNA sequences in the promoter region of contractile protein gene (e.g., SM  $\alpha$ -actin) contribute significantly to SM  $\alpha$ -actin mRNA and protein expression. To determine the promoter activity of contractile protein gene in human vascular SMCs, we therefore used the DNA oligonucleotide sequences (Integrated DNA Technologies) specific for contractile protein genes such as SM  $\alpha$ -actin, SM22 $\alpha$ , and calponin ([Table 2](#)). To understand the relationship between contractile proteins and proliferative genes (e.g., cFos), we also used the DNA oligonucleotide sequence (that has SRE binding site) specific for c-Fos in parallel experiments.

Since nuclear proteins contain key transcription factors (e.g., SRF or Sp1) that would regulate the promoter activity of contractile protein genes, we prepared the nuclear extracts from human aortic SMCs. The nuclear and cytoplasmic extracts of human aortic SMCs were prepared using nuclear and cytoplasmic reagent kit (NE-PER; Pierce, Rockford, IL) and stored at -80°C until analysis. The reagent kit consists of cytoplasmic extraction reagent I (CER I), cytoplasmic extraction reagent II (CER II), and nuclear extraction reagent (NER). Prior to extraction, CER I and NER reagents were supplemented with Halt<sup>TM</sup> protease and phosphatase inhibitor cocktail (NE-PER; Pierce, Rockford, IL) and 1  $\mu$ M LR-microcystin. Protease and phosphatase inhibitors were added to prevent protein degradation and protein dephosphorylation, respectively, during

nuclear and cytoplasmic extraction procedures. The purities of nuclear and cytoplasmic fractions were assessed using CREB and superoxide dismutase (SOD), respectively.

To determine the promoter activity of contractile genes in human vascular SMCs, our initial experiments were aimed toward determining the extent to which nuclear proteins were bound to the DNA-binding sequence of contractile genes using electrophoretic mobility shift assays (EMSAs). [Table 2](#) shows the binding site (in red color) in the respective DNA oligonucleotide sequence for the specific gene. For EMSAs, double-stranded DNA was prepared by heating single-stranded oligonucleotides in equimolar concentrations at 95°C followed by cooling to room temperature over 2 hours. In brief, this was followed by i) DNA labeling/phosphorylation reaction using double-stranded DNA, T4 polynucleotide kinase (Promega) and [ $\gamma$ -<sup>32</sup>P]ATP; ii) removal of unlabeled DNA using Sephadex G-25 spin columns (Roche); iii) DNA binding reaction using human aortic SMC nuclear extracts and <sup>32</sup>P-labeled double-stranded DNA; iv) electrophoresis of DNA-protein complexes using DNA retardation gels; and v) autoradiography.

[Figure 4 A and B](#) shows the binding of nuclear proteins to the CArG-A and CArG-B containing DNA sequences specific for SM  $\alpha$ -actin. In parallel, [Figure 4 C](#) shows the binding of nuclear proteins to the SRE binding site on the proliferative gene, c-Fos. While the DNA binding activity was observed with CArG-B containing DNA sequence specific for SM22 $\alpha$  ([Figure 5](#)), there was no detectable DNA binding activity with Sp1 containing DNA sequence specific for calponin ([Figure 6](#)). Further studies will determine whether the promoter activity of contractile genes is constitutively active (under serum-free conditions) or inducible.

Together, EMSA, RT-PCR, and immunoblot analysis will provide a better understanding of diabetic alterations in the promoter activity of the contractile protein gene, mRNA levels of the contractile protein, and protein levels of the contractile protein in arterial *vs.* venous grafts from human subjects undergoing CABG surgery. Thus, changes in the promoter activity and expression levels of one or more contractile proteins may be associated with altered contractile responses in arterial *vs.* venous grafts.

**Table 1.** Primer sequences for contractile genes.

mRNA	PCR product size (bp)	Strand	Primer Sequence (5'-3')
SM $\alpha$ -actin	965	Forward Reverse	CCA GCT ATG TGT GAA GAA GAG G GTG ATC TCC TTC TGC ATT CGG T
SM22 $\alpha$	928	Forward Reverse	CGC GAA GTG CAG TCC AAA ATC G GGG CTG GTT CTT CTT CAA TGG GC
Calponin	671	Forward Reverse	GAG TGT GCA GAC GGA ACT TCA GCC GTC TGT GCC CAG CTT GGG GTC
MHC	479	Forward Reverse	CAG ATC CGA GCT CGC CAT CCG AGT AGA TGG GCA GGT GT
c-Fos	348	Forward Reverse	CCT GTC AAG AGC ATC AGC AG GTC AGA GGA AGG CTC ATT GC
GAPDH	302	Forward Reverse	AGC CAC ATC GCT CAG ACA CC GTA CTC AGC GCC AGC ATC G

**Table 2.** Oligonucleotide probes specific for contractile protein genes to determine DNA binding activity in EMSAs using the nuclear extracts of human aortic SMCs.

Promoter/Gene	Binding domain/site	Oligonucleotide sequence (5'-3')
SM $\alpha$ -actin	<b>CArG-A</b>	CTTTGCT <b>CCTTGT</b> TTGGGAAGCAA (F) TTGCTT <b>CCAAACAAGG</b> AGCAAAG (R)
SM $\alpha$ -actin	<b>CArG-B</b>	CTGAGGT <b>CCCTATATGG</b> TTGTGTT (F) AACACAA <b>CCATATAGGG</b> ACCTCAG (R)
SM 22 $\alpha$	<b>CArG-B</b>	GGGCAGGGTCCTGT <b>CCATAAAAGG</b> C TTT (F) AAAG <b>CCTTTTATGG</b> ACAGGACCCTGCCC (R)
Calponin	<b>Sp1</b>	AGGTGCC <b>CCGCC</b> CCTTGCA (F) TGCCAAG <b>GGCGGG</b> GCACCT (R)
c-Fos	<b>SRE</b>	ACAGGATGT <b>CCATATTAGG</b> ACAT (F) ATGT <b>CCTAATATGG</b> ACATCCTGT (R)

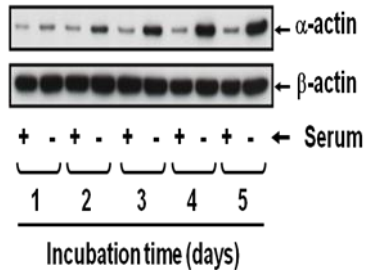


**Figure 1.** Human aortic SMCs were maintained in culture in the presence or absence of serum for up to 5 days. The SMC lysates were subjected to immunoblot analysis using the primary antibody specific for SM  $\alpha$ -actin.  $\beta$ -actin was used as an internal control (n = 2 to 3).

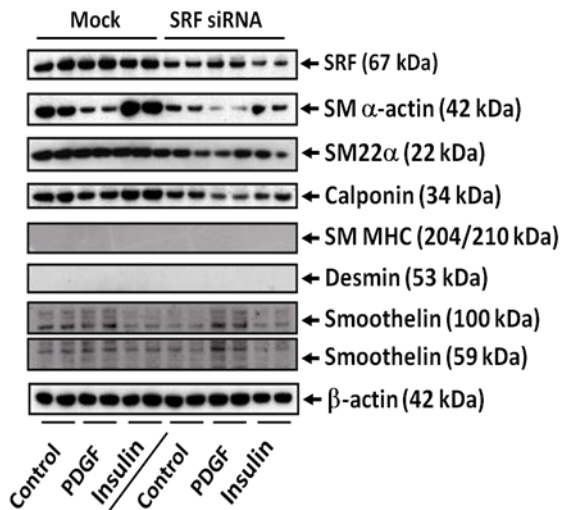


**Figure 2.** Comparison of contractile protein expression in human aortic SMCs under control or SRF-downregulated conditions. Mock control and SRF siRNA (400 pmoles)-transfected SMCs were incubated in complete medium for 3 days. Subsequently, SMCs were serum-deprived for 2 days in the absence or presence of PDGF-BB (30 ng/ml) or insulin (100 nM). SMC lysates were then subjected to immunoblot analysis using the respective primary antibodies.  $\beta$ -actin was used as an internal control (n = 2).

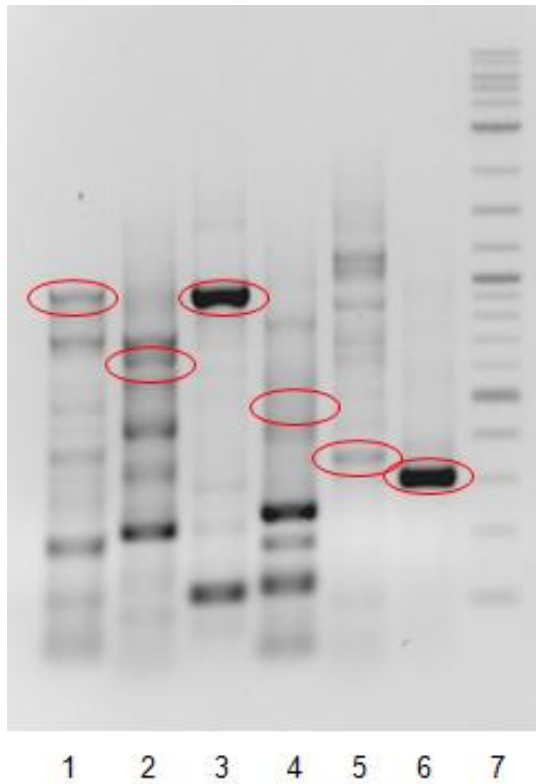


**Figure 3.** RT-PCR analysis of contractile protein mRNA in human aortic SMCs. The ethidium bromide-stained PCR products in agarose gel electrophoresis are shown in the following order: 1) SM α-actin; 2) calponin; 3) SM22α; 4) SM MHC; 5) c-Fos; and 6) GAPDH. Lane 7 shows the 100 bp DNA ladder. These data are representative of 2-3 experiments.

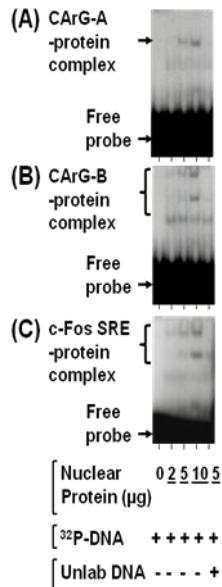


**Figure 4.** Effects of increasing concentrations of SMC nuclear proteins on DNA binding activity. Subconfluent human aortic SMCs were deprived of serum for 4 days. The respective nuclear extracts (2 to 10 μg protein) were then subjected to EMSAs to determine the binding of nuclear proteins to <sup>32</sup>P-labeled (A) CArG-A; (B) CArG-B; or (C) c-Fos SRE containing oligonucleotide probe. For competition experiments, the nuclear extracts were pre-incubated with 50 molar excess concentration of the respective unlabeled double-stranded DNA oligonucleotide prior to the addition of <sup>32</sup>P-labeled DNA (n = 2 to 3).

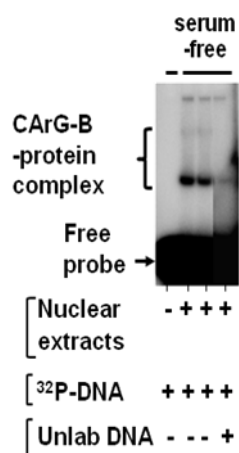


**Figure 5.** Nuclear protein binding to CArG-B containing region of SM22 $\alpha$  gene promoter. Subconfluent human aortic SMCs were deprived of serum for 4 days. The respective nuclear extracts (10  $\mu$ g protein) were then subjected to EMSAs to determine the binding of nuclear proteins to <sup>32</sup>P-labeled CArG-B containing oligonucleotide probe. For competition experiments, the nuclear extracts were pre-incubated with 100 molar excess concentration of the unlabeled double-stranded DNA oligonucleotide prior to the addition of <sup>32</sup>P-labeled DNA.



**Figure 6.** Nuclear protein binding to the Sp1 binding region of calponin gene promoter. Subconfluent human aortic SMCs were maintained in complete medium or deprived of serum for 24 hours. During serum deprivation, 30 ng/ml PDGF or 100 nM insulin was included in the incubation medium. The samples included for EMSAs were as follows: 1) no nuclear extract; and 2-6) nuclear extracts from SMCs  $\rightarrow$  2) complete medium; 3) serum-free, 24 hr; 4) serum-free with PDGF for 24 hr; 5) serum-free with insulin for 24 hr; and 6) serum-free for competition studies. The respective nuclear extracts (10  $\mu$ g protein) were then subjected to EMSAs to determine the binding of nuclear proteins to <sup>32</sup>P-labeled Sp1 binding site containing oligonucleotide probe. For competition experiments, the nuclear extracts were pre-incubated with 100 molar excess concentration of the unlabeled double-stranded DNA oligonucleotide prior to the addition of <sup>32</sup>P-labeled DNA.

## **Research Project 31: Project Title and Purpose**

*Autism Indicators: Erythrocyte Membrane Fluidity and/or Lipid Composition* – To determine whether fluidity and/or lipid composition of isolated red blood cell membranes differ in children with autism compared to age and gender matched children who are developing normally. If consistent differences are observed, funding to determine whether they are of diagnostic value will be sought.

### **Duration of Project**

7/8/2009 - 6/30/2011

### **Project Overview**

Autism is diagnosed by a set of behaviors most often initially noticed by the parents. While researchers agree that the earlier the diagnosis is made and treatment started, the more likely improvement will be noticed. Children are frequently three years of age or older by the time the diagnosis is able to be made. Recent research has indicated that even though autism affects most obviously specific areas of the brain, other organ systems may be involved as well. Therefore, abnormalities of membrane function/lipid composition may well be a fundamental difference that could affect neurological functioning and explain the multisystem pathology of autism. For example, a generalized membrane dysfunction could provide a reason for the observation of gastrointestinal malfunction, including diarrhea, in a significant fraction of children with autism. Erythrocytes from children with autism may have membranes that are less “fluid” than those of erythrocytes from normal children. Membrane fluidity reflects its lipid composition. Therefore, the aim of this project is to ascertain whether there is a consistent change in fluidity of membranes isolated from erythrocytes from children with autism relative to that of erythrocytes from age, gender, and geographic residence matched comparison children who are developing typically. If a difference is evident, then the study will determine whether that difference is accompanied by changes in glycerophospholipid (GPL), sphingolipid and/or cholesterol content/composition of the membrane. Fluidity of isolated red blood cell membranes will be measured by monitoring fluorescence depolarization using 1,6-diphenyl-1,3,5-hexatriene as the probe. Lipids will be extracted and aliquots taken for analysis of total lipid phosphorous, amino-glycerophospholipids, and cholesterol and the rest used for sphingolipid isolation and analysis. A significant change in fluidity coupled with a change in lipid content or composition might provide a simple test for predicting at a young age children who are or might become affected with autism.

### **Principal Investigator**

Cara-Lynne Schengrund, PhD  
Professor  
Penn State College of Medicine  
Department of Biochemistry and Molecular Biology H171  
500 University Drive  
Hershey, PA 17033

## **Other Participating Researchers**

Jeanette C. Ramer, MD – employed by The Milton S. Hershey Medical Center

Fatima Ali-Rahmani - employed by Penn State College of Medicine

## **Expected Research Outcomes and Benefits**

The results of the project should indicate whether the lipid composition of membranes isolated from red blood cells obtained from children diagnosed as having autism differs from those of normally developing, age, gender, and location-matched controls. If a difference is observed it may be possible to 1) develop a simple diagnostic test to identify children with autism and 2) determine what cell function(s) the changes may affect and whether they contribute to the problem.

## **Summary of Research Completed**

Children enrolled in this research were evaluated for symptoms of autism using a two step procedure. Initially each potential enrollee was evaluated in the pediatric Autism clinic by an experienced developmental pediatrician. Individuals that met DSM-IV-R criteria to have autism, had their diagnosis confirmed using an interview specialized for research use, the Autism Diagnostic Interview-Revised. Blood was drawn and serum separated for analysis. Comparison children (controls) were also evaluated using normed questionnaires completed by a parent in order to exclude children with symptoms of autism or other developmental disorders. Information about age and sex of participants is given in Table 1.

Erythrocytes were isolated from blood samples by centrifugation on Ficoll-Paque at 400xG for 30 min at room temperature. The erythrocytes, recovered at the bottom of the tube, were washed (20mM Tris-HCl containing 0.13M NaCl, pH 7.4) prior to lysis in cold 5mM sodium phosphate, pH8.0. Membranes were recovered by centrifugation (14,000xG, 4°C) and the ghosts washed until hemoglobin free. Protein concentration was determined using the Bio-Rad protein assay with bovine serum albumin as the standard. Samples were then stored at -80°C until used.

Anisotropy measurements were done on membranes isolated from erythrocytes obtained from children that were diagnosed with autism or from age, gender, and geographic residence matched controls in order to obtain a first approximation of whether a difference in membrane fluidity was associated with autism. The hypothesis that it might be was based on the report of elevated levels of amino-glycerophospholipids in erythrocytes and plasma from children with autism compared to controls and that fluorescence anisotropy measurements of erythrocyte membranes isolated from the blood of autistic children indicated they were less fluid than erythrocyte membranes isolated from blood of typically developing peers. Anisotropy experiments were done as follows: tetrahydrofuran containing 2mM 1,6-diphenyl-1,3,5-hexatriene was pipetted into a 1000-fold volume of phosphate buffered saline, pH7.4 and stirred to allow evaporation of the tetrahydrofuran. Sample containing ~0.1mg of protein/ml of phosphate buffered saline was then diluted with an equivalent volume of the fluor. To allow the fluor to interact with the protein, samples were incubated at 37°C for two hours. Anisotropy measurements were then made using an ISS PC1™ spectrofluorimeter using an excitation wavelength of 365nm and a

400nm Ealing colored glass filter for emitted light ( $\lambda_{\max}$  for the fluor is 435nm, a wavelength transmitted by the filter). It can be seen (Figure 1) that results obtained for erythrocyte membranes isolated from 11 samples from children with autism did not differ from samples obtained from 14 controls. Interestingly, results were similar whether samples were analyzed within 24hrs of preparation or after storage at  $-80^{\circ}\text{C}$  for several weeks.

While failure to see differences in anisotropy was not the anticipated result, experiments are underway to determine whether changes in one lipid that might affect membrane fluidity are offset by changes in another. Because cholesterol is known to affect membrane fluidity, its presence in the isolated membranes was determined using the Amplex Red<sup>®</sup> cholesterol assay (Invitrogen) according to the manufacturer's instructions. Since membranes contain cholesterol and not cholesterol esters, cholesterol esterase was not used to catalyze hydrolysis of fatty acid from cholesterol prior to analysis. In this assay cholesterol oxidase is used to oxidize the hydroxyl group on cholesterol to the ketone with the concomitant production of hydrogen peroxide. In the presence of horse radish peroxidase, 10-acetyl-3,7-dihydroxyphen-oxazine interacts on a 1:1 basis with hydrogen peroxide, to give resorufin (see Fig. 2) which is fluorescent (excitation range of 530-560nm, emission at  $\sim 590\text{nm}$ ). Known concentrations of cholesterol were used as standards. Results obtained thus far are shown in Table 1. No significant differences were seen between values obtained for samples from children with autism and controls. Based on the anisotropy data, this observation was not unexpected since cholesterol is known to reduce lateral mobility within the membrane when it is above the transition temperature and to enhance it below. To counteract a significant change in cholesterol concentration would require a significant change in other lipid components (eg unsaturated fatty acid composition of phospholipids). Because only four samples from children with autism were analyzed, additional samples will be measured to ascertain whether these preliminary results are reproducible.

Studies of the phospholipid composition of the membranes have been started. For these studies lipids were extracted from 1mg of isolated membranes and analyzed using shotgun lipidomics (electrospray ionization mass spectrometric analysis). Phospholipid standards were prepared using phospholipids having fatty acid compositions not found *in vivo*. Samples containing 1 mg of protein were added to a test tube containing dried phospholipid standards and extracted using chloroform-methanol-0.05M LiCl (protocol obtained from Dr. X. Han, Washington Univ. School of Medicine, St. Louis, MO). Phospholipid standards provided the internal standard for quantification of each of the phospholipids analyzed. The first six extracts were analyzed by Dr. Han. Analysis of the data indicated no significant differences between the ratios of the different classes of phospholipids, or in the fatty acid composition of those isolated from membranes isolated from erythrocytes from children with autism and those from controls (Table 2 for the ratio of different phospholipid classes). However, the numbers of samples are too small to permit firm conclusions to be made. A check of the literature indicated four papers in which lipids were analyzed with one indicating that the results of their analyses of the fatty acids present in erythrocyte membranes obtained from autistic subjects and controls did not provide "strong evidence for the hypothesis that abnormal fatty acid metabolism plays a role in the pathogenesis of autism spectrum disorder." Interestingly, another paper suggested that the fatty acid composition of erythrocyte phospholipids contained more highly unsaturated fatty acids than controls. Differences could also reflect diet or whether samples were obtained from children who

had been fasted for a fixed length of time prior to the time blood was taken. This point emphasizes the need to study multiple samples to determine whether there is a consistent difference regardless of the conditions under which samples are obtained.

The possibility of using NMR to obtain an indication of the relative amounts of the different classes of phospholipids present in the membranes is currently under investigation with Dr. Fang Tian. Phosphatidylcholine (PC) and sphingomyelin (SM) were readily identified by NMR while characterization of phosphatidylserine (PS) and phosphatidylethanolamine (PE) was less clear. The interesting point is that the NMR signal was very strong for both PC and SM, indicating that they are present in greater concentrations than PS and PE. This is the inverse of the results shown in Table 3 and is currently under investigation.

In conclusion: 1) Results of the anisotropy measurements indicate that if there are changes in fluidity in membranes of erythrocytes isolated from children with autism compared to those from children developing neurotypically, they are not sufficient to permit distinctions to be made using anisotropy measurements. 2) Cholesterol measurements made thus far indicate no significant difference in total membrane cholesterol. 3) Phospholipid measurements done so far failed to show significant differences in the PE/PS ratios as found by Chauhan et al. While more measurements must be done to solidify the data on which conclusions 2 and 3 are based, the results obtained thus far indicate that changes in lipid composition of erythrocyte membranes will not provide a relatively simple diagnostic possibility for the early identification of children with autism.

Table 1: Sex and ages of children from whom blood samples were taken for analysis.

Autism samples		Control samples	
Sex	Age	Sex	Age
14 males	3 – 3yr old	16 males	3 – 3yr old
	3 – 4yr old		1 – 4yr old
	2 – 5yr old		2 – 5yr old
	6 – 6yr old		5 – 6yr old
	1 – 7yr old		4 – 7yr old
1 female	6yr old	14 females	1 – 8yr old
			1 – 3yr old
	1 – 4yr old		
	2 – 5yr old		
	3 – 6yr old		
	3 – 7yr old		
	4 – 8yr old		

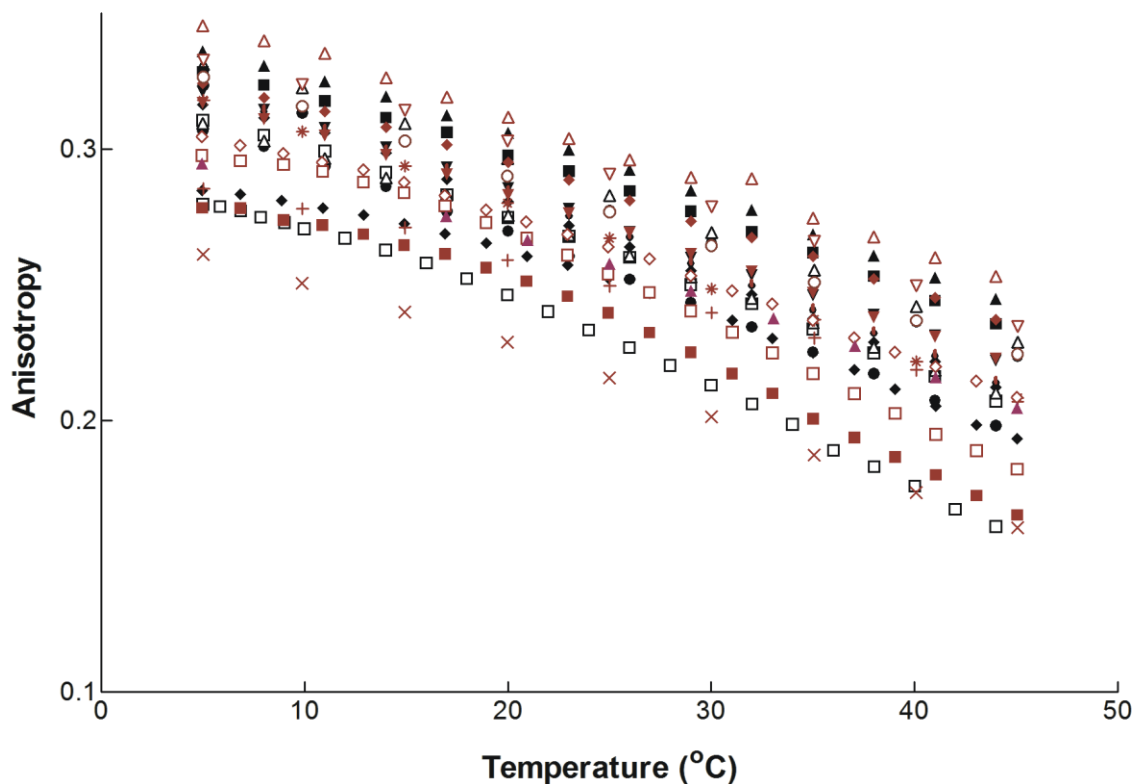


Figure 1: Anisotropy measurements. Red symbols indicate anisotropy measurements made for 14 different samples of red blood cell membranes isolated from blood from controls, black symbols – measurements made for 11 samples obtained from children diagnosed as having autism. Control samples were from both males and females aged 4-8; autism samples were from males aged 3-6. Differences do not reflect age and for controls do not reflect sex.

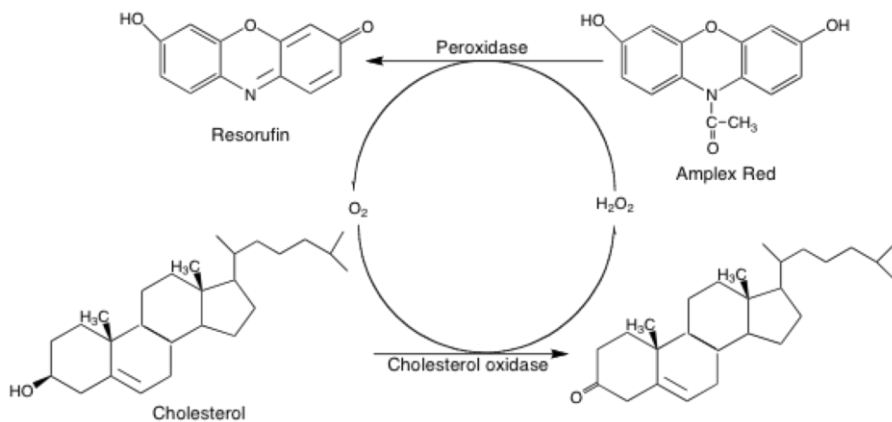


Figure 2: Cholesterol assay

Table 2: Cholesterol content per mg of red blood cell membrane protein taken for analysis. Cholesterol was determined using the Amplex Red Cholesterol Assay method (Invitrogen).

Sample	µg chol/mg protein
CO41	240
CO42	240
CO44	206
CO46	216
CO47	250
CO48	228
CO50	178
CO51	265
CO53	247
CO55	231
CO58	290
Aver+/- SD	236+/-29.8
AO8/10	280
AO47	240
AO49	240
AO28 9/26/08	235
Ave+/-SD	249+/-21.0

ρ=0.43

Table 3: Phospholipid composition of erythrocyte membranes isolated from four children with autism and two control children.

Phospholipid	AO	AO	AO	AO	CO	CO
PC	88	82	135	76	101	87
PE	342	288	572	280	380	352
PS	200	164	359	197	216	191
SM	158	171	278	154	179	171
PC:PE	0.25	0.28	0.24	0.27	0.27	0.25
PC:PS	0.44	0.5	0.38	0.38	0.47	0.46
PC:SM	0.55	0.48	0.48	0.49	0.57	0.51
PE:PS	1.7	1.8	1.6	1.4	1.8	1.8
PE:SM	2.2	1.7	2.1	1.8	2.1	2.1
PS:SM	1.3	1.0	1.3	1.3	1.2	1.1

AO indicates the sample is from an autistic child; CO from a control.

PC, phosphatidylcholine; PE, phosphatidylethanolamine; PS, phosphatidylserine; and SM, sphingomyelin

## **Research Project 32: Project Title and Purpose**

*Efficacy of Gemcitabine for Pancreatic Cancer: Role of DNA Polymerases* – Pancreatic ductal adenocarcinoma is a very aggressive malignancy that is treated by gemcitabine. Its efficacy is thought to be due to inhibition of DNA synthesis. It is our hypothesis that newly discovered DNA polymerases modulate gemcitabine toxicity and thereby decrease its efficacy. The purpose of the present experiments is to test the hypothesis that inter-individual differences in the levels of these polymerases affect incorporation of gemcitabine into the DNA and its efficacy in pancreatic cancer patients receiving gemcitabine.

### **Anticipated Duration of Project**

7/8/2009 - 12/31/2010

### **Project Overview**

The nucleotide analog, gemcitabine, a promising agent for a variety of cancers, is the most active chemotherapy agent for metastatic pancreatic cancer. Its efficacy is thought to be due to inhibition of DNA synthesis by stalling the DNA replication fork. However, it is our central hypothesis that newly discovered DNA polymerases ( $\kappa$ ,  $\iota$ ,  $\eta$ , and  $\zeta$ ) can rescue the stalled replication forks and incorporate gemcitabine into the DNA and consequently modulate gemcitabine toxicity and efficacy. The long-term goal of this research is to more fully understand the anti-cancer mechanisms of gemcitabine so that we can design a more effective treatment protocol and/or identify which patients will be more likely to respond to gemcitabine treatment. In the present experiments we plan to test the hypothesis that inter-individual differences in the levels of these polymerases affect incorporation of gemcitabine into the DNA and its efficacy. Specifically we will isolate white blood cells from patients who received gemcitabine. From these cells we will measure the levels of DNA polymerases  $\delta$ ,  $\kappa$ ,  $\iota$ ,  $\eta$ , and  $\zeta$ . In addition, we will measure the amount of gemcitabine incorporated into the DNA by an HPLC-MS/MS method, and after two months of treatment, determine the efficacy of the treatment. Upon successful completion of this research, we will have discovered whether levels of DNA polymerases  $\delta$ ,  $\kappa$ ,  $\iota$ ,  $\eta$ , and  $\zeta$  can modulate gemcitabine efficacy and determine whether the measurement of gemcitabine incorporation into the DNA of lymphocytes is a biomarker of efficacy of treatment.

### **Principal Investigator**

Thomas E Spratt, PhD  
Associate Professor  
Pennsylvania State University  
500 University Dr  
H171  
Hershey, PA 17033

## Other Participating Researchers

Yixing Jiang, MD, PhD, Kristin Eckert, PhD, Kwangmi Ahn, PhD, AS Prakasha Gowda, PhD – employed by Pennsylvania State University

## Expected Research Outcomes and Benefits

Gemcitabine, while a potent anti-cancer drug, is successful in only a minority of cases. The effectiveness of gemcitabine is believed to be due to the ability of gemcitabine to become incorporated into the DNA and then inhibit DNA synthesis. Our hypothesis is that individuals differ in their ability to incorporate gemcitabine into their DNA and that these differences lead to differences in efficacy. We expect to determine if the ability of an individual to incorporate gemcitabine into the DNA influences the effectiveness of the therapy. If true, then we would have designed a simple diagnostic test to determine whether gemcitabine therapy would be effective in an individual.

## Summary of Research Completed

The major goal of this project was to measure gemcitabine levels on blood cells of patients undergoing gemcitabine therapy for pancreatic cancer. However, in contrast to our expectations, in the 9 months that we have had to opportunity to obtain patients, only one has been a candidate. With a change in the IRB, we hope to get more patients enrolled.

We have evaluated a mechanism by which gemcitabine is incorporated into the genome. This has resulted in a publication in *Biochemistry*. A.S. Prakasha Gowda, Joanna M. Polizzi, Kristin A. Eckert and Thomas E. Spratt (2010) The incorporation of gemcitabine and cytarabine into DNA by DNA polymerase  $\beta$  and ligase III/XRCC1. *Biochemistry* **49** 4833-4840.

1- $\beta$ -D-Arabinofuranosylcytosine (cytarabine, araC) and 2', 2'-difluoro-2'-deoxycytidine (gemcitabine, dFdC), are effective cancer chemotherapeutic agents due to their ability to become incorporated into DNA and then subsequently inhibit DNA synthesis by replicative DNA polymerases. However, the impact of these 3'-modified nucleotides on the activity of specialized DNA polymerases has not been investigated. The role of polymerase  $\beta$  and base excision repair may be of particular importance due to the increased oxidative stress in tumors, increased oxidative stress caused by chemotherapy treatment, and the variable amounts of polymerase  $\beta$  in tumors. We directly investigated the incorporation of the 5'-triphosphorylated form of araC, dFdC, 2'-fluoro-2'-deoxycytidine (FdC) and cytidine into two nicked DNA substrates and the subsequent ligation. See Scheme 1 for structures.

We examined the steady-state and pre-steady-state rate of incorporation of dCTP and analogs into the gapped DNA substrates 1 and 3, shown in Scheme 2. The summary of the results are presented in Figure 1. Opposite template dG, the relative  $k_{pol}/K_d$  for incorporation was dCTP > araCTP, dFdCTP  $\gg$  rCTP. The relative  $k_{pol}/K_d$  for FdCTP depended on sequence. The effect on  $k_{pol}/K_d$  was due largely to changes in  $k_{pol}$  with no differences in the affinity of the nucleotide triphosphates to the polymerase. Ligation efficiency by T4 ligase and ligase III/XRCC1 was largely unaffected by the nucleotide analogs.

The results with pol  $\beta$  show that dFdC and araC are incorporated about 10-fold less efficiently than dC and but > 100-fold more efficiently than rC. The ligation experiments show that the modification of the sugar does not impact the rate of reaction with ligase III. Thus, the overall conclusion is that BER is capable of incorporating araC and dFdC into the genome.

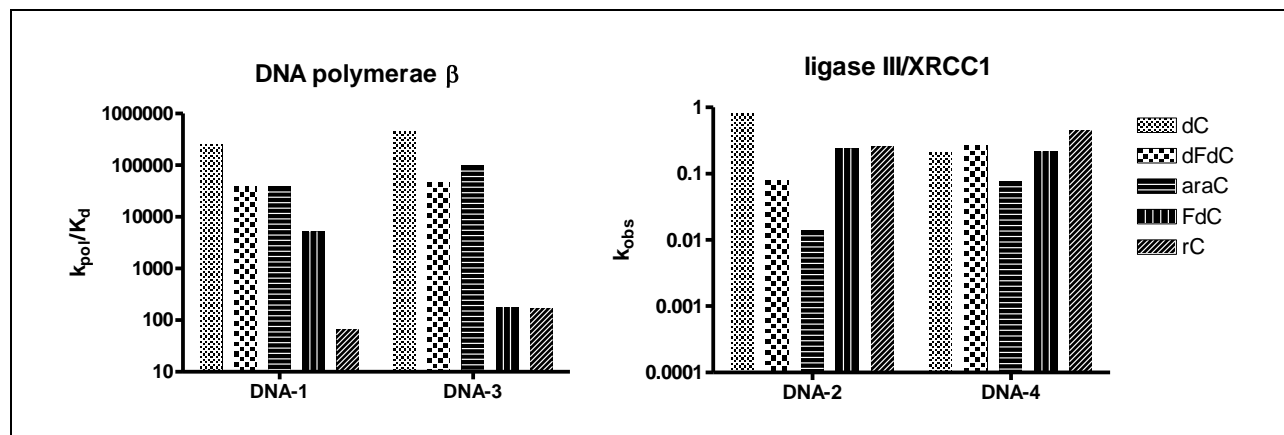
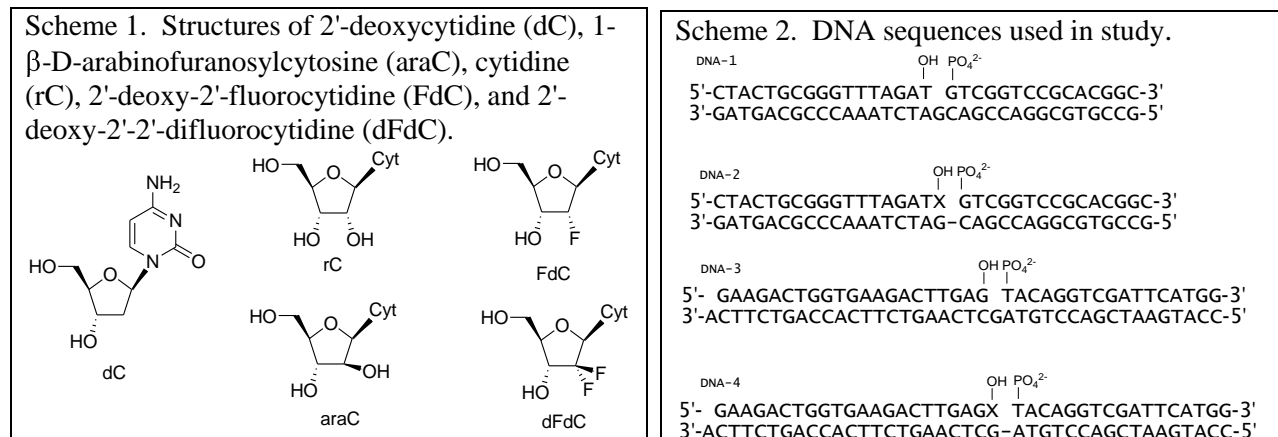


Figure 1. Summary of the reactivity of dC, dFdC, araC, FdC, and rC with DNA polymerase  $\beta$  and ligase III/XRCC1. A. Relative  $k_{pol}/K_d$  values for the incorporation of the dC analogs into DNA-1 and DNA-3 with 40 nM pol  $\beta$  and 25 nM. B. First-order rate constants for the ligation of DNA-2 and DNA-4 with 10 nM DNA, 10 nM ligase III, 10 nM XRCC1, and 2 mM ATP.

## **Research Project 33: Project Title and Purpose**

*Embedded Rural Clinical Research Infrastructure: Utilization of Community Based Nurses and Paramedics* – This project establishes the foundation for a research and community health approach that will be applicable to rural Americans nationwide. Rural Pennsylvanians are an underserved and aging population who suffer from an increased rate of elder falls and poor rates of influenza immunization. This project will deploy an innovative strategy to engage this community by using Penn State Cooperative Extension agents working together with newly trained and embedded health assessment staff. Embedded nurses and emergency medical technicians may offer an effective solution to furthering community assessment, improving important health measures, and creating new employment opportunities for these providers. Home safety assessment recommendations will be collected and recommendations for aging in place re-construction will be made with preferred local contractors.

### **Anticipated Duration of Project**

7/8/2009 - 6/30/2011

### **Project Overview**

This project will focus on establishing a Rural Embedded Assessment Community Health (REACH) Network of research coordinators in central Pennsylvania to meet the health care needs of the elderly. Objectives & Specific Aims: This study will test the hypothesis that in-home interventions to make the home safer will reduce the risk of falls and fall-related injuries compared to a control group not receiving the intervention. Embedded central Pennsylvania (PA) regional registered nurses (RN) and emergency medical technicians and paramedics (EMT) can successfully complete training and maintain adequate competency in the good clinical practice of research (GCPR), as established by the World Health Organization. Elder fall prevention and influenza immunization will serve as initial targets of our rural community health improvement efforts. Design & Methods: Distance learning programs delivered via the Penn State University (PSU) will achieve an adequate level of competency on appropriate outcome metrics in these RN&EMT populations in central PA. The density of GCPR graduates within the central PA region will allow representation in targeted central PA communities at a proportion of 1:2,500 population. Community participation to achieve a sample size of 25 elders will be considered as a threshold for participation. Continuing education units will be offered as an incentive to improve student enrollment in the program and coordination with county extension services will be performed. Additionally, selected graduates with a community commitment and excellent skills will be offered employment opportunity in representing their respective communities in this clinical research network. Facilitation will be carried out using computer desk-top based, web-conferencing tools to reduce travel, expense and enhance participation. Initial communities with strong commitment and agreeable participants will be selected for pilot programs, with regional expansion in future years. Generalizeability, for rural and small towns will be assessed. Expected Outcomes: Groups of embedded trained staff will work to identify community needs and engagement by holding standardized meetings focused on eliciting community perception on health needs, coordinating with county extension office staff. Trained community research staff from the embedded pool will work with local community leaders in identifying acceptable

methods to improve fall risk and immunization of elder citizens. Outcome measures include percentage of elder homes assessed and approval recommendations and actual modifications accepted by elders. Before and after proportions of community based elders receiving influenza vaccination will be assessed.

### **Principal Investigator**

Thomas E. Terndrup, MD  
Associate Dean for Clinical Research  
Emergency Medicine  
Penn State College of Medicine  
500 University Drive  
Hershey, PA 17033

### **Other Participating Researchers**

Ted Alter, PhD, Marilyn Corbin, PhD, Gregory Olsen, PhD, MLA – employed by Pennsylvania State University  
Claire Flaherty-Craig, PhD - employed by Penn State College of Medicine

### **Expected Research Outcomes and Benefits**

The REACH Network would capitalize on the experience and expertise of nurses and emergency medical technicians (nurse/EMTs) who are part of the social fabric of rural communities, and team these workers with Penn State University cooperative extension staff to perform detailed assessments in the homes of elderly individuals. After completing training, the nurse/EMTs will conduct a safety analysis of living conditions in the home, complete a neurocognitive questionnaire, and make recommendations for preventive health care (eg, immunizations), using an innovative mobile data acquisition device for facilitated and enhanced site data input. This approach should reduce the incidence of fall-related injuries and increase the immunization rates compared with elders who do not receiving this intervention. Our transformational approach to community engaged research will address the challenges of a lack of understanding of local health needs, poor community trust in research, and the absence of trained research personnel domiciling within those communities.

### **Summary of Research Completed**

REACH's Community Advisory Board was convened in July 2009. The board consists of local health professionals and leaders: Phyllis Mitchell, VP Marketing & Community Affairs, Lewistown Hospital, Dr. David Schooley, Retired Public Health Physician, Maureen Hoffman, Nurse Administrator for PRN, Phyllis Palm, Retired Senior VP of Operations, Lewistown Hospital, Patrick Shoop, Chief, Fame Emergency Medical Services, and CAB co-chair, Ellen Weaver, Regional Director, Centre HomeCare, VNA of Pennsylvania. The Board met with all network members on August 4, 2009 and subsequently on the following dates September 8<sup>th</sup>, October 13<sup>th</sup>, November 17<sup>th</sup>, January 11<sup>th</sup>, February 16<sup>th</sup>, March 23<sup>rd</sup>, April 20<sup>th</sup>, and May 21<sup>st</sup>.

Research coordinator, Leigh Gordon, was hired to work full time beginning on July 20, 2009. The coordinator was responsible for hiring local nurses and emergency medical technicians (EMTs) known as Community Health Assistants (CHAs) to administer interventions to the participants. Four EMTs and four nurses were hired. Each CHA was required to successfully complete online good clinical practices of research training (CITI training – Collaborative Institutional Training Initiative). The Institutional Review Board (IRB) approved the application to allow participants to be recruited into the study on August 19, 2009. After successful completion of CITI training and the IRB's approval, the CHAs were able to begin recruiting participants. This was done mainly by word of mouth, at local churches, visits to senior centers, asking neighbors, etc. Recruitment was aided by the use of informational brochures and articles in local media. The CHAs receive a yearly stipend of \$2500 for their services with the payments being dispersed after certain milestones have been met. To date, \$2250 has been paid out to the CHAs during this fiscal year. Each CHA was also required to attend iPod Touch/home visit training.

A methodologist with experience in community engaged research and collaboration, Louis Brown, Ph.D., from Penn State's Research Prevention Center was hired on July 31, 2009 to help create the study design. A crossover study design was decided upon after receiving feedback from network participants and the community advisory board. The study design randomizes participants into either the fall prevention treatment group or the seasonal flu vaccine intervention treatment group. If a participant is randomized into the fall prevention group in year 1, they will be crossed over to the season flu vaccine intervention group in year 2. The immunization treatment group will not receive their initial home visit until approximately September 2010 when flu shot season begins. Each participant will receive four visits per year; the initial home visit which includes the assessment and three quarterly follow-up visits.

Jessica Cook, a project coordinator at Penn State's Hamer Center for Community Design and graduate student in landscape architecture was also hired in July 2009 to assist with the selection and design of the home safety assessment survey. HomeFast, a validated survey tool, was selected and approved by the board at the meeting held on September 8, 2009. After deciding on the use of HomeFast, the survey was built into an application for the iPod Touch device. The application not only included the home safety survey but also collected pertinent information such as participant's name and date of assessment. The application was completed at the end of October 2009. Testing of the application took place the first week in November 2009. A secure password protected server was created so that survey data from the iPod Touch could be downloaded and exported to Excel for data analysis purposes. A home safety recommendation brochure was also designed. Based on the results of each participant's HomeFast survey, a personalized brochure was created to give participants tips and recommendations on how to make their homes safer.

A baseline questionnaire to be administered to each participant was created. The baseline questionnaire collects information regarding the participant's fall and flu shot history, medical conditions, current medications, lifestyle factors and demographics. The baseline questionnaire was approved by the board and was implemented in December 2009. Initial home visits for the fall prevention group began in January 2010. They include the HomeFast safety assessment, a

brief neurocognitive screening (mini-cog) and the Timed Get Up and Go test that measures one's mobility.

In order to assess the network's level of community engagement, a collaboration survey was created by Louis Brown in February 2010. A community engagement subcommittee comprised of both network and community members met several times to discuss how to go about implementing the survey and follow-up discussions. The survey was presented to the entire group in March 2010 and time was given for everyone to give input and feedback. The survey was submitted to the IRB for approval which was granted on April 12, 2010. The anonymous survey was placed on Survey Monkey. The survey aimed to assess members' involvement, effectiveness of leadership and communication, network participation, community support and barriers. Network members were given 2 weeks to complete the survey. 17 network members completed the survey. At the end of the two week period, results were downloaded into a report. A meeting was held on May 21<sup>st</sup> to discuss the results of the survey, identifying strengths and weaknesses of the collaboration and ways community engagement strategies can be improved. Results of the survey and meeting discussion will be used as part of a journal article.

The REACH Network has also been involved in several presentations and poster sessions. In March 2010, a presentation was given to the Mifflin County Cooperative Extension board. An "Establishment of the REACH Network" poster was displayed during the Center for Integrated HealthCare Delivery Systems (CHIDS) workshop held in State College, PA on March 29, 2010. The network also presented at a Kiwanis club meeting in Burnham, PA on April 20, 2010. REACH also participated in AcademyHealth's 2010 Annual Research Meeting poster session that was held in Boston on June 28, 2010. Currently, a first person accounts article is being compiled to be submitted to the American Journal of Community Psychology.

To date, 157 participants have been recruited. 106 baseline questionnaires have been completed. 47 participants have received their initial home visits, timed get up and go tests, and mini-cog assessments. Preliminary data from the initial home visits show that the most common fall risks found were: lack of non-slip floor surfaces, no slip resistant mats and/or strips in the bath/shower recess, lack of sturdy grab rails in the shower/beside the bath, loose throw rugs (not securely fixed to the floor) and not being able to easily switch on a light from their bed. In addition, 11 follow up visits have been completed. There were zero falls reported from baseline to the follow up visit.